SYNTHESIS AND INVESTIGATION OF NEW ELECTRONICALLY AND IONICALLY CONDUCTING POLYMERS

HUANYU MAO

Synthesis and Investigation of New Electronically and Ionically Conducting Polymers

By

Huanyu Mao

Submitted to the School of Graduate Studies in partial fulfilment of the requirements for the degree of Doctor of Philosophy

Department of Chemistry
Memorial University of Newfoundland
St. John's Newfoundland, Canada

1991

ISBN 0-315-73348-9

To Naming and Duncan

Abstract

The electronically and ionically conducting ion exchange polymers, protonated poly-[3-(pyrrol-1-ylmethyl)pyridine](poly-HPMP$^+$), poly-[1-methyl-3-(pyrrol-1-ylmethyl)pyridinium tetrafluoroborate] (poly-MPMP$^+BF_4^-$), poly-[1-(3-[pyrrol-3-yl]propyl)pyridinium tetrafluoroborate] (poly-PPP$^+BF_4^-$) and poly-[(3-[pyrrol-3-yl]propyl)trimethylammonium tetrafluoroborate] (poly-PPTA$^+BF_4^-$) have been electrochemically synthesised. Elemental analysis, cyclic voltammetry, gravimetry and scanning electron microscopy have been used to characterize the prepared polymers. The structures and electrochemical properties of these polymers are similar to those of other N- and 3-substituted polypyrrole based polymers. However, the high concentration (5 ~ 6 M) of permanent positively charged sites improve their electrochemical properties.

The *in situ* electronic conductivity of poly-MPMP$^+$ was measured using rotating disc voltammetry. An empirical method was developed to extract potential profiles and conductivities from rotating disc voltammograms of ferrocene at poly-MPMP$^+$ coated electrodes. This treatment was tested using *in situ* dual electrode methods, and confirmed. A relationship between the polymer conductivity and potential was obtained. The electronic conductivity increases

exponentially with potential (90 mV per decade) and levels off when the potential is more positive than the polymer's formal potential.

Ion exchange properties, such as the binding of an anionic electrocatalyst, for poly-$MPMP^+$, poly-PPP^+ and poly-$PPTA^+$ have been quantitatively investigated. The partition coefficients of ferrocyanide for these polymers range from 3.2×10^4 to 5.5×10^4 and their saturation concentrations are $1.3 \sim 1.4$ M. The charge transport of ferrocyanide is faster in poly-PPP^+ and poly-$PPTA^+$ than in poly-$MPMP^+$ due to the significant difference in each polymer's conductivity at the formal potential of ferrocyanide.

Transport of I^-, Cl^-, and $Fe(CN)_6^{4-}$ in poly-$MPMP^+$ have been studied using rotating disc voltammetry and ionic conductivity methods. Ion transport in the film is strongly dependent on the solvent. The diffusion coefficient of I^- in water (1.5×10^{-7} cm^2 s^{-1}) is over 2 orders of magnitude higher than in acetonitrile. Poly-$MPMP^+$ is significantly more permeable in water than polypyrrole. The diffusion coefficient for $Fe(CN)_6^{4-}$ is over 3 orders of magnitude higher than in reduced polypyrrole. The increased solvation and swelling of poly-$MPMP^+$ in water, which are due to the high concentration of positively charged sites in the polymer, result in improved ion transport properties.

Ascorbic acid oxidation is catalysed by these polymers (pH = 7.4) and mediated by electrostatically bound $Fe(CN)_6^{4-}$ (pH = 2.3). Cyclic voltammograms

for ascorbate oxidation show that the peak potential at poly-$PPTA^+$ coated Pt electrodes can be as much as 350 mV less than that at a bare Pt electrode. The peak current for poly-PPP^+ coated electrodes is more than 10 times greater than that at a bare Pt electrode. The 3-substituted polymers (poly-PPP^+ and poly-$PPTA^+$) show a greater electron transfer rate than does the N-substituted polymer (poly-$MPMP^+$), mainly due to the higher electronic conductivity for 3-substituted polymers at the ascorbate oxidation potential. The three polymers have enhanced, analytically significant peak currents which have allowed the generation of linear calibration curves for the analysis of ascorbic acid in aqueous solution.

Acknowledgements

I wish to express my deep sense of gratitude to my supervisor, Peter G. Pickup for his great help, stimulating advice, continued encouragement and patient guidance throughout the course of the degree.

I would like to thank the staff of Memorial University's Technical Services department for the help in construction of electrochemical cells and electrodes, and, in particular I am indebted to Mr. Martin Hatswell and Mr. Tom Perks for the construction and repair of glass apparatus. I am most grateful to Ms. Marion Baggs and Dr. Brian Gregory for their help in operating the mass spectrometer, and also to Dr. C. Jablonski, Ms. Nathalie Brunet for NMR operations. I would like also to thank Ms. Carolyn Emerson for her help in operating the scanning electron microscope.

Financial support in the form of a Memorial University of Newfoundland Graduate Fellowship, a Teaching Assistantship offered by the Department of Chemistry, and supplements from an NSERC grant are gratefully acknowledged.

Contents

Abstract	ii
Acknowledgements	v
List of Tables	ix
List of Figures	x
List of Abbreviations and Symbols Used	xvi
Chapter 1 Introduction	1
1.1 Chemically Modified Electrodes	1
1.1.1 Monolayers.	2
1.1.2 Polymeric Modifications	3
1.2 Polypyrrole: A Conducting Polymer	5
1.2.1 Electrochemical Polymerization	5
1.2.2 Structure of Polypyrrole	7
1.2.3 Electrochemistry of Polypyrrole	9
1.2.4 Electrocatalysis at Polypyrrole Electrodes	12
1.2.5 Applications of Polypyrrole	14
1.2.6 Polypyrroles with Cation Substituents	15
Chapter 2 Experimental	22
2.1 Synthesis of Monomers	22
2.2 Equipment for Electrochemical Experiments	33
2.3 Chemicals for Electrochemical Experiments	37
2.4 Scanning Electron Microscopy	38
2.5 Ionic Conductivity Measurements	38
2.6 Electronic Conductivity Measurements	42
2.7 Temperature, Errors and Precision of Results	42
Chapter 3 Synthesis and Characterization of Polymers	44
3.1 Synthesis of Polymers	44
3.2 Film Thickness and Morphology	54
3.3 Cyclic Voltammetry	63
3.4 Gravimetry, Chemical Analysis and Oxidation Level	74
3.5 Conclusions	80

Chapter 4 In Situ Electronic Conductivity Measurements 83
4.1 Rotating Disc Voltammetry 84
4.1.1 Rotating Disc Voltammetry of Ferrocene Oxidation at Poly-MPMP$^+$ Coated Electrodes 86
4.1.2 Data Analysis 89
4.2 Dual Electrode Measurements 100
4.2.1 Conductivity Measurement for Poly-MPMP$^+$ by Dual Electrode Voltammetry at Fixed Gold Potential 102
4.2.2 Conductivity Measurement for Poly-MPMP$^+$ Using Dual Electrode Voltammetry with a Small Potential Difference 105
4.2.3 Conductivity Measurement for Poly-PPP$^+$ and Poly-PPTA$^+$ Using Dual Electrode Voltammetry with a Small Potential Difference 108
4.2.4 Summary of Results for Poly-MPMP$^+$ 111
4.3 Electronic Conductivity of Poly-BPP 111
4.4 Conclusion 117

Chapter 5 Ion Exchange And Electrostatic Binding 120

5.1 Ion Exchange in Poly-MPMP$^+$ 121
5.1.1 Ion Exchange Process 121
5.1.2 Iodide Partition Coefficient Measurement by Ion Exchange 124
5.2 Electrostatic Binding of Ferrocyanide by Poly-[1-methyl-3-(pyrrol-1-ylmethyl)pyridinium], (Poly-MPMP$^+$) 129
5.2.1 Qualitative Aspects 130
5.2.2 Ferrocyanide Saturation Concentration Measurement 134
5.3 Electrostatic Binding of Ferrocyanide by Poly-[1-(3-[pyrrol-3-yl]propyl)pyridinium], (Poly-PPP$^+$) and Poly-[(3-[pyrrol-3-yl]propyl)trimethyl ammonium], (Poly-PPTA$^+$) 138
5.4 Kinetics of Ferrocyanide Electrochemistry within the Polymers 145
5.5 Discussion 151
5.6 Conclusions 153

Chapter 6 Ion Transport in Poly-[1-methyl-3-(pyrrol-1-ylmethyl) pyridinium], (poly-MPMP$^+$) 156

6.1 Investigation of Transport of Electroactive Ions by Rotating Disc Voltammetry 157
6.1.1 Principle of Rotating Disc Voltammetry Measurement 157
6.1.2 Transport of I^- within Poly-MPMP$^+$ in Acetonitrile 160

6.1.3 Transport of I^- within Poly-MPMP$^+$ in Water 166
6.1.4 Transport of $Fe(CN)_6^{4-}$ within Poly-MPMP$^+$ in Water 169
6.2 DC Ionic Conductivity Measurements 173
6.3 Estimation of Swelling Factor 177
6.4 Discussion 181
6.5 Conclusions 189

Chapter 7 Electrocatalysis of Ascorbic Acid Oxidation 192

7.1 The Mechanism of Electrooxidation of Ascorbic Acid 192
7.1.1 General Mechanism 192
7.1.2 Mechanism of Electrooxidation of Ascorbic Acid at Polymer Coated Electrodes 195
7.2 Ascorbic Acid Oxidation at Polymer Coated Electrodes 201
7.2.1 Poly-[1-methyl-3-(pyrrol-1-ylmethyl)pyridinium],Poly-MPMP$^+$ 201
7.2.2 Poly-[1-(pyrrol-3-ylpropyl)pyridinium], Poly-PPP$^+$ 207
7.2.3 Poly-[1-(pyrrol-3-ylpropyl)trimethylammonium], Poly-PPTA$^+$ 212
7.3 An Application in Analytical Chemistry 214
7.4 Discussion 219
7.5 Conclusions 225

List of Tables

Table 3.1 Film polymerization conditions at constant current.

Table 3.2 Formal potential change as a function of scan rate for poly-$MPMP^+$.

Table 3.3 Results of elemental analysis for poly-$MPMP^+$

Table 3.4 Mass, degree of oxidation, and coulombic polymerization efficiency for poly-$MPMPBF_4$ films by gravimetry.

Table 4.1 Data of DEV with a small fixed potential difference.

Table 4.2 Conductivities of poly-PPP^+ and poly-$PPTA^+$.

Table 4.3 The conductivity change for poly-BPP with reaction time in NMe_3/MeOH solution.

Table 5.1 Partition coefficients for I^- in poly-$MPMP^+$ (C_s = 1.0 mM)

Table 5.2 Variation of ferrocyanide concentration with potential.

Table 6.1 Ionic conductivities and Cl^- diffusion coefficients for poly-$MPMP^+$ in aqueous solutions

Table 6.2 Comparison of the current, i, due to electronic conductance with the limiting current, i_L, in RDV experiments.

Table 6.3 Half wave potentials for the second ferrocyanide rotating disc wave at poly-$MPMP^+$ coated electrodes.

Table 6.4 Summary of ion transport measurements

Table.7.1 Film thickness and peak current for poly-$MPMP^+$ in 0.5 mM ascorbic acid and 0.01 M phosphate buffer, pH = 7.4.

Table 7.2 Cyclic voltammetry results for poly-PPP^+ coated Pt electrodes.

Table 7.3 Comparison of cyclic voltammetry data for electrocatalysis of ascorbate oxidation at polypyrrole, poly-$MPMP^+$, poly-PPP^+ and poly-$PPTA^+$ coated electrodes.

List of Figures

Figure 1.2.1. Proposed mechanism for polypyrrole formation by oxidative electro-polymerization.

Figure 1.2.2. Cyclic voltammograms of polypyrrole (0.6 μm thick) in 0.1 M Et_4NClO_4/CH_3CN solution.

Figure 2.2.1. Three compartment cell for small disc electrode.

Figure 2.2.2. Three compartment cell for rotating disc electrode.

Figure 2.5.1. Two compartment cell for the measurement of ionic conductivity perpendicular to the film plane.

Figure 2.5.2. Two compartment cell for the measurement of ionic conductivity parallel to the film plane.

Figure 3.1.1. Structures of polymers.

Figure 3.1.2. Optimization of polymerization conditions for poly-$MPMP^+$.

Figure 3.1.3. A plot of anodic peak current *vs.* concentration of monomer (PMP).

Figure 3.1.4. A plot of anodic peak current *vs.* water concentration.

Figure 3.2.1. Indium/tin oxide electrodes for film thickness measurement.

Figure 3.2.2. Scanning electron micrographs of poly-$MPMP^+$ films.

Figure 3.2.3. Plot of polymerization charge density *vs.* film thickness for poly-$MPMP^+$ films.

Figure 3.2.4. Plot of polymerization charge density *vs.* film thickness for poly-PPP^+ films.

Figure 3.2.5. SEM pictures of poly-PPP^+ and poly-$PPTA^+$.

Figure 3.3.1. Cyclic voltammogram of a poly-$HPMP^+$ coated Pt electrode.

Figure 3.3.2. Cyclic voltammograms of a poly-$MPMP^+$ coated Pt electrode.

Figure 3.3.3. Plot of anodic and cathodic peak currents *vs.* scan rate for poly-$MPMP^+$.

Figure 3.3.4. Cyclic voltammograms of a poly-PPP^+ coated Pt electrode.

Figure 3.3.5. Cyclic voltammograms of a poly-$PPTA^+$ coated Pt electrode.

Figure 3.3.6. Plot of anodic peak current *vs.* scan rate for poly-PPP^+ and poly-$PPTA^+$.

Figure 3.3.7. Formal potential changes with scan rates for poly-PPP^+.

Figure 3.3.8. Cyclic voltammograms of a poly-BPP coated Pt electrode.

Figure 4.1.1. Schematic diagram of Ferrocene oxidation at the polymer/solution interface.

Figure 4.1.2. Rotating disc voltammograms in 5 mM ferrocene $LiClO_4/CH_3CN$ solution.

Figure 4.1.3. Plot of equation 4.1.2 for ferrocene oxidation at a bare rotating disc Pt electrode.

Figure 4.1.4. A schematic diagram of the dependence of film potential with the distance to the Pt surface.

Figure 4.1.5. A plot of potential at Pt *vs.* the logarithm of film thickness.

Figure 4.1.6. Linear relations between constants c, s and current *i*.

Figure 4.1.7. A schematic diagram of measuring data from rotating disc

voltammograms.

Figure 4.1.8. A plot of Log(conductivity) *vs.* potential for poly-$MPMP^+$.

Figure 4.2.1. Schematic diagram of dual electrode.

Figure 4.2.2. Voltammogram of dual electrode experiment at a fixed gold potential.

Figure 4.2.3. A plot of Log(conductivity) *vs.* potential for poly-$MPMP^+$ coated electrodes at a fixed gold potential.

Figure 4.2.4. Voltammogram of dual electrode experiment at fixed small potential difference.

Figure 4.2.5. A plot of Log(conductivity) *vs.* potential for poly-$MPMP^+$ coated electrodes at fixed small potential difference.

Figure 4.2.6. A comparison of conductivity of poly-$MPMP^+$ measured by different methods.

Figure 4.3.1. Voltammogram of dual electrode experiment at fixed small potential for poly-BPP.

Figure 4.3.2. A plot of conductivity *vs.* potential for poly-BPP coated electrode.

Figure 5.1.1. Schematic diagram of anion exchange of ClO_4^- by $Fe(CN)_6^{4-}$ for an ion exchange polymer.

Figure 5.1.2. Calibration curve of potential *vs.* Log (iodide concentration).

Figure 5.1.3. Plot of moles of iodide extracted from poly-$MPMP^+$ *vs.* film thickness.

Figure 5.2.1. Cyclic voltammograms at a poly-$MPMP^+$ coated Pt electrode in a $K_4Fe(CN)_6$ solution.

Figure 5.2.2. Cyclic voltammograms for the stability test for electrostatically bound $Fe(CN)_6^{4-}$ within poly-$MPMP^+$.

Figure 5.2.3. Slow cyclic voltammogram for $Fe(CN)_6^{4-}$ containing poly-$MPMP^+$ coated electrode.

Figure 5.2.4. Plot of the equilibrium concentration of $Fe(CN)_6^{4-}$ in poly-$MPMP^+$ films *vs.* its concentration in the bulk solution.

Figure 5.3.1. Cyclic voltammograms at a poly-PPP^+ coated Pt electrode in a $K_4Fe(CN)_6$ solution.

Figure 5.3.2. Cyclic voltammograms of a poly-PPP^+ coated Pt electrode in a $K_4Fe(CN)_6$ and a $K_4Fe(CN)_6$ free solution.

Figure 5.3.3. Plot of the equilibrium concentration of $Fe(CN)_6^{4-}$ in poly-PPP^+ films.

Figure 5.3.4. Cyclic voltammograms of a poly-$PPTA^+$ coated Pt electrode in a $K_4Fe(CN)_6$ solution.

Figure 5.4.1. A comparison of the kinetics of ferrocyanide electrochemistry in poly-$MPMP^+$ and poly-PPP^+.

Figure 5.4.2. Plot of peak current density for ferrocyanide oxidation in poly-$MPMP^+$ *vs.* (scan rate)$^{1/2}$.

Figure 5.4.3. Plots of peak current density for ferrocyanide oxidation in poly-PPP^+ and poly-$MPMP^+$ *vs.* scan rate.

Figure 6.1.1. Schematic diagram of ion transport pathways within the polymer film and in solution during rotating disc voltammetry.

Figure 6.1.2. Rotating disc voltammetry of tetrabutylammonium iodide at poly-$MPMP^+$ coated Pt electrode.

Figure 6.1.3. Rotating disc voltammetry of tetrabutylammonium iodide at poly-$MPMP^+$ coated electrodes at different rotation rates.

Figure 6.1.4. Inverse Levich plots for I^- (1.0 mM) oxidation at naked Pt and poly-$MPMP^+$ coated Pt electrodes.

Figure 6.1.5. Plot of intercept *vs.* film thickness.

Figure 6.1.6. Cyclic voltammograms of four successive scans for a 0.3 μm poly-MPMP$^+$ film.

Figure 6.1.7. Rotating disc voltammetry of I^- at a naked Pt electrode and at poly-MPMP$^+$ coated electrodes.

Figure 6.1.8. Rotating disc voltammograms of $Fe(CN)_6^{4-}$ at naked Pt and poly-MPMP$^+$ coated electrodes.

Figure 6.1.9. Inverse Levich plots for $Fe(CN)_6^{4-}$ (0.10 mM) oxidation at naked Pt and poly-MPMP$^+$ coated Pt electrodes.

Figure 6.1.10. Plot of intercept *vs.* film thickness.

Figure 6.2.1. Ionic resistance *vs.* time for a poly-MPMP$^+$ film.

Figure 6.3.1. Schematic diagram of the estimation of the swelling factor.

Figure 7.1.1. Proposed mechanism for the electrooxidation of ascorbic acid.

Figure 7.1.2. Schematic diagram of dissociated ascorbic acid oxidation at conducting polymer chains.

Figure 7.2.1. Cyclic voltammograms of ascorbate at a naked Pt electrode and at a poly-MPMP$^+$ coated electrode.

Figure 7.2.2. Rotating disc voltammograms of ascorbic acid oxidation at a naked Pt electrode and a poly-MPMP$^+$ coated Pt electrode.

Figure 7.2.3. Cyclic voltammograms of ascorbate oxidation at poly-PPP$^+$ coated electrode.

Figure 7.2.4. Cyclic voltammograms of ascorbate oxidation at poly-PPP$^+$ coated electrode and a naked Pt electrode.

Figure 7.2.5. Cyclic voltammograms of ascorbate oxidation at a poly-PPTA$^+$ coated electrode.

Figure 7.3.1. Calibration plot of peak current *vs.* ascorbic acid concentration for a poly-$MPMP^+$ coated electrode.

Figure 7.3.2. Calibration plot of peak current *vs.* ascorbic acid concentration for a poly-PPP^+ coated electrode.

Figure 7.3.3. Calibration plot of peak current *vs.* ascorbic acid concentration for a poly-$PPTA^+$ coated electrode.

List of Abbreviations and Symbols Used

Symbol	Meaning	Dimensions	Section
A	electrode area	cm^2	3.2
c	intercept of E_{Pt} *vs.* Ln(*d*) plot	V	4.1.1
C_I	concentration of iodide in extraction solution	M	5.1.1
C_{IE}	concentration of ion exchange sites in polymer	M	3.4
C_P	equilibrium concentration of substrate in polymer	M	5.1.1
C_S	equilibrium concentration of substrate in solution	M	5.1.1
d	film thickness	μm	3.2
D	diffusion coefficient	$cm^2\ s^{-1}$	5.4
DEV	dual electrode voltammetry		4.2
D_S	diffusion coefficient of substrate in solution	$cm^2\ s^{-1}$	6.1.1
$D_{S,pol}$	diffusion coefficient of substrate in polymer	$cm^2\ s^{-1}$	6.1.1
$E^{o'}$	formal potential	V	3.3
E_{app}	applied potential	V	4.1.1
E_{FWHM}	full width at half maximum	V	1.2.3
$E_{1/2}$	half wave potential	V	4.1.1
$E_{p,a}$	anodic peak potential	V	3.3
$E_{p,c}$	cathodic peak potential	V	3.3
E_{Pt}	potential of the polymer contacting Pt electrode	V	4.1.1
E_S	potential at polymer/solution interface	V	4.1.1
F	Faraday constant	$C\ mol^{-1}$	3.2
i	current	A	4.1.1
i_o	selected anodic current from rotating disc voltammogram of ferrocene oxidation	A	4.1.1
i_l	limiting current	A	4.1.1

Symbol	Meaning	Dimensions	Section
i_p	peak current	A	1.2.3
i_{DC}	constant current passing through a DC cell	A	6.2
k^o	standard heterogeneous rate constant	cm s^{-1}	7.1.1
Log	Log_{10}		4.1.1
M	molar mass of monomer	g mol^{-1}	3.2
M_c	mass of the counterion	g	3.4
M_p	formula mass of the reduced monomer unit in polymer film	g mol^{-1}	3.4
m_{ox}	mass of the oxidized film	g	3.4
m_{red}	mass of the reduced film	g	3.4
n	oxidation level		3.2
	electrons per molecule oxidized or reduced		4.1.1
n_α	number of electrons involved in rate determining step		7.1.1
P	partition coefficient		5.1.1
Q_{CV}	charge under cyclic voltammogram	C	3.4
Q_{pol}	polymerization charge	C	3.4
R	gas constant	J $mol^{-1}K^{-1}$	4.1.1
RDV	rotating disc voltammetry		4.1.1
R_u	uncompensated resistance	Ω	4.1.1
R⊥	perpendicular resistance	Ω	6.3
R//	parallel resistance	Ω	6.3
s	slope of E_{Pt} *vs.* Ln(d) plot	V	4.1.1
	swelling factor		6.3
SEM	scanning electron microscope		3.2.2
SSCE	sodium chloride saturated calomel electrode (0.24 V *vs* SHE)		1.2.3
v	scan rate	mV s^{-1}	1.2.3
	viscosity	cm^2 s^{-1}	6.1.1
V	film volume	cm^3	7.1.1
α	transfer coefficient		7.1.1
δ	film density	g cm^{-3}	3.2

Symbol	Meaning	Dimensions	Section
ΔE	peak separation	V	3.3
	potential difference in DEV	mV	4.2.2
ΔE_{DC}	potential difference between two reference electrodes in DC cell		6.2
η	coulombic efficiency		3.1.4
σ	conductivity	S cm^{-1}	4.1.1
σ_i	ionic conductivity	S cm^{-1}	6.2
ρ	resistivity	Ω cm	6.3
$\rho\perp$	perpendicular resistivity	Ω cm	6.3
$\rho//$	parallel resistivity	Ω cnm	6.3
ω	rotating rate	s^{-1}	6.1.1

Chapter 1

Introduction

One of the most active and interesting research areas in today's electrochemistry concerns chemically modified electrodes. These electrodes have received a great deal of attention over the past twenty years because they have many novel properties and also a wide range of applications in electrochemical analysis, energy conversion, microelectronics, information storage, and display. Conducting polymers, an important class of chemically modified electrodes, form the basis of this thesis. As an introduction, chemically modified electrodes will be briefly discussed, followed by a review of some specific polymers which are similar to those studied in this work.

1.1 Chemically Modified Electrodes

Chemically modified electrodes are defined as electrodes which have their surfaces deliberately modified so that the properties of the surface are dictated and controlled[1]. Two kinds of chemically modified electrodes have attracted much

attention in the past decade, those coated with monolayers and those with polymer coatings.

1.1.1 Monolayers

Early work involved the modification of electrodes by means of chemisorptive bonding. Usually only one layer of modifying molecules is formed on a carbon, tin dioxide, or platinum electrode surface. Specially treated carbon electrode surfaces have a very high density of pi-electrons and can adsorb large aromatic molecules such as porphyrins[2]. Porphyrins, as free bases as well as their metalloderivatives, greatly affect surface properties. An important modification of the monolayer technique was then developed. Organosilanes were bound to tin dioxide electrodes, and, subsequently, various molecules were bound to the organosilane monolayer. Tin dioxide and some superficially oxidized metals such as Au and Pt[3] have hydroxy surfaces which can react with organosilane compounds. These organosilane compounds can contain active groups at the end which can further react to incorporate redox couples. The electrochemistry of the electrodes can be greatly altered by these chemical reactions and this, perhaps, represents the true beginning of chemically modified electrodes. Extensive work has been carried out since[4] that time and many more reagents have been immobilized *via* silane chemistry. This kind of modification is called covalent

bonding modification. The formal potentials for the immobilized species have been found to be not much different from those of the dissolved analog. The significance of the use of such electrodes is that the electrochemical properties of a modified surface are predictable by analogy with solutions. One can therefore design and tailor electrodes. However, the stability of such monolayer coatings is not adequate in most cases. A lot of recent effort has therefore been centred on polymeric coatings to improve the stability and other properties[5].

1.1.2 Polymeric Modifications

The polymeric modification of electrodes is realized by depositing a polymer film on a noble metal or carbon. These polymeric films generally contain the equivalent of many monolayers, thus higher stability normally results[6]. For catalysis, polymer films have fundamental advantages over covalently bonded monolayers of catalyst[7]. They show great chemical and electrochemical stability and possess a high density of active-centres. Technically, electrochemical signals obtained from polymer coated electrodes are greatly enhanced compared to monolayer coated electrodes and therefore easy to measure. The preparation of polymer films can be very simple, involving methods such as dip coating, spin coating, electropolymerization and so on[4]. Among the methods of preparing polymer films, electrochemical polymerization of an electroactive monomer has

become one of the most versatile methods of modifying the surface of an electrode. Most electropolymerized films are highly adherent and are relatively resistant to solvents. Also, surface coverage can be easily controlled.

Polymers used to coat electrodes can be divided into three groups: redox polymers, ion exchange polymers[8] and conducting polymers. Redox polymers contain redox couples fixed to the polymer backbone. One of the examples of redox polymer electrodes involved a polymer containing aromatic nitro groups[9]. Soon the electrochemical study of redox polymers containing transition metals was begun by Oyama and Anson[10]. Considerable work has been reported[11] and metal containing polymers have been employed to explore electrochemical processes such as electrocatalysis[12], charge transport phenomena[13,14,15], and photoactive interfaces[16].

Ion exchange polymers have the ability to exchange counterions (cations or anions) and thereby electroactive ions with favourable ion exchange partition coefficients can be incorporated *via* an electrostatic binding mechanism[17]. Cationic polymers (anion exchange polymers) contain fixed cation sites and anions can be electrostatically bound. Quaternized polyvinylpyridine is an example. Similarly, cations can be incorporated into anionic polymers (cation exchange polymers). The sulphonated fluorocarbon, Nafion, is a widely used anionic polymer in this area. The noteworthy advantages of ion exchange polymers are

that a wide range of different ions can be incorporated and the modification process is relatively simple.

Among polymeric electrode modifiers, conducting polymers play an important role. Examples are polyacetylene, polyparaphenylene, polyanilines, polypyrrole, and polythiophene. Most conducting polymers have conjugated π-electron systems and transport electrons *via* the delocalized band structure. Generally conducting polymers can be reversibly oxidized and reduced. The properties of conducting polymers such as conductivity, doping level, and permeability are strongly dependent on the oxidation states and can be easily controlled by changing the applied potential. For example, the conductivity of the polymers can be varied over many orders of magnitude by changing the oxidation state. Among the variety of conducting polymers, polypyrrole is one of the most interesting electrode modification materials. It has high chemical and thermal stability, it is simple to prepare, and a wide range of derivatives and copolymers have been made.

1.2 Polypyrrole: A Conducting Polymer

1.2.1 Electrochemical Polymerization

Polypyrrole was first made as a black powder by Angeli[18] in 1916. It did

not arouse any interest among electrochemists until polypyrrole films were prepared electrochemically by Dall'Olio [19]. The polymer was brittle with a conductivity of 8 S cm^{-1}. The study of polypyrrole by electrochemists was stimulated by Diaz and co-workers[20] when they reported that the anodic oxidation of pyrrole in acetonitrile containing 1% water resulted in stable conducting films. Subsequently a great many papers have been published on this subject.

Pyrrole can be easily electrochemically polymerized on noble metals (*e.g.* Pt and Au), carbon, or indium/tin oxide coated glass by oxidation either at constant potential, at constant current, or during potential scanning in conventional three compartment cells. Most electrochemically polymerized polypyrroles are dense and have the same structure throughout. Fiber structures have not been observed under electron scanning microscopy.

Polypyrrole is usually prepared in acetonitrile, water, or a mixture of acetonitrile and water. The most commonly used electrolytes are Et_4NClO_4 (Et $=C_2H_5$) and Et_4NBF_4. However, the types of anion used in the electrolyte can greatly affect the physical properties of the polypyrrole film. Salmon *et al*[21] studied nine anions and found that the density of the films varied from 1.37 to 1.51 g cm^{-3} and the conductivity changed from 10^{-2} to 100 S cm^{-1}. The mechanical property (tensile strength) of polypyrrole grown in a toluenesulfonate anion solution was reported to be superior to other forms of polypyrrole[22]. Another

method of growing the polymer used an aqueous solution of pyrrole and copper sulphate in a one compartment cell[23]. The conductivity for this polypyrrole film was about 100 S cm^{-1}. Street *et al*[24] grew polypyrrole film in a dry box using carefully dried and deoxygenated acetonitrile to make the $AgClO_4$ and pyrrole solution. They reported that extremely smooth films with high coulombic efficiency were obtained. A lot of work has been done to reveal the mechanism of the electrochemical polymerization of pyrrole. The radical-cation coupling mechanism[25] shown in Fig.1.2.1 is now widely accepted[26]. Pyrrole is initially oxidized at the anode to form an unstable radical cation which then reacts with another radical cation to form a pyrrole dimer after loss of two protons. This dimer can further react with more radicals to form a growing polymer chain. Eventually the chain becomes too inactive or sterically inhibited, or growth is quenched by some inert species.

1.2.2 The Structure of Polypyrrole

It is believed that the pyrrole units are linked through the 2-2' positions, based on the experimental evidence that, predominantly, the 2,5- dicarboxylic acid was obtained after oxidation of polypyrrole powder with $KMnO_4$[27]. The degree of polymerization is believed to be greater than ten[26]. An interesting experiment was conducted by Street and coworkers[28]. They used 2,5-tritiated 3,4- dimethyl-

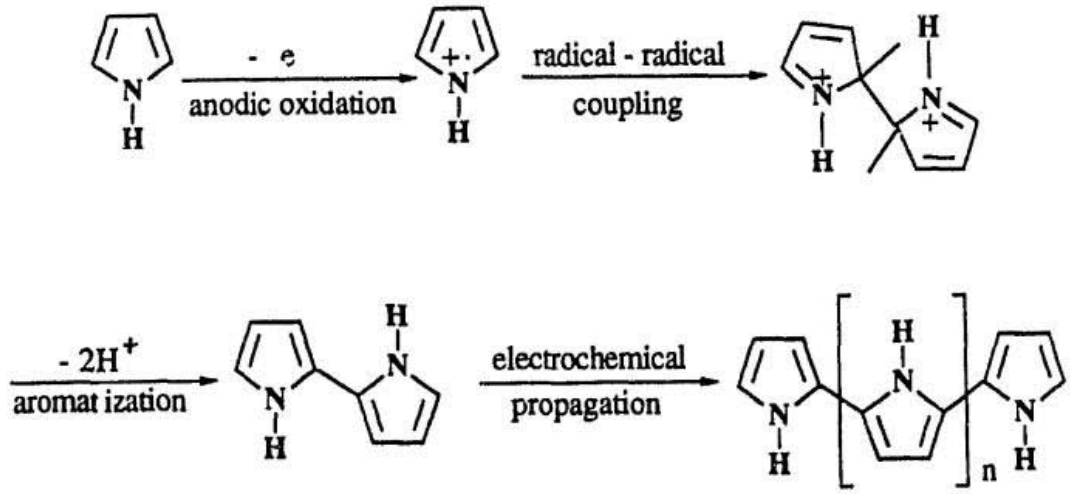

Figure 1.2.1. Proposed mechanism for polypyrrole formation by oxidative electropolymerization.

pyrrole monomers to determine the chain length by radiochemical techniques. Once the pyrrole rings were linked at the 2,5 positions, there could be no tritium atoms in the chain except at the ends. Average chain lengths of 100 to 1000 pyrrole units were calculated, depending on conditions, by comparing the radioactivity of the final polymer and that of the monomer.

Along the chain, the pyrrole rings are arranged in a planar manner. *Ab initio* calculations[29] on polypyrrole show that a linear, completely planar and alternately orientated structure (as shown in Figure 1.2.1) has the lowest energy. This structure leads to electron delocalization on a large conjugated chain[30] and is believed to greatly affect the conductivity of the polymer.

Oxidized polypyrrole is a cationic polymer because every third or forth pyrrole rings carry a positive charge. These positive sites are compensated for by incorporation of anions into the film. Recent research shows that the role of the anion in the film remains one of the key questions in polypyrrole chemistry[31].

1.2.3 Electrochemistry of Polypyrrole

An important electrochemical property of polypyrrole is its ability to undergo electrochemical switching. Polypyrrole can be electrochemically switched between conducting and insulating states at different applied potentials. Switching is fast and electrochemically reversible. A 10 micron thick film in acetonitrile

takes approximately 30 seconds to complete the transition from the conducting to the insulating state when the potential is changed from +2 to -2 volts[32]. For a thin film (*e.g.* 0.2 micron), the switching is accompanied by a colour change which has led to many electrophotometric investigations of this polymer[33,34].

Cyclic voltammetry has been widely employed to explore the electrochemistry of polypyrrole. Fig.1.2.2 shows typical cyclic voltammograms of polypyrrole in 0.1 M Et_4NClO_4/acetonitrile solution. The film starts to be oxidized at about -0.3 V [*vs.* sodium chloride saturated calomel electrode (SSCE) unless indicated otherwise] with insertion of the anion ClO_4^-. The current peaks at about -0.1 V show that the polypyrrole is electroactive and is able to undergo a redox reaction. A larger capacitive current appearing after the peak is perhaps due to the increased effective area of the polymer. Feldberg[35] has treated the total current as a mixture of faradaic current and a capacitive current. It is not possible to separate these currents without additional physical-chemical information. Recently, this interpretation has been questioned[36] due to the unusually high capacitance of the polymer coating. The value of E_{FWHM} (Full Width at Half Maximum) for the broad anodic peaks, especially at higher scan rates, are clearly a lot higher than the theoretical value of 90.6 mV for a one electron transfer reaction[37]. However, they are difficult to measure accurately due to the large background currents. The reasons for non-ideal behaviour could be that different

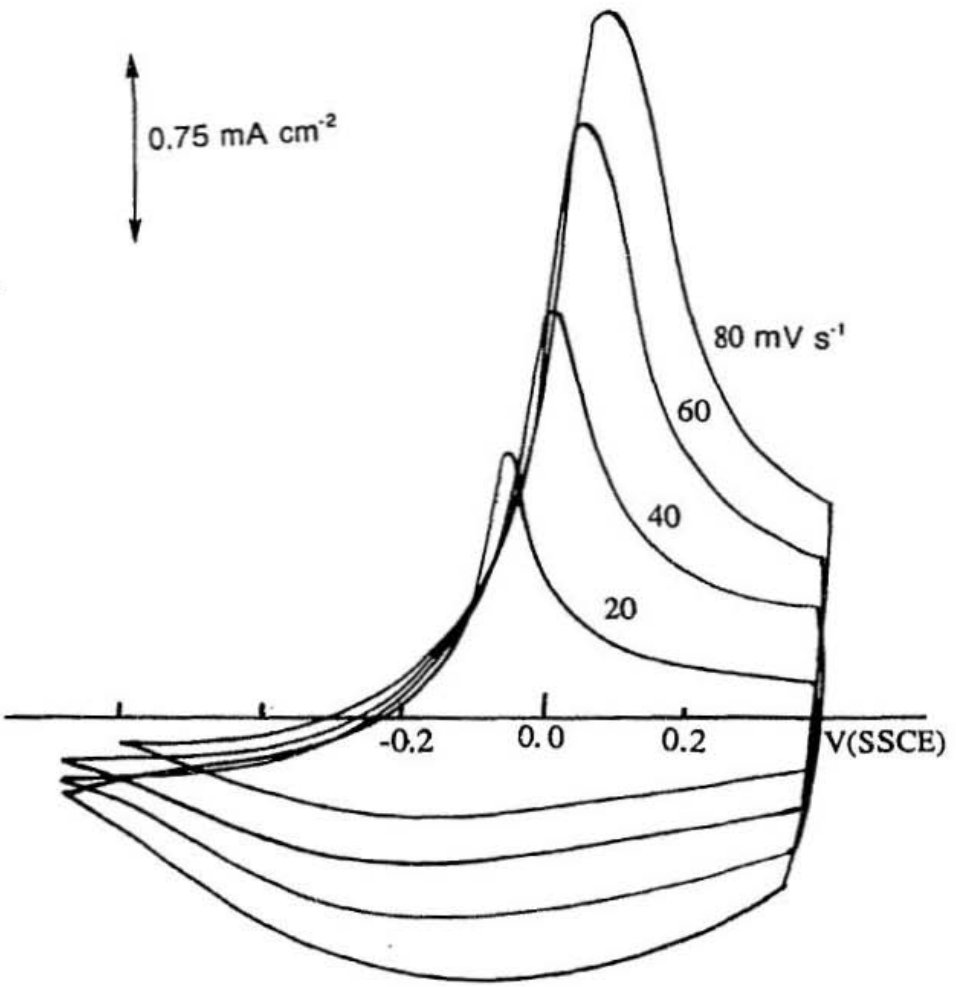

Figure 1.2.2. Cyclic voltammograms of polypyrrole (0.6 μm thick) in 0.1 M Et_4NClO_4/CH_3CN solution. Scan rates were 20,40,60 and 80 mV s^{-1}.

sites in the film have different formal potentials because of the interactions between sites.

An expected feature of the voltammograms is that the peak current (i_p) is proportional to the scan rate (v) rather than to the square root of scan rate. This indicates that the redox centres are fixed in the film and therefore the total amount of charge required to change the oxidation state of the film is independent of scan rate. This relation only holds when the scan rate is slow enough (10 - 200 mV/s) and the kinetics of the charge transfer are fast enough to complete oxidation and reduction within each scan cycle. The value of i_p reverts to a normal square root relation with respect to v if the scan rate is high or the rate of charge transfer is so slow that the process becomes diffusive. The square root relation has been seen by decreasing the temperature to -70 °C, where the rate of charge transfer is greatly reduced[38].

1.2.4 Electrocatalysis at Polypyrrole Electrodes

Electrocatalysis is also an important property of polypyrrole. Ewing[39] compared the behaviour of a polypyrrole coated carbon electrode with that of a bare electrode for the oxidation of ascorbic acid, dihydroxyphenylacetic acid and dopamine. It was found that the ascorbic acid oxidation occurs at potentials which are 300 mV more negative than at the bare electrode and that the rising slope of

the rotating disc voltammogram decreased by over 100 mV, indicating that the reversibility of the reaction is increased. Similar enhanced electrochemical reversibility was also observed for dihydroxyphenylacetic acid and dopamine. The mechanism is assumed to involve some electrostatic interactions between the anionic solutes and cationic fixed sites in the oxidized polypyrrole.

For polypyrrole, electrocatalysts can be easily incorporated in the film to form a built-in catalyst[26,40]. The electrocatalysts are usually anions which can be incorporated during the electrochemical polymerization. An example is polypyrrole incorporating tetrasulfonated iron phthalocyanine which was employed as a catalyst in the reduction of O_2[41]. The reduction potential, using this polypyrrole, is 0.2-0.8 V less negative than that at a bare glassy carbon electrode. Selectivity for the reduction of O_2 to water over that to hydrogen peroxide is remarkably enhanced compared to the reduction at a bare electrode[42].

Another way of introducing the catalyst is *via* some functional group on the polypyrrole ring which binds the electrocatalyst[43]. One can attach almost any functional group to polypyrrole. For example, N-substituted redox-active groups have potential catalytic activity, and a great many papers have been published on incorporation *via* N-substituted polypyrrole. There are polypyridyl complexes of ruthenium(II)[44,45], iron(II),[46] and many other metal ions and porphyrins[47,48] with their metallated complexes including cobalt, nickel and manganese[49] and so on.

1.2.5 Applications of Polypyrrole

The applications of polypyrrole have been a subject of much research. Potential applications are mainly in areas related to electrical materials, batteries, catalysis, display devices, and analysis.

The mechanical and electrical properties of polypyrrole have been examined for applications as an electrical material in mind. For example, a 0.1 mm thick film made electrochemically on a 10 x 10 cm electrode had a tensile strength of about 3000 psi and a Young's modulus of 1 x 10^5 psi[50]. The tensile strength and the Young's modulus were increased by 33% when the film was dried in a vacuum. The mechanical properties can be improved by growth, at elevated temperatures, from tetrabutylammonium hexafluoroarsenate solutions in dimethylsulfate[51]. With such mechanical strength, polypyrrole has obvious uses as a new conductive plastic in electrical systems.

Polypyrrole has been used in analytical chemistry. Miasik[52] *et al* made a gas sensor with a polypyrrole coated electrode based on the observation that the conductivity of polypyrrole decreases when exposed to NH_3 and increases in NO_2 and H_2S. The concentration of the above gases can be closely monitored. An electrochemical detector system was produced by using a polypyrrole coated Pt electrode for flow injection analysis[53]. The detector response is based on the repetitive doping-undoping of polypyrrole. A linear relation was obtained between

the electrode response and the concentrations of phosphate and carbonate over 3 orders of magnitude. The electrode was stable for two weeks. In another application, polypyrrole, which was electrochemically deposited on vitreous carbon particles from a KCl solution, served as a chromatographic stationary phase[54]. The polypyrrole functions as a reversed phase and shows characteristics of an anion exchange resin.

Although polypyrrole has been playing an important role among the conducting polymers, its electrochemical functions are limited and the study of its properties is still far from completed. The introduction of functional groups onto the polypyrrole ring appears to extend the functions of polypyrrole, but new methods are needed to investigate the properties of polypyrrole and the new polypyrrole based polymers. This work is devoted to synthesis and electrochemical study of new polypyrrole based conducting polymers with cation substituents.

1.2.6 Polypyrrole with Cationic Substituents

As described earlier, the applications of polypyrrole are limited by the lack of electrochemical functions. For example, the extent of incorporation of catalytic species by ion exchange into a pre-formed polypyrrole is very limited. The ion exchange capacity of the polypyrrole varies with potential and vanishes when

polypyrrole is reduced. The maximum capacity is restricted to one negative charge per three pyrrole rings[55]. Furthermore, bulky anions such as ferrocyanide, or porphyrins, cannot be incorporated. Considering the ion exchange properties, a very popular anion exchange system, quaternized polyvinylpyridine (QPVP), should be mentioned. This system has shown excellent ion exchange properties for incorporating various metal complexes and numerous studies have been conducted on electrodes modified with QPVP[56,57,58]. However, QPVP has some drawbacks in that it cannot be prepared electrochemically and it is not an electronic conductor. The superior ion exchange properties of QPVP and high electronic conductivity of polypyrrole can be combined by using substituted polypyrroles. The anion exchange properties have been greatly improved by linking cation (alkylammonium or pyridinium) containing groups to the pyrrole skeleton[59,60,61]. Also, other properties such as ionic conductivity, permeability, and catalytic properties are improved in the substituted polymers.

With the intention of extending the functions of polypyrrole in mind, four polypyrrole based cationic polymers have been synthesised and studied in this work. They are polymers of protonated 3-(pyrrol-1-ylmethyl)pyridine, (poly-HPMP$^+$), 1-methyl-3-(pyrrol-1-ylmethyl)pyridinium tetrafluoroborate, (poly-MPMP$^+BF_4^-$), 1-(3-[pyrrol-3-yl]propyl)pyridinium tetrafluoroborate, (poly-

PPP$^+BF_4^-$), and (3-[pyrrol-3-yl]propyl)trimethylammonium tetrafluoroborate, (poly-PPTA$^+BF_4^-$) (structures are shown in Fig.3.1.1). These polymers possess the electronically conducting polypyrrole chain and a high concentration of positively charged sites. Hence, they are electronically and ionically conductive. Similar polypyrrole based cationic polymers have been reported recently[59,60,61] and have shown excellent ion exchange properties for the incorporation of ferrocyanide, oxometallates and the cluster $[Fe_4S_4(SPh)_4]^{2-}$. These reports have demonstrated that the alkylammonium and pyridinium containing polypyrrole based polymers have formed a new class of electronically conducting anion exchange polymers.

The polymers synthesised in this work have shown high electronic and ionic conductivity, and excellent ion exchange properties. Also they have proven to be excellent for the electrostatic binding of metal complexes, and in the electrocatalysis of ascorbic acid. Some of this work has already been published[62,63,64,65].

References

1. P. R. Moses, L. M. Wier and R.W. Murray. Anal. Chem., 47 (1975) 1882.

2. C. M. Elliott and C. A. Marrese, J. Electroanal. Chem., 119 (1981) 395.

3. J. R. Lenhard and R. W. Murray, J. Electroanal. Chem., 78 (1977) 195.

4. R. W. Murray in A.J. Bard (Ed.), Electroanalytical Chemistry, Vol. 13, M. Dekker, New York, 1984, p. 236.

5. A. R. Hillman, in R. G. Linford (Ed.), Electrochemical Science and Technology of Polymers 1, Elsevier Applied Science, London and New York, 1987, P.241.

6. R. W. Murray, A. G. Ewing and R.A. Durst, Anal. Chem., 59 (1987) 382A.

7. R. W. Murray, Annu. Rev. Mater. Sci. 14 (1984) 145.

8. R. W. Murray in A.J. Bard (Ed.), Electroanalytical Chemistry, Vol. 13, M. Dekker, New York, 1984, p. 297.

9. L. L. Miller and M. R. Van de Mark, J. Am. Chem. Soc., 100 (1978) 639 and 3223.

10. N. Oyama and F.C. Anson, J. Am. Chem. Soc., 101 (1979) 739.

11. H.D. Abruna, P. Denisevich, M. Umana, T. J. Meyer and R. W. Murray, J. Am. Chem. Soc., 103 (1981) 1.

12. T. Ikeda, C.R. Leidner and R.W. Murray, J. Am. Chem. Soc., 103 (1981) 7422.

13. C.E.D. Chidsey and R.W. Murray, Science, 231 (1986) 25.

14. B. J. Feldman, A.E. Ewing and R. W. Murray, J. Electroanal. Chem., 194 (1985) 63.

15. P. G. Pickup, W. Kutner, C. R. Leidner and R. W. Murray, J. Am. Chem. Soc., 106 (1984) 1991.

16. L. D. Margerum, T. J. Meyer and R. W. Murray, J. Electroanal. Chem., 149 (1983) 279.

17. N. Oyama and F. C. Anson, J. Electrochem. Soc., 127 (1980) 247 and 249.

18. A. Angeli, Gazz. Chim. Ital., 46,II (1916) 279 and 283.

19. A. Dall'Olio, C.R. Hebd. Sciences Acad. Sci., Ser. C, 267 (1969) 433.

20. A. F. Diaz, K. K. Kanazawa, and G. P. Gardine, J. Chem. Soc., Chem. Commun., (1979) 635.

21. M. Salmon, A. F. Diaz, A. J. Logan, M. Krounbi, and J. Bargon, Mol. Cryst. Liq. Cryst., 83 (1982) 265.

22. A. F. Diaz and B. Hall, IBM J. Res. Dev., 27 (1983) 342.

23. T. A. Skothein (Ed), Handbook of Conducting Polymers, Marcel Dekker, New York, 1986, p.268.

24. G. B. Street, T. C. Clarke, M. Krounbi, K. K. Kanazawa, V. Lee, P. Pfluger, J. C. Scott, and G. Weiser, Mol. Cryst. Liq. Cryst., 83 (1982) 253.

25. A. F. Diaz and K.K.Kanazawa, in J.S. Miller (Ed.), Extended Linear Chain Compounds, Vol.3, 1982, P.417.

26. E. Barendrecht, J. Applied Electrochemistry, 20 (1990) 175.

27. G. P. Gardini, Adv. Heterocyclic Chem., 15 (1973) 67.

28. A. Nazzal and G. B. Street, J. Chem. Soc. Chem. Commun., (1984) 83.

29. H. Mao, unpublished results, 1988

30. K. Yakushi, L. J. Lauchlan, T.C. Clark and G.B.Street, J. Chem. Phys., 79 (1983) 4774.

31. G. K. Chandler and D. Pletcher, Spec. Period, Rep. Chem. Soc. Electrochem., 10 (1985) 117.

32. A. F. Diaz, J. I. Castillo, J. A. Logan and W-Y. Lee, J. Electroanal. Chem., 129 (1981) 115.

33. E. M. Genies and J. M. Pernaut, Synthetic Metals, 10 (1984/85) 117.

34. E. M. Genies G. Bidan and A. F. Diaz, J. Electroanal. Chem., 149 (1983) 101.

35. S. W. Feldberg, J. Am. Chem. Soc., 106 (1984) 4671.

36. R. Greef, M. Kalaji and L. M. Peter, Faraday Discuss. Chem. Soc., 88 (1988) 277.

37. A. P. Brown and F. C. Anson, Anal. Chem., 49 (1977) 1589.

38. P. Daum, J. R. Lenhard, D. Rolison, and R. W. Murray, J. Am. Chem. Soc., 102 (1980) 4649.

39. R. A. Saraceno. J. Pack and A. G. Ewing, J. Electroanal. Chem., 197 (1986) 265.

40. W-H Kao and T. Kuwana, J. Am. Chem. Soc. 106 (1984) 473.

41. R. A. Bull, F.R. Fan, and A. J. Bard, J. Electrochem. Soc., 130 (1983) 1636.

42. R. C. M. Jakobs, L. J. J. Janssen and E. Barendrecht, Electrochim. Acta, 30 (1985) 1433.

43. A. Deronzier and J-C. Moutet, Acc. Chem. Res., 22 (1989) 249.

44. J. Ochmanska and P.G.Pickup, J. Electroanal. Chem., 271 (1989) 83.

45. S. Cosnier, A. Deronzier and J-C. Moutet, J. Electroanal. Chem., 193 (1985) 193.

46. J. G. Eaves, H.S. Munro and D. Parker, Inorg. Chem., 26 (1987) 644.

47. O. Ikeda, K. Okabayashi, N. Yoshida and H. Tamura, J. Electroanal. Chem, 191 (1985) 157.

48. A. Bettelheim, B. A. White, S. A. Raybuck and R. W. Murray, Inorg. Chem., 26 (1987) 1009.

49. F. Bedioui, A. Merino, J. Devynck and C. E. Bied-Charreton, J. Electroanal. Chem., 239 (1988) 433.

50. G.B. Street, S.E. Lindsey, A. I. Nazzai and K.J. Wynne, Mol. Cryst. Liq. Cryst. 118 (1985) 137.

51. S. Hotta , T. Hosaka , and W. Shimotsuma, Synth. Met., 6 (1983) 319.

52. I. Miasik, A. Hooper and B. C. Tofield, J. Chem. Soc. Faraday Trans. 1, 82 (1986) 1117.

53. Y. Ikariyama and W. R. Heineman, Anal. Chem., 58 (1986) 1803.

54. G. Hailin and G. G. Wallace, Anal. Chem., 61 (1989) 198.

55. K. K. Kanazawa, A. F. Diaz, W. D. Gill, P. Grant, G. B. Street, G. P. Gardini and J. K. Kwak, Synth. Met., 1 (1979/80) 329.

56. N. Oyama, T. Shimomura, K. Shigehara, and F. C. Anson, J. Electroanal. Chem., 112 (1980) 271.

57. S. M. Oh and L. R. Faulkner, J. Electroanal. Chem., 269 (1989) 77.

58. A. R. Hillman, in R. G. Linford (Ed.), Electrochemical Science and Technology of Polymers 1, Elsevier Applied Science, London and New York, 1987, P.103.

59. J-C. Moutet and C. J. Pickett, J. Chem. Soc., Chem. Commun., (1989) 188.

60. S. Cosnier, A. Deronzier, J-C. Moutet and J. F. Roland, J. Electroanal. Chem., 271 (1989) 69.

61. B. Keita, D. Bouaziz, L. Nadjo, A. Deronzier, J. Electroanal. Chem., 279 (1990) 187.

62. H. Mao and P. G. Pickup, J. Am. Chem. Soc., 112 (1990) 1776.

63. H. Mao and P. G. Pickup, J. Phys. Chem., 93 (1989) 6480.

64. H. Mao, J. Ochmanska, C. D. Paulse and P.G. Pickup, Faraday Discuss. Chem. Soc., 88 (1989) 163.

65. H. Mao and P. G. Pickup, J. Electroanal. Chem., 265 (1989) 127.

Chapter 2

Experimental

2.1. Synthesis of Monomers

2.1.1 Synthesis of 1-methyl-3-(pyrrol-1-ylmethyl)pyridinium tetrafluoroborate ($MPMPBF_4$)

The reaction for preparation of $MPMPBF_4$ is shown in Scheme 1.

Scheme 1

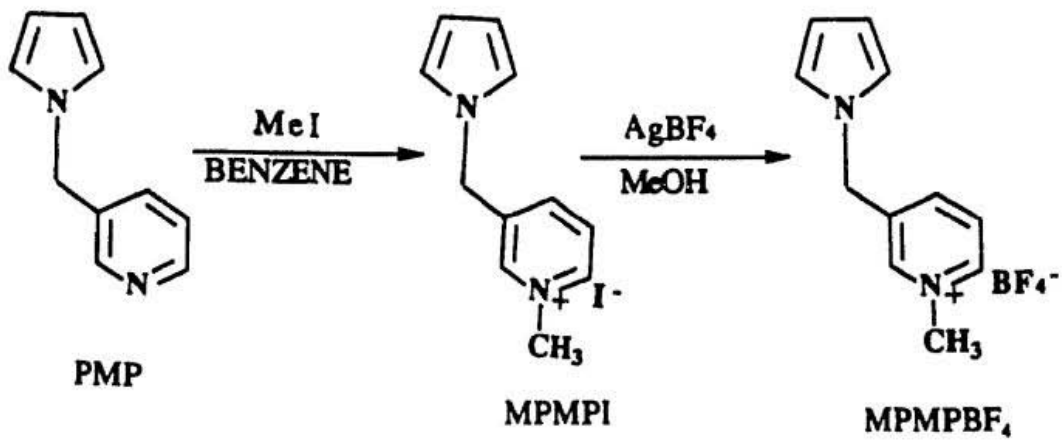

3-(pyrrol-1-ylmethyl)pyridine (PMP, Aldrich) was purified on an aluminium oxide/acetonitrile column followed by recrystallization from acetonitrile.

PMP (5.1 g, 0.032 mol) was dissolved in about 10 ml (minimum amount) of benzene in a round bottom flask and CH_3I (10.5 g, 0.064 mol) was slowly added at room temperature. After mixing, the solution was swirled until a white precipitate appeared. The mixture was kept at room temperature overnight to complete the reaction. After washing with benzene and recrystallizing from acetonitrile, 1-methyl-3-(pyrrol-1-ylmethyl)pyridinium iodide (MPMPI), a pale yellow powder was obtained. The yield for this process was 90%.

For the second step in Scheme 1, iodide was replaced by tetrafluoroborate *via* precipitation. Stoichiometric quantities of silver tetrafluoroborate and MPMPI were separately dissolved in methanol (20 ml per gram of solid). The $AgBF_4$ solution was added dropwise to the MPMPI solution with vigorous stirring. The yellow AgI precipitate appeared immediately and was removed by filtration. A 92% yield of $MPMPBF_4$ was obtained after recrystallization from methanol. The product was characterized with high resolution mass spectroscopy (by fast atom bombardment) and ^1H NMR spectroscopy. MS: m/z = 173.08. ^1H NMR in D_2O: δ = 4.19(s.3H), 5.26(s.2H), 6.15(t.2H), 6.75(t.2H), 8.05(t.1H), 8.24(t.2H), 8.50(t.1H).

2.1.2 Synthesis of (pyrrol-3-ylmethyl)dimethylamine (PMDMA)

The three steps shown in Scheme 2 for the preparation of PMDMA were

based on literature methods[1,2].

Scheme 2

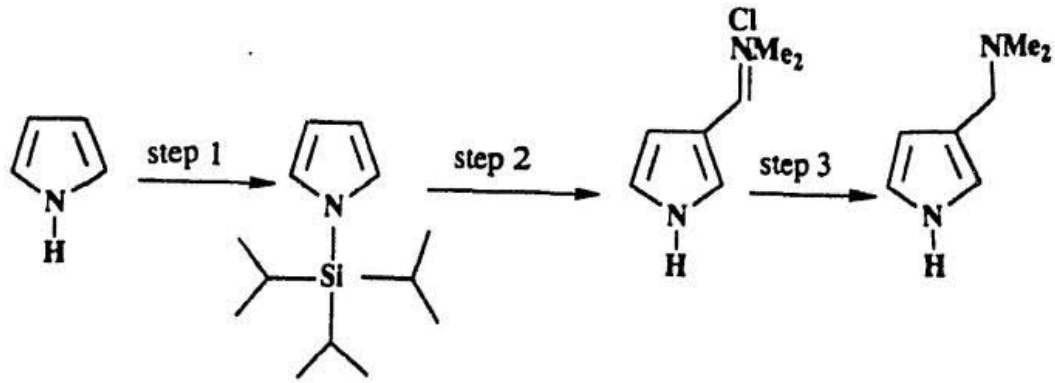

Step 1: N-triisopropylsilylpyrrole (TISP) In order to substitute at the 2-position of the pyrrole ring, the alpha position is protected by introducing a bulky triisopropylsilyl group at the nitrogen[1]. These reactions are shown in Scheme 3:

Scheme 3

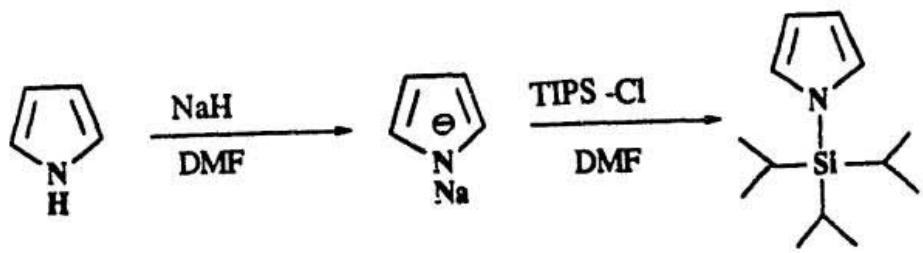

TISP

4.0 g of NaH in mineral oil (60%, Aldrich) was thoroughly washed with hexane. About 200 ml of dried (molecular sieves) dimethyl-formamide (DMF, Aldrich) was added to the resulting fine grey powder of NaH (~ 100 mmol). 6

ml (5.8 g, 86 mmol) of pyrrole (purified through an aluminium oxide column) was added rapidly to the reaction flask while stirring, under a nitrogen flow. Hydrogen evolution occurred during the reaction. When the hydrogen bubbling ceased, 16g of triisopropylsilylchloride (TIPSCl, Aldrich) was added dropwise at 0 °C. Upon finishing the addition of TIPSCl, the temperature was allowed to rise to room temperature and stirring was maintained for one hour. Then the reaction mixture was poured into 200 ml of 10% $NaHCO_3$ and the product was extracted with ether. The crude product (16.6 g, yield 86%) was then vacuum distilled twice at 67 °C and 3 mmHg to provide pure TISP: ^1H NMR ($CDCl_3$) δ = 1.10(d.18H); 1.45(heptad,3H); 6.12(s.1H); 6.25(s.1H); 6.72(d.2H); MS: m/z= 223.13.

Step 2: N,N-dimethylpyrrole-3-formiminium Chloride (NDPF) Scheme 2 illustrates this step[2]. 2.94 g (40 mmol) of DMF was added to a stirred solution of oxalyl chloride (18.4 ml, 2M, 36.8 mmol) in 100 ml dichloromethane at 0 °C. After 20 minutes, 7.75 g (34.7 mmol) TISP in 15 ml of dichloromethane was added rapidly; solid immediately appeared. The reaction flask was immersed in an oil bath to increase the temperature to 60 °C. The solid dissolved and, then, another solid formed. At this temperature, the mixture was refluxed for 30 minutes in order to complete the reaction. The reaction mixture was cooled to 0

°C, and more precipitate formed. The product was collected by filtration under nitrogen, washed 5 times with ether, and then dried *in vacuo*. The product (4.97 g, 31.6 mmol, 91% yield) consisted of white crystals: MS, m/z = 123.04.

Step 3: (Pyrrol-3-ylmethyl)dimethylamine (PMDM) The purified NDPF (4.97 g, 31.6 mmol) from Step 2 was reduced with $NaBH_3CN$ as shown in Scheme 2. A solution of 3.2 g N,N-dimethylpyrrole-3-formiminium chloride in 20 ml methanol was added to a solution of 1.3 g $NaBH_3CN$ in 100 ml methanol with stirring at room temperature. The reaction was allowed to proceed overnight, and then stopped by adding *ca.* 100 ml 10% $NaHCO_3$ aqueous solution to the reaction flask. Then this mixture was extracted with ether three times. A 60% yield of a white powder was obtained. NMR: 2.26 (s.6H);3.40 (s.2H);6.18(d.1H);6.65 (s.1H);6.70 (d.1H). ^{13}CNMR: 45 (s.2xMe); 57(s.CH_2); 110(s.βC); 117(d. 2xαC) and all the C-H correlations are correct.MS: m/z = 124.00

2.1.3 Synthesis of 3-(3-Bromopropyl)pyrrole (BPP)

The synthesis of 3-(3-Bromopropyl)pyrrole (BPP) was based on literature methods[3,4,5] with some modifications. The reactions for BPP are shown as in Scheme 4:

Scheme 4

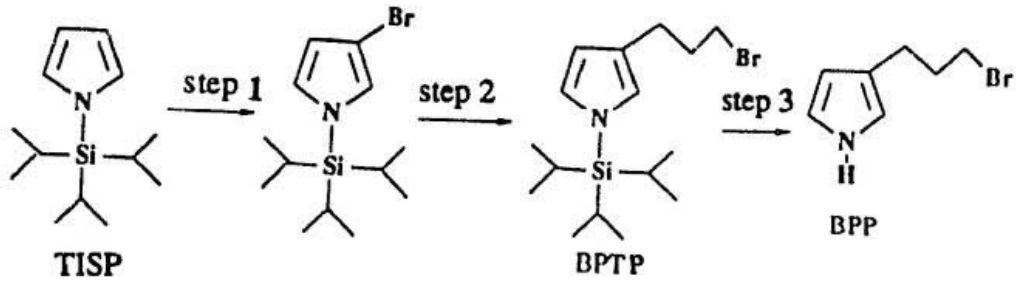

Step 1: 3-Bromo-1-triisopropyl)pyrrole (BTP) The literature method for preparing BTP[5] was modified for our use. Our method is significantly simpler, and a higher yield was obtained. Instead of adding N-bromosuccinimide (NBS) solution dropwise, the NBS powder (9.7 g,0.055 mol) was directly added into precooled (-78°C) N-triisopropylsilyl-pyrrole (11.1 g 0.05 mol) in 150 ml THF solution. The reaction flask was kept in the dark to avoid the decomposition of NBS by light. The photo decomposition of NBS in THF is significant at room temperature (as can be seen from the quick coloration of the solution) but insignificant at -78°C. This decomposition leads to a lower yield of BTP and adds to difficulties with purification. After addition of NBS, the mixture was stirred overnight in an acetone/dry ice bath. The temperature gradually raised to ambient temperature upon the vaporization of the dry ice. The solvent was removed by vacuum evaporation until a precipitate appeared. Then, dry CCl_4 was added, and the whole mixture was stored in a freezer for a few hours to complete the precipitation of succinimide. The mixture was filtered and the filter cake was

washed three times with additional carbon tetrachloride. After removing the solvent *in vacuo*, a light tea coloured oil was obtained. The reaction is shown in Scheme 5.

Scheme 5

TISP BTP

After purification through a silica gel column, the final product of BTP was a colourless oil (2.8 g, 92.4%). NMR ($CDCl_3$) δ = 1.10(d.18H); 1.45(heptad, 3H); 6.22(s.1H); 6.61(s.1H); 6.702(s.1H); MS:m/z = 300.99 and 303.00.

Step 2: 3-(3-Bromopropyl)-1-(triisopropyl)pyrrole (BPTP) from BTP

The reactions for making BPTP are shown in Scheme 6. The steps were carried out in one pot[5].

n-Butyllithium in hexane (8.5 ml, 2M, Aldrich) was added dropwise to a solution of 2.8 g BTP in 100 ml of freshly distilled THF at -23 °C (CCl_4/dry ice bath). After 2 hours of stirring in the dark, 3-lithio-1-(triisopropylsilyl)pyrrole had

Scheme 6

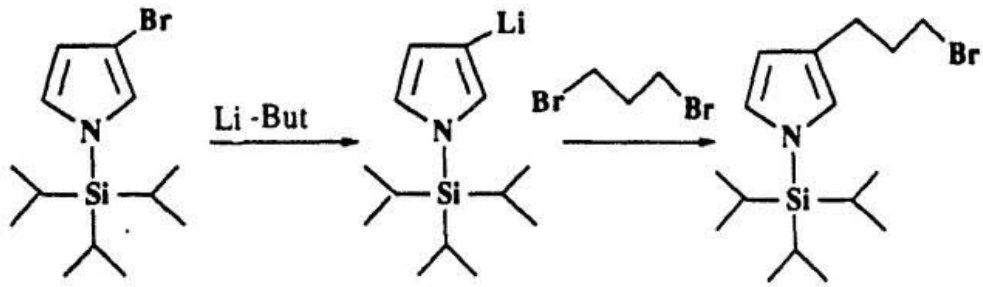

BTP BPT P

formed; then 3.5 ml 1,3-dibromopropane (Aldrich) in 50 ml of THF was added dropwise. The reaction mixture was allowed to warm to room temperature for about 40 minutes in the dark. The mixture was then poured into 20 ml water and extracted with ether three times. The combined organic phase was dried with anhydrous Na_2SO_4. A colourless oil was obtained after removal of solvents under reduced pressure. The excess dibromo-propane was removed by vacuum distillation at about 30 °C and 10 mmHg. Other impurities were removed through a silica gel column with ACS grade hexane. The yield was 61%.

Step 3: 3-(3-Bromopropyl)pyrrole (BPP) The reaction is shown in Scheme 7[4]. A solution of 0.47 g (1.4 mmol) BPTP in 15 ml ether was placed in a 50 ml separating funnel. To this solution, 1.5 ml tetraethylammonium fluoride (Et_4NF, 1 M in THF, <5% water, Aldrich) was added with the ratio at Et_4NF:BPTP = 1.1:1. The mixture was vigorouslyshaken for 5 minutes; then the non-aqueous

Scheme 7

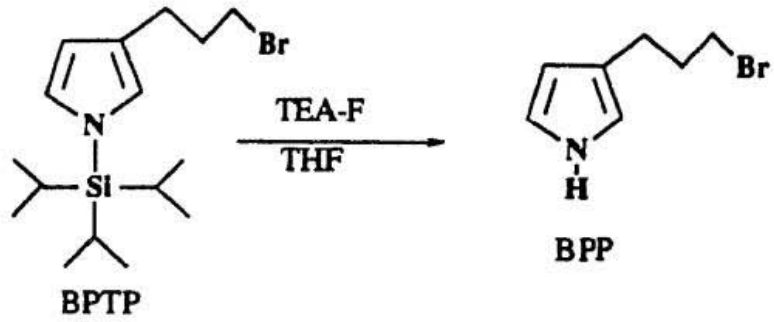

BPTP BPP

phase was washed four times with water (5 ml each). The ether was then removed at reduced pressure. After purification through a silica gel column with 10% acetone in hexane, 0.26 g product (BPP) was obtained (98% yield): NMR ($CDCl_3$): δ = 2.15 (pent. 2H); 2.65 (t. 2H); 3.45 (t. 2H); 6.10 (s.1H); 6.62 (s.1H); 6.73 (s.1H).

2.1.4 Synthesis of 1-(3-[pyrrol-3-yl]propyl)pyridinium tetrafluoroborate ($PPPBF_4$)

Scheme 8 shows the reaction:

Scheme 8

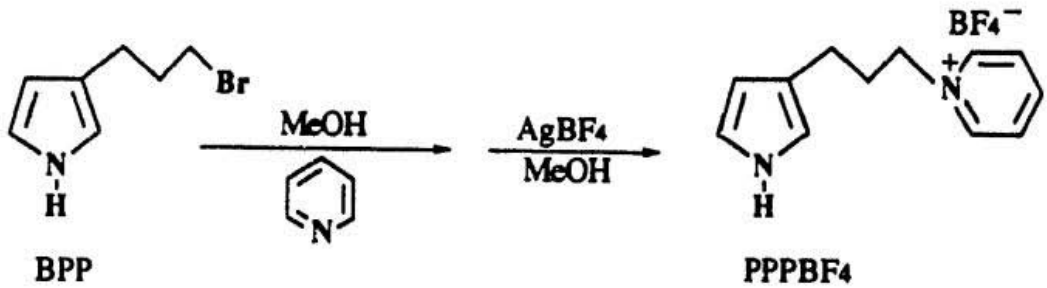

BPP PPPBF4

A solution of 3-(3-bromopropyl)pyrrole (0.21 g, 1.2 mmol) and pyridine (1 g, 13 mmol) in methanol was stirred overnight in the dark. The methanol was removed under reduced pressure and excess pyridine was eliminated by washing the residue with hexane (the PPPBr salt is insoluble in hexane). This salt was then dissolved in methanol and one equivalent of silver tetrafluoroborate in methanol was added to precipitate AgBr. The product ($PPPBF_4$) was recrystallized from methanol, and the yield was 80%. NMR (CD_3OD): δ = 2.15 (pent. 2H); 2.61 (t. 2H); 4.66(t.2H); 5.92(s.1H); 6.55(s.1H); 6.62(s.1H); MS: m/z = 186.99.

2.1.5 Synthesis of (3-[pyrrol-3-yl]propyl)trimethylammonium tetrafluoroborate ($PPTABF_4$)

Trimethylamine was prepared from trimethylamine hydrochloride (Aldrich) by reacting it with NaOH. The trimethylamine gas was condensed at -78°C after drying through a $CaCl_2$ column. The cold liquid trimethylamine was quantitatively dissolved in methanol at room temperature and used immediately.

3-(3-Bromopropyl)pyrrole (0.26 g, 1.5 mmol) was mixed with 5 equivalents of trimethylamine in methanol with stirring in a sealed container at room temperature overnight. The reaction is shown in Scheme 9. The methanol and trimethylamine were removed under reduced pressure leaving a white powder of PPTABr (0.24 g, 76%, b.p. 166 - 167°C). The NMR spectrum (same as $PPTABF_4$

Scheme 9

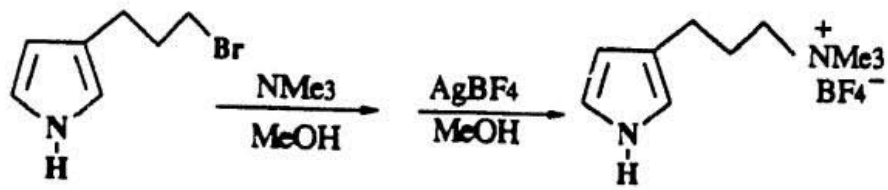

BPP PPTABF$_4$

below) supported the structure.

The PPTABr was converted to the PPTABF$_4$ salt in the same way as described in Section 2.1.4. The NMR and mass spectra for PPTABF$_4$ are as follows: NMR: (CD_3OD) δ = 2.04(pent.2H); 2.58(t.2H); 3.30(t.2H); 6.01(s.1H); 6.60(s.1H); 6.68(s.1H); MS: m/z =167.07.

2.1.6 Equipment for synthesis

A Hewlett Packard 5890A GC-MS was extensively used to determine the purity and structure for the synthesized compounds. A Varian Model 3700 GC and Varian 5000 HPLC were used for the same purposes. Three kinds of NMR spectrometers were used. They are Varian EM-360 (60 MHz), Bruker WP80F (80 MHz) and General Electric GN NB-300 (300 MHz). A Perkin-Elmer 283 IR and high resolution VG Micromass 7070 HS mass spectrometer were also used.

2.2. Equipment for Electrochemical Experiments

2.2.1 Electrodes

An aqueous sodium chloride saturated calomel electrode (SSCE, Fisher) was used as reference electrode for all work and potentials quoted in this thesis are on the SSCE scale. Platinum wire counter electrodes were used in all electrochemical experiments. The following working electrodes were used:

1. Platinum disc: These were made by sealing a piece of 0.75 mm diameter platinum wire in a soft glass tube with a Bunsen flame. The end was subsequently polished, first with sand paper, and then by 0.3 micron alumina. The geometric area was 0.0045 cm^2. The majority of the cyclic voltammetry experiments were carried out with this small disc electrode.

2. Rotating Pt disc electrode: This was manufactured by Pine Instruments. The 0.458 cm^2 platinum disc was sealed in PTFE.

3. Pt flag electrode: A thin Pt wire (0.1 mm in diameter) was spot welded onto a 0.5 cm x 1.88 cm, 0.1 mm thick Pt foil. The total geometric area (both sides) was 1.88 cm^2. This electrode was used for the gravimetry and I^- partition coefficient determinations.

4. Dual electrode: This electrode was made by sealing two identical Pt wires (0.1 mm diameter) in soft glass. The end was polished (as for the platinum

disc electrode) to a mirror finish.

5. Indium/tin oxide coated glass plate electrodes (NESATRON glass, 20 ohm/sq. PPG Industries Inc.) were used, both to determine the film thickness by scanning electron microscopy and to the prepare large area films for elemental analysis. The electrical connection was made by a piece of copper foil.

6. An iodide-selective electrode[6] was made to determine the concentration of I^- for the partition coefficient measurements. This electrode was made by first dipping a well polished silver strip into a melted mixture of KI and $AgNO_3$ (1:1 mol) at about 400 °C and then quickly pulling it out in order to evenly coat it with a thin layer of AgI. This electrode was calibrated in standard I^- solutions before use.

2.2.2 Electrochemical Cells

Two kinds of conventional three compartment glass cells were used. One was for small disc electrode measurements (Figure 2.2.1). The volume of solution could vary from 2 to 10 ml. Argon was introduced with small plastic tubing parallel to the working electrode to remove oxygen from the electrolyte solution. Figure 2.2.2 shows a typical cell for the rotating disc electrode experiments. The reference electrode was connected through a tube with a tip pointed towards the working electrode to reduce the uncompensated resistance. This cell contained a

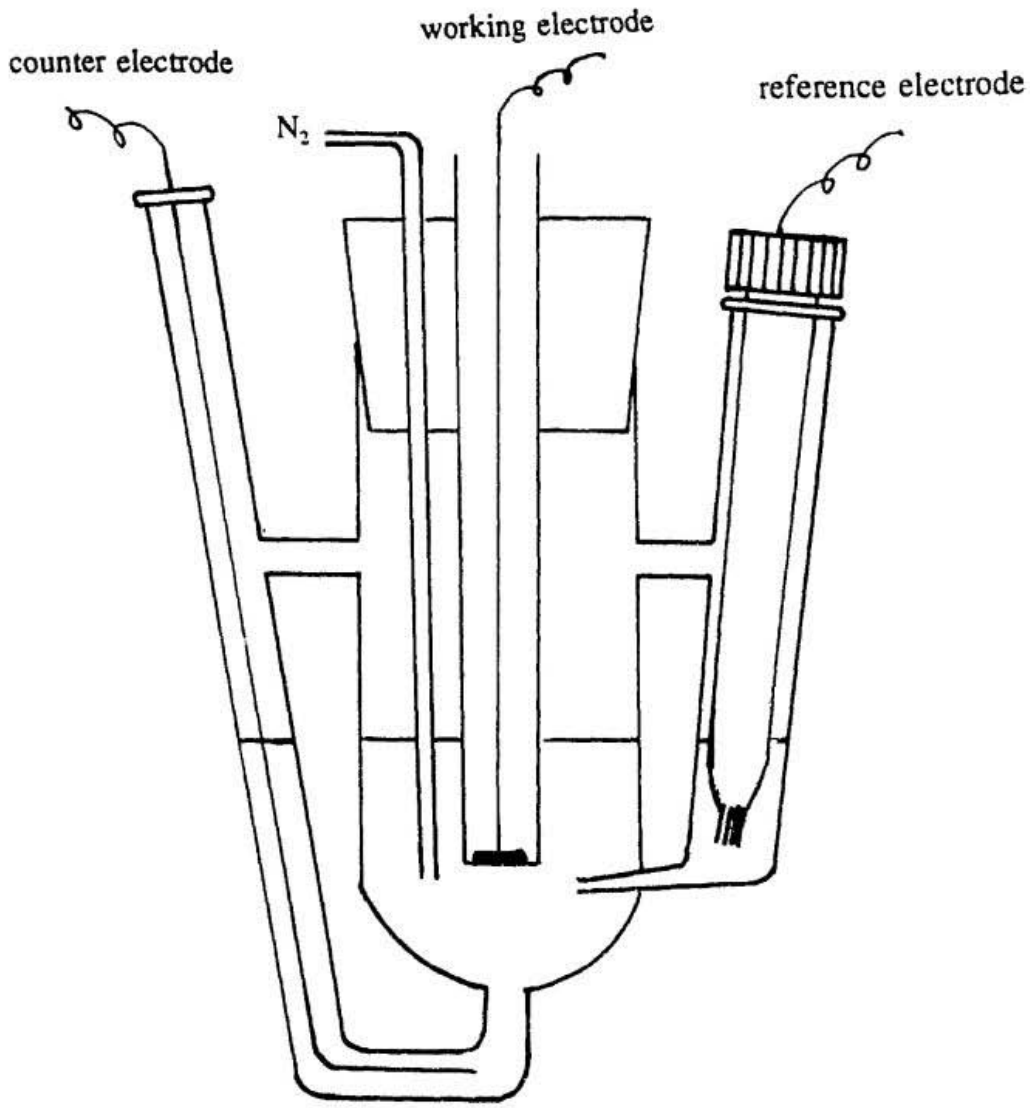

Figure 2.2.1 Three compartment cell for small disk electrode.

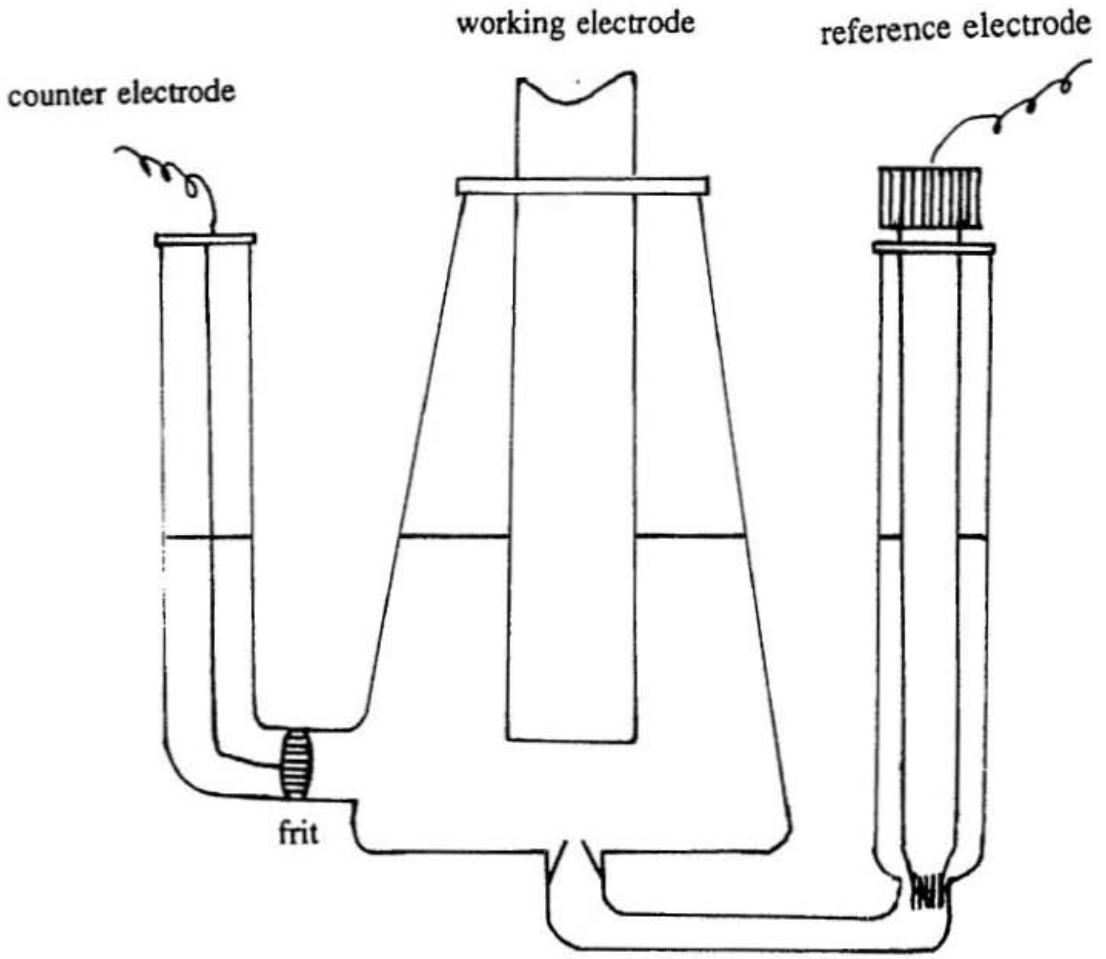

Figure 2.2.2. Three compartment cell for rotating disk electrode.

maximum of 100 ml of solution. A two compartment cell was employed to measure ionic conductivities (see section 2.5).

2.2.3 Instrumentation

A Pine Instruments RDE4 potentiostat/galvanostat, a HB-104 Hokuto Denko function generator and HA-301 potentiostat/galvanostat were used along with a BBC MDL780 X-Y recorder. A Pine Instruments ASR electrode rotator was used for rotating disc voltammetry. A 80286 PC (Tatung TS-7000) was interfaced to the potentiostat and the rotator by a Data Translation DT2801 ADC/DAC card. An Orion Research 601 Digital Ionanalyser was used for conductivity measurements. Gravimetry was carried out using a Perkin-Elmer AD-2Z Auto Microbalance. A Hitachi S570 scanning electron microscope was used for electron micrographs. An Edwards (Model 4) vacuum coating machine was used to coat gold on the dual electrodes for the electronic conductivity measurements.

2.3 Chemicals for Electrochemical Experiments

Tetraethylammonium tetrafluoroborate (Et_4NBF_4, Aldrich) was recrystallized twice from methanol before use. Tetraethylammonium perchlorate (Et_4NClO_4, Purum, Fluka), $LiClO_4$ (Fluka), tetrabutylammonium chloride (But_4NCl, Eastman) and tetrabutylammonium iodide (But_4NI, Eastman) were used as received without

further purification. In most cases, acetonitrile (HPLC, Fisher) was used as a solvent. Buffers were made with potassium dihydrogen orthophosphate (Analar, BDH), potassium phosphate (Fisher) and orthophosphoric acid (Analar, BDH). Potassium iodide (Fisher), potassium ferrocyanide (ACS, BDH), L-ascorbic acid (Gold Label, Aldrich), ferrocene (Aldrich) were used as received.

2.4 Scanning electron microscopy

Scanning electron microscopy (SEM) was used to reveal polymer morphology and to determine the thickness of polymer films. The samples were made by coating the films, each having a different thickness, onto indium/tin oxide electrodes. The glass and the film were broken in the middle to expose a sharp cross-section of the film. The film cross-sections were then examined using the scanning electron microscope (SEM). Film thicknesses were determined from the scales on the SEM pictures.

2.5 Ionic Conductivity measurements

Ionic conductivities were measured perpendicular and parallel to the direction of film plane for poly-$MPMP^+$ using two compartment cells. For the perpendicular measurement,the cell was divided into two parts by two glass slides, each with a hole (3.5 mm in diameter) at the centre as shown in Figure 2.5.1. A

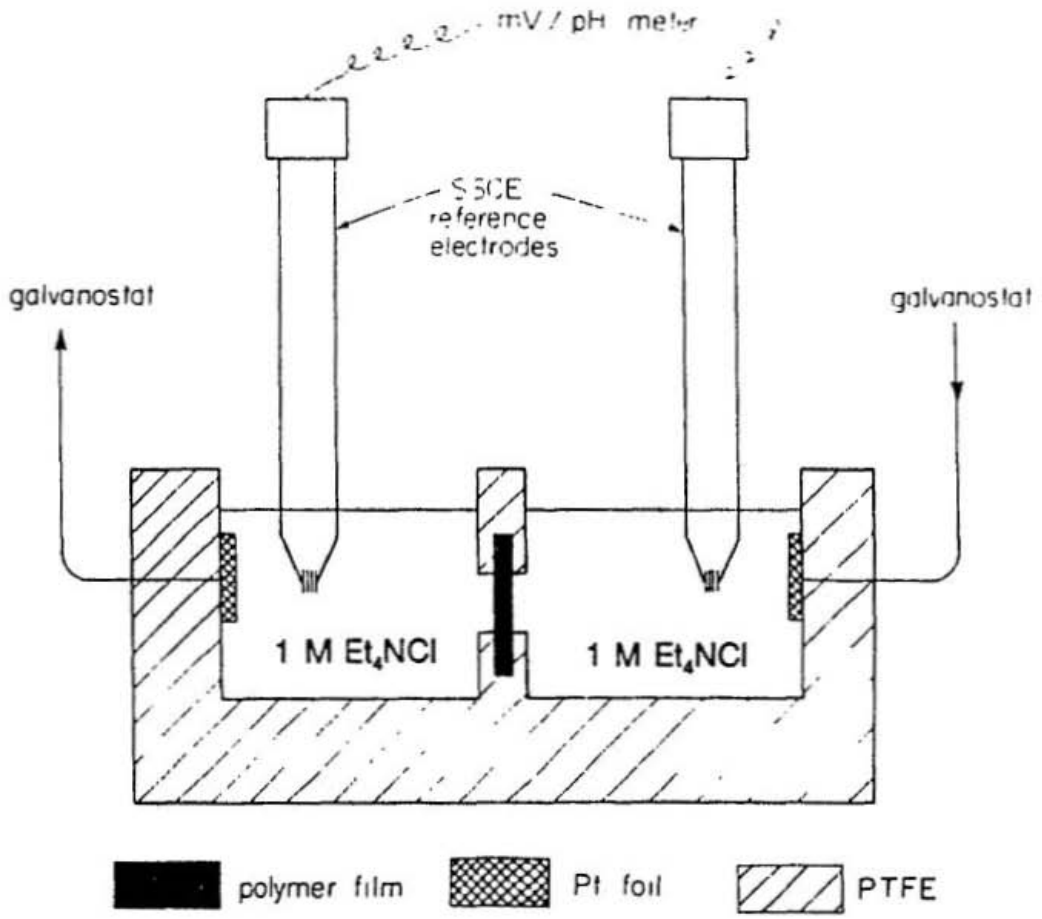

Figure 2.5.1. Two compartment cell for the measurement of ionic conductivity perpendicular to the film plane.

0.45 cm^2 (5 ~ 40 μm thick) polymer film was sandwiched between the two glass slides to fully block the hole and to contact the solutions in both sides of the cell. There are two Pt foils at the ends of the cell so that a constant current can be passed through the polymer film. A SSCE reference electrode is dipped in the electrolyte solution in each compartment. The potential difference between the two sides of the cell was measured using the two SSCEs. The solution resistance, which was determined without blocking the hole with a film, was subtracted from the total resistance to yield the resistance of the film. Such an arrangement was previously used in this lab[7]. Tetrabutylammonium chloride (But_4NCl) and KCl aqueous solutions were used as electrolytes.

For the parallel measurement, the cell was completely separated (Figure 2.5.2) and the connection of solution to film was made through a salt bridge filled with tetrabutylammonium chloride or KCl saturated agar. A rectangular shaped 0.8 X 0.3 cm film (also 5 ~ 40 μm thick) was washed with distilled water, wiped dry with filter paper, and mounted between the two bricks of agar located 0.3 cm apart. The whole agar assembly was covered to prevent the film from drying. The resulting measurement was similar to that for the perpendicular ionic conductivity. To determine the cell resistance, the film was replaced by a large piece of But_4NCl or KCl saturated agar; the measured resistance was then subtracted from the resistance measured with the film. The large piece of gel had

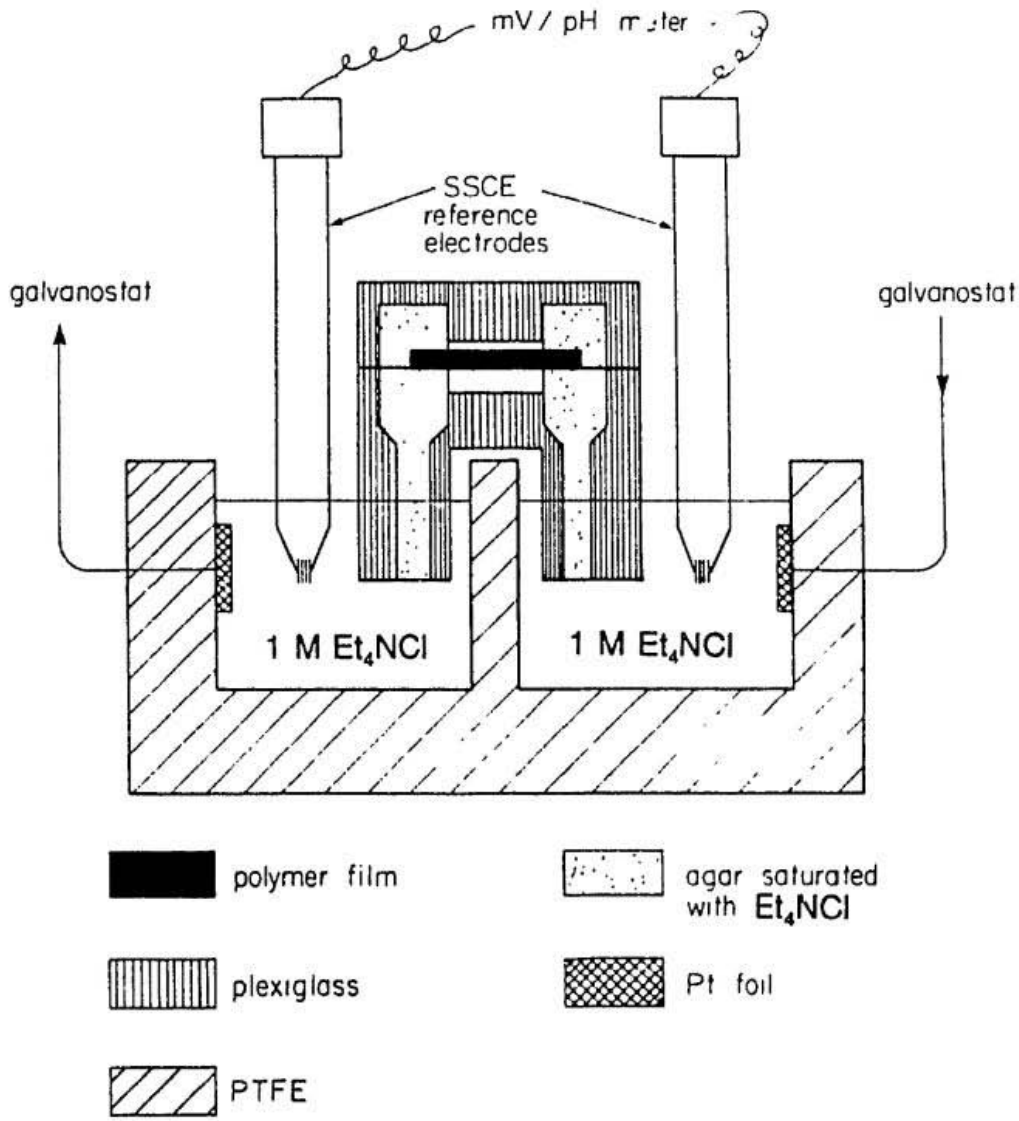

Figure 2.5.2. Two compartment cell for the measurement of ionic conductivity parallel to the film plane.

negligible resistance compared with the polymer. With both parallel and perpendicular ionic conductivities, the ionic conductivity and the swelling factor can be calculated.

2.6 Electronic Conductivity measurements

Electronic conductivities for all the films were measured by various methods. The simplest way employs a mercury contact. The film coated electrode was dipped into a clean mercury pool and resistance was calculated from the applied potential and the observed current.

The most informative conductivity measurement involved connecting a polymer coated Pt electrode to a second Pt electrode using an evaporated gold film. A polymer film was grown on one of the discs of a dual electrode and then both were coated with gold by vacuum coating after thoroughly washing and drying the film in air. The film was in electrical contact with the Pt disc on one side and with the gold on the other. The electronic conductivity was measured *in situ* in 0.1 M Et_4NBF_4/acetonitrile solution. A dual potentiostat was used as discussed in Chapter 4.

2.7 Temperature, Errors and Precision of Results

Electrochemical experiments in this work were carried out at room

temperature without temperature control (23 ± 2 °C). Temperature control was not warranted given the inherent imprecision of the experiments performed. All quoted errors (indicated by " ± ") are standard deviations. Fairly large standard deviations were observed in many experiments. These are mainly caused by the inherent imprecision due to inadequate reproducibility of the polymer preparation.

References

1. J. M. Muchowski and D. R. Solas, Tetrahedron Letters, 33, 24 (1983) 3455.
2. B. L. Bray and J. M. Muchowski, J. Org. Chem., 53 (1988) 6117.
3. K-P. Stefan, W. Schuhmann, H. Parlar and F. Korte, Chem. Ber., 122 (1989) 169.
4. A.P. Kozilowski and X-M. Cheng, J. Org. Chem., 49 (1984) 3239.
5. J. M. Muchowski and R. Naef, Helvetica Chimica Acta, 67 (1984) 1168.
6. V.M.Jovanovic, M. Radovanovic, M. S. Jovanovic, In Ion-Selective Electrodes, 4: Analytical Chemistry Symposium Series 22; Pungor, E., Ed.; Elsevier: Budapest, 1985,489-500.
7. C.D. Paulse and P.G. Pickup, J. Phys. Chem., 92 (1988) 7002.

Chapter 3

Synthesis and Characterization of Polymers

3.1. Synthesis of Polymers

The polymers in this work were all electrochemically synthesized. The following five polymers were investigated: protonated poly-[3-(pyrrol-1-ylmethyl)pyridine], (poly-HPMP$^+$), poly-[1-methyl-3-(pyrrol-1-ylmethyl) pyridinium tetrafluoroborate], (poly-MPMP$^+BF_4^-$), poly-[1-(3-[pyrrol-3-yl]propyl)pyridinium tetrafluoroborate], (poly-PPP$^+BF_4^-$), poly-[(3-[pyrrol-3-yl]propyl)trimethylammonium tetrafluoroborate], (poly-PPTA$^+BF_4^-$) and poly-[3-(3-bromopropyl)pyrrole], (poly-BPP). The structures of these polymers are shown in Figure 3.1.1.

Polymer films were at first prepared by potential cycling (applying cyclic potential to the working electrode) between 0.3 V and 1.3 V in 0.1 M Et_4NClO_4/ CH_3CN for poly-HPMP$^+$ and poly-MPMP$^+$ or between 0 and 1.0 V in the same solution for poly-PPP$^+$, poly-PPTA$^+$ and poly-BPP. Satisfactory films, as judged by cyclic voltammetry, were obtained, and the potentials at which the polymers

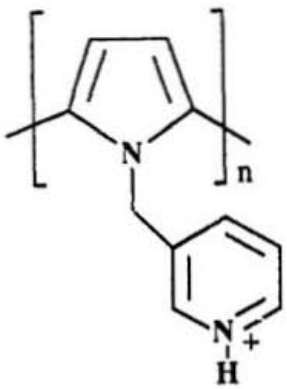

poly - HPMP^{+}

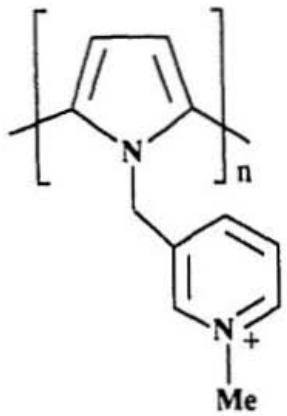

poly - MPMP^{+}

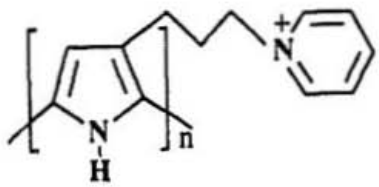

poly-PPP^{+}

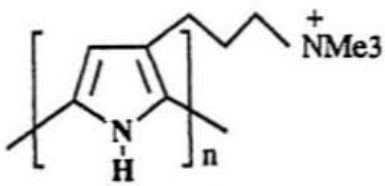

poly- PPTA^{+}

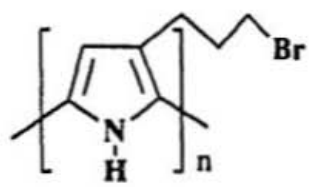

poly - BPP

Figure 3.1.1. Structures of polymers

started to grow were observed (see Table 3.1). However, potential cycling was not convenient for control of film thickness. Constant current polymerization (applying constant current to the anode) produced films that were reproducible, both in quality and thickness. Therefore this method was routinely used for later polymer preparations. For the best film quality, current density should be optimized. This optimization was carried out by growing a series of films using different current densities with identical charge. The resulting films were then tested with cyclic voltammetry. The best current density should have the smallest peak separation and highest peak current of the cyclic voltammogram. Figure 3.1.2 shows this optimization for poly-$MPMP^+$. The minimum peak separation and maximum peak current are found at a current density of 0.8 ± 0.2 mA cm^{-2}. It is noted that the polymerization potential increases with current density. Hence, at high current densities over-oxidation of the film can result. From Figure 3.1.2., it can be seen that the film was severely damaged at current densities of 3.2 mA cm^{-2} or higher. The best upper current density limit should allow the polymerization potential to be slightly lower than the oxidation potential as listed in Table 3.1.

The lower current density limit for constant current polymerization is determined by the onset of uneven film coverage at the electrode. Low current densities result in poor coverage (in most cases the polymerization only occurs at

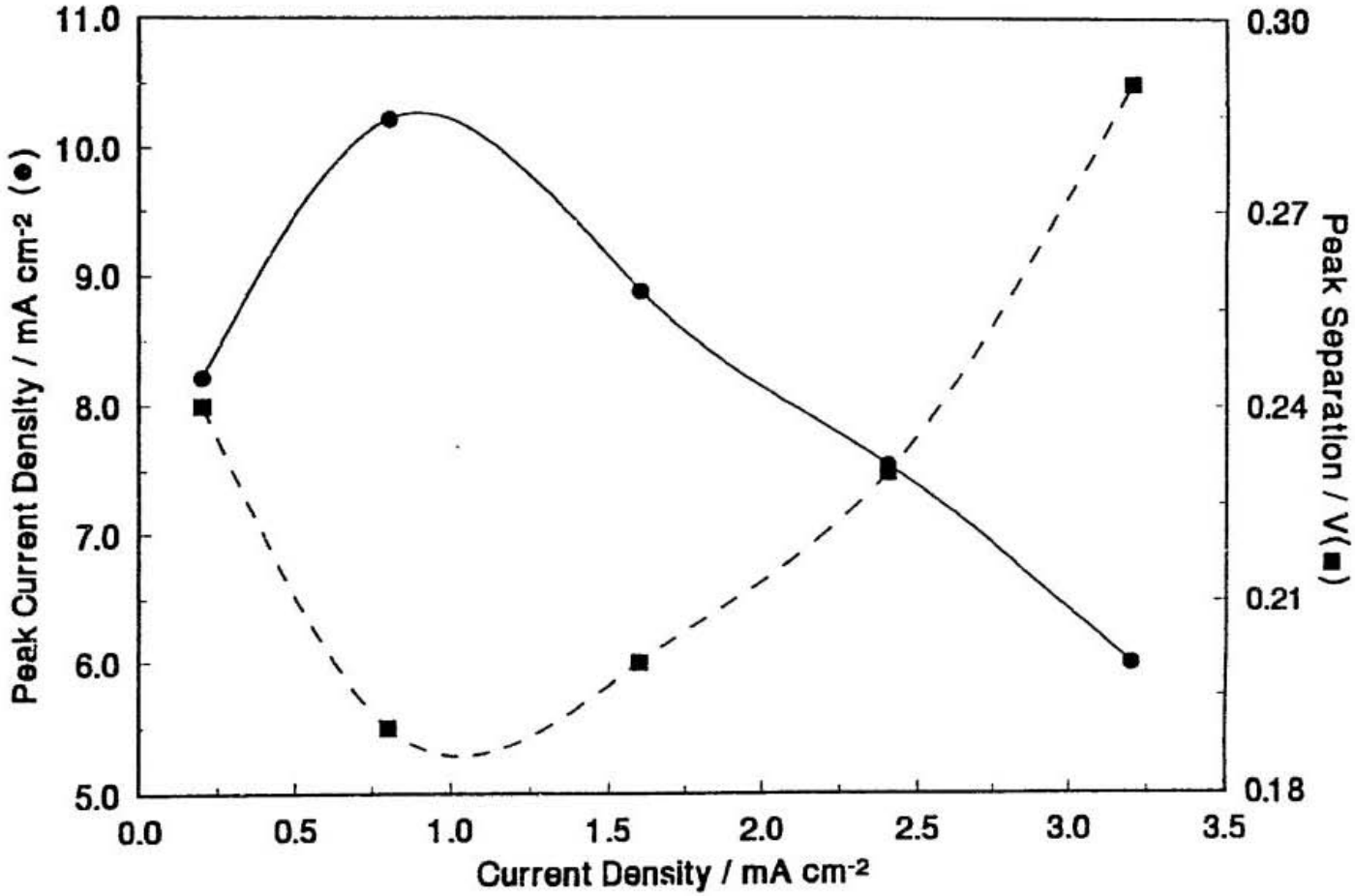

Figure 3.1.2. Optimization of polymerization conditions for poly-MPMP$^+$ in 0.1 M Et_4NClO_4/CH_3CN solution. Lines were drawn by spline fit.

the centre of the Pt disc electrode). It was found that different polymers showed different coverage behaviour. Electrochemical polymerization of $HPMP^+$, $MPMP^+$ and BPP exhibit better coverage than do PPP^+ and $PPTA^+$. For the former polymers, the coverage was poor when the current density was less than 0.2 mA cm^{-2}. For poly-PPP^+ and poly-$PPTA^+$, a range of current densities from 0.4 to 1.4 mA cm^{-2} was tried, and satisfactory coverage required a current density at least 0.6 mA cm^{-2}. All of the polymers were grown in still solutions. If the growth solution is stirred during the polymerization at a current density above the lower limit, the coverage is very poor (only a small spot of film grew at the centre of the disc electrode). Insufficient nucleation may be the cause for the poor coverage because a low current density dictates a low polymerization potential. Also, since poor coverage usually occurs at the edge of the Pt disc electrode, this could be due to a difference in diffusion rates at the edge and centre. Perhaps the products formed initially at the edge is less easily precipitated as polymers than is the film polymerized at the centre, because the diffusion rate at the edge of the disc electrode is greater than at the centre. The optimum constant current polymerization conditions were used for all polymer preparations (except for poly-$HPMP^+$) and listed in Table 3.1 (next page).

The data show that the polymerization potentials for N-substituted pyrroles are much higher than those for 3-substituted pyrroles. This is consistent with

literature values[1].

Table 3.1. Film polymerization conditions at optimum constant current.

Polymer	Concentration of monomer* (mM)	Oxidation potential** (V)	Current density (mA/cm^2)	Potential during polymerization (V)
poly-$HPMP^+$	10-30'	1.26	----	---
poly-$MPMP^+$	50-100	1.20	0.80	1.06-1.08
poly-PPP^+	25	0.70	0 58	0.7-0.8
poly-$PPTA^+$	25	0.80	0.40	0.7-0.8
poly-BPP	25	0.75	0.21	0.7-0.8

* in 0.1M Et_4NBF_4/acetonitrile solution. ' in 0.1M Et_4NClO_4/acetonitrile and 10 ~ 30 mM $HClO_4$ solution. ** potential at which the film starts to grow recorded from potential cycling polymerization.

Poly-$HPMP^+$ could not be synthesized unless at least one equivalent of $HClO_4$ (70%, Fisher) was added to the polymerization solution. In other words, monomer cannot be in excess with respect to $HClO_4$. Potential cycling polymerizations of $HPMP^+$ were carried out in a series of solutions made by

adding different amounts of the monomer to an acetonitrile solution containing a fixed amount of perchloric acid and 0.1 M Et_4NClO_4. For each polymerization in a different solution, 20 polymerization cycles between 0.3 and 1.3 V were used and the polymer quality was assessed by the anodic peak current on the final cycle. As shown in (Figure 3.1.3), the voltammetric peak current increases with increasing monomer concentration. However, once the concentration of monomer exceeds the stoichiometric amount of acid, the polymerization stops declines to zero. The best film (maximum peak current) was produced with the stoichiometric amount of monomer. This result demonstrates that free pyridine groups strongly inhibit the electro-polymerization of PMP.

Morse *et al*[2] mentioned 3-(pyrrol-1-ylmethyl)pyridine (PMP) in their investigation of pyridine intervention in the electrooxidation of pyrrole. They suggest that because pyridine forms a C-N bond with pyrrole during the polymerization, as shown in the scheme below, the polymer is neither conjugated nor planar.

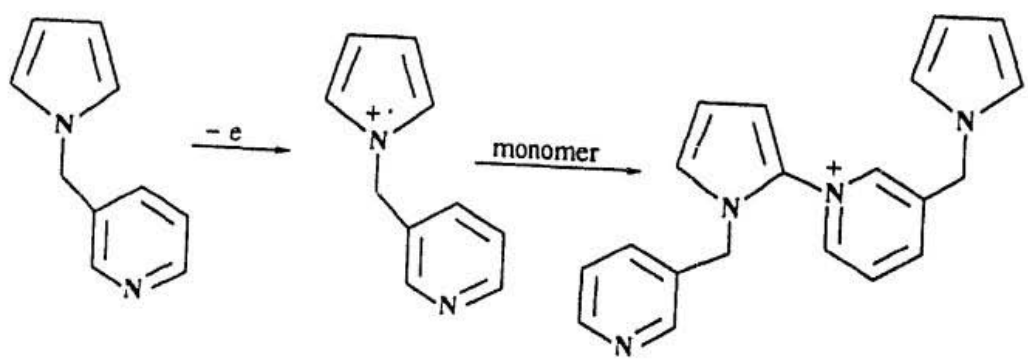

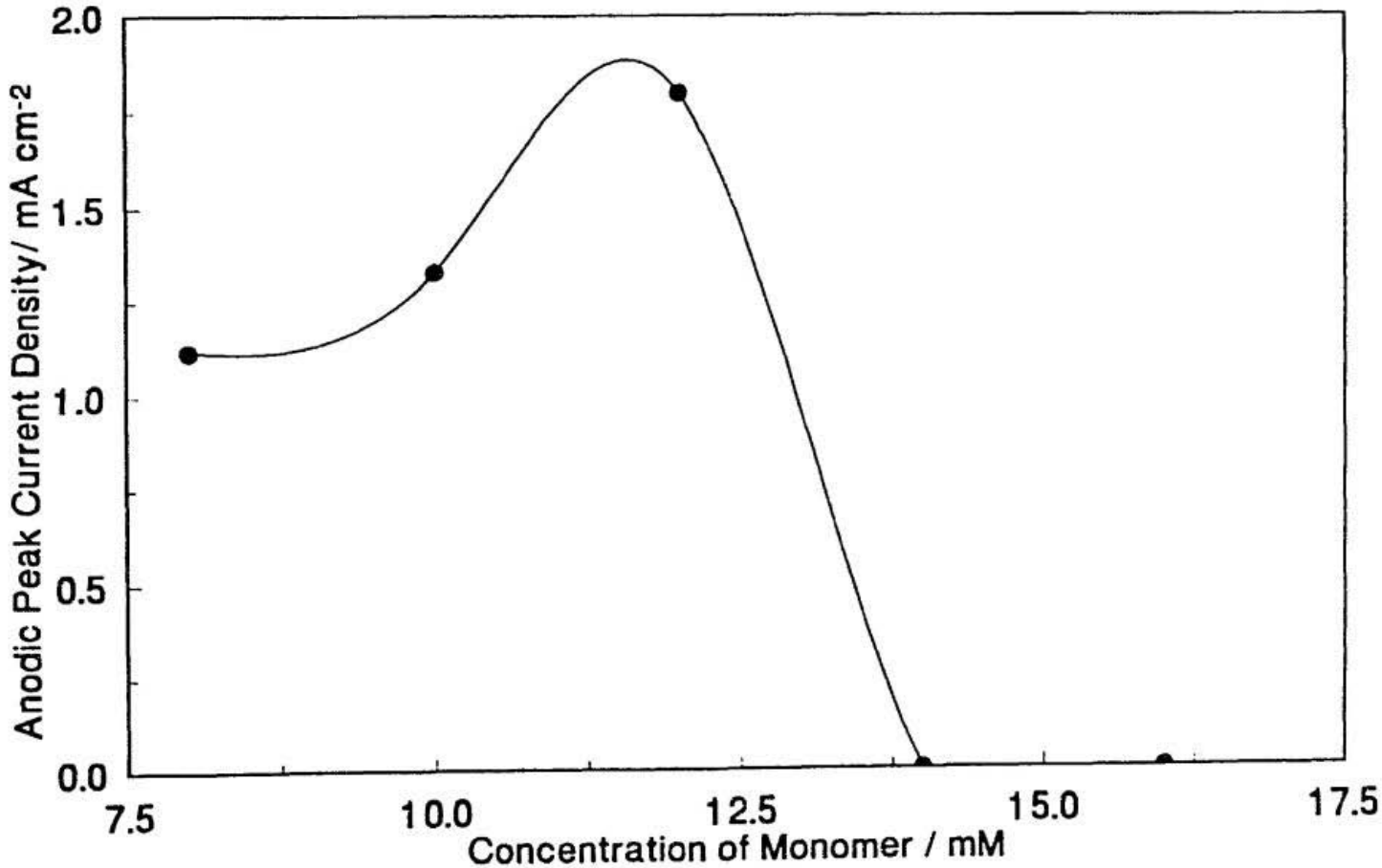

Figure 3.1.3. A plot of anodic peak current *vs.* concentration of monomer (PMP) in 12 mM $HClO_4$, 0.1 M Et_4NClO_4/CH_3CN solution. Line was drawn by spline fit.

Bartlett[3] *et al* have reported an investigation of the feasibility of polymerization of polypyrrole derivatives. They conclude that without added catalysts, it is impossible to polymerize pyrrole derivatives containing a basic nitrogen group. The suppression of polymerization is due to the basicity of the nitrogen groups. The catalysts, such as acids or hydrated metal salts (acting as strong proton sources), protonate the basic groups which leads to a promotion of electrochemical polymerization. Our experiments show that at least one equivalent of acid is needed to start polymerization of PMP; this is consistent with the work of Bartlett *et al*.

Although poly-HPMP$^+$ can be prepared in acidic solution, the use of excess acid resulted in an inferior polymer. This appears to be due to water introduced to the solution by adding 70% $HClO_4$. As shown in Figure 3.1.4, peak currents decrease as water is added to the polymerization solution. In order to grow a film without introducing any water, the pyridine group was quaternized with CH_3I prior to polymerization. Acid was no longer required to cause polymerization and consequently, no water is introduced into the electrolyte. Compared with poly-HPMP$^+$, cyclic voltammograms for poly-MPMP$^+$ exhibit a smaller peak separation and are more symmetrical.

The monomer (pyrrol-3-ylmethyl)dimethylamine (PMDMA, section 2.1.2, Scheme 2) could not be polymerized with any polymerization methods (potential

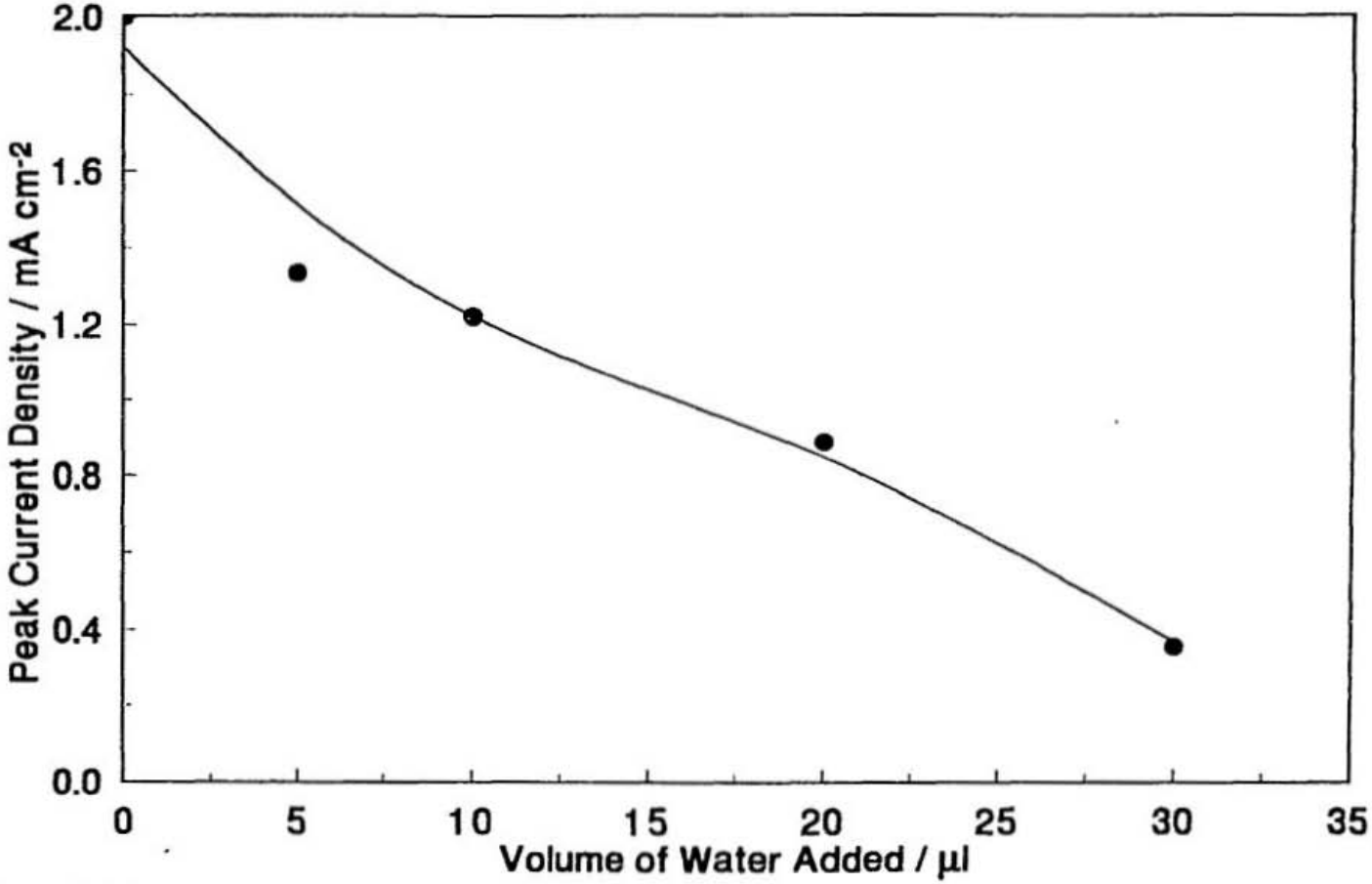

Figure 3.1.4. A plot of anodic peak current *vs* amount of water added to 10 ml, 12 mM PMP and $HClO_4$, 0.1 M Et_4NClO_4/CH_3CN solution.

scanning, constant potential and constant current) even in the presence of acid. The reason is not steric hindrance since PPP^+ and $PPTA^+$ have similarly bulky substituents and do polymerize. The only alternative that one can suggest is that the positively charged site is too close to the pyrrole ring. According to the accepted mechanism for film polymerization (see Chapter 1), the monomer is oxidized to form a cation radical. The positively charged substituent of protonated PMDMA is close enough to draw the electron cloud from the pyrrole ring. Also, the extra electrostatic repulsion due to the substituent could prevent radical cations from coupling.

3.2 Film Thickness and Morphology

Accurate determination of polymer conductivity and other properties is largely dependent on the precision of the film thickness measurement. However, measurement of film thickness is an arduous task. There has been a lot of effort, but not many consistent results reported. For polypyrrole, most workers calculate film thicknesses using a conversion factor based on the charge required to polymerize a 1 μm thick film on a 1 cm^2 electrode, which ranges[4] from 30 to 400 mC. Diaz[5] reported that a 0.1 μm thick film is produced by a charge of 24 mC cm^{-2}, and a conversion factor of 4.16 μm cm^2 C^{-1} results. However, Martin[6]

obtained a plot of film thickness *vs.* polymerization charge, and a conversion factor of 2.64 μm cm^2 C^{-1} by using a profilometer. Ellipsometrical determination also yielded such a plot in Murao and Suzuki's work[7]. In many other publications, film thicknesses have been estimated from cyclic voltammetry (CV) using thickness/charge relationships quoted from early papers.

In this work film thicknesses were estimated in a convenient and accurate way from the charge used to prepare the film. Conversion factors were determined by scanning electron microscopy (SEM) as follows.

Indium/tin oxide coated glass electrodes were used and the exposed area was precisely measured. The electrode was then coated with polymer by constant current polymerization under the optimized conditions (Section 3.1). The polymerization charge, Q, is the product of the current i and the polymerization time, t.

The indium/tin oxide coated glass was cut into 2 mm wide and 10 mm long pieces. The assembly of the electrode is shown in Figure 3.2.1A. Electrical connection was made to one end of the slide with copper foil. The copper slide joint and part of the glass were sealed with epoxy to leave about 2 mm of the indium/tin oxide coating exposed. The uncovered electrode area was precisely measured under an optical microscope. A film was then polymerized onto the conducting side at the desired current. After thoroughly washing with acetone and

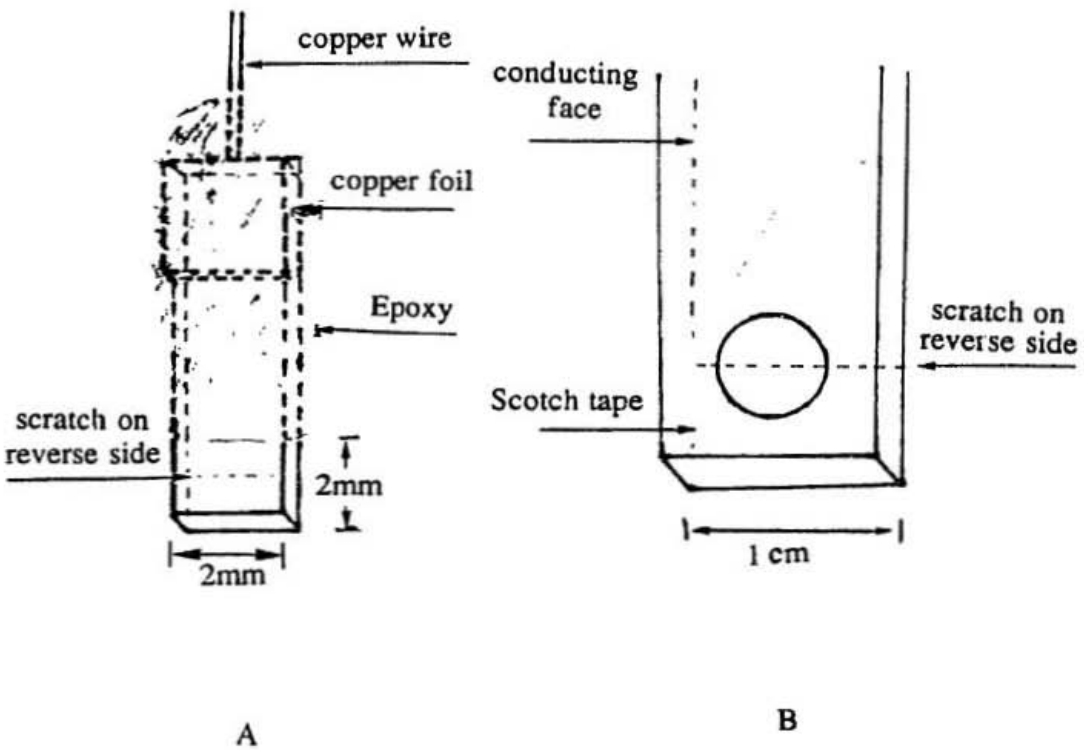

Figure 3.2.1. Indium/tin oxide electrodes for film thickness measurement.

drying under vacuum, the electrode was broken at the scratch as shown in Figure 3.2.1A. A cross-section of the film was exposed and observed parallel to the surface of the film using the scanning electron microscope (Figure 3.2.2). Film thicknesses were measured from the micrographs. Figure 3.2.3 and 3.2.4 show plots of film thickness *vs.* polymerization charge density for poly-MPMP$^+$ and poly-PPP$^+$ films. The data were fitted to linear equations. The slopes of 150 mC cm^{-2} μm^{-1} for poly-MPMP$^+$, and 95 mC cm^{-2} μm^{-1} for poly-PPP$^+$ serve as conversion factors. The thickness of poly-PPTA$^+$ could not be precisely measured because the SEM pictures of this film show a very uneven surface. Since this polymer has similar morphology to poly-PPP$^+$ the same factor of 95 mC cm^{-2} μm^{-1} was used.

Similar electrodes were made in early work by masking the indium/tin oxide slide by adhesive tape with a hole in it so that the exposed area was determined by the size of the hole as shown in the schematic diagram in Figure 3.2.1B. However the boundary of the film was not very sharp due to the dissolution of the adhesive tape in acetonitrile.

The micrographs shown in Figure 3.2.2, and Figure 3.2.5 reveal the difference in morphology between N-substituted poly-MPMP$^+$ and 3-substituted poly-PPP$^+$, poly-PPTA$^+$. Figure 3.2.2A shows a dense morphology for poly-MPMP$^+$. This morphology is similar to that of polypyrrole[8]. Neither pore

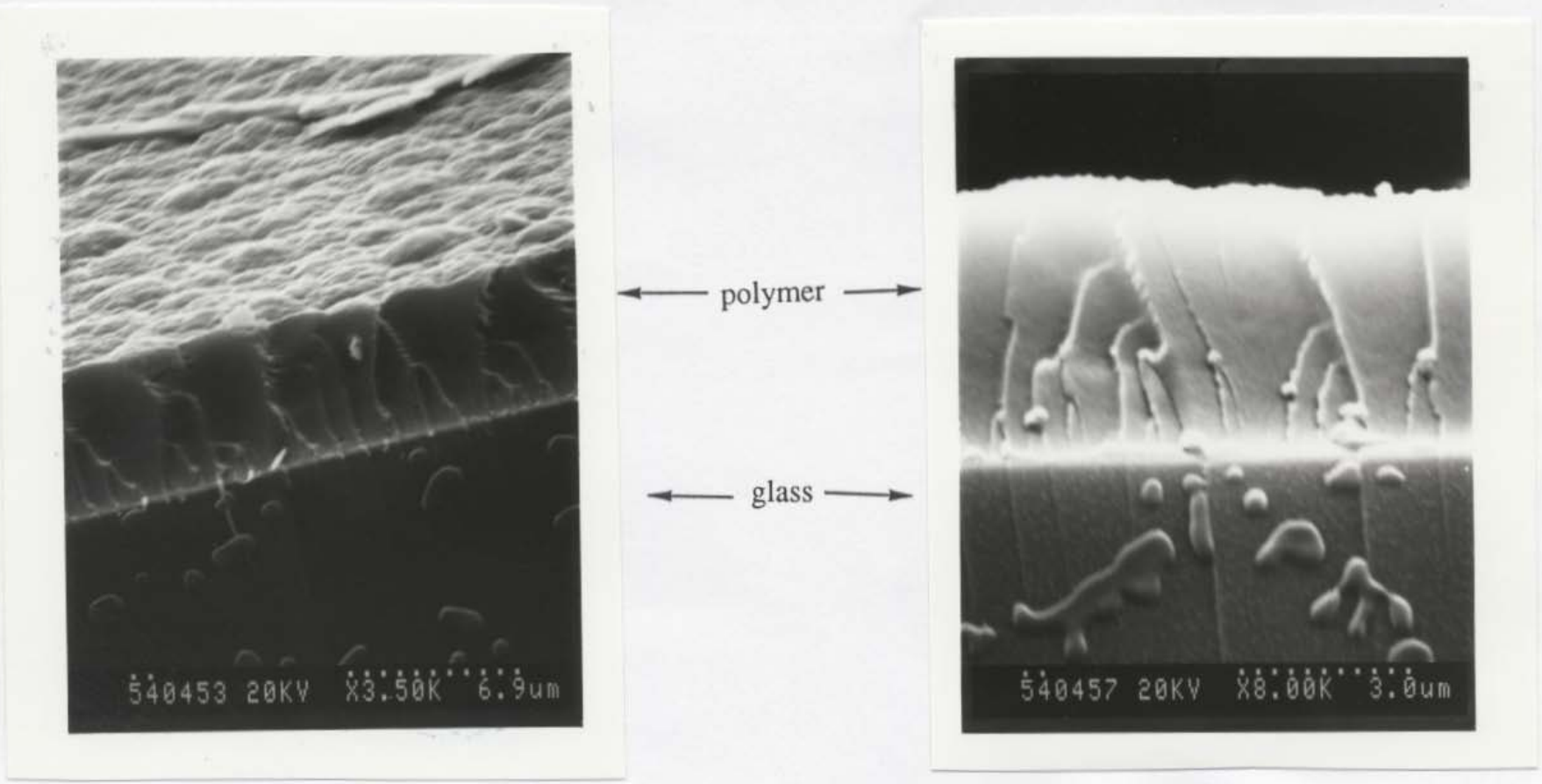

Figure 3.2.2. Scanning electron micrographs of poly-MPMP$^+$ films on indium/tin oxide coated glass slides.

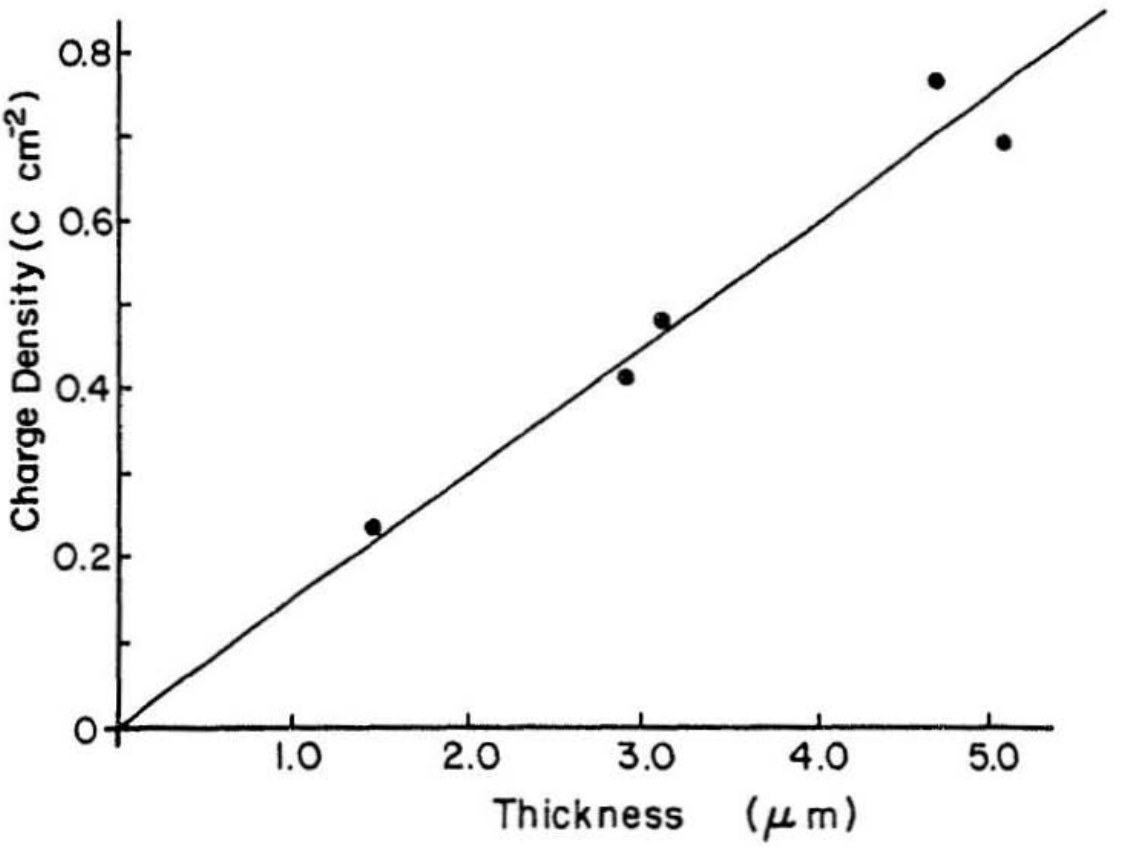

Figure 3.2.3. Plot of polymerization charge density vs. film thickness for poly-MPMP$^+$ films.

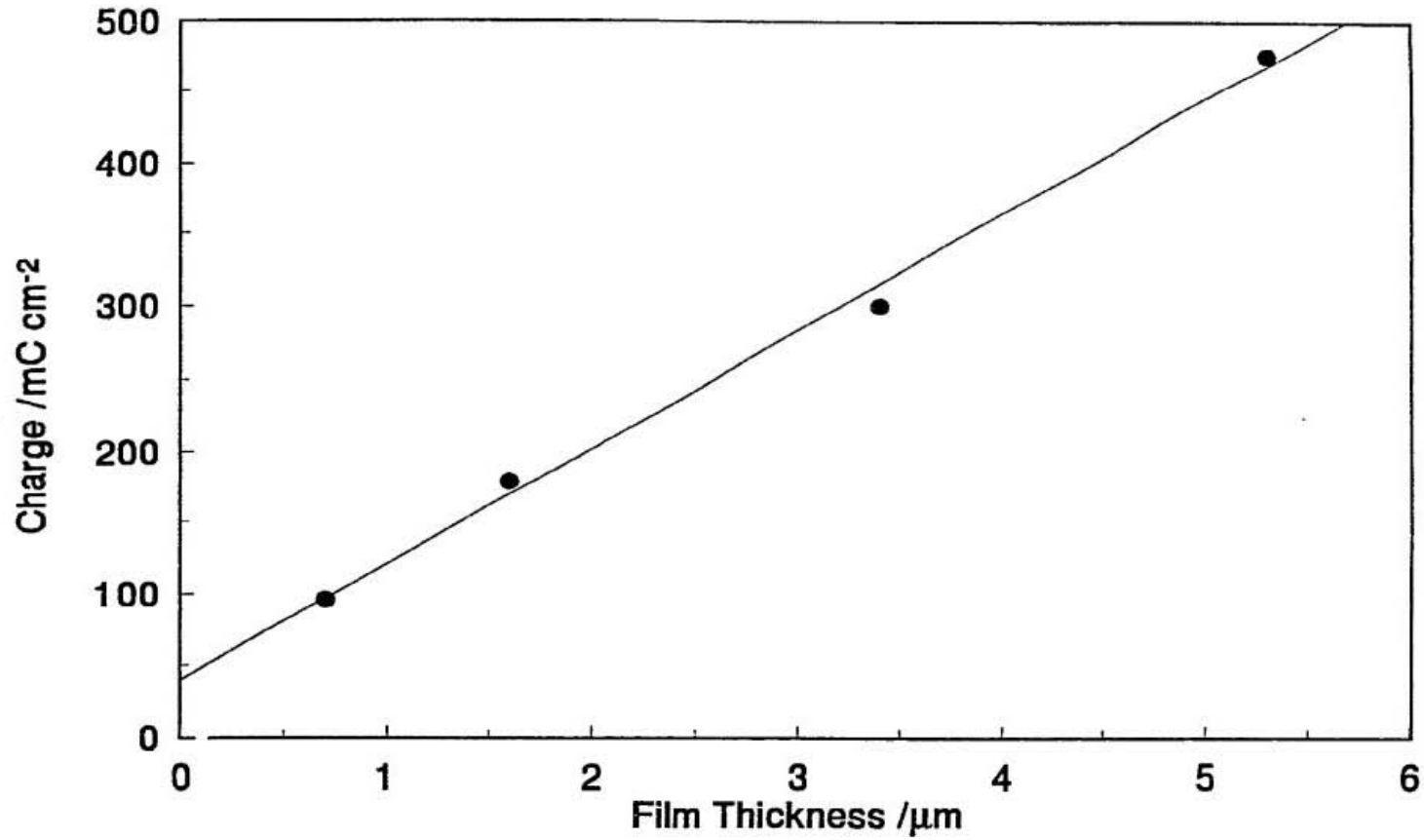

Figure 3.2.4 Plot of polymerization charge density vs. film thickness for poly-PPP+ films.

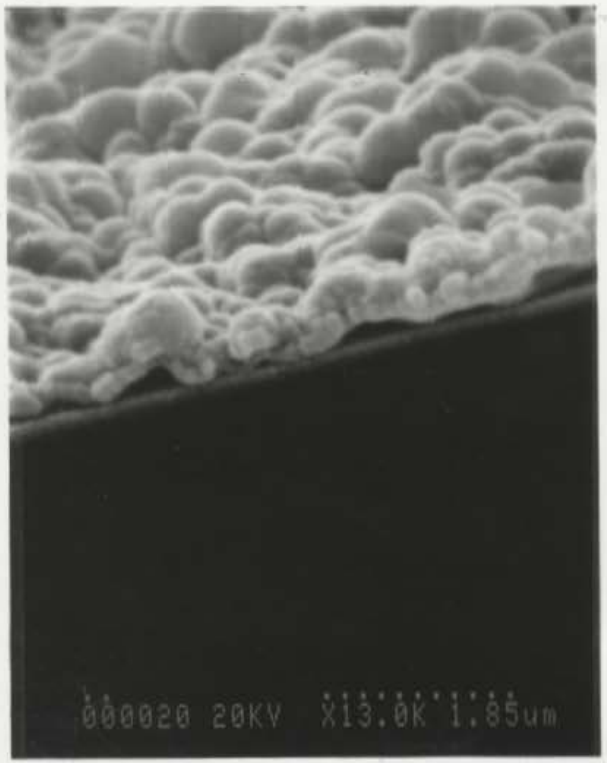

(A)

poly-PPP^+

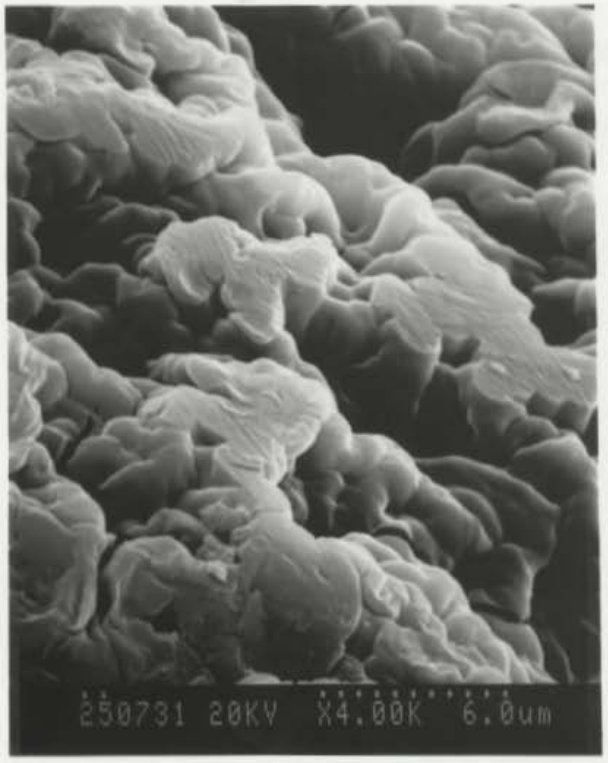

(B)

poly-$PPTA^+$

Figure 3.2.5. SEM pictures of poly-PPP^+(A) and poly-$PPTA^+$ (B).

structure nor fibers could be resolved. Poly-PPP^+ and poly-$PPTA^+$ display a rough surface. Figure 3.2.5B is a micrograph of the poly-$PPTA^+$ surface facing to the working electrode. It is clear that the film only grew at some of the sites of the electrode (see those bright and flat parts on the picture). The reason for this morphology is not clear.

In the case of potential scanning polymerization, the calculation of polymerization charge is complicated by the charging current which causes difficulty in obtaining an accurate measurement of the polymerization current. Film thicknesses were then estimated from cyclic voltammograms (CV). The area under the anodic or cathodic part of the CV is proportional to the film thickness (d) as described in the following equation:

$$d = QM/nFA\delta \qquad (3.2.1)$$

Where Q and M are the measured charge from CV and the molar mass for the monomer, respectively; δ is the film density (1.45 g cm^{-3}, see section 3.4) and n is the oxidation level of 0.16 (measured in section 3.4). In practice this method is imprecise because of difficulty in choosing the upper potential for the CV area measurement.

3.3 Cyclic Voltammetry

Only cyclic voltammograms for poly-MPMP$^+$, poly-PPP$^+$ and poly-BPP will be discussed since the voltammograms of poly-MPMP$^+$ and poly-PPP$^+$ are very similar to those of poly-HPMP$^+$ (as shown in Figure 3.3.1) and poly-PPTA$^+$, respectively. Figure 3.3.2 shows examples of cyclic voltammograms of a poly-MPMP$^+$ coated Pt electrode in 0.1 M Et_4NBF_4/acetonitrile solution. Well defined cathodic and anodic peaks are observed. The peak separation of 30 mV at 20mV s^{-1} is small for a polypyrrole based film. A formal potential of 0.77 V is obtained by taking the average of the anodic and the cathodic peak potentials. The shape of the anodic and cathodic peaks for the scans are similar. The peak current increases linearly with scan rate for both the anodic and cathodic scans as shown in Figure 3.3.3. This relationship is expected for an immobilized electroactive film and indicates the fast charge transport kinetics of the polymer[9]. Compared to polypyrrole (Figure 1.2.2), the symmetry is obviously improved.

Figure 3.3.4 and 3.3.5 are examples of cyclic voltammograms for poly-PPP$^+$ and poly-PPTA$^+$. Formal potentials from these voltammograms range from -0.04 to -0.125 V depending on scan rate, much lower than that of poly-MPMP$^+$ and characteristic of 3-substituted polypyrroles[10]. Figure 3.3.6 reveals a linear relationship between peak current and scan rate. As compared to poly-HPMP$^+$

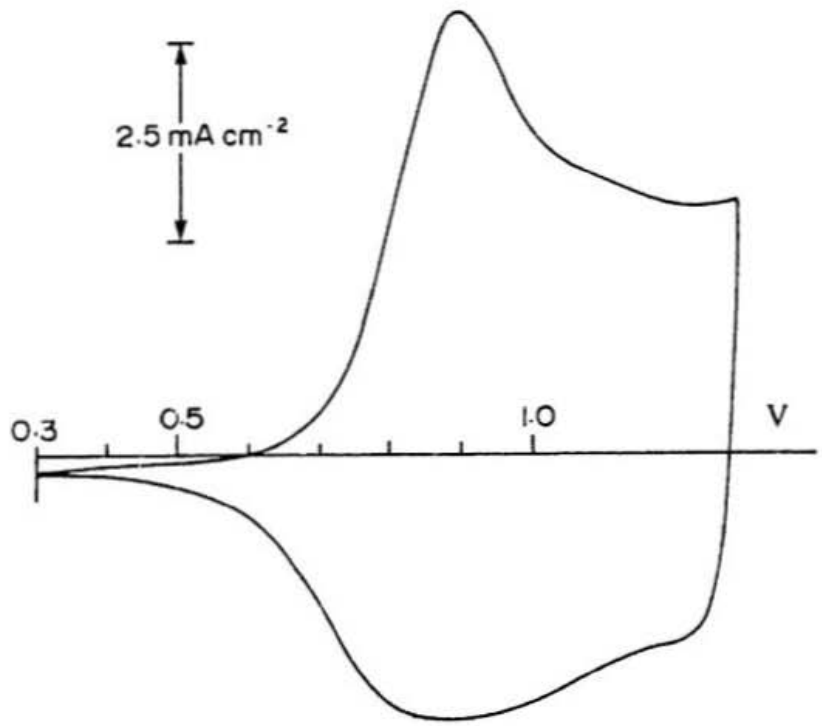

Figure 3.3.1. Cyclic voltammogram of a poly-$HMPM^+$ coated Pt electrode in 0.1 M Et_4NBF_4/CH_3CN solution. Scan rates was 100 mV s^{-1}.

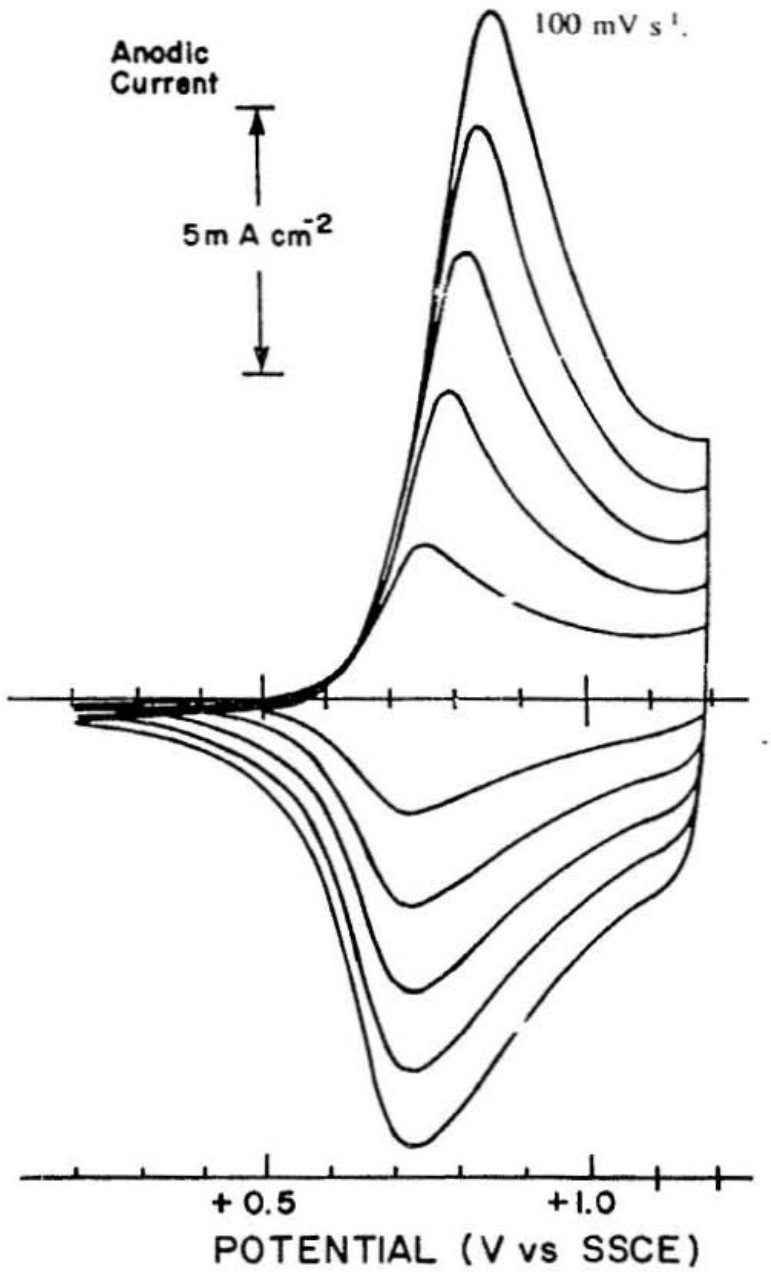

Figure 3.3.2. Cyclic voltammograms of a poly-MPMP$^+$ coated Pt electrode in 0.1 M Et_4NBF_4/CH_3CN solution. Film thickness = 3.2 μm. Scan rates were 20,40,60,80 and 100 mV s^{-1}.

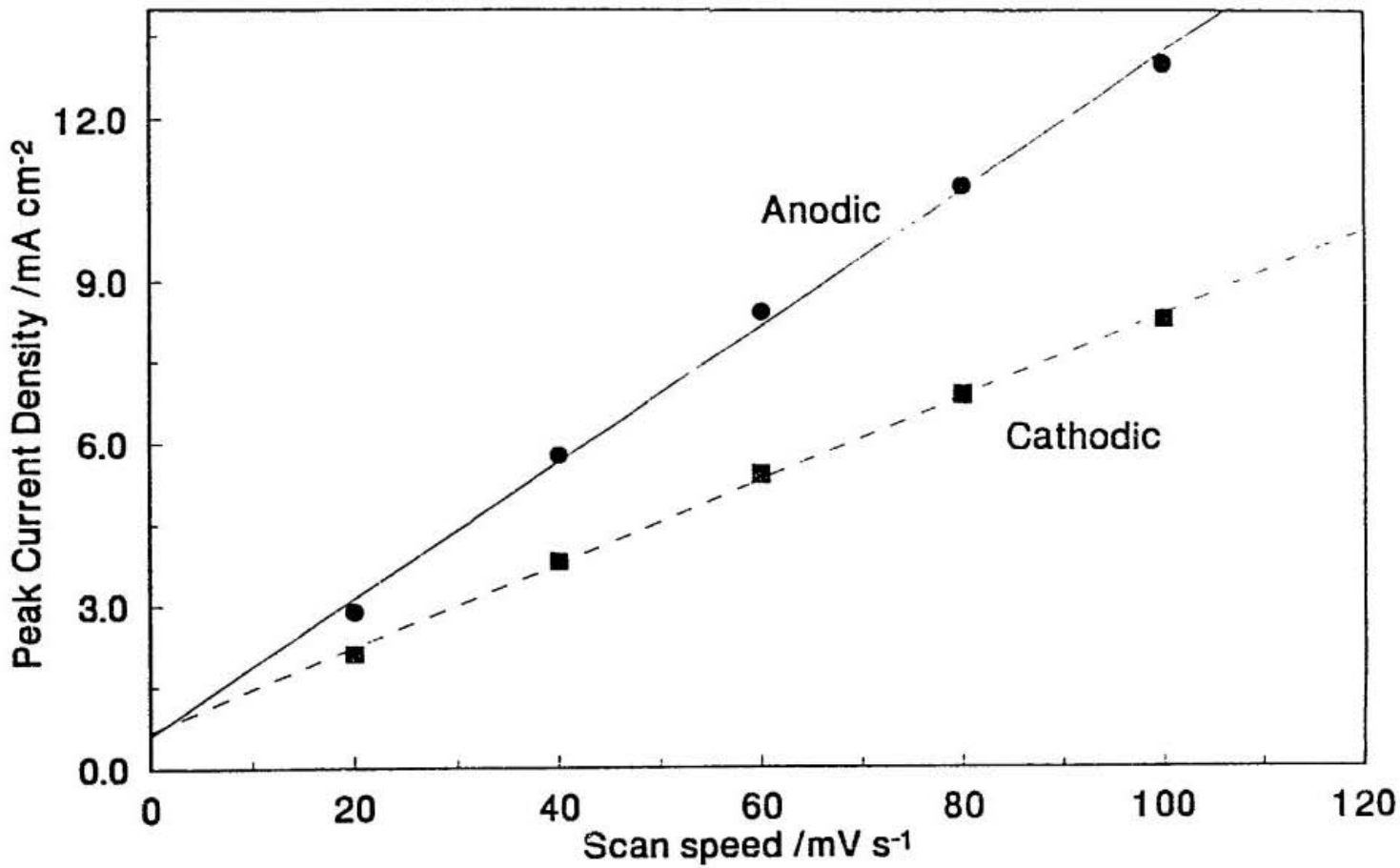

Figure 3.3.3. Plot of peak current *vs.* scan rate for poly-MPMP^{1}; anodic(—) and cathodic (----). Data are from cyclic voltammograms in Figure 3.3.1.

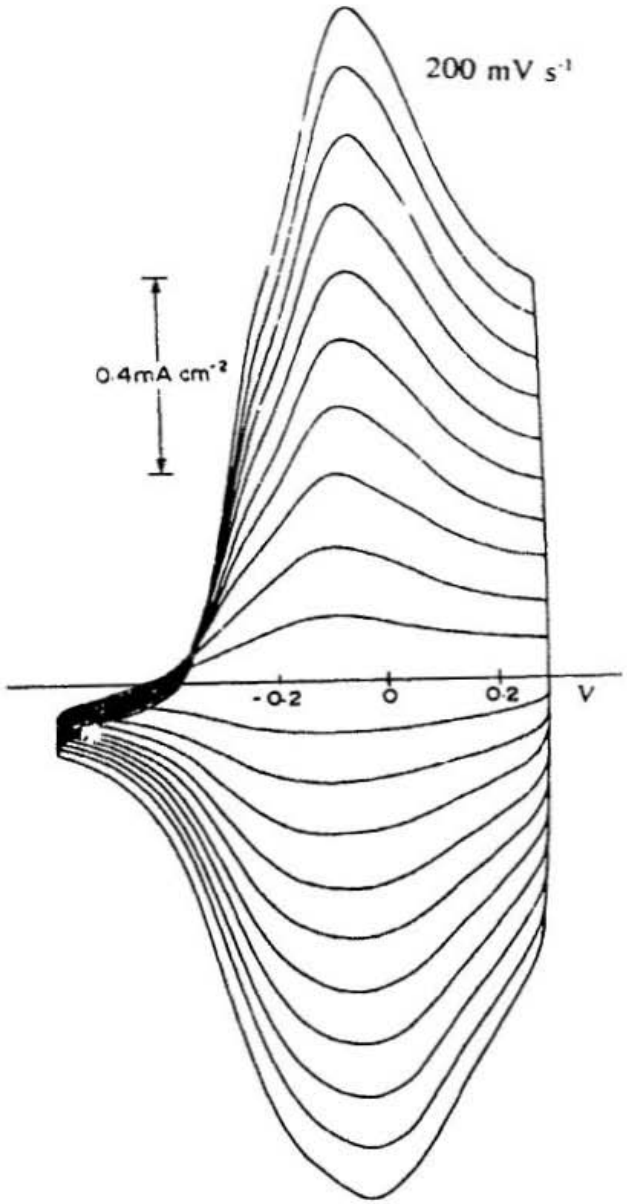

Figure 3.3.4. Cyclic voltammograms of a poly-PPP^+ coated Pt electrode in 0.1 M Et_4NBF_4/CH_3CN solution. Film thickness = 0.5 μm. Scan rates were from 20 to 200 mV s^{-1} (20 mV increment).

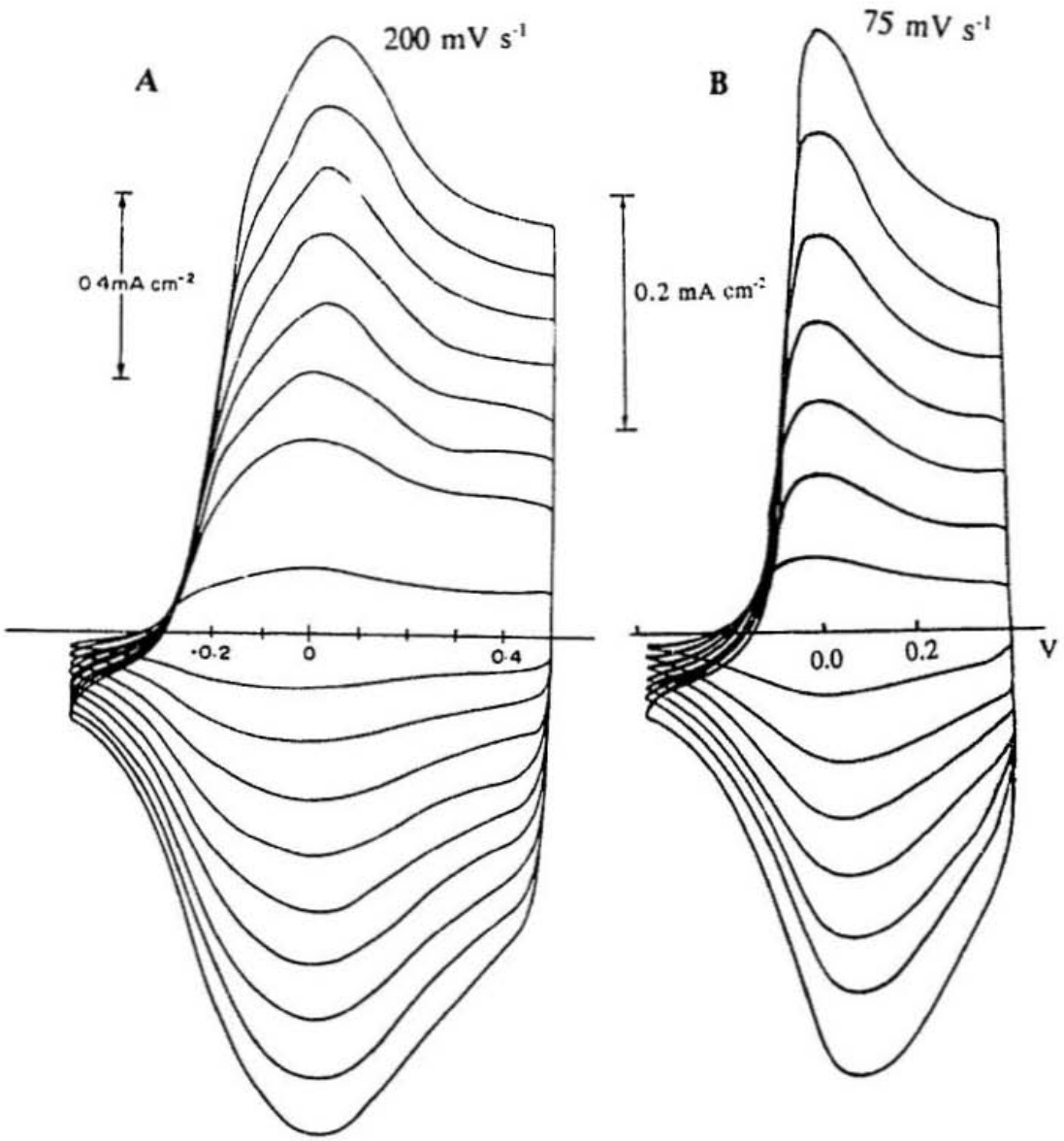

Figure 3.3.5. Cyclic voltammograms of a poly-PPTA$^+$ coated Pt electrode in 0.1 M Et_4NBF_4/CH_3CN solution. Film thickness = 0.5 μm. (A) polymerized at 400 μA cm^{-2}; scan rates were from 20 to 200 mV s^{-1} (20 mV increment). (B) polymerized at 600 μA cm^{-2}, scan rates were 10,20,30,40,50,60,75 mV s^{-1}.

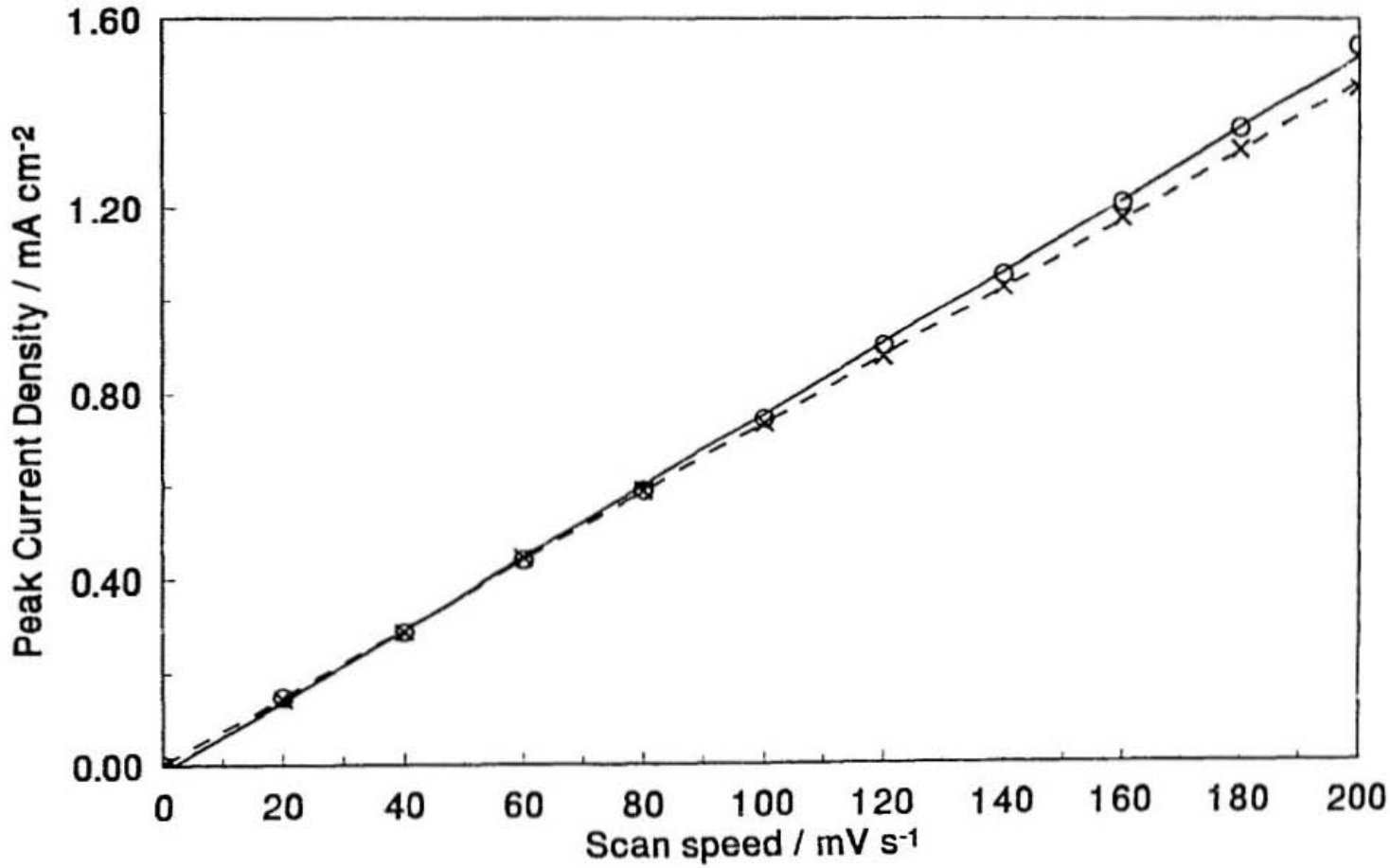

Figure 3.3.6. Plot of anodic peak current *vs.* scan rate for poly-PPP'(----) and poly-PPTA'(----) from cyclic voltammograms in Figure 3.3.3 and Figure 3.3.4A.

and poly-MPMP$^+$, the symmetry shows improvement as judged by the near zero peak separation at scan rates up to 200 mV s^{-1}. When poly-PPTA$^+$ was polymerized at a larger current density, e.g. 600 μA cm^{-2} instead of 400 μA cm^{-2}, a negative peak separation was observed as shown in Figure 3.3.5B. The origin of this is not clear.

The formal potential is usually measured from the average of the cathodic and anodic peak potentials. However the average potential changes with scan rate as shown in Table 3.2 for poly-MPMP$^+$:

Table 3.2: Formal potential change as a function of scan rate for poly-MPMP$^+$.

Scan Rate (mV/s)	$E_{p,a}$ (V)	$E_{p,c}$ (V)	ΔE (V)	$E^{o'}$ (V)
20	0.75	0.72	0.03	0.74
40	0.79	0.73	0.06	0.76
60	0.82	0.73	0.09	0.77
80	0.84	0.73	0.11	0.78
100	0.86	0.73	0.13	0.80

Where ΔE, $E^{\circ\prime}$, $E_{p,a}$ and $E_{p,c}$ are the peak separation, the formal potential, anodic peak potential and cathodic peak potential, respectively. The average formal potential of 0.77 ± 0.02V is similar to that of other N-substituted pyrrole polymers[1]. For poly-PPP^+, Figure 3.3.7 shows a plot of formal potential vs. scan rate. The measured formal potential ranges from -120 mV at a scan rate of 20 mV s^{-1} to -40 mV at 200 mV s^{-1}. This variation complicates the measurement of formal potential.

The peak separation ΔE for poly-$MPMP^+$, at 20 mV s^{-1} appears much lower than at other scan rates (Table 3.2). One may assume that ΔE could be zero at an extremely low scan rate. According to the trends of the $E^{\circ\prime}$s in the table, the formal potential could be even lower than 0.74 V. This suggests that the formal potential should be determined at extremely low scan rate so that the film is completely in equilibrium and scan rate effects are avoided. However, one can not extrapolate the formal potential to a zero scan rate because the relationship between the $E^{\circ\prime}$ and scan rate is not linear as seen from Figure 3.3.7 for poly-PPP^+ and from Table 3.2.

Figure 3.3.8 shows a cyclic voltammogram for poly-BPP in acetonitrile. Two oxidation and reduction peaks appear and the formal potentials (measured from the average of the cathodic and anodic peak potentials) are 0.35 V for the first oxidation and +0.08 V for the second. It is interesting to note that this film

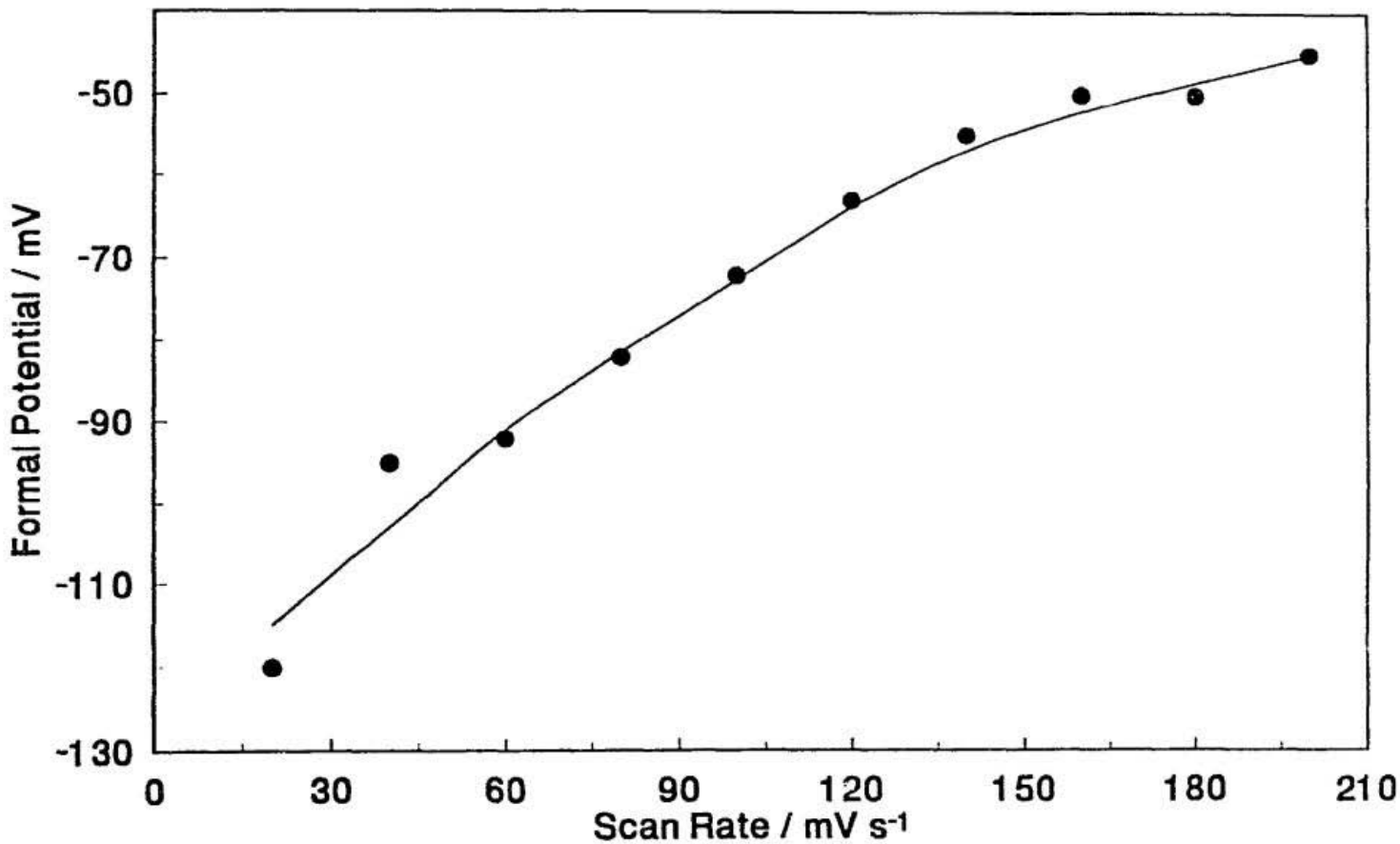

Figure 3.3.7. Formal potential changes with scan rates for poly-PPP^{+}. Data are from Figure 3.3.3.

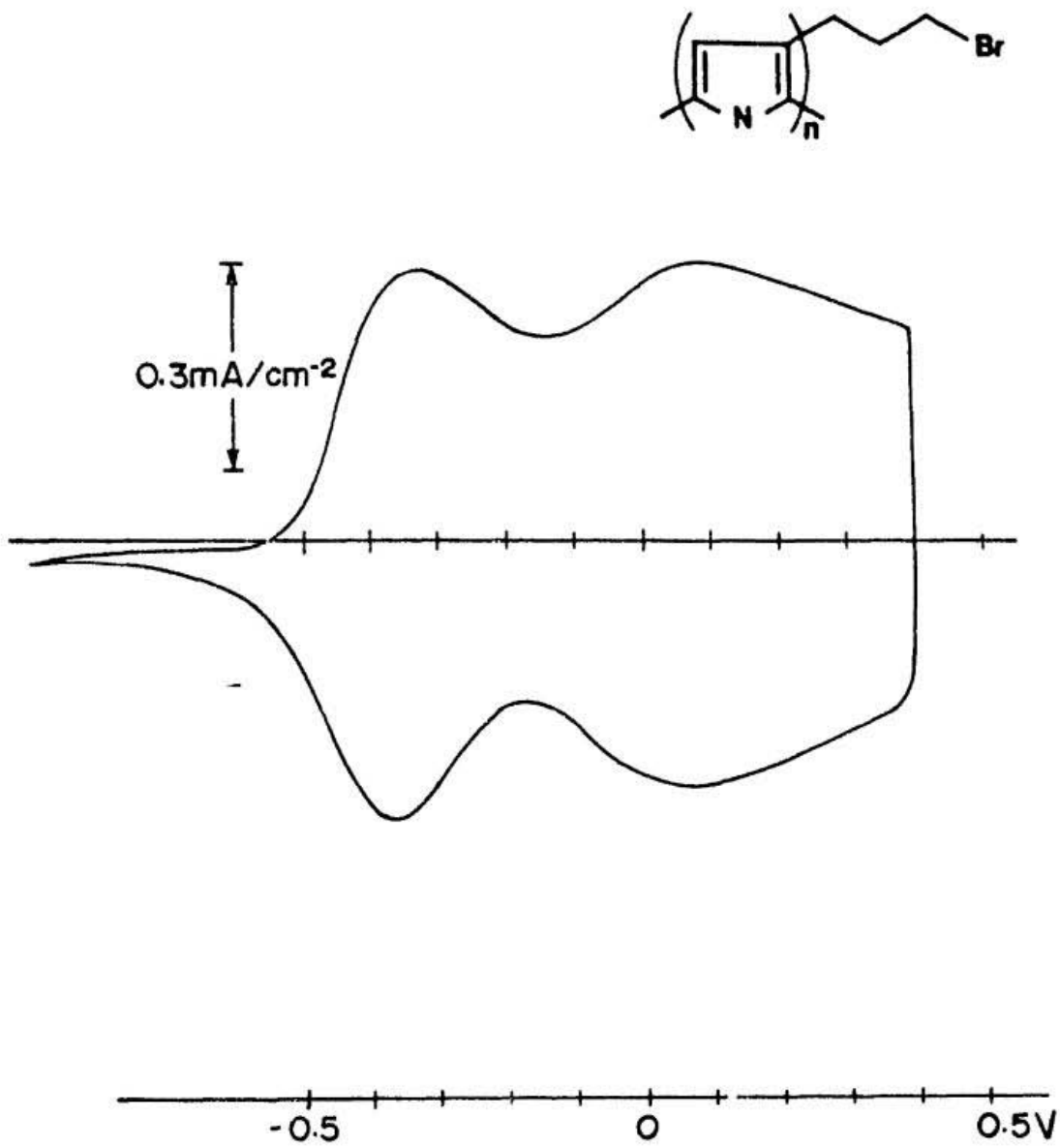

Figure 3.3.8. Cyclic voltammograms of a poly-BPP coated Pt electrode in 0.1 M Et_4NBF_4/CH_3CN solution. Film thickness = 0.4 μm. Scan rate was 50 mV s^{-1}.

exhibited no electrochemical properties in aqueous solution. Presumably, this polymer is so hydrophobic that a double layer is formed only at the polymer/solution interface; hence, no ions can enter the polymer. Further investigation of this polymer is needed, but it is beyond the scope of this dissertation.

3.4 Elemental Analysis, Gravimetry and Oxidation Level

Gravimetry and elemental analysis were employed to determine the oxidation level for poly-MPMP$^+$. By analogy with polypyrrole[8], the expected electrochemical reduction of the polymer is:

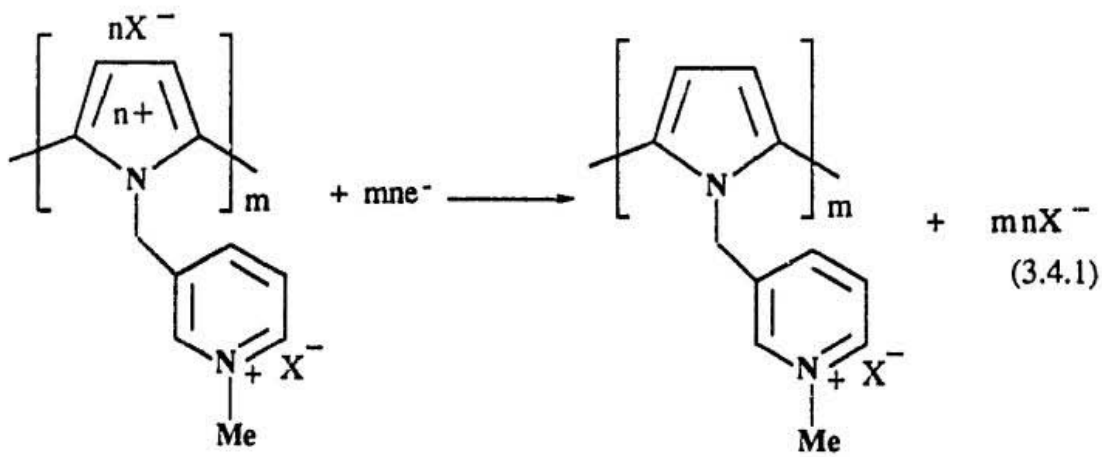

(3.4.1)

where n is the degree of oxidation of one pyrrole unit or the average positive

charge on the polypyrrole chain per pyrrole unit; m is the average chain length and X^- is an anion associated with the positive charge. The value of m is not known, but is assumed to be large enough to have no influence on the following calculations. The oxidation level, n, can either be obtained by comparing the atomic ratio of C:X (number of carbon atoms : number of chlorine atoms if $X^- = ClO_4^-$) from elemental analysis for reduced and oxidized films, or by determining the mass of a film in its reduced and oxidized forms, by gravimetry.

Samples of poly-$MPMP^+$ for the elemental analysis were prepared by polymerizing a film onto a 1 cm^2 indium/tin oxide coated glass electrode at constant current for 15 minutes from a 0.1 M $MPMP^+$, 0.1 M Et_4NClO_4/ acetonitrile solution. Oxidized films were produced by holding the potential at 1.1 V for 4 minutes in $MPMP^+$ free 0.1 M Et_4NClO_4/acetonitrile solution with constant stirring. Reduced films were produced similarly at 0 V. All films were peeled off the electrode after either oxidation or reduction, then thoroughly washed with acetone and dried in air. The oxidized films were black while the reduced films were semitransparent with a green coloration. Samples consisting of 6 films each were sent to Canadian Microanalytical Services Ltd. (New Westminster, British Columbia) for elemental analysis. The results are listed in Table 3.3 (next page).

For the reduced film, the calculated values are obtained based on the

Table 3.3. Results of Elemental Analysis for poly-MPMP$^+$

ELEMENT	OXIDIZED FILMS		REDUCED FILMS	
	Calculated %	Found %	Calculated %	Found %
C	43.36	42.85	45.75	46.41
H	4.27	3.87	4.51	3.99
N	9.20	9.00	9.71	9.57
Cl	13.51	13.36	12.29	12.52
C:Cl ratios				
	9.47	9.47	11	10.94

formular $C_{11}H_{11}N_2Cl_1O_4$ H_2O with the addition of one molecule of water per monomer unit. The hydration is supported by the weight loss when films were dried at room temperature in vacuo. Also, hydration was previously reported[11] for polypyrrole. The results in Table 3.3 are in good agreement between the calculated and analyzed values. It confirms that each unit of the polymer retains the same structure as the monomer.

A degree of oxidation of 0.16 is calculated from the amount of excess ClO_4^- by using the atomic ratio C:Cl for oxidized films [$9.47 = 11/(1 + n)$]. This assignment of the oxidation level is lower than the literature value for polypyrrole based films ($n \sim 0.25$)[12]. The reason is not clear but the lower C:Cl ratio for the oxidized films indicates that the counter ion, ClO_4^-, has been incorporated into the backbone (poly-MPMP$^+$ chain) of the polymer.

For gravimetry, poly-MPMP$^+$ was grown onto a Pt foil flag electrode (described in Section 2.2.1) at constant current from a 0.1 M MPMPBF$_4$ and 0.1 M Et_4NBF_4/acetonitrile solution. After the desired polymerization period, the flag electrode was disconnected at the polymerization potential (1.07 -1.13 V) to maintain the oxidation state of the film. The film and the Pt foil were weighed after being washed with acetonitrile and acetone, and dried at room temperature *in vacuo*. The mass of the foil was subtracted from the total mass to yield the mass of the oxidized poly-MPMP$^+$ film. The reduced form of the film was prepared by holding the potential at 0 V in MPMP$^+$ free 0.1 M Et_4NBF_4/ acetonitrile solution for 15 minutes. Procedures for washing, drying and weighing were repeated for the reduced film, in order to obtain its mass. The gravimetric results are listed in Table 3.4 (next page).

As shown in equation 3.1.4, the number of moles of monomer units in a film can be calculated from the mass of the reduced form which has a formula mass of 258.5 g mol^{-1} ($C_{11}H_{11}N_2B_1F_4$, no H_2O included). The molar mass for the oxidized form of the polymer can then be obtained from the oxidized film mass. The degree of oxidation, n, can be obtained from Equation 3.4.2.

$$n = (m_{ox} - m_{red})M_p / m_{red}M_c \qquad (3.4.2)$$

where the m_{ox} and m_{red} are the masses of the oxidized and reduced film

Table 3.4 Mass, degree of oxidation, and coulombic polymerization efficiency for poly-MPMPBF$_4$ films by gravimetry.

polymerize charge (C)	film mass (mg)		degree of oxidation	coulombic efficiency (%)	density (g cm^{-3})
	reduced	oxidized			
0.20[a]	0.212	0.225	0.17±0.12	86.0±3.9	1.59±0.07
0.50	0.465	0.496	0.20	76.5	1.40
0.90[b]	0.873	0.935	0.22±0.02	80.2±0.5	1.45±0.01
1.20	1.078	1.156	0.21	74.0	1.35

[a] Averages for 4 films. [b] Averages for 5 films.

respectively; their difference is the mass of counter ion inserted during oxidation. M_p and M_c are the formula masses of the reduced monomer unit in the film and the counter-ion respectively. The calculated results are listed in Table 3.4. The average degree of oxidation for a number of poly-MPMP$^+$ films is 0.20±0.07 at the potential at which the films were prepared (1.1 V).

The degree of oxidation can also be determined by combining the gravimetry data and cyclic voltammetry data. The charge, Q_{CV}, under a slow cyclic voltammogram integrated from 0.3V to the polymerization potential (about 1.1 V) gives the total number of moles of electrons x*ne*$^-$ in the reaction 3.4.1. The

number of moles of monomer units, x, can be obtained from the mass of the reduced film. Using this relationship:

$$n = Q_{CV}M_p/Fm_{red} \qquad (3.4.3)$$

the average value of n for poly-MPMP$^+$ is 0.21 ± 0.03 calculated this way. It is in reasonable agreement with the values determined using the masses of the oxidized films. However, both "faradaic" and "capacitive" currents contribute to the measured charge even at extremely low scan rate, and it is impossible to distinguish the two without another physical measurement[13].

The gravimetric experiment provides the coulombic efficiency, η, from the polymerization charge and the number of moles of the polymer units in the reduced form as described in Equation 3.4.4.

$$\eta = (2 + n)Fm_{red}/M_pQ_{pol} \qquad (3.4.4)$$

where Q_{pol} is the polymerization charge. Coulombic efficiencies for the polymerization are listed in Table 3.4. The average is 80% for the range of film thicknesses studied (0.7 to 4.3 μm) and the efficiency is roughly constant.

The film density (δ) can be calculated by combining the result of the

gravimetric experiment and the polymerization charge/film thickness relationship, 150mC cm^{-2} μm^{-1} or 1.50 x 10^3C cm^{-3}, in Figure 3.2.3. The film volume, Vol, can be obtained from the polymerization charge Q_{pol}, that is Vol = $Q_{pol}/1.50 \times 10^3$ (cm^3). With use of the film mass m_{red}, we have:

$$\delta = 1.5 \times 10^3 \, m_{red}/Q_{pol} \qquad (3.4.4)$$

The units for m_{red} and Q_{pol} are respectively grams and coulombs. An average film density of 1.45 $\pm$ 0.12 g cm^{-3} is obtained for reduced poly-MPMPBF_4. This is in good agreement with the literature value (1.36 ~ 1.48 g cm^{-3}) for polypyrrole based polymers[10].

The concentration of pyridinium sites, which serve as ion exchange sites, C_{IE}, in poly-$MPMP^+$ is therefore calculated for the reduced film to be 5.6 M using the film density and the formula mass of the reduced form of the polymer (258.5 g mol^{-1} with BF_4^- as counterion).

3.5 Conclusion

Five pyrrole based polymers have been electrochemically synthesized. Constant current polymerization was used and the polymerization conditions have

been optimized. The polymerization conditions for poly-HPMP$^+$ demonstrate that free pyridine groups strongly inhibit electropolymerization. The film thicknesses for poly-MPMP$^+$ and poly-PPP$^+$ have been precisely determined by measuring the cross section of the film from scanning electron microscope pictures. The obtained conversion factors between polymerization charge and film thickness were 150 mC cm^{-2} μm^{-1} for poly-MPMP$^+$ and 95 mC cm^{-2} μm^{-1} for poly-PPP$^+$. The micrographs also reveal different morphology comparing poly-MPMP$^+$ with poly-PPP$^+$ and poly-PPTA$^+$. The former shows a dense morphology whereas the latter have a rough surface. Cyclic voltammograms of poly-MPMP$^+$ and poly-PPP$^+$, poly-PPTA$^+$ coated electrodes show well defined cathodic and anodic peaks with a linear relationship between the scan rate and peak current. The peak separation is near zero for poly-PPP$^+$ and poly-PPTA$^+$ at scan rates up to 200 mV s^{-1}, and 130 mV at 100 mV s^{-1} for poly-MPMP$^+$ coated electrodes. Elemental analysis of poly-MPMP$^+$ shows good agreement between the theoretical and analyzed values, and the degree of oxidation is calculated to be 0.16. Gravimetric experiments for poly-MPMP$^+$ were carried out to yield the film density (1.45 g cm^{-3}), the degree of oxidation (0.20), and the coulombic efficiency (0.8).

Reference

1. A.F. Diaz, J. Castillo, K. K. Kanazawa, J. A. Logan, M. Salmon and O. Fajardo, J. Electroanal. Chem., 133(1982)233.

2. N. J. Morse, D. R. Rosseinsky, R. J. Mortimer and D.J. Walton, J. Electroanal. Chem., 255 (1988) 119.

3. P. N. Bartlett, L-Y. Chung and P. Moore, Electrochimica Acta, 35 (1990) 1273.

4. P. G. Pickup and R. A. Osteryoung, J.Am. Chem. Soc., 106 (1984) 2294.

5. A. F. Diaz and J. I. Castillo, J. Chem. Soc. Chem. Commun., (1980) 397.

6. R. M. Penner, L. S. Van Dyke and C. R. Martin, J. Phys. Chem., 92 (1988) 5274.

7. K. Murao and F. Suzuki, Electrochem. Soc., 6, 135 (1988) 1415.

8. A. F. Diaz, J. I. Castillo, J. A. Logan and W. Lee, J. Electroanal. Chem., 129 (1981) 115.

9. P. Daum, J. R. Lenhard, D. Rolison and R. W. Murray, J. Am. Chem. Soc., 102 (1980) 4649.

10. G. K. Chandler and D. Pletcher, Spec. Period. Rep. Chem. Soc. Electrochem., 10 (1985) 117.

11. M. Salmon, A.F.Diaz, A.J. Logan, M. Krounbi and J. Bargon, Mol. Cryst. Liq.Cryst., 83(1982)265.

12. F. A. Diaz, Chem. Scr., 17 (1981) 145.

13. S. W. Feldberg, J. Am. Chem. Soc., 106 (1984) 4761.

Chapter 4

In Situ Electronic Conductivity Measurements

Electronic conductivity, or the rate of electron transport, is an important property of conducting polymers because it influences both electrochemical and catalytic processes (see Chapter 7). Therefore, the mechanism of electron transport in organic polymers is of particular interest. One of the most interesting aspects of conducting polymers is that their electronic conductivity is known to be a strong function of their oxidation state. Thus, they can reversibly be "switched" between their electronically conductive and their insulating states (see Section 1.1.2.). Therefore, it is important to measure conductivity as a function of potential. In order to obtain this dependence, an *in situ* technique, such as rotating disc voltammetry or a dual electrode method, is required. Another important reason for the use of an *in situ* technique is that most of the electrochemical applications involve an electrolyte; it is only *in situ* studies that are relevant to these applications. The results of electronic conductivity measurements are also of value in understanding charge transport mechanisms (see Chapter 5 and 6).

4.1 Rotating Disc Voltammetry

Rotating disc voltammetry (RDV) is an accurate and convenient method for investigating electron transport through polymer films. Steady state mass transport of electroactive species, *e.g.* ferrocene, to the polymer is ensured by the rotation of the electrode. The advantages of using rotating disc voltammetry have been shown in investigations of the kinetics of electron transport in redox polymer films[1], the mechanisms of charge transport through ion exchange polymer films[2], and the conductivity of conducting polymers[3,4]. The substrate (probe ion or molecule) can react (give or take electrons) either at the polymer/solution interface or at the underlying Pt electrode surface (type t_e in Albery's description[5]) by diffusion through the film. Conductivity measurements require the former pathway only. The film resistance is then evaluated by monitoring the flow of electrons between the Pt/polymer and polymer/solution interfaces. The size of the substrate molecule or ion must be large enough to prevent significant penetration into the film. The usual evidence for absence of penetration is the shifting of the apparent formal potential of the substrate to a higher potential, with the magnitude of the shift rising with increasing film thickness. Ferrocene has been chosen as a probe substrate in this work. Not only is ferrocene sufficiently large but it also is neutral (or positively charged when oxidized) and it would not be incorporated into the cationic ion exchange polymer, poly-MPMP$^+$. As shown in Figure 4.1.1,

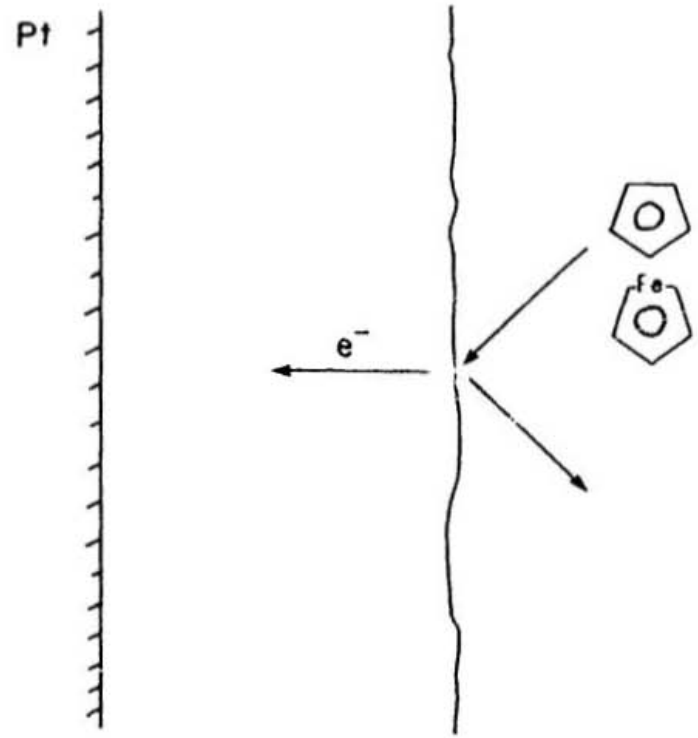

Figure 4.1.1. Schematic diagram of Ferrocene oxidation at the polymer/solution interface.

the ferrocene acts as an electron source at the surface of the polymer, and the electron flow (current) at different potentials provides information on the conductivity of the polymer.

4.1.1. The Rotating Disc Voltammograms of Ferrocene Oxidation at Poly-MPMP$^+$ Coated Electrodes

To achieve a steady mass transport state and to avoid a capacitance current, rotating disc voltammograms were recorded using small potential steps with current collection after 20 seconds at each desired potential. Figure 4.1.2. shows rotating disc voltammograms of 5.0 mM ferrocene in acetonitrile at: A, a bare Pt electrode; B, a thin film of poly-MPMP$^+$ (0.5 μm): and C, a thick film 10 μm.

The voltammograms at the coated electrodes shift to higher potentials as the film thickness increases. Near the formal potential of ferrocene (0.405 V), no current is observed for polymer coated electrodes. This is an indication that the ferrocene molecules do not diffuse through the polymer to react at the underlying Pt electrode. Although the formal potential may shift in some cases when the substrate reacts within a polymer film because of the different electrochemical environment, the dependence of the potential shift on the film thickness in Figure 4.1.2 rules out the this explanation here. The potential shift of ferrocene oxidation at poly-MPMP$^+$ must be caused by the resistance of the polymer film, which

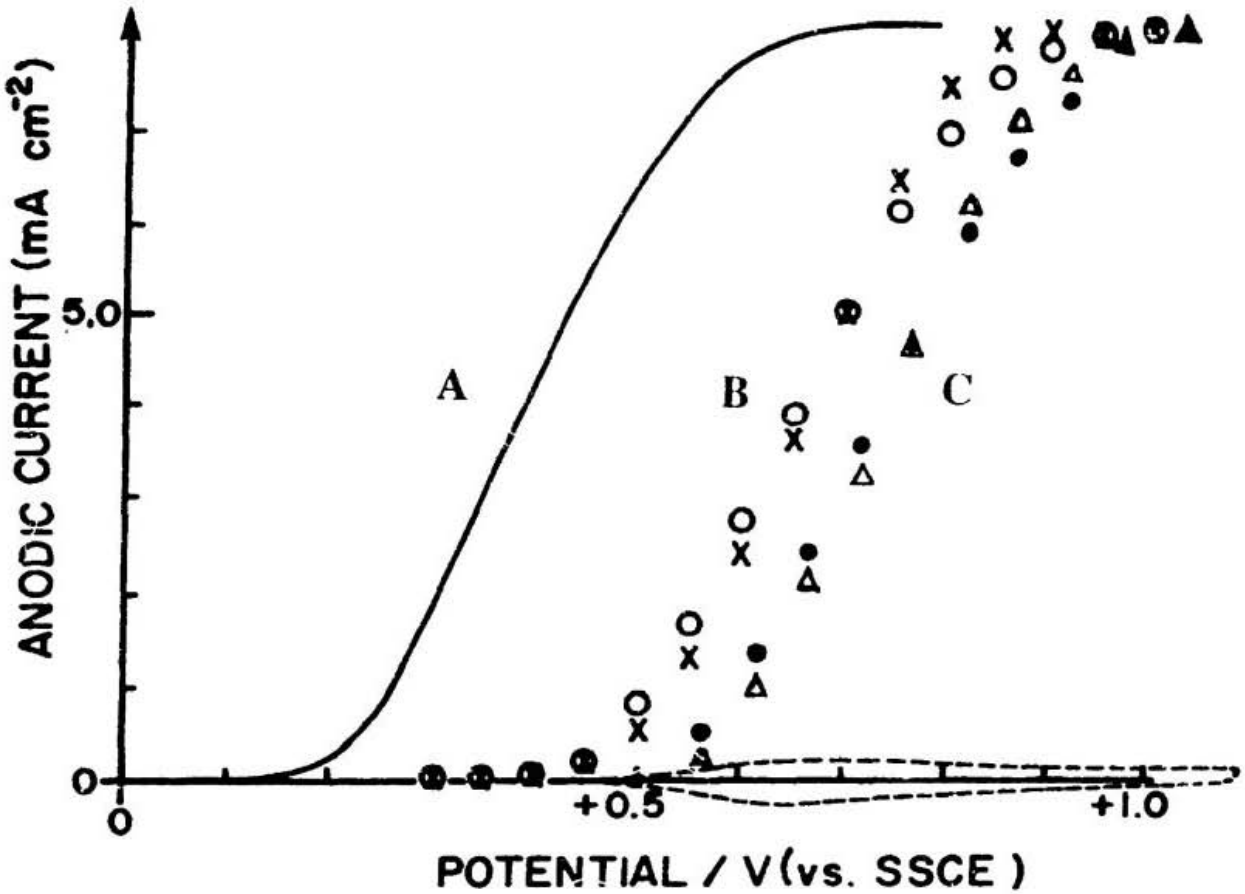

Figure 4.1.2. Rotating disc voltammograms (2000 rpm) in 5 mM ferrocene $LiClO_4/CH_3CN$ solution. (A): a bare Pt electrode; (B): thin film (0.5 μm) of poly-$MPMP^+$ coated electrode; (C):thick film (10 μm) of poly-$MPMP^+$ coated electrode. o and ● represent the forward scan; x and Δ are cathodic scans. Current was measured after 20 s at each potential. The dashed line is a cyclic voltammogram (10 mV s^{-1}) of a stationary, 0.5 μm poly-$MPMP^+$ coated Pt electrode in the same solution.

changes with film thickness Ferrocene acts solely as an electron source at the film/solution interface.

The shapes of the voltammograms for coated electrodes are almost identical to the shape at the bare electrode. The difference in potential between a coated electrode and a bare Pt electrode at any current is approximately constant. This demonstrates that mass transport and electron transfer at the polymer/solution interface are similar to the processes that occur at a Pt/solution interface for a bare Pt electrode. In other words, ferrocene oxidation at the film/solution interface is controlled by the film surface potential.

The effects of ohmic potential drop, iR_u, in these experiments must be accounted for because the currents are high and uncompensated resistance distorts the rotating disc voltammograms. This correction has been made by using the general equation[6]:

$$E_{app} = E_{1/2} + \frac{RT}{nF} Ln(\frac{i}{i_l - i}) + iR_u \qquad (4.1.1)$$

where E_{app} and $E_{1/2}$ are respectively the applied and half wave potentials; and i_l and R_u are the limiting current and uncompensated resistance respectively. Other parameters, i, R, T, n and F retain their usual meanings. Rearrangement gives:

$$[E_{app} - \frac{RT}{nF} Ln(\frac{i}{i_l - i})] = R_u i + E_{1/2} \qquad (4.1.2)$$

By plotting the left hand side of equation (4.1.2) against i, a linear relation is revealed in Figure 4.1.3. The slope and intercept give the uncompensated resistance (48 $\pm$ 2 Ω) and half wave potential (0.398 $\pm$ 0.004 V) respectively. This correction has been applied to all data reported in this chapter, which were obtained from rotating disc voltammetry.

4.1.2. Data Analysis

It is clear from the rotating disc voltammograms in Figure 4.1.2 that the conductivity of poly-MPMP$^+$ is strongly dependent on the potential applied to the polymer. Accordingly, the potential profile across a film during the mediated oxidation of ferrocene will be similar to that shown in Figure 4.1.4. E_{Pt} and E_S are the potential of the Pt electrode and potential at the polymer/solution interface, respectively. d is the film thickness. Simplistically, the conductivity of a film can be estimated by using the following equation:

$$\sigma = id/(E_{Pt} - E_S)A \qquad (4.1.3)$$

where σ is an average conductivity across the film, i and A are the current and electrode area, respectively. However, the potential to which this conductivity corresponds is not clear. The polymer closest to the Pt surface will have the highest conductivity and conductivity sharply decreases near the solution/film interface. Therefore this average conductivity is not a useful parameter. The true

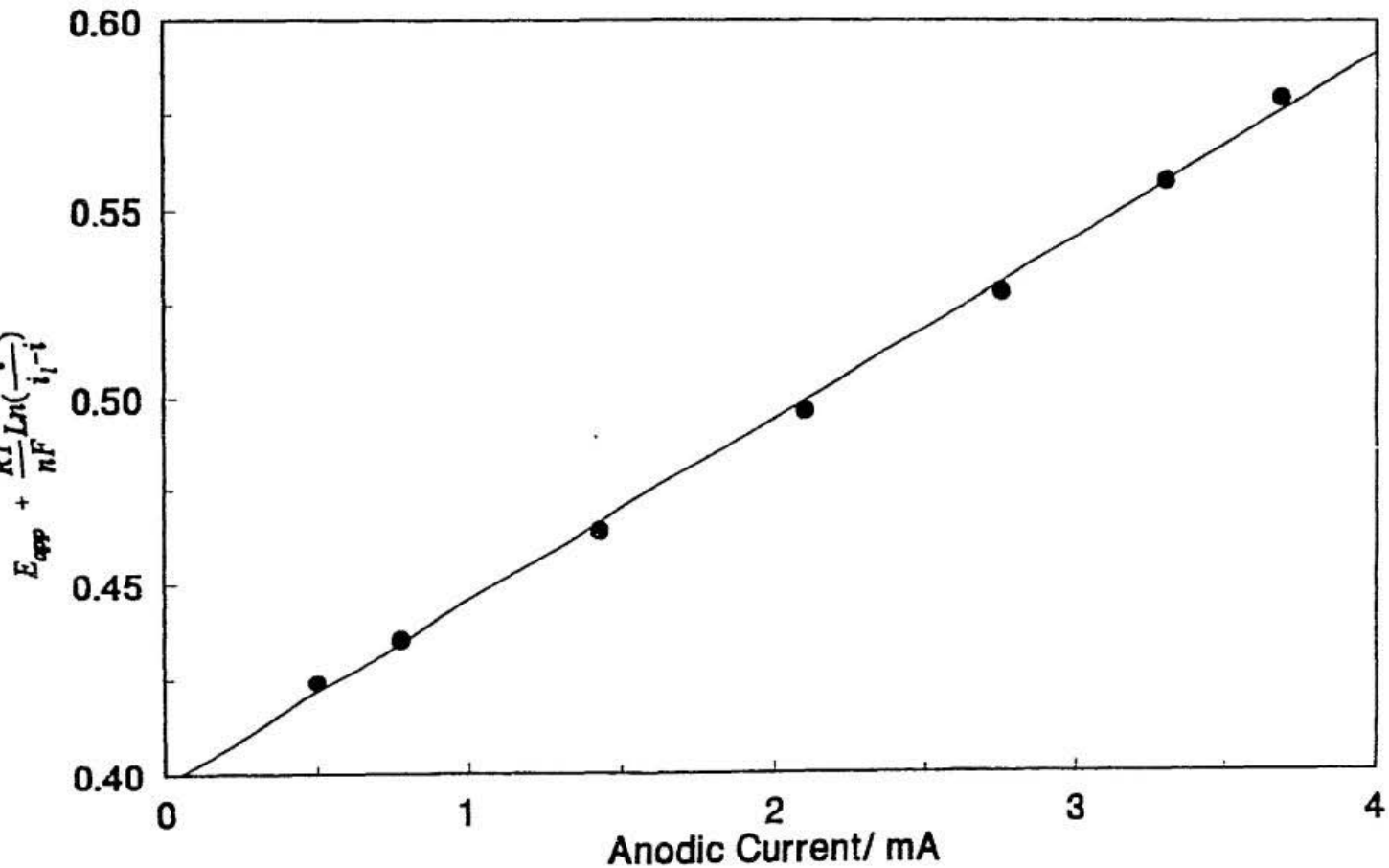

Figure 4.1.3. Plot of equation 4.1.2 for ferrocene oxidation at a bare rotating disc Pt electrode (2000 rpm) in 5 mM ferrocene Et_4NBF_4/CH_3CN solution.

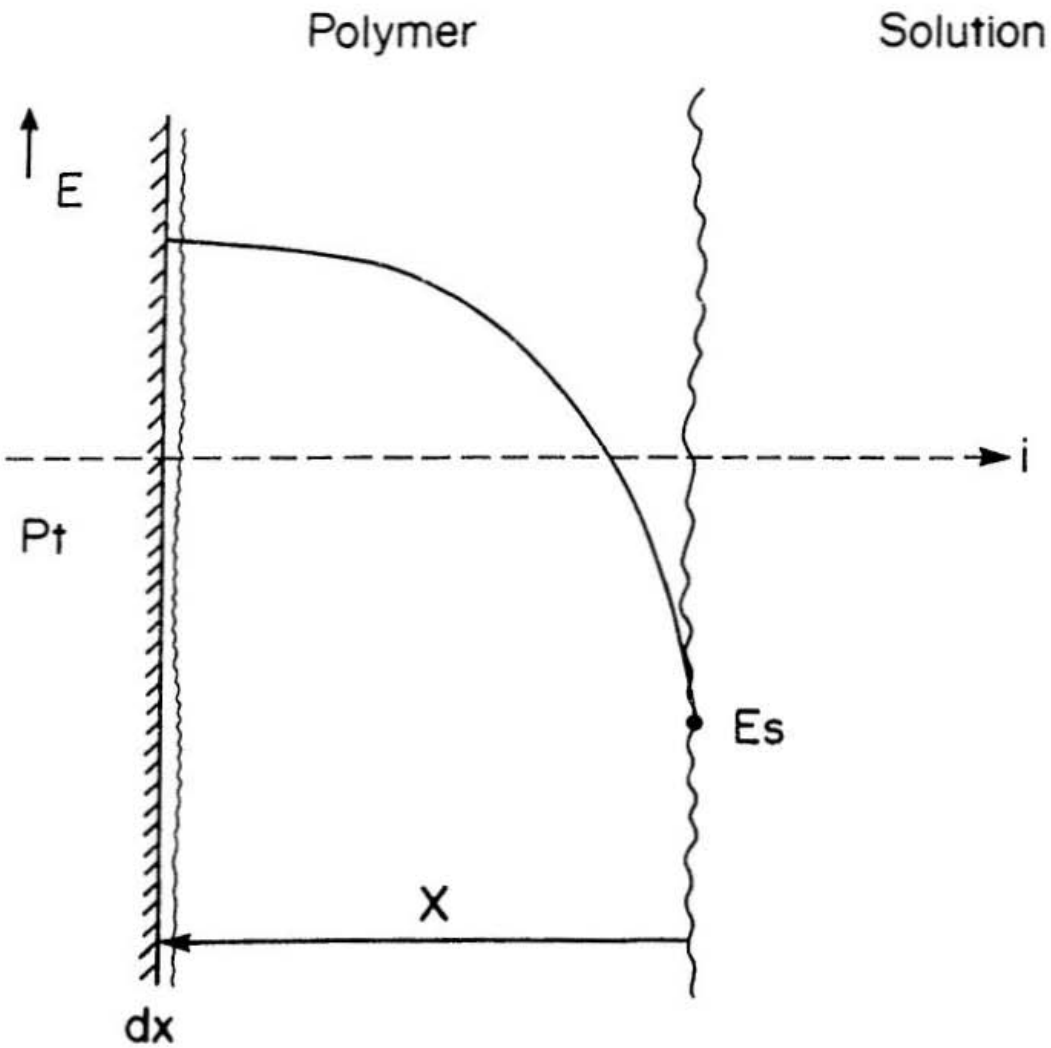

Figure 4.1.4. A schematic diagram of the dependence of film potential on the distance to the Pt surface.

conductivity of the polymer at the applied potential can be obtained only if a layer of film nearest to the Pt surface with an infinitesimally small thickness, dx, is considered, as shown in Figure 4.1.4. This layer is held at the potential of the Pt electrode which is set by the potentiostat and is recorded in the rotating disc voltammogram. In the following discussion, E_{Pt} represents the potential of the polymer contacting the Pt electrode.

As mentioned in the last section, voltammograms of coated electrodes shift to more positive potential as the film thickness increases. If we plot the film potential, E_{Pt}, against film thickness at a certain current i_{ss}, an exponential curve is revealed. Therefore, a linear relationship between E_{Pt} and logarithm of film thicknesses ranging from 0.5 μm to 10 μm is shown in Figure 4.1.5 and this can be expressed as:

$$E_{Pt} = s\,Ln(d) + c \qquad (4.1.4a)$$

Equation (4.1.4a) expresses the exponential relationship between the film potential and film thickness at a specific current. This relationship also applies to the potential profile across a film which can be written as:

$$E = s\,Ln(x) + c \qquad (4.1.4)$$

The constants s and c are slightly dependent on the value of the current. This equation is not rigours if x is so small that the film potential is dominated by the

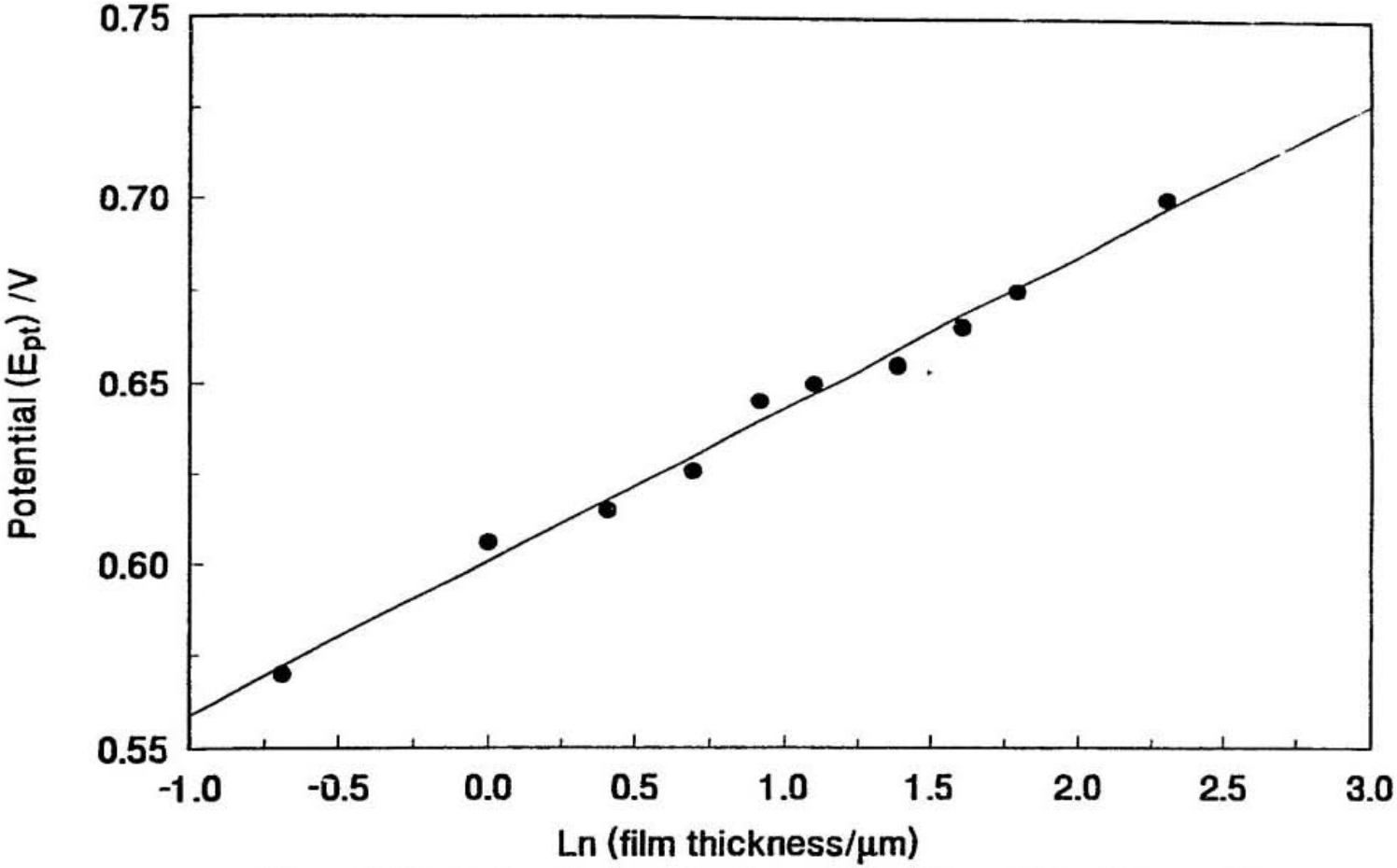

Figure 4.1.5. A plot of potential at Pt *vs.* the logarithm of film thickness. Film thicknesses range from 0.5 to 10 μm; potentials measured at 0.25 mA (see Figure 4.1.7).

solution potential E_s. Figure 4.1.6 shows that the relationships between both *s*, *c* and the current are linear. The origin of these relationships is not clear.

A plot of conductivity against film potential is the best way to display the *in situ* results. In order to draw this plot, an equation which gives a relationship between film thickness and conductivity is needed to calculate conductivity. Looking back to Figure 4.1.4, one can assume that the imagined very thin layer of polymer with a thickness of *dx* obeys Ohm's law. Then the resistance, R, for this layer of film should be the ratio of the potential difference *dE* and the current i_o:

$$R = dE/i_o \tag{4.1.5}$$

Converting this resistance to a conductivity, we have:

$$\sigma = \frac{i_o}{(\frac{dE}{dx})\,A} \tag{4.1.6}$$

Differentiating both sides of equation (4.1.4), we have

$$\frac{dE}{dx} = \frac{s}{x} \tag{4.1.7}$$

Substituting equation (4.1.7) into equation (4.1.6), we get:

$$\sigma = \frac{i_o x}{sA} \tag{4.1.8}$$

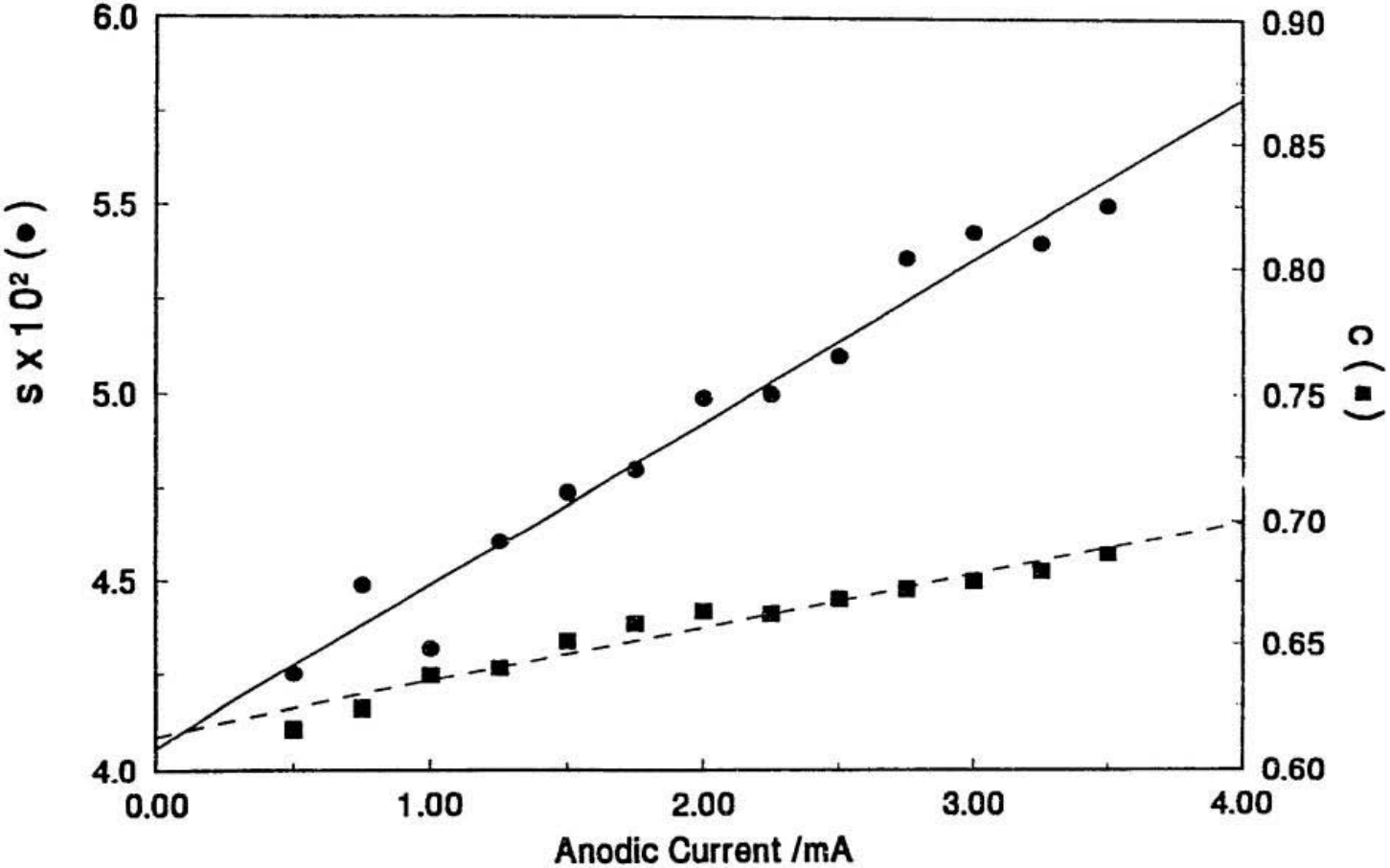

Figure 4.1.6. Linear relations between constants c, s and current *i*.

for constant i_o. This equation predicts that the film conductivity measured by RDV should be independent of the properties of the probe ion or molecule since the equation does not involve any terms which are related to the properties of probe ion or molecule. In other words, whatever electroactive species (as long as no penetration into the film occurs) is used in the solution, the half wave potential of the RDV will remain unchanged. If any other substrate with a different formal potential is employed in the solution, only the potential at the film/solution interface will be different at the same current. This property has been confirmed by Pickup[7]. The current at the coated electrode rises at the same potential regardless of whether $Cr(bp)_3^+$, $Cr(bp)_3^{2+}$ or ferrocene is being oxidized. Pickup used the assumption that conductivity increases exponentially with potential to derive equation 4.1.8. It was reported that the equation was not accurate for potentials above 0.6 V for poly-$MPMP^+$. However, the validity of equation 4.1.8 can be extended if s is allowed to vary with potential.

Solving equation (4.1.8) for x, and substitution into equation 4.1.4, gives:

$$Ln(\sigma) = \frac{1}{s}E - [Ln(\frac{sA}{i_o}) + \frac{c}{s}] \qquad (4.1.9)$$

This equation indicates that conductivity for a conducting polymer is exponentially related to potential. Naturally, the experimental data follow the equation since x was merely converted linearly to conductivity σ by using equation (4.1.8). This

equation is rigorous only at the current to which the values of s and c apply. Thus, for accurate measurements, s and c have to be determined for each current used. In summary, the procedure of the *in situ* conductivity measurement is listed as follows:

(1) Chose a moderate rotating rate to obtain the highest current without causing turbulence and wide range of potential can be covered. As shown in Figure 4.1.7, at a desired current i_o (less than 96% of limiting current), the potentials E_{Pt} are measured at films with corresponding film thicknesses d.

(2) Plot the potentials E_{Pt} against logarithmic film thicknesses d to obtain a slope s.

(3) The conductivity at potential of the polymer/electrode enterface, E_{Pt}, for a film with thickness d at current i_o, is calculated from equation 4.1.8 ($\sigma = i_o x/sA$), with $x = d$.

(4) Steps (1) to (3) are repeated at different currents to obtain more data, and a wider range of potentials are covered.

(5) The relationship between conductivity and potential is obtained by a plot of Log (conductivity) against corresponding potentials.

Figure 4.1.8. depicts the plot of the logarithm of conductivity vs. potential for poly-MPMP$^+$ in acetonitrile solution. For these data, the current covers the range from 3% up to 96% of the limiting current while the film thicknesses ranged

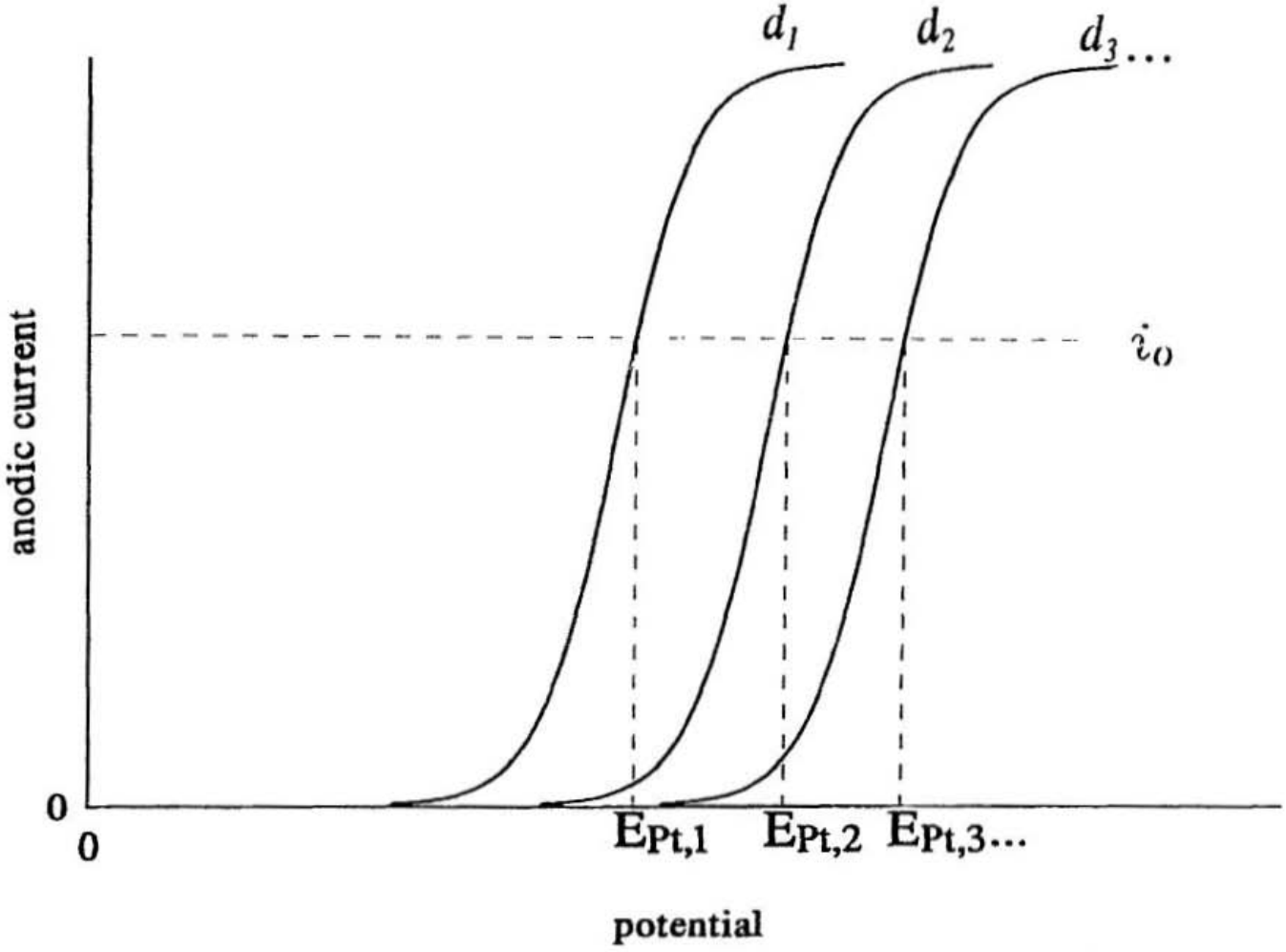

Figure 4.1.7. A schematic diagram of measuring data from rotating disc voltammograms. d_1, d_2, d_3... represent different film thicknesses.

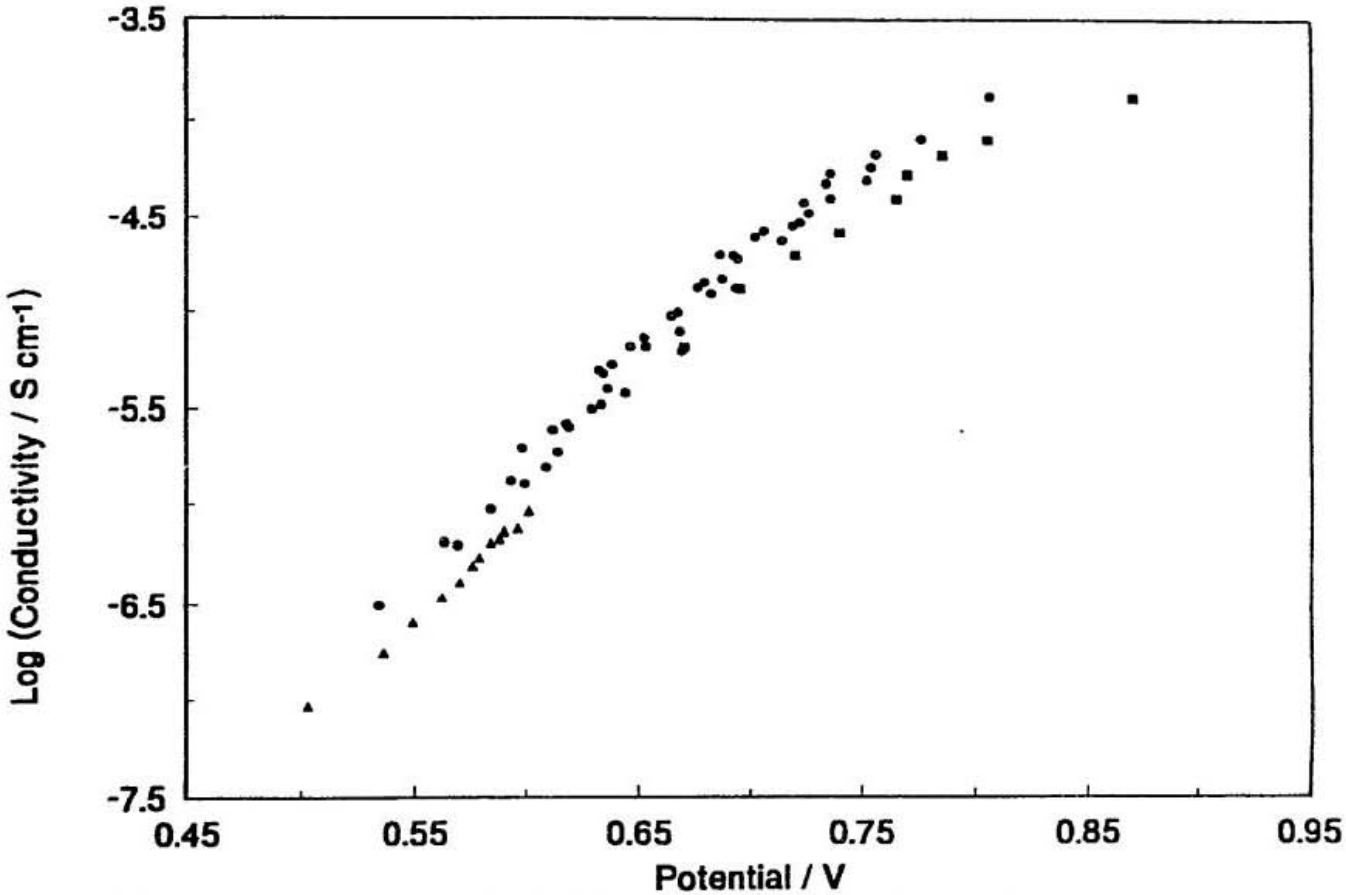

Figure 4.1.8. A plot of Log_{10}(conductivity) *vs.* potential for poly-MPMP$^+$ coated electrode on 0.1M Et_4NBF_4/CH_3CN solution. Different symbols represent different film thicknesses from 0.5 (▲) to 10 (■) μm and others in between.

from 0.5 μm to 10μm. The conductivity increases exponentially with potential but begins to level off at potentials above 0.77 V. The levelling of the curve could be due to the electrical conductivity of the polymer becoming ohmic (independent of potential) at potentials above +0.77 V (formal potential of poly-MPMP$^+$). This phenomenon has been reported for polypyrrole by Murray and coworkers[8] and many other groups. The highest conductivity is *ca* 1 x 10^{-4} S cm^{-1} for poly-MPMP$^+$.

4.2 Dual Electrode Conductivity Measurements

Dual electrode voltammetry (DEV) is a sandwich electrode technique[9]. Figure 4.2.1. shows a dual electrode. The polymer is coated onto one of the Pt disc electrodes; then a thin layer of gold is deposited onto the polymer and the second Pt disc in vacuum. Both sides of the film are attached to metals. The gold layer is porous enough to allow access of both the solvent and the electrolyte. The potentials at each side of the film can be conveniently controlled by a dual potentiostat. This technique does not require any electroactive species in solution.

The potentials applied to each side of the film are controlled in two different ways. In one experiment, the potential of the gold coated side is fixed at a low potential relative to the reference electrode in order to keep the polymer reduced, and the potential of the other side is scanned. This experiment is called "fixed

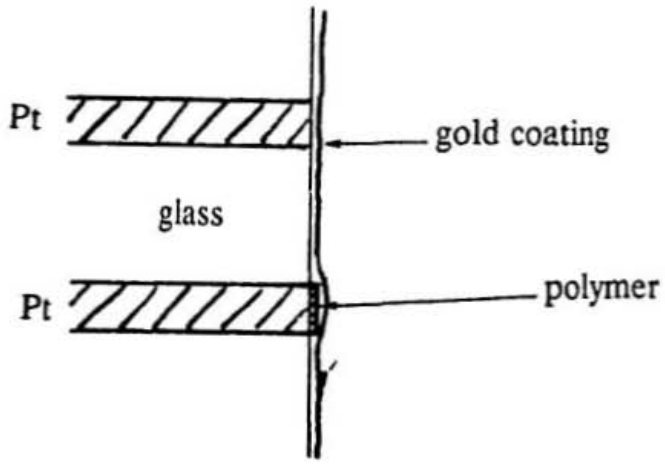

Figure 4.2.1. Schematic diagram of dual electrode.

gold potential" in later discussions. In the second experiment, DEV is conducted by keeping a small constant potential difference (5 - 10 mV) between the two sides of the polymer; both are scanned synchronously relative to the reference electrode. The conductivity is calculated from the potential difference and the current passing through the film.

4.2.1. Conductivity Measurement for Poly-MPMP$^+$ by Dual Electrode Voltammetry at Fixed Gold Potential

Figure 4.2.2 shows a dual electrode voltammogram of poly-MPMP$^+$ in 0.1 M Et_4NBF_4/CH_3CN solution. A potential of +0.3 V was applied to the gold electrode throughout the experiment while a potential scan was applied to the Pt electrode. This arrangement is similar to rotating disc voltammetry of ferrocene at the poly-MPMP$^+$ coated electrode (section 4.1.1). The principle is the same as the case in section 4.1.2. Conductivities at different potentials are calculated using the same procedures as in RDV (see the list (1) to (5) in section 4.1.2). The results are shown in Figure 4.2.3. The conductivity increases exponentially with potential but begins to level off at potentials above 0.8 V. The data below the formal potential of 0.77 V (because of the levelling off) in Figure 4.2.3 were fitted to a linear equation to give $y = 10.75\ x\ -12.51$. The data ($E_{Pt} < 0.77$ V) in Figure 4.1.8 were also fitted to a linear equation: $y = 11.11\ x\ -12.53$. The

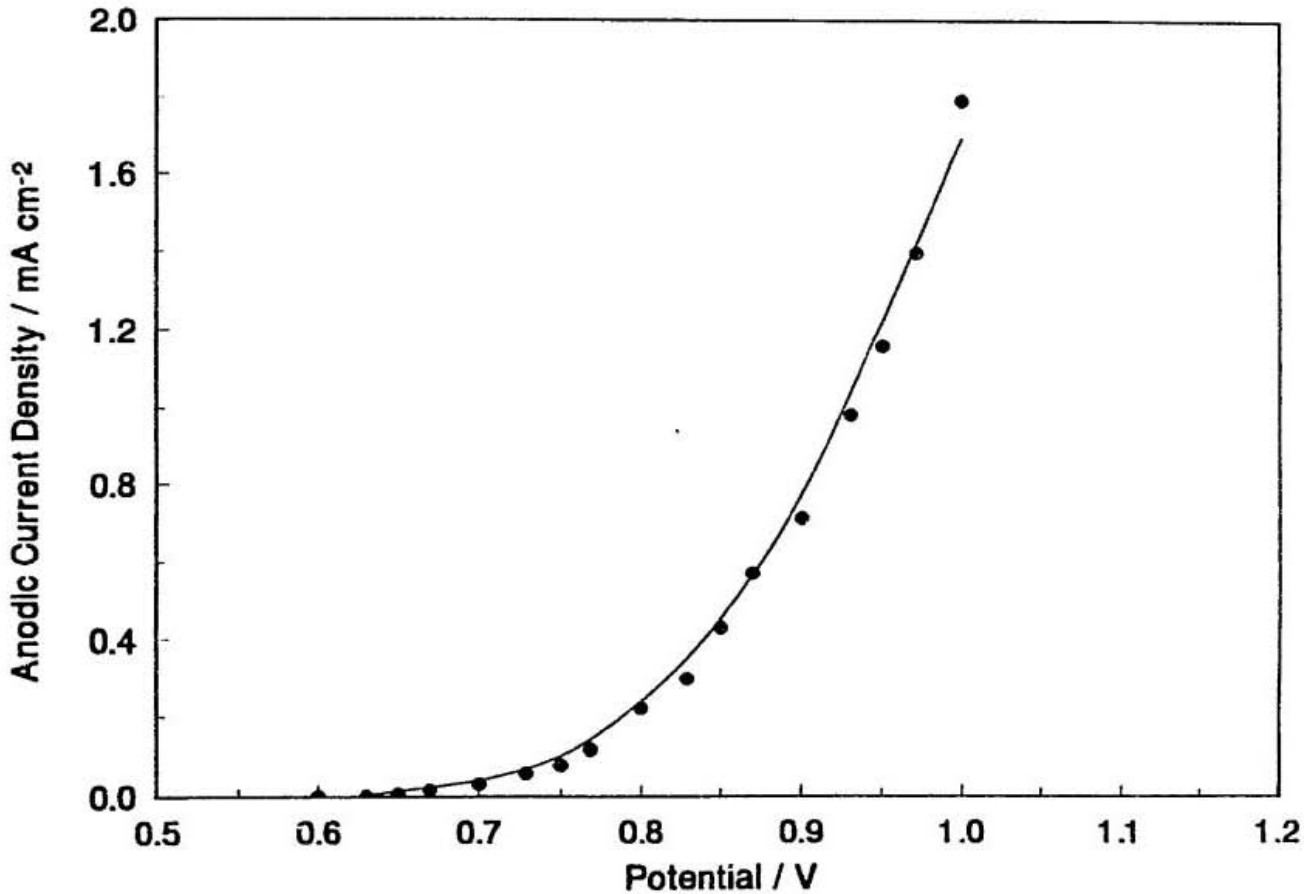

Figure 4.2.2. Voltammogram of dual electrode experiment at a fixed gold potential of 0.3V for poly-MPMP$^+$ in 0.1 M Et_4NBF_4/CH_3CN solution. Film thickness = 0.5 μm.

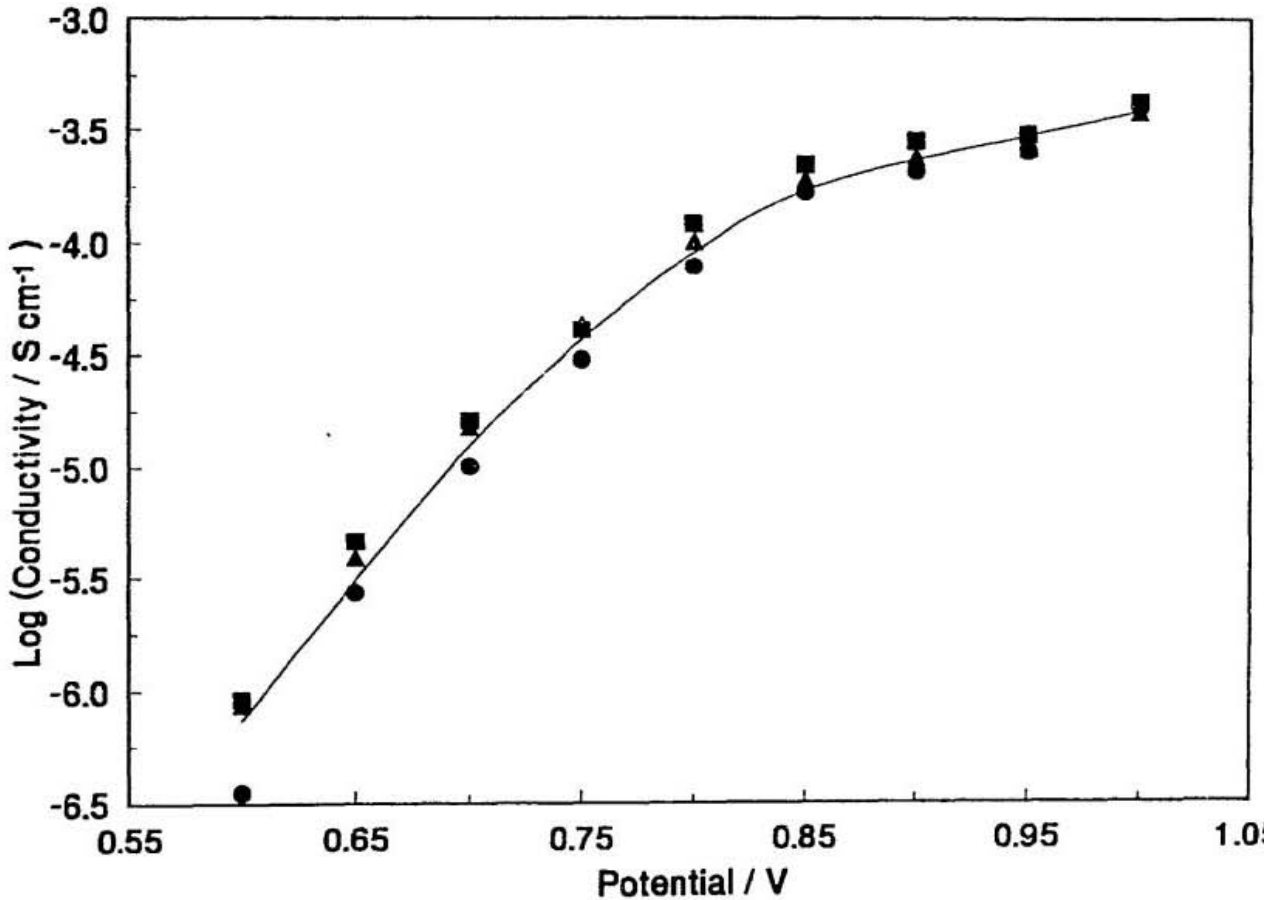

Figure 4.2.3. A plot of Log_{10}(conductivity) *vs.* potential for poly-MPMP$^+$ coated electrodes at a fixed gold potential of 0.3V in 0.1 M Et_4NBF_4/CH_3CN solution. ●, ■ and ▲ represent film thicknesses 0.25,0.5 and 0.75 μm respectively.

similarity of the slopes and intercepts demonstrates that the method derived in section 4.1 is also applicable here.

4.2.2. Conductivity Measurements for Poly-MPMP$^+$ Using Dual Electrode Voltammetry with A Small Fixed Potential Difference.

This measurement was carried out with a small potential difference, ΔE = 10 mV, and the film potential was scanned using the dual potentiostat. The conductivity across the film is considered constant because each side of the film is at approximately the same potential. A simple equation is used to calculate the film conductivity:

$$\sigma(E) = id/A\Delta E \qquad (4.2.1)$$

where d and A are the film thickness and electrode area respectively. Figure 4.2.4. shows the dual electrode voltammogram for a dual electrode with one disc coated with poly-MPMP$^+$ in 0.1 Et_4NBF_4/CH_3CN solution. A potential difference of 10 mV was held throughout the synchronous potential scanning. The forward scan overlaps with the cathodic scan, but a loop appears at high potentials. With the loop present, the average of the cathodic and anodic currents were used in the measurement. The film potential is measured in the following way. At a desired potential E on Figure 4.2.4, a corresponding current i is measured and the conductivity is calculated from equation 4.2.1 for this potential. More conductivity

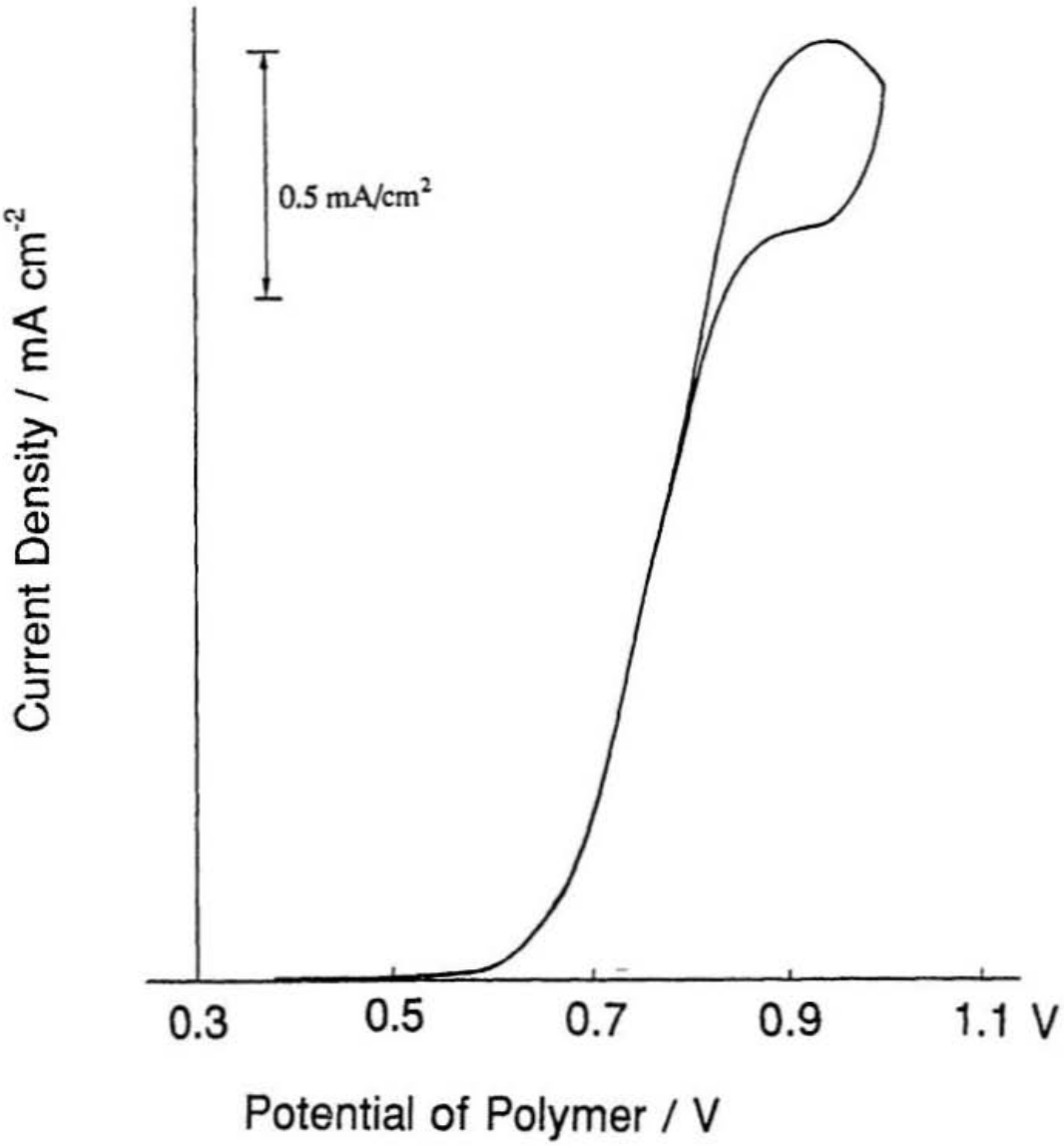

Figure 4.2.4. Voltammogram of dual electrode experiment at fixed small potential difference (ΔE = 10 mV) for poly-MPMP$^+$ in 0.1 M Et_4NBF_4/CH_3CN solution. Film thickness = 0.5 μm; scan rate = 10 mV s^{-1}.

and corresponding potential data for different films are listed in Table 4.1.

Table 4.1 Data of dual electrode voltammetry with a small fixed potential difference for poly-$MPMP^+$.

film thickness (μm)	film potential (V)	current density (mA cm^{-2})	conductivity,σ (S cm^{-1} x10^{-5})	$Log_{10}(\sigma)$
0.25	0.60	1.4	0.35	-5.45
	0.65	3.9	0.98	-5.01
	0.70	13	3.4	-4.47
	0.75	30	7.4	-4.13
	0.80	47	12	-3.93
	0.85	57	14	-3.85
	0.90	64	16	-3.80
	0.95	68	17	-3.77
	1.00	69	17	-3.76
0.50	0.60	0.39	0.20	-5.70
	0.65	1.6	0.71	-5.15
	0.70	6.0	3.0	-4.52
	0.75	13	6.3	-4.20
	0.80	19	9.3	-4.03
	0.85	22	11	-3.95
	0.90	24	12	-3.92
	0.95	24	12	-3.91
	1.00	25	12	-3.91
0.75	0.60	0.39	0.29	-5.54
	0.65	1.4	1.1	-4.97
	0.70	4.6	3.4	-4.47
	0.75	10	7.8	-4.11
	0.80	16	12	-3.91
	0.85	20	15	-3.83
	0.90	22	16	-3.79
	0.95	23	17	-3.77
	1.00	24	18	-3.74

conductivity is plotted against film potential as shown in Figure 4.2.5. Similar to the RDV measurement, the conductivity increases exponentially with potential and levels off at ca. 0.8 V. The conductivity becomes independent of potential above 0.8 V, characteristic of an ohmic conductor. Figure 4.2.5 also shows that the conductivity can be measured at potentials as high as 1.0 V by dual electrode voltammetry, while the RDV method would require a film as thick as ca. 30 μm to achieve the same potential.

4.2.3. Conductivity Measurements for Poly-PPP$^+$ And Poly-PPTA$^+$ Using Dual Electrodes with a Small Fixed Potential Difference

Many attempts were made to use dual electrodes to measure the conductivity of poly-PPP$^+$ and Poly-PPTA$^+$ in solution. They were unsuccessful due to the excessively rough surfaces of these polymers (see the scanning electron microscope pictures in Section 3.2, Figure 3.2.5). Useful dual electrode voltammograms in solution could not be obtained. However, the maximum conductivities of poly-PPP$^+$ and poly-PPTA$^+$ were estimated by measuring the resistances of the dry sandwiched films (dual electrode) in their oxidized form. The results are listed in Table 4.2. The failure of these experiments for poly-PPP$^+$ and poly-PPTA$^+$ tells us that although the dual electrode method has several advantages, technical difficulties can be encountered in its application.

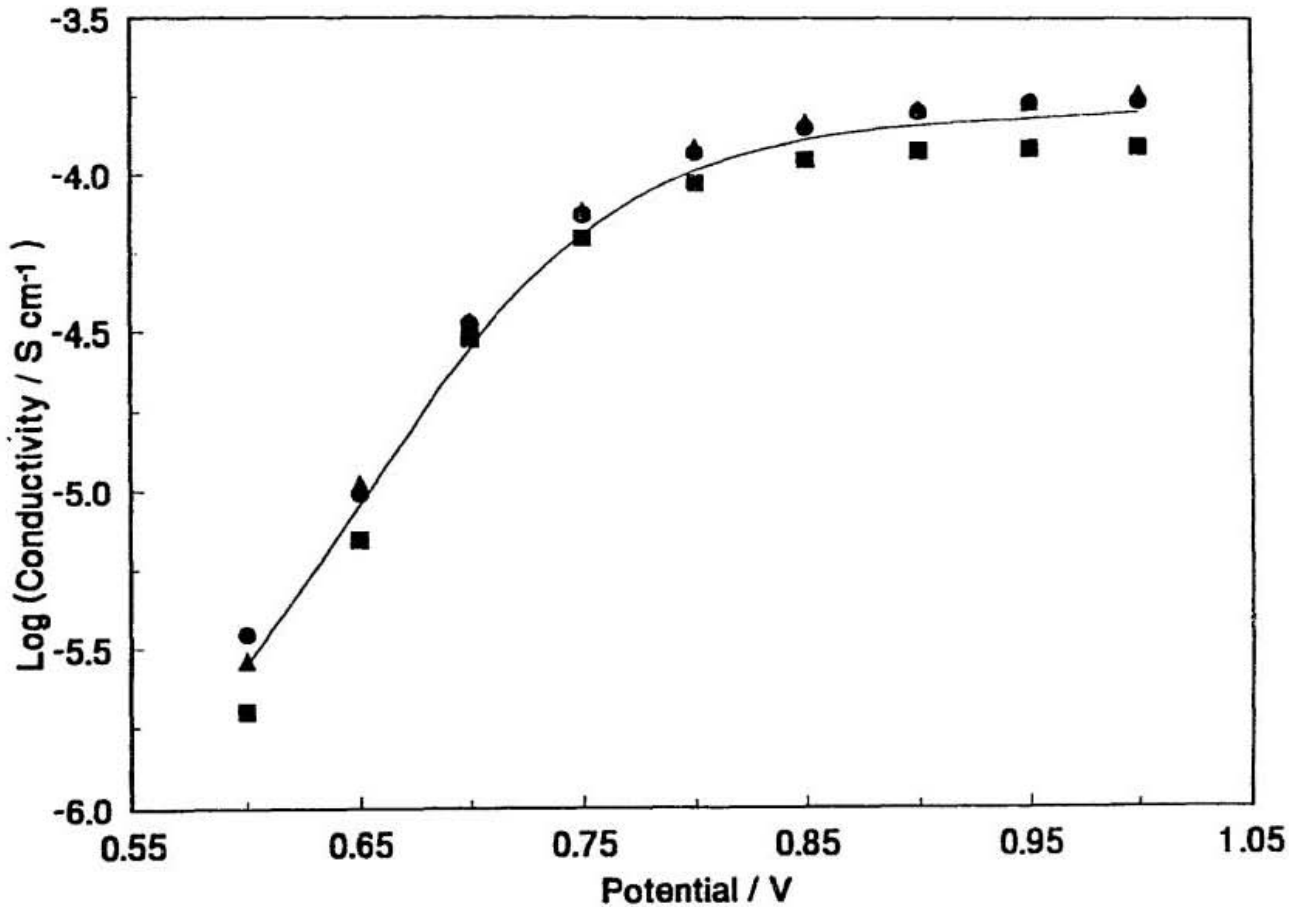

Figure 4.2.5. A plot of conductivity *vs.* potential for poly-MPMP$^+$ coated electrodes at fixed small potential difference ($\Delta E = 10$ mV) in 0.1 M Et_4NBF_4/CH_3CN solution. Different lines represent data from different film thicknesses of 0.25(●), 0.5(▲) and 0.75(■)μm.

Table 4.2. Conductivities of poly-PPP$^+$ and poly-PPTA$^+$.

polymer	film thickness (μm)	conductivity, σ x 10^5 (S cm^{-1})	average σ x 10^5 (S cm^{-1})
poly-PPP$^+$	0.46	6.1	6.1 $\pm$ 0.4
	0.90	5.7	
	1.0	6.0	
	2.8	6.7	
poly-PPTA$^+$	0.5	1.6	3.4 $\pm$ 1.8
	1.8	3.2	
	2.7	5.9	
	3.6	2.8	

The gold coating could penetrate deep into the film or a short could occur to give overestimated results. It could also be broken along some vertical surfaces which would give underestimated conductivity or yield no conductivity. In some cases, rather high conductivity could be measured immediately after gold coating when the film was dry, but the conductivity was not measurable once the electrode was immersed in the solution. This suggests that swelling of the film in the acetonitrile solvent causes cracks in the gold coating. Thick polymer films frequently failed to provide reliable results presumably due to the large vertical area around the edge where it is difficult to obtain a good gold coating.

4.2.4 Summary of Results for Poly-MPMP$^+$

The conductivity results for poly-MPMP$^+$ determined from the three *in situ* methods are plotted in Figure 4.2.6. The circles, triangles and squares are respectively the results from ferrocene RDV, fixed gold potential dual electrode voltammetry and small potential difference dual electrode voltammetry. They are in reasonably good agreement. The conductivity changes over 4 orders of magnitude from the reduced form to the oxidized form. The linear section up to 0.8 V indicates that the conductivity of poly-MPMP$^+$ increases approximately exponentially with potential before the film is fully oxidized (the formal potential of this polymer is 0.77 V). It then appears to be an ohmic conductor when it is oxidized. The slope of the linear portion shows that for every 90 mV change of potential, the conductivity changes by one order of magnitude. The maximum conductivity is about 1 x 10^{-4} S cm^{-1}.

4.3. Electronic Conductivity of Poly-BPP

The conductivity of poly-BPP has been measured by DEV in acetonitrile using the small potential difference technique. A dual electrode voltammogram and a cyclic voltammogram are shown in Figure 4.3.1. The forward and reverse scans do not overlap so the average of cathodic and anodic current were used in

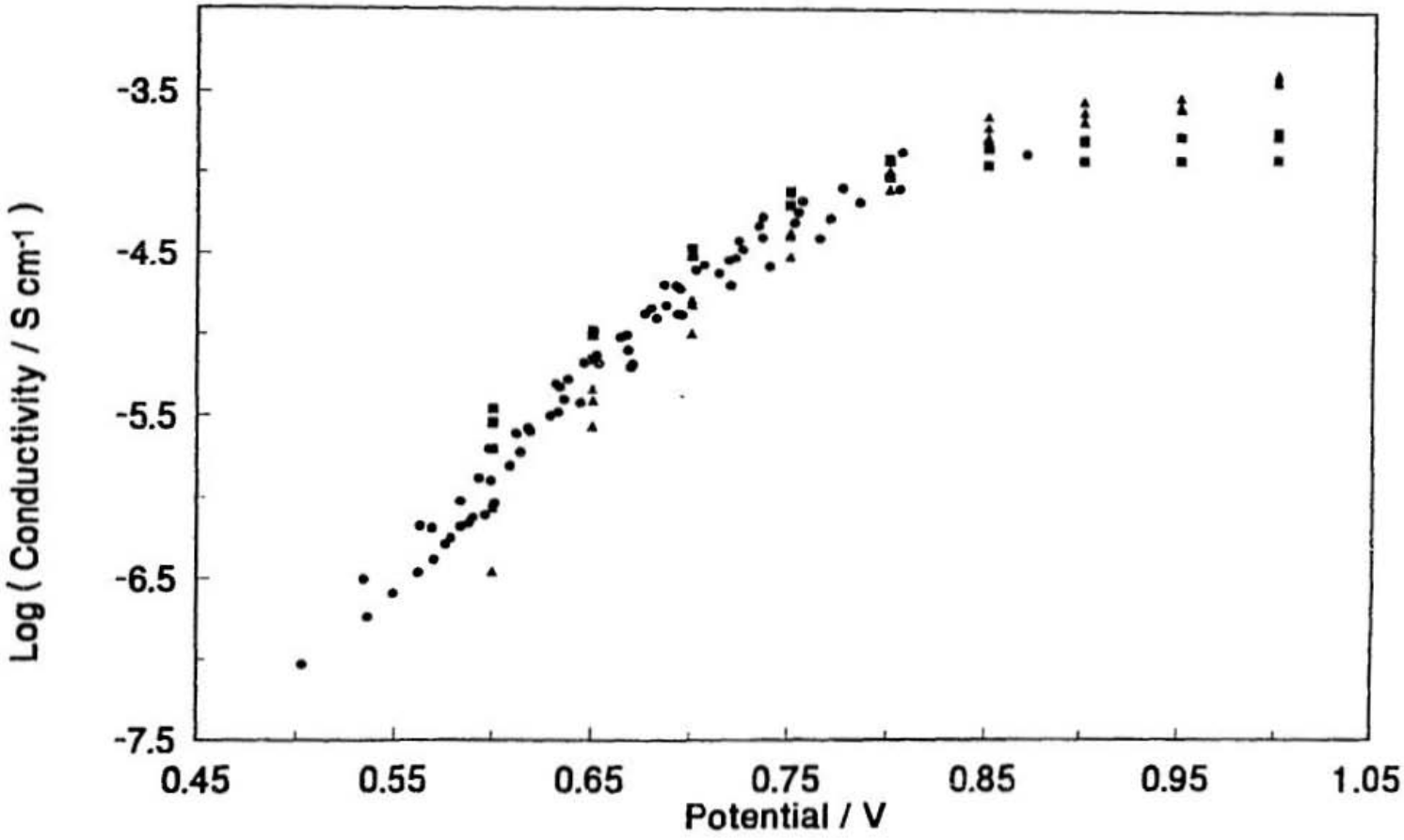

Figure 4.2.6. A comparison of conductivity of poly-MPMP$^+$ measured by different methods: Rotating disc voltammetry(●); Dual electrode voltammetry at 10 mV potential difference(■); Dual electrode voltammetry at fixed gold potential(▲).

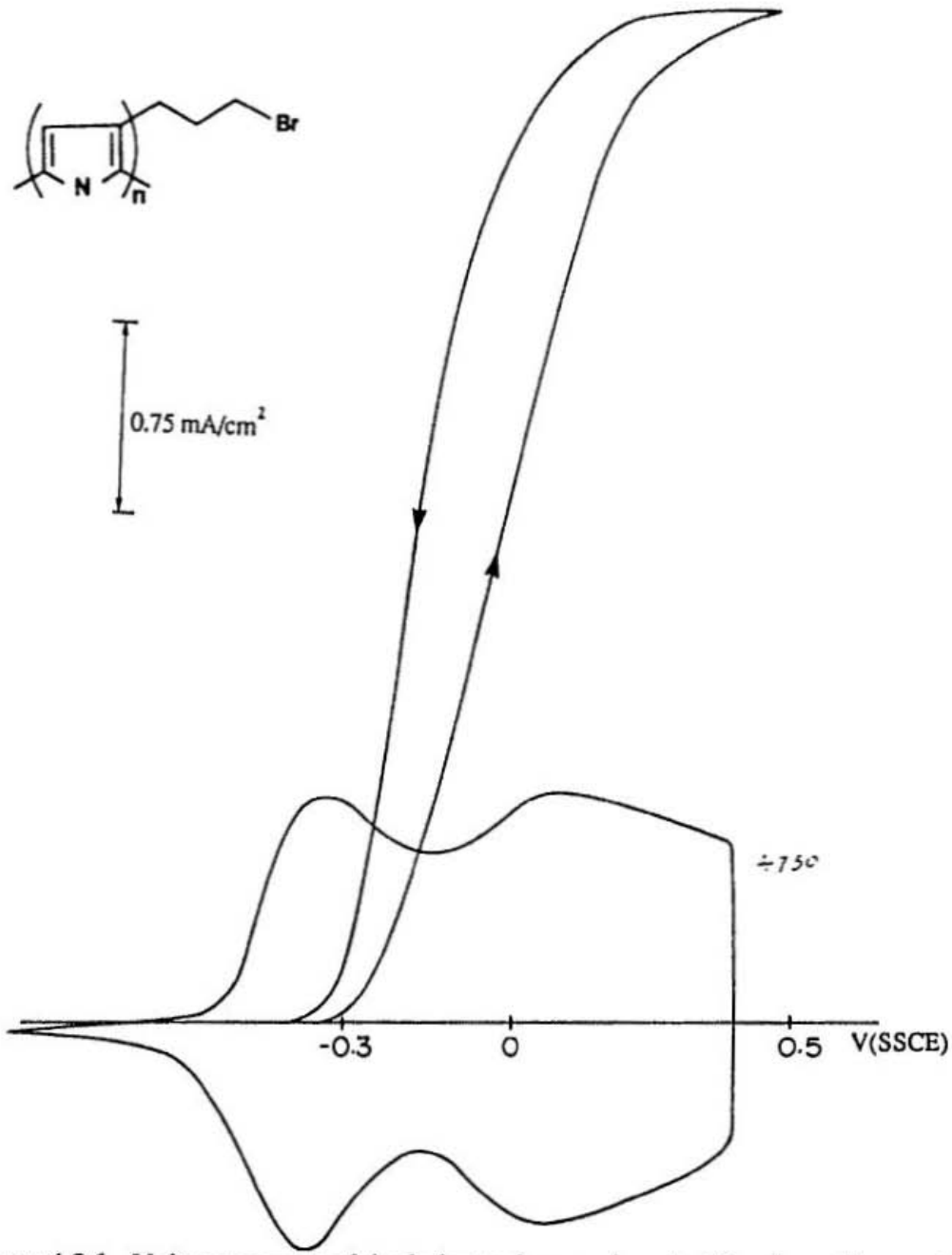

Figure 4.3.1. Voltammogram of dual electrode experiment at fixed small potential (ΔE = 10 mV) for poly-BPP in 0.1 M Et_4NBF_4/CH_3CN solution. Film thickness = 0.5 μm.

the calculation for film conductivity. Surprisingly, the conductivity does not rise until the first oxidation peak at -0.35 V has been passed. The first oxidation process of the film does not appear to make it conductive.

Figure 4.3.2 shows how the conductivity varies with potential for two films (0.44 and 0.55 μm). A linear portion appears at low potential with a slope of *ca.* 70 mV per decade, which is not higher than for poly-MPMP$^+$. This demonstrates that the slope may be a characteristic of the polymer. Also, the conductivity becomes independent of potential at potentials above -0.2 V, exhibiting a maximum conductivity *ca.* 10^{-2} S cm^{-1}. This is about two orders of magnitude higher than that of poly-MPMP$^+$.

The following experiment helps to explain the origin of the conductivity difference between the two polymers. The reaction below was carried out on a poly-BPP dual electrode assembly in which the bromine is gradually replaced with trimethylamine.

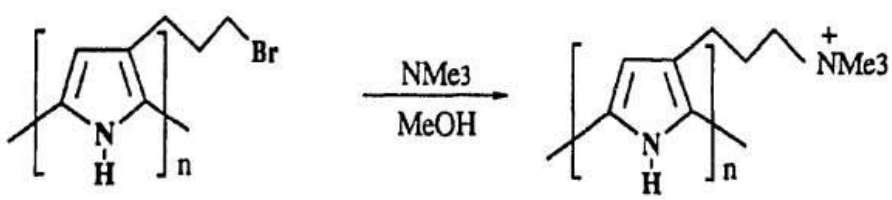

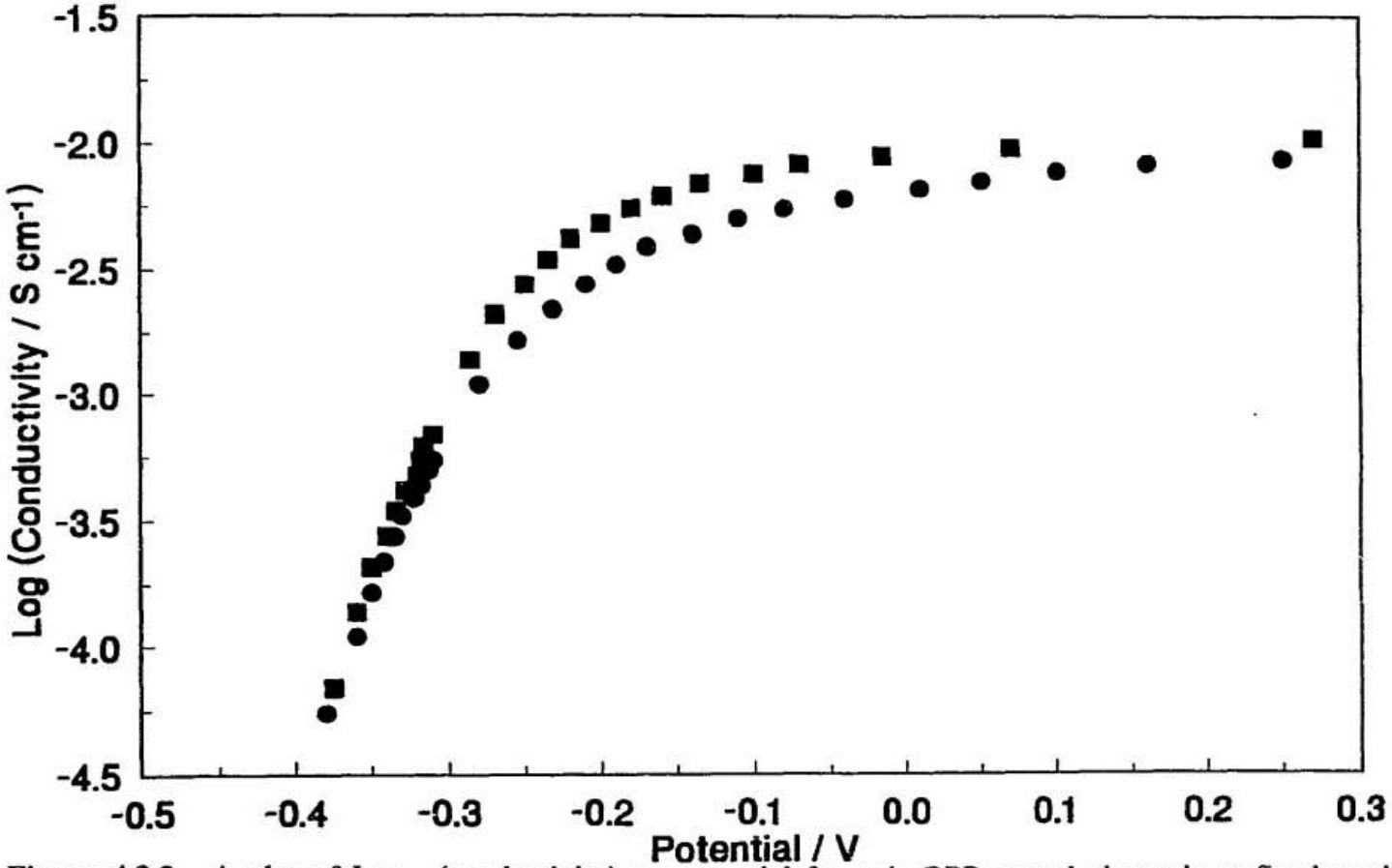

Figure 4.3.2. A plot of Log_{10} (conductivity) *vs.* potential for poly-BPP coated electrode at fixed small potential difference (ΔE = 10 mV) in 0.1 M Et_4NBF_4/CH_3CN solution for films 0.5 (●) and 0.75(■) μm.

The conductivity of the virgin polymer was measured with dual electrode voltammetry and then it was soaked in a trimethylamine/methanol solution for a certain time at room temperature. The conductivity was then measured again. This procedure was repeated several times and the results are listed in Table 4.3.

Table 4.3. The conductivity change for poly-BPP with reaction time in NMe_3/MeOH solution.

reaction time (hours)	max. conductivity (S cm^{-1})
0.0	1.0×10^{-2}
1.0	1.0×10^{-3}
12	4.7×10^{-5}
24	3.8×10^{-6}

Evidence of the replacement of bromine by trimethylamine is the electrostatic binding of ferrocyanide in the polymer, which will be described in chapter 5. Ferrocyanide was not electrostatically bound by the virgin poly-BPP because of the absence of positively charged sites but it was bound in the reacted

polymer. A concentration of 0.48 M ferrocyanide was obtained from the cyclic voltammogram for the ferrocyanide bound film. This indicates that about 34% of bromo- groups have been converted to alkyl ammonium groups.

The conductivity drops by 4 orders of magnitude as the bromine substituent is replaced with the positively charged trimethylammonium groups. Presumably, the decrease in conductivity is caused by solvation and swelling since the positively charged group increases the solvation and swelling of the film, a property which will be discussed in chapter 6.

The bulkiness of the substituent may also be partly responsible for the loss in conductivity since the $-N(CH_3)_3^+ X^-$ group (where X is BF_4 since the conductivity was measured in 0.1 M Et_4NBF_4 acetonitrile solution) is certainly much larger than a single bromine atom. This is supported by the work of Andrieux *et al*[10] who reported that the conductivity for poly-3-alkylpyrrole is higher than that for more bulky 3-functionalized poly-pyrrole.

4.4 Conclusion

The electronic conductivity of poly-$MPMP^+$ has been measured using the *in situ* techniques of rotating disc voltammetry and dual electrode voltammetry. An empirical method for calculating the *in situ* conductivity of the polymer from

rotating disc data is developed. The accuracy of the method is supported by the conductivity results from an independent technique, dual electrode voltammetry with a small fixed potential difference. The conductivity of poly-$MPMP^+$ increases approximately exponentially with potential before the polymer is fully oxidized (potential below 0.8V). For every 90 mV change of potential, the conductivity changes by one order of magnitude. It is then almost independent of applied potential and the polymer appears to be an ohmic conductor. The maximum conductivity is about 1×10^{-4} S cm^{-1}.

Dual electrode voltammetry was used to measure the electronic conductivity for poly-BPP. Similarly to poly-$MPMP^+$, the conductivity increases approximately exponentially with potential before the formal potential (-0.2 V) and levels off at higher potentials. Poly-BPP shows high conductivity ($\sim 1 \times 10^{-2}$ S cm^{-1}), but it decreases to $\sim 4 \times 10^{-6}$ S cm^{-1} if the bromo is replaced by trimethylamino. The presence of the positively charged sites and the bulkiness of the substituent may be responsible for the decrease of conductivity.

Dual electrodes were used to measure the maximum conductivity of poly-PPP^+ and poly-$PPTA^+$. They are $(6.1 \pm 0.4) \times 10^{-5}$ S cm^{-1} for poly-PPP^+, and $(3.4 \pm 1.8) \times 10^{-5}$ S cm^{-1} for poly-$PPTA^+$. These results indicate that moving the propylpyridinium or propyltrimethylammonium group to the 3-position of the pyrrole ring does not increase the electronic conductivity.

References

1. T. Ikeda, C. R. Leidner and R. W. Murray, J. Electroanal. Chem., 138 (1982) 343.

2. F. C. Anson, J-M. Saveant, and K. Shigehara, J. Am. Chem. Soc., 105 (1983) 1096.

3. J. Rault-Berthelot and M-A. Orliac, J. Simonet, Electrochim. Acta, 33 (1988) 811.

4. P. G. Pickup and R. A. Osteryoung, J. Electroanal. Chem., 195 (1985) 271.

5. W. J. Albery and A.R. Hillman, Ann. Reports Chem. Soc., C (1981) 377.

6. A. J. Bard and L. R. Faulkner, "Electrochemical Methods", Wiley, New York, 1980, P.290.

7. H. Mao and P. G. Pickup, J. Am. Chem. Soc., 112 (1990) 1776.

8. B. J. Feldman, P. Burgmayer and R. W. Murray, J. Am. Chem. Soc., 107 (1985) 872.

9. P. G. Pickup, W. Kutner, C. R. Leidner, and R. W. Murray, J. Am. Chem. Soc., 106 (1984) 1991.

10. C. P. Andrieux and P. Audebert, J. Electroanal. Chem., 261 (1989) 443.

Chapter 5

Ion Exchange And Electrostatic Binding

One main purpose for studying modified electrodes is to utilize the coating material as an electron transfer mediator in electrochemical reactions. Transition metal complexes are of great interest because they possess excellent electron-mediation properties[1]. Instead of using transition metal complexes in homogeneous solutions, these complexes can be incorporated into an electrode coating, such as a polymer. Polypyrrole has been used to incorporate a number of different complexes[2,3,4,5]. Current research utilizes two means of incorporating metal complexes in polypyrrole. The first method involves incorporating an anionic complex into the polypyrrole film as a counterion by growing the polymer in a solution containing the metal complex. The second method involves incorporation through ion exchange after synthesis of the film. Conventional ion exchange principles are applicable to the incorporation of ionic redox species into polyelectrolyte films on electrodes as counterions of the films[6]. However, ion exchange for polypyrrole is of very limited utility. The exchange capacity depends on the oxidation state of the film because polypyrrole must be oxidized to provide positively charged sites for ion exchange. Even when it is oxidized, four of the

polypyrrole units provide only one such site. The reduced form has no ion exchange capacity. Moreover, large anions such as ferrocyanide cannot be incorporated by ion exchange because of the low density of positively charged sites. In order to improve ion exchange capacity and stability, additional positive or negative sites have been introduced into the polypyrrole chain[7,8,9,10]. Metal complexes with negative or positive charges can be easily incorporated into these films regardless of the pyrrole oxidation state. Members of this new class of polymer have been called electronically conducting ion exchange polymers. All of the polymers discussed in this chapter have permanent positively charged sites and their quantitative anion exchange properties will be described.

5.1 Ion Exchange in Poly-MPMP$^+$

5.1.1 The Ion exchange Process

Ion exchange is a class of reversible reaction. If a solution of an anion X^- is brought into contact with a anion exchange polymer in the Y^- form (the positively charged sites are associated with the Y^- counterion), the following reaction will occur:

$$X^-_{sol} + Y^-_{pol} = X^-_{pol} + Y^-_{sol} \qquad (5.1.1)$$

where the subscripts *sol* and *pol* denote whether the anion is in solution or associated with the polymer, respectively. The equilibrium constant for reaction 5.1.1 is:

$$K = [X^-_{pol}][Y^-_{sol}]/[X^-_{sol}][Y^-_{pol}] \qquad (5.1.2)$$

The value of the equilibrium constant depends on the properties of the ion exchange polymer and the properties of the two ions. Figure 5.1.1 is a schematic diagram of the exchange of ClO_4^- with $Fe(CN)_6^{4-}$ for an anion exchange polymer film on an electrode. The solid lines in the polymer represent the polymer chains. There are many positive sites attached to each polymer chain. Anions can move within the polymer while cations from the solution are generally excluded from the polymer. Ion exchange can be carried out by soaking the ion exchange polymer film (Y^- form) in the X^- containing solution. To reduce the time required to reach equilibrium, potential cycling can be used for electrochemically active anions, e.g. $Fe(CN)_6^{4-}$. The ion exchange reaction can then be observed by cyclic voltammetry.

Instead of using the equilibrium constant in equation 5.1.2, the ion exchange properties of a polymer are often expressed by the saturation concentration and partition coefficient[11,12]. When an ion exchange polymer has fully equilibrated with a solution, the concentration of a particular ion within the film is governed

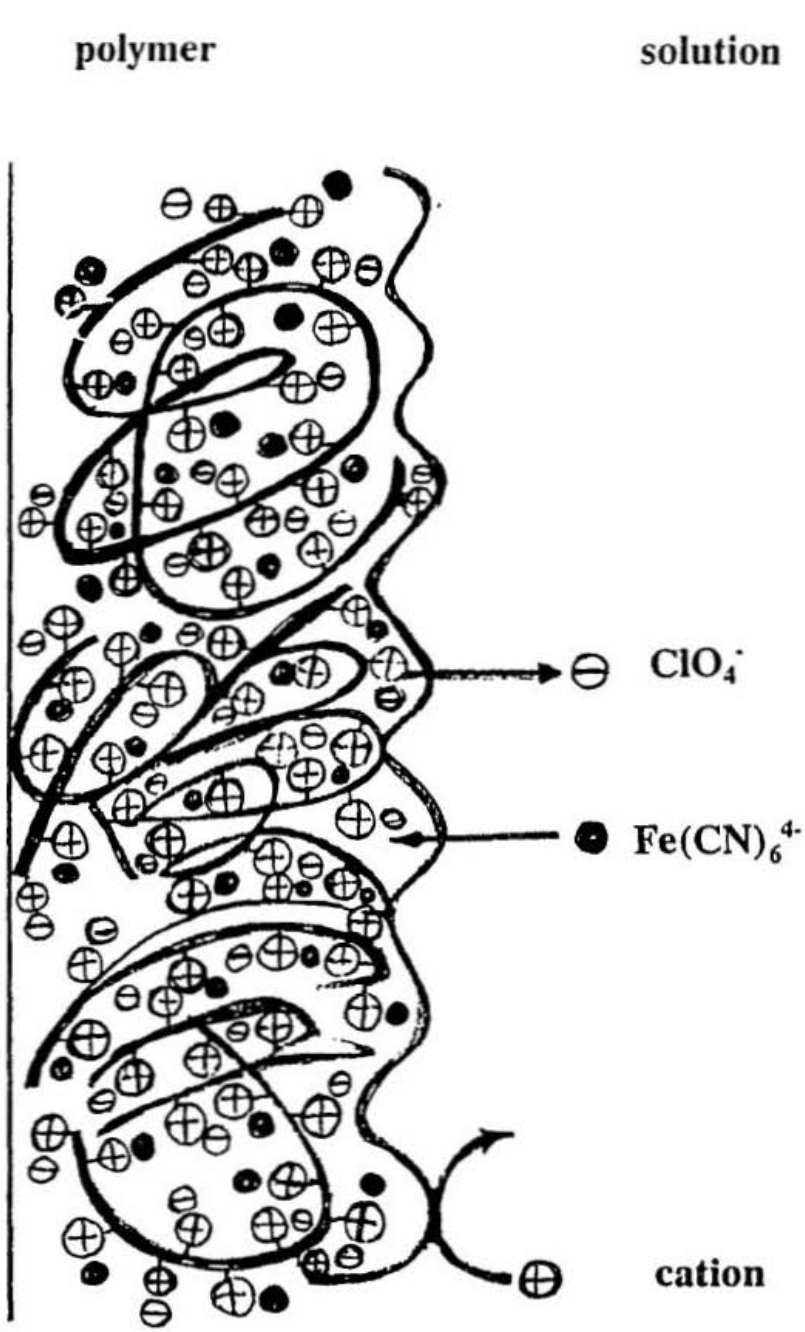

Figure 5.1.1. Schematic diagram of anion exchange of ClO_4^- by $Fe(CN)_6^{4-}$ for an ion exchange polymer. Solid lines represent the polymer chains and ⊕ are the positively charged sites around the chains.

by the partition coefficient, P. The partition coefficient has also been called a distribution coefficient or extraction coefficient. It is defined as $P = C_p/C_s$, where C_p and C_s are respectively the equilibrium ion concentrations in the polymer and solution, corresponding to $[X^-_{pol}]$ or $[Y^-_{pol}]$ and $[X^-_{sol}]$ or $[Y^-_{sol}]$ in equation 5.1.2. If the solution concentration of an ion is high or its partition coefficient is high, then almost all the ion exchange sites in the polymer can become associated with that ion. The concentration of the ion within the film is then called "saturation concentration" and it serves as the limiting concentration of the ion in the film.

In this chapter, the saturation concentration for $Fe(CN)_6^{4-}$ in poly-$MPMP^+$ is more useful than the partition coefficient because the maximum incorporation of ferrocyanide is desired. For the I^- transport study (Chapter 6), the concentration of I^- in the film is much below the saturation concentration, thus the partition coefficient dominates the ion exchange property of the polymer for iodide.

5.1.2. Iodide Partition Coefficient Measurement by Ion Exchange

For poly-$MPMP^+$, which is an anion exchange polymer, C_p for I^- under various conditions can be conveniently obtained by ion exchange processes. A Pt flag electrode (see Section 2.2.1) coated with poly-$MPMP^+$ (1.0 μm) was

equilibrated with I^- by immersing the electrode in an I^- solution (in either acetonitrile or water) for 20 minutes with stirring. The following equation describes the ion exchange process:

$$[\text{Poly-MPMP}]^+ClO_4^- + I^- = [\text{Poly-MPMP}]^+I^- + ClO_4^- \qquad (5.1.3)$$

The I^- concentration (C_s) was 1.0×10^{-3} M, in 0.1 M $LiClO_4/CH_3CN$ or in 0.1 M $NaClO_4/H_2O$. The completion of equilibrium was tested by determining the amount of I^- in the film (see below) at different times varying from 5 to 20 minutes. The same amount of I^- detected over different equilibrium times confirms the establishment of equilibrium.

To measure the content of I^- in the film the process in equation 5.1.3 is reversed to extract the I^- for analysis as illustrated in the following equation:

$$[\text{Poly-MPMP}]^+I^- + ClO_4^- = [\text{Poly-MPMP}]^+ClO_4^- + I^- \qquad (5.1.4)$$

The electrode was removed from the I^- solution and thoroughly washed with the solvent. It was then immersed in 5.00 ml of aqueous 2 M $NaClO_4$ solution for 5 minutes to allow the ion exchange. The I^- released in the process was then analyzed using an ion selective electrode (see section 2.2.1). After extraction the

film was again soaked in another 5.00 ml of 2M $NaClO_4$ solution. This solution was then analyzed and no detectable I^- was found. This confirms that no I^- was left in the film following the first extraction.

All of the I^- analyses were carried out using an iodide selective electrode. Figure 5.1.2 shows a calibration curve for the I^- selective electrode. This electrode was an excellent tool for the determination of I^- as its wide linear region, from 10^{-4} M to 10^{-8} M, covered the range of concentrations required for I^- partition coefficient measurements both in aqueous solutions and acetonitrile.

From the definition of partition coefficient, $P = C_P/C_S$ (C_P is the concentration of I^- in the film), we can obtain the following equation:

$$5C_I = C_S APd \qquad (5.1.5)$$

Where C_I is the concentration of I^- in the 5.00 ml extraction solution, A and d are the film area (cm^2) and thickness(cm) respectively. The left hand side represents the number of moles of I^- in the film obtained from the potentiometric analysis. A plot of number of moles of I^- vs. film thickness is linear as shown in Figure 5.1.3. The partition coefficient is then obtained from the slope. I^- partition coefficients from different solutions and films are listed in Table 5.1. These partition coefficients will be used in the analysis of ion transport properties of

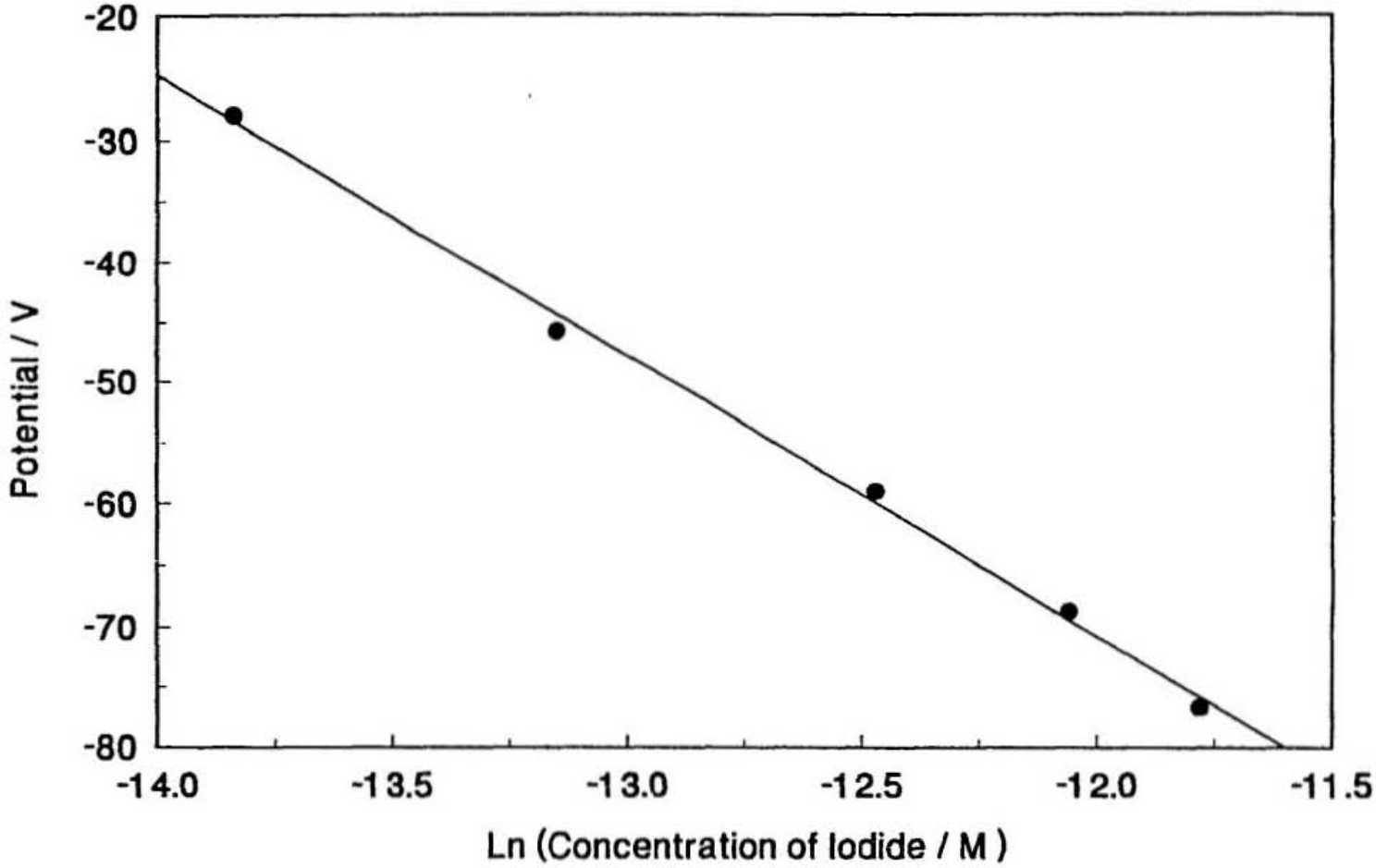

Figure 5.1.2. Calibration curve of potential *vs.* Ln (iodide concentration).

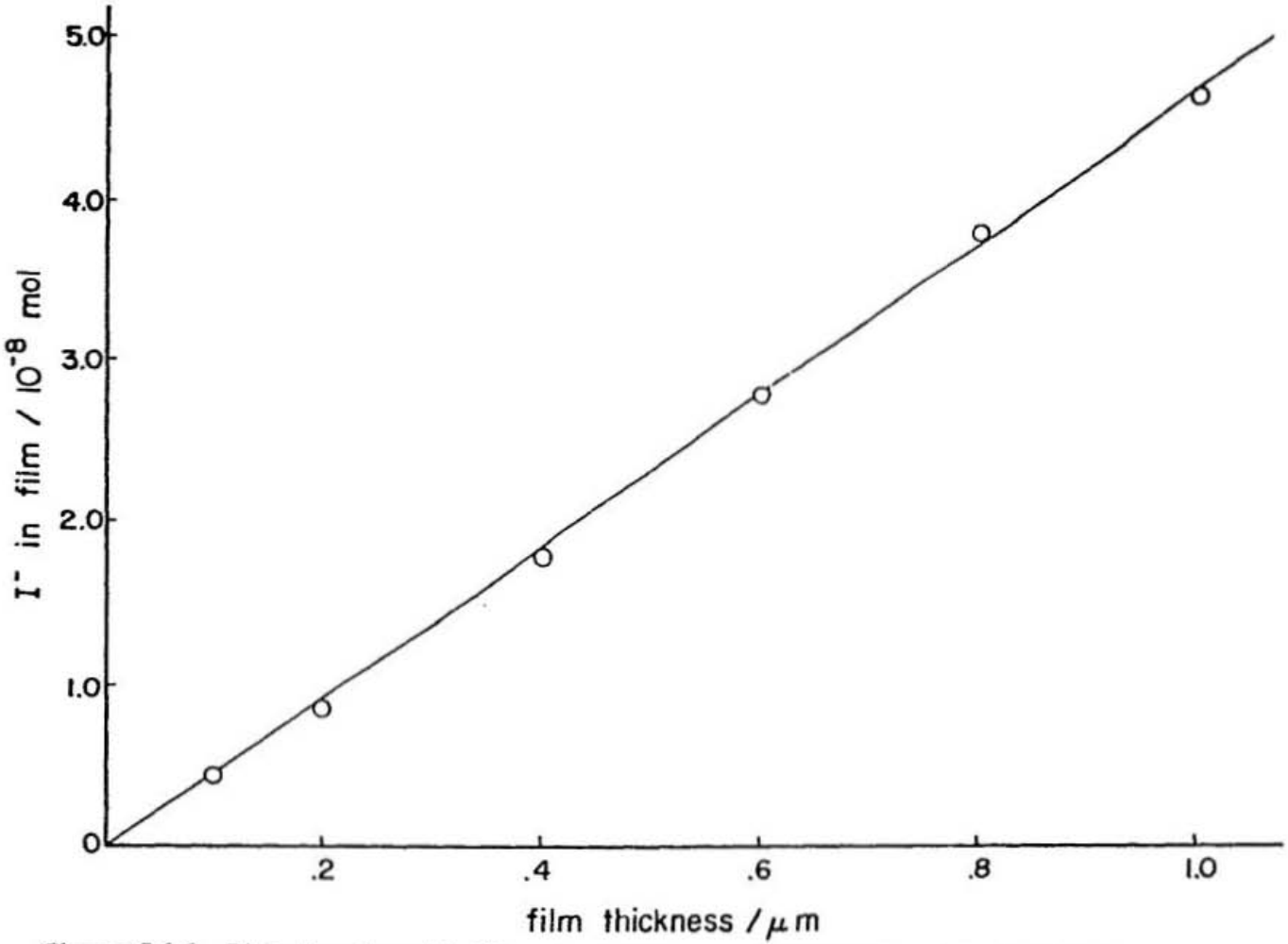

Figure 5.1.3. Plot of moles of iodide extracted from poly-MPMP$^+$ vs. film thickness.

Table 5.1 Partition coefficients for I^- in poly-$MPMP^+$ (C_s = 1.0 mM)

solvent/electrolyte	C_P (M)	partition coefficient
0.1 $MLiClO_4/CH_3CN$	0.24 ± 0.01	240 ± 10
0.1 M $NaClO_4/H_2O$	0.021 ± 0.002	21 ± 2
0.1 M $NaClO_4^*/H_2O$	0.019 ± 0.002	19 ± 2

* For deactivated films (see section 6.1.2).

5.2 Electrostatic Binding of Ferrocyanide by Poly-[1-methyl-3-(pyrrol-1-ylmethyl)pyridinium], (poly-$MPMP^+$)

Electrostatic binding is a process whereby ionic redox species can be incorporated as counterions into a polymer film on an electrode[13]. This process is an application of the ion exchange principles illustrated in Section 5.1.1. The study of the electrostatic binding of ferrocyanide in this section comprises both qualitative and quantitative aspects. The qualitative study explores the nature of the electrostatic binding of ferrocyanide by poly-$MPMP^+$. The quantitative study

investigates the extent of ferrocyanide incorporation into the film in terms of the saturation concentration.

5.2.1 Qualitative Aspects

Ferrocyanide can be electrostatically bound (or ion exchanged) into poly-MPMP$^+$ simply by soaking a polymer coated electrode in a ferrocyanide aqueous solution. Scanning the potential of the electrode through the ferro/ferri-cyanide redox wave speeds up the electrostatic binding process and allows it to be monitored by cyclic voltammetry. Figure 5.2.1A shows a series of cyclic voltammograms of ferrocyanide at a 0.33 μm poly-MPMP$^+$ coated electrode in an aqueous solution of 0.1 mM $K_4Fe(CN)_6^{4-}$ and 0.1 M phosphate buffer at pH = 9.12. The cyclic voltammogram with the lowest peak current is the first scan and this peak current is similar to that for a naked Pt electrode (same diameter). As more cycles are applied, the peak current increases and maximizes at about 100 cycles. The steadily growing peak current before the limit indicates an increase in the amount of ferrocyanide within the polymer. The size of the final voltammogram implies that the concentration of ferrocyanide in the film is much greater than the solution concentration (corresponding roughly to the size of the first scan). This coated electrode, containing a high concentration of ferrocyanide in the film, was thoroughly washed with water and transferred to a ferrocyanide

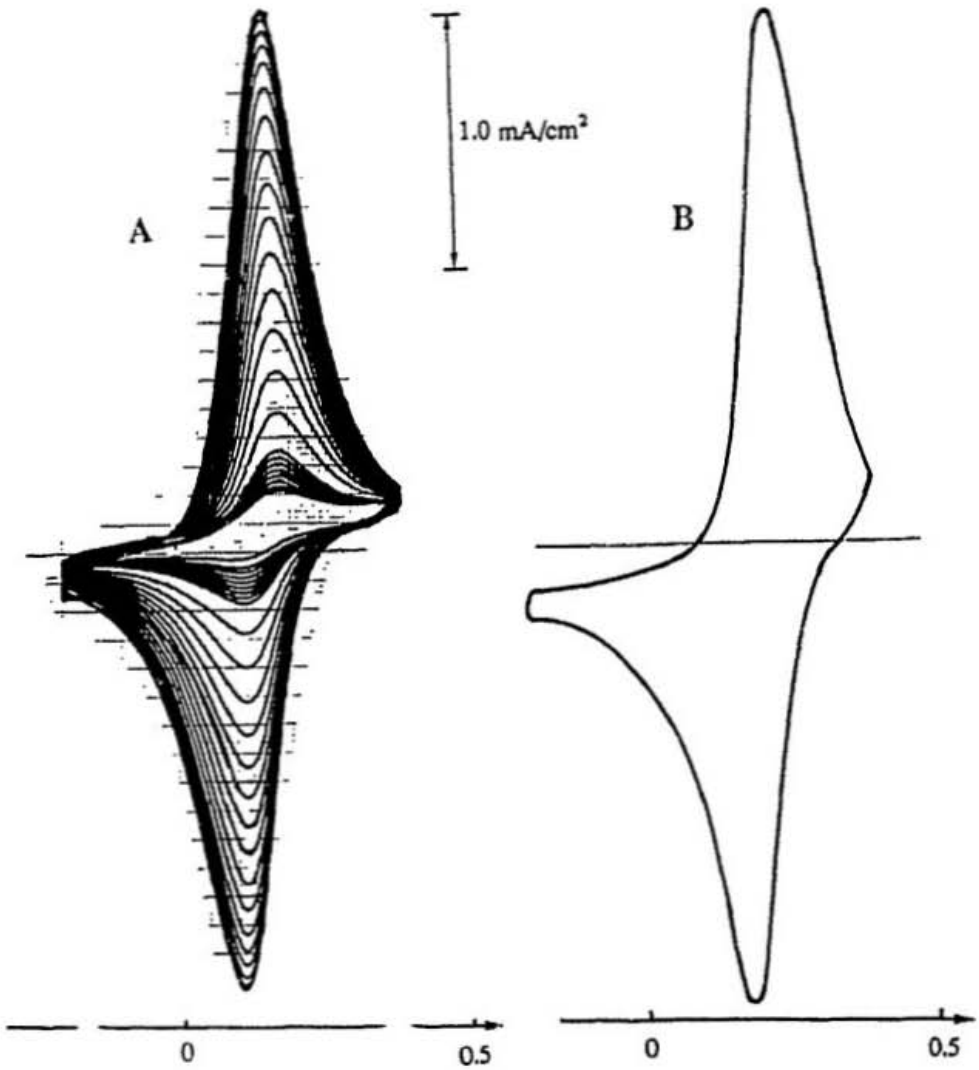

Figure 5.2.1. Cyclic voltammograms at a poly-MPMP$^+$ coated Pt electrode: (A) Peak currents increase during potential cycling in 0.1 M K_2HPO_4 containing 0.1 mM $K_4Fe(CN)_6$. The first scan (the lowest peak current) has a size similar to a voltammogram at a bare Pt electrode. (B) Cyclic voltammogram for the ferrocyanide loaded electrode from (A) in 0.1 M K_2HPO_4 solution containing no $K_4Fe(CN)_6$. All scan speeds are 100 mV/s.

free solution (0.1 M phosphate buffer). A cyclic voltammogram is shown in Figure 5.2.1B. The peaks displayed are approximately the same size as the final peaks in the ferrocyanide containing solution. This indicates that the ferrocyanide is strongly bound to poly-MPMP$^+$ and is trapped within the film. Electrostatic binding should be considered as the mechanism.

The stability of ferrocyanide loaded films were tested by potential scanning in the ferrocyanide-free 0.1 M K_2HPO_4 aqueous buffer solution. Potential scanning through the ferro/ferri-cyanide wave on a 0.4 μm ferrocyanide loaded film for 3 hours caused only a 6% loss of trapped ferrocyanide (shown in Figure 5.2.2A). Soaking the film at open circuit in the same solution for 14 hours produced almost no change in the cyclic voltammogram. However, ferrocyanide leaves the film at a much higher rate in sodium perchlorate solutions. Consequently, after only 20 cycles, voltammograms recorded in 0.01 M $NaClO_4/H_2O$ show a significant loss of ferrocyanide (shown in Figure 5.2.2B). The trapped ferrocyanide is completely lost after soaking the loaded film in 1 M $NaClO_4/H_2O$ for 30 seconds without cycling. Apparently, the process of replacing ferrocyanide by perchlorate is much faster than that for phosphate. No further study was made to reveal the reason for this characteristic but it has provided a convenient way of releasing ferrocyanide so that the film can be reused. Consecutive loading/releasing of ferrocyanide does not affect the ion exchange

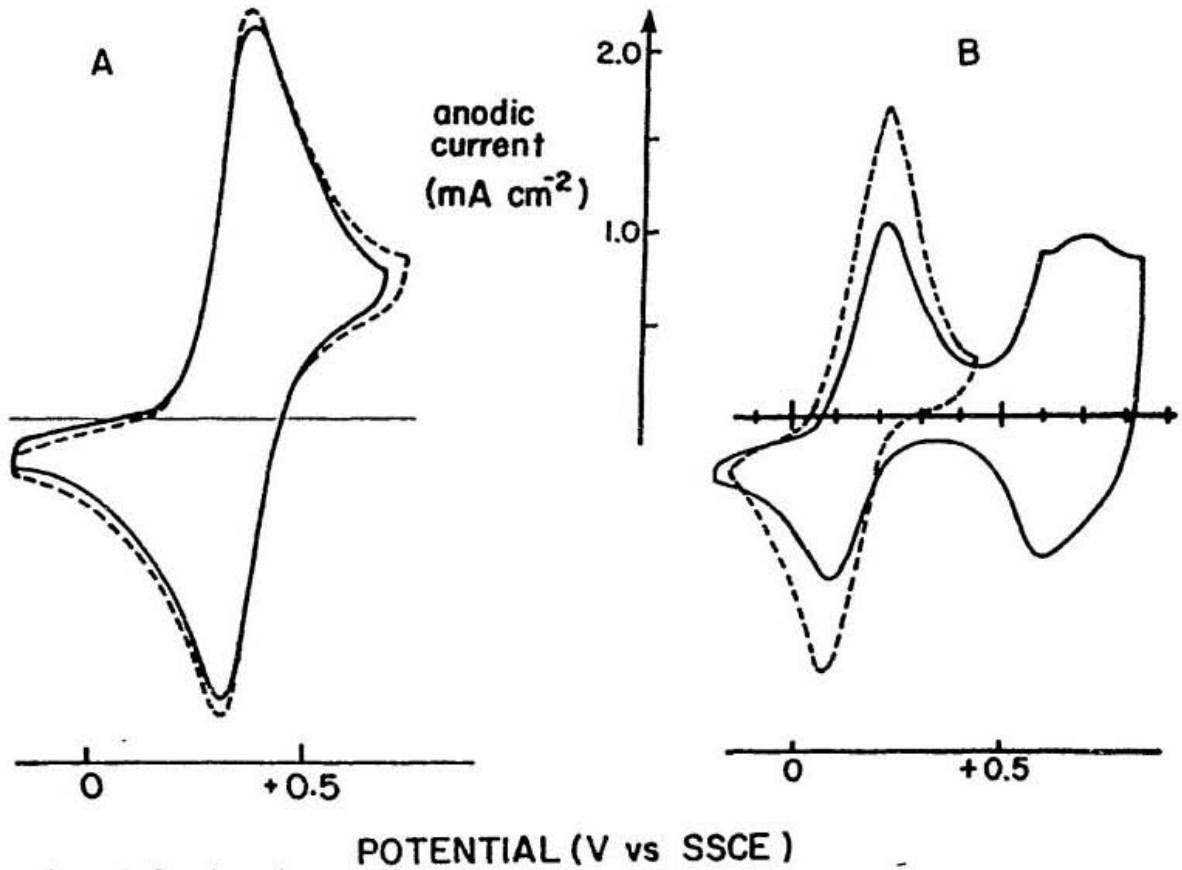

Figure 5.2.2. (A) Cyclic voltammograms for the stability test for electrostatically bound $Fe(CN)_6^{4-}$ within poly-$MPMP^+$ in 0.1 M K_2HPO_4/H_2O solution containing no $K_4Fe(CN)_6$. Dashed line: original cyclic voltammogram; solid line: the cyclic voltammogram after soaking in 0.1 M K_2HPO_4 solution containing no $K_4Fe(CN)_6$ for 14 hours.(B)Cyclic voltammograms of the polymer coated electrode from (A) in 0.01 M $NaClO_4$ containing no $Fe(CN)_6^{4-}$ (----) 1st scan, (_____)20th scan to 0.85 V. All scan rates are 100 mV/s.

capacity of the poly-$MPMP^+$ as evidenced by a less than 1 % decrease in the cyclic voltammogram peak area after 8 loading-releasing operations.

Poly-$MPMP^+$ can only be used at potentials below its formal potential (0.77V) in phosphate solution because the polymer loses its electroactivity completely when it is oxidized in this medium. However, the polymer exhibits reversible electrochemistry in perchlorate solution up to about 1.0 V. Voltammetric peaks due to ferrocyanide and the polymer can be recorded in 0.01 M $NaClO_4$ solution as shown in Figure 5.2.2B.

The ferrocyanide binding process occurs over a wide pH range. Approximately the same amount of ferrocyanide is bound from phosphate solutions from pH = 0.93 to 9.12. This may be an attractive feature in applications such as drug release or automated analysis where media of different pH are encountered.

5.2.2. Ferrocyanide Saturation Concentration Measurement

The saturation concentration of $Fe(CN)_6^{4-}$ was measured by determining the equilibrium concentration of ferrocyanide within poly-$MPMP^+$ films (C_P) immersed in solutions containing ferrocyanide at various concentrations (C_S). When C_S is sufficiently low, C_P increases with C_S, and the slope in the region gives the partition coefficient. Once ferrocyanide saturates the film, C_P no longer changes with bulk concentration. Thus the saturation concentration is equivalent

to the constant C_P.

The electrostatic binding (or ion exchange) of $Fe(CN)_6^{4-}$ was carried out by holding a 0.21 μm poly-$MPMP^+$ film at a potential of -0.1 V in the stirred ferrocyanide solution for 4 minutes. Longer soaking time, such as 8, 10 minutes was tried but resulted no increase in the amount of ferrocyanide bound in the film. The ferrocyanide loaded film was then washed with water and transferred to a solution without ferrocyanide. A slow cyclic voltammogram at 5 mV s^{-1} was recorded as shown in Figure 5.2.3 and the concentration of ferrocyanide trapped in the film was determined from the charge (Q_{CV}) under the voltammogram. The following equation gives the concentration of ferrocyanide in film:

$$C_P = 10^3 Q_{CV}/nFAd \qquad (5.2.1)$$

This procedure was repeated in solutions containing different ferrocyanide concentrations to obtain the relationship between C_S and C_P. The experiment was carried out using both 0.1 M KH_2PO_4 and 0.01 M $NaClO_4$ electrolytes in water. The measurements were reproducible from one film to another. Four different films were used in the experiment. Since the loading and release of ferrocyanide is repeatable, each film was reused after soaking in 1 M $NaClO_4$ solution for one minute.

Figure 5.2.4 shows plots of log C_P *vs* log C_S for ferrocyanide exchange from both 0.1 M KH_2PO_4 and 0.01 M $NaClO_4$ electrolytes. The solid line in

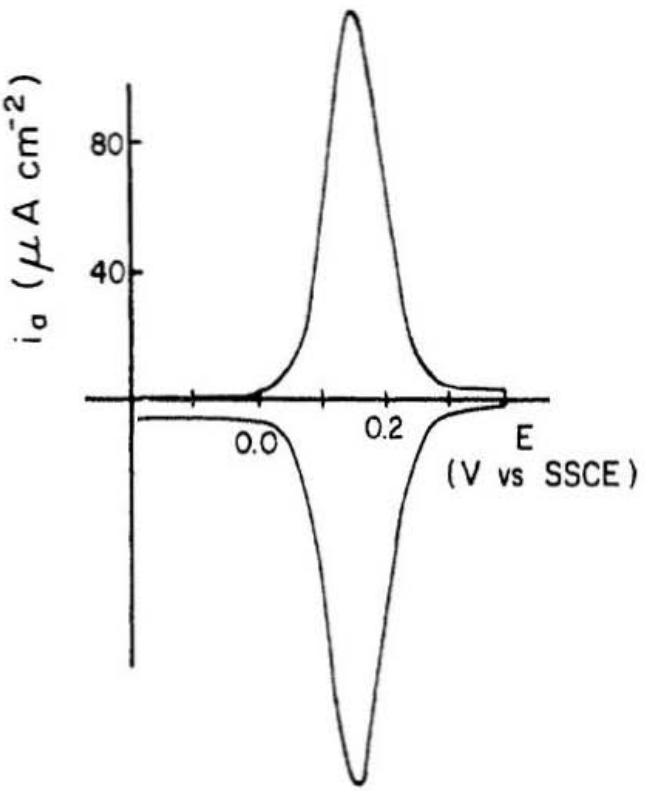

Figure 5.2.3. Slow cyclic voltammogram at 5 mV/s for $Fe(CN)_6^{4-}$ containing poly-MPMP$^+$ coated electrode in 0.1 M KH_2PO_4 solution containing no $K_4Fe(CN)_6$.

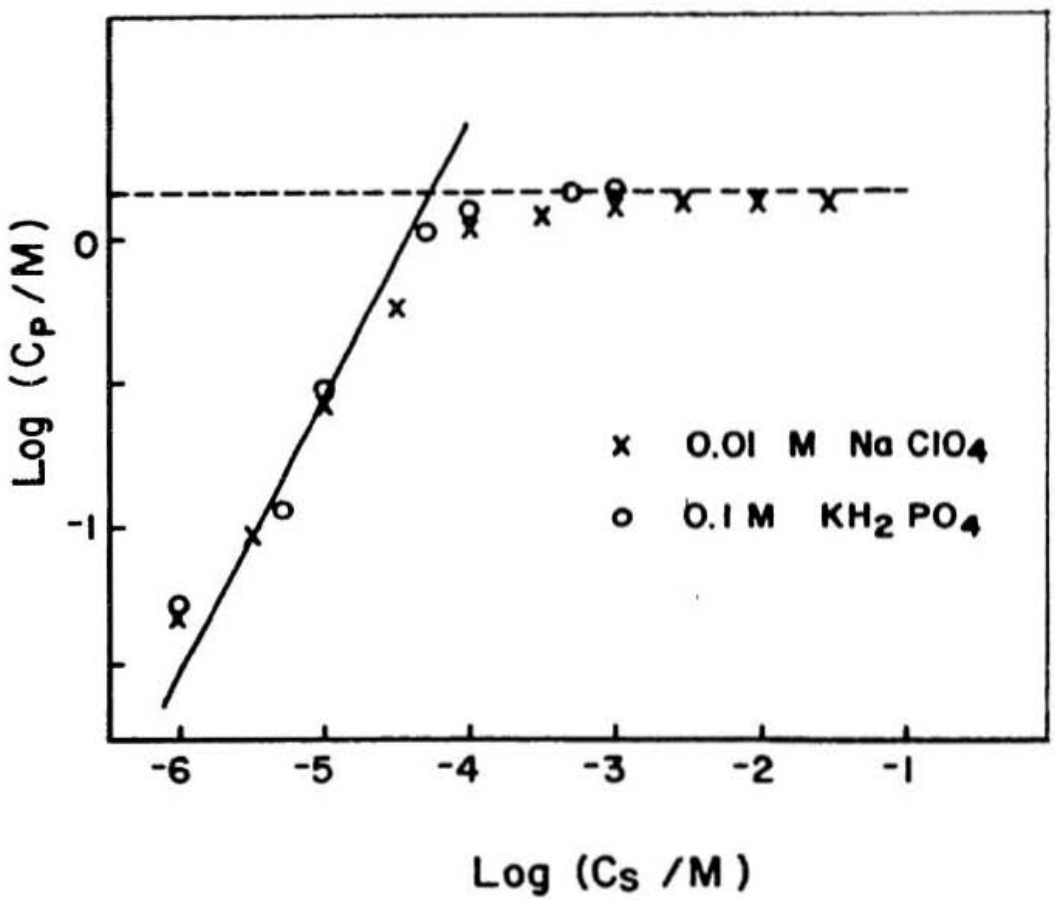

Figure 5.2.4. Plot of the equilibrium concentration of $Fe(CN)_6^{4-}$ in poly-MPMP$^+$ films (Cp) as a function of its concentration in the bulk solution (Cs).

Figure 5.2.4 represents an average partition coefficient of (3.2 ± 1.2) x 10^4 in 0.01 M $NaClO_4$ and (3.2 ± 1.5) x 10^4 in 0.1 M KH_2PO_4 solution. The approximately linear relationship between Log(C_P) and Log(C_S) with nearly unit slope for $C_S < 10^{-4}$ M indicates that C_P and C_S follow the expected linear relationship ($P = C_P/C_S$). For solution concentrations higher than 10^{-4} M, C_P becomes constant and is represented by the dashed line on Figure 5.2.4. Clearly, the ferrocyanide in the film has reached the saturation concentration which is 1.3 M in 0.01 M $NaClO_4$ and 1.4 M in 0.1 M KH_2PO_4 solution. These concentrations are in excellent agreement with the theoretical value of 1.4 M calculated from the pyridinium concentration (section 3.4) assuming four pyridinium units accommodate one ferrocyanide ion.

5.3 Electrostatic Binding of Ferrocyanide by Poly-[1-(3-[pyrrol-3- yl]propyl)pyridinium], (Poly-PPP$^+$) and Poly-[(3--[pyrrol-3-yl]propyl)trimethyl ammonium], (Poly-PPTA$^+$)

Figure 5.3.1 shows an example of the electrostatic binding of ferrocyanide by a poly-PPP$^+$ film. Similar to the electrostatic binding of $Fe(CN)_6^{4-}$ by poly-MPMP$^+$, the steadily growing peaks demonstrate that the amount of ferrocyanide incorporated in the film increases with the number of potential cycles. The peaks

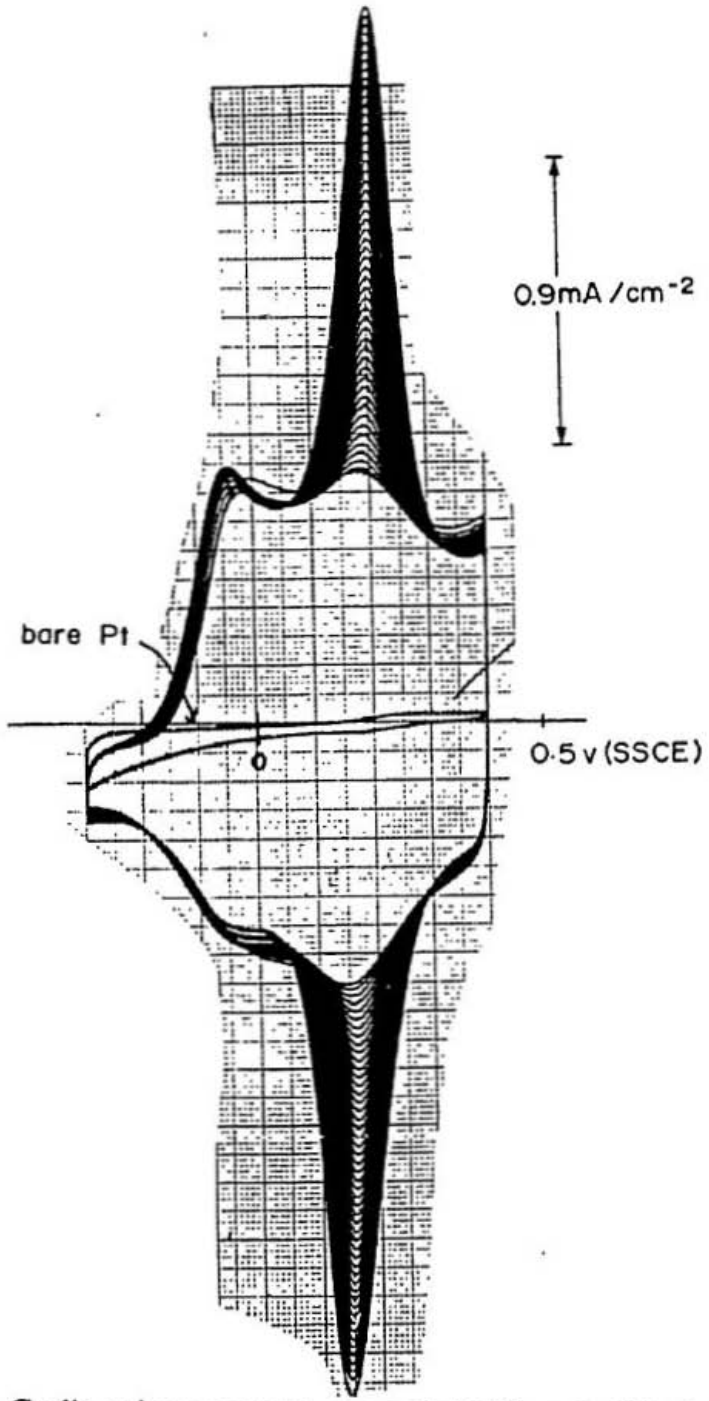

Figure 5.3.1. Cyclic voltammograms at a poly-PPP$^+$ coated Pt electrode. Peak currents increase during potential cycling in 0.1 M KH_2PO_4 containing 0.1 mM $K_4Fe(CN)_6$. The voltammogram along the potential axis is from a bare Pt electrode in the same solution and same current scale. All scan speeds were 100 mV s^{-1}.

cease to increase after about 100 cycles which indicates saturation of the film by the incorporated ion. The redox peaks have been intensified by more than two orders of magnitude compared to a cyclic voltammogram at a bare Pt electrode in the same solution as shown by the solid line (near potential axis). A noteworthy difference from the electrostatic binding of $Fe(CN)_6^{4-}$ by poly-MPMP$^+$, is that the ferrocyanide peaks are now superimposed on the capacitive current due to the oxidized polymer as illustrated in Figure 5.3.1. Figure 5.3.2 shows cyclic voltammograms for a ferrocyanide loaded poly-PPP$^+$ film in a 10^{-4} M $Fe(CN)_6^{4-}$ solution (dashed line) and in a ferrocyanide free solution (solid line). Clearly, ferrocyanide has been incorporated into the film of poly-PPP$^+$ in the same manner as it was in the film of poly-MPMP$^+$.

Since ferrocyanide is electrostatically bound by the positive sites in the film, the amount of bound ferrocyanide should be related to the oxidation state of the complex. In other words, a film should bind less $Fe(CN)_6^{4-}$ than $Fe(CN)_6^{3-}$ under similar conditions. The electrostatic binding of $Fe(CN)_6^{3-/4-}$ at different oxidation states was quantified by the following experiment. Ferrocyanide (0.1 mM in 0.1 M KH_2PO_4/K_2HPO_4 buffer solution at pH = 2.3 solution) was electrostatically bound by a 0.11μm poly-PPP$^+$ film under the following different conditions: (1) a constant potential of 0 V; (2) potential scanning between 0 to 0.35 V (the formal potential of ferrocyanide oxidation is 0.14 V); (3) constant potential of 0.35V. The

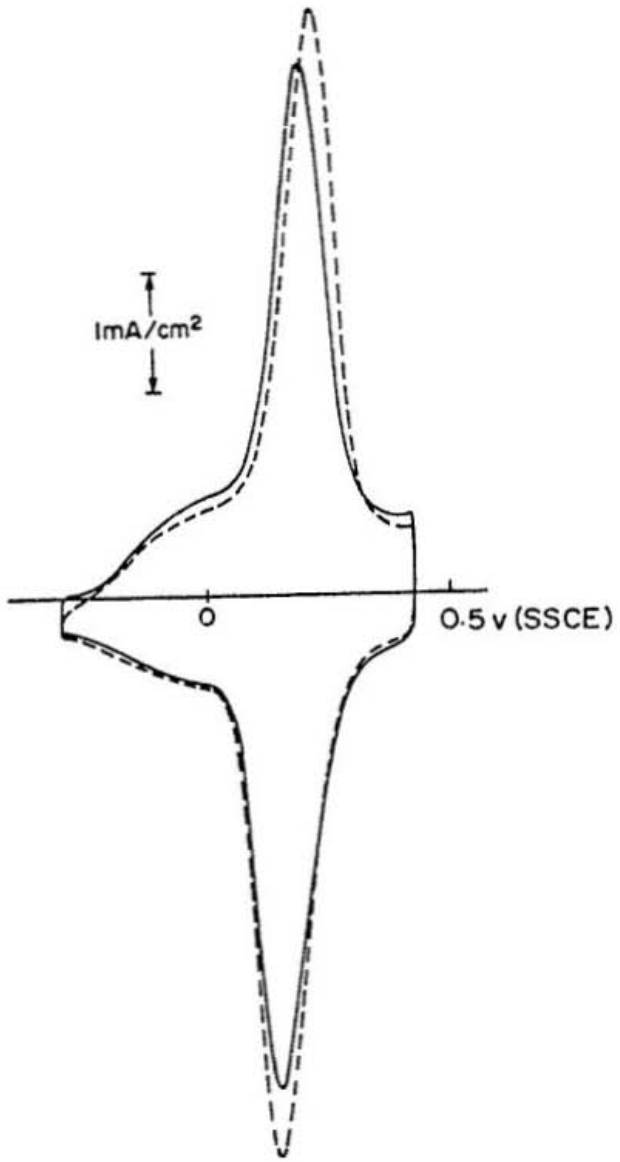

Figure 5.3.2. Cyclic voltammograms of a poly-PPP$^+$ coated Pt electrode. The dashed line is in 0.1 M KH_2PO_4 containing 0.1 mM $K_4Fe(CN)_6$. The solid line is the voltammogram in 0.1 M KH_2PO_4 containing no $K_4Fe(CN)_6$.

concentration of the bound ferro/ferri-cyanide under each condition was measured from a slow cyclic voltammogram using the same procedures as in section 5.2.2. Table 5.2 shows that the concentration of ferrocyanide bound by poly-PPP^+ film varies with potential.

Table 5.2 Variation of ferro/ferri-cyanide concentration with potential.

binding potential (V)	concentration of ferro/ferri-cyanide (M)
0.0	0.50
0 ↔ 0.35	0.56
0.35	0.62

As shown in the table, $Fe(CN)_6^{3-}$ has the highest concentration and $Fe(CN)_6^{4-}$ the lowest. The ratio of the amount of trapped $Fe(CN)_6^{4-}$ to $Fe(CN)_6^{3-}$ is 1.3, which agrees with the theoretical value of 1.33 within experimental error. This result indicates that $Fe(CN)_6^{4-}$ is bound at 0 V and $Fe(CN)_6^{3-}$ at 0.35 V. Under potential scanning the amount of incorporation is in between the potentiostatic values and a mixture of ferro- and ferri-cyanide is incorporated into the film.

The stability of the incorporated ferrocyanide was tested using the same

procedures as for poly-MPMP$^+$ (section 5.2.1). About 5 % of the bound ferrocyanide was lost after continual potential cycling of a loaded film at 100 mV/s for 3⅓ hours in a 0.1 M KH_2PO_4/K_2HPO_4 buffer (pH = 2.3) solution containing no ferrocyanide. Approximately the same percentage loss was observed for a loaded film after soaking in the solution for 15 hours at open circuit.

The saturation concentration and the partition coefficient were measured for a 0.2 μm thick film in 0.1 M KH_2PO_4 solution at pH = 2.3 in the same manner as for poly-MPMP$^+$(section 5.2.2); the results are shown in Figure 5.3.3. A partition coefficient of $(5.5\pm0.5) \times 10^4$ was obtained from the average C_P/C_S ratio (represented by the solid line) for solution concentrations below 10^{-5} M. The data below $C_S = 10^{-5}$ M was treated as linear between $\text{Log}(C_P)$ and $\text{Log}(C_S)$ and gave a slope of 1.1. The suggests that C_P and C_S follow the expected linear relationship ($P = C_P/C_S$) for poly-PPP$^+$. The partition coefficient is significantly higher than that for poly-MPMP$^+$. The saturation concentration is 1.3 M which is the same as the value for poly-MPMP$^+$ (section 5.2.2) within experimental error. Surprisingly, the fact that poly-PPP$^+$ is oxidized at the formal potential of the ferro/ferri-cyanide couple does not increase the saturation concentration. However, the partition coefficient is increased compared with poly-MPMP$^+$.

Electrostatic binding of ferrocyanide also occurs in poly-PPTA$^+$ as shown in Figure 5.3.4. With respect to binding of ferrocyanide this polymer is very

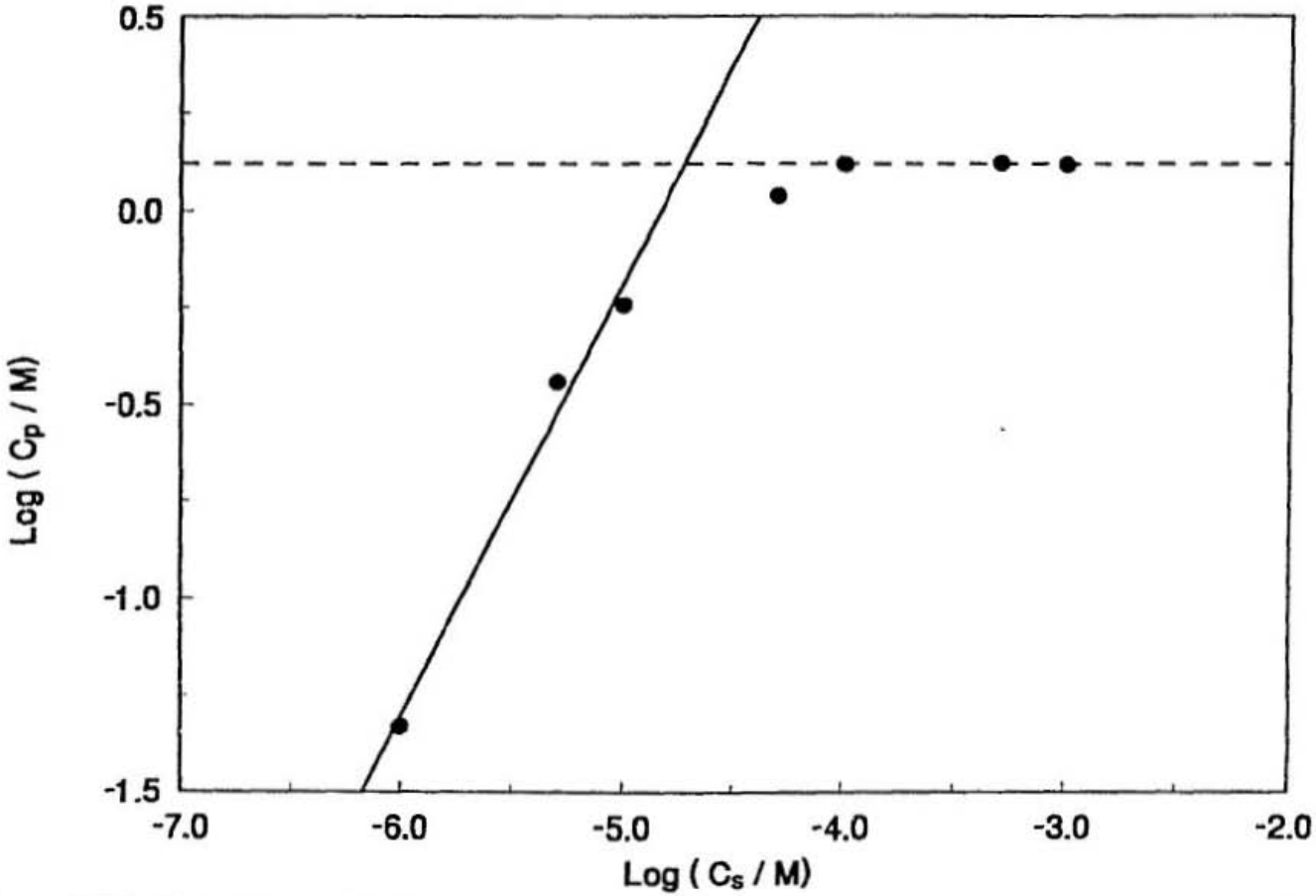

Figure 5.3.3. Plot of the equilibrium concentration of $Fe(CN)_6^{4-}$ in poly-PPP^+ films, Log (Cp), as a function of its concentration in the bulk solution Log (Cs).

similar to poly-PPP^+. This demonstrates that the binding properties are not sensitive to the nature of the positively charged group. Since no significant difference were found in preliminary experiments, trapping of ferrocyanide by poly-$PPTA^+$ was not investigated in detail.

5.4 Kinetics of Ferrocyanide Electrochemistry within the Polymers

The kinetics of ferrocyanide electrochemistry in different polymers have been investigated by cyclic voltammetry. Figure 5.4.1A shows cyclic voltammograms at different scan rates of ferrocyanide electrostatically bound by poly-$MPMP^+$. The ferrocyanide was bound by soaking the film in a ferrocyanide solution, similar to the procedures used in section 5.2.2. The cyclic voltammograms, at scan rates over 40 mV s^{-1}, exhibit a shape indicative of diffusion control[1]. The peaks are broad with significant diffusion tails for both anodic and cathodic scans. The E_{FWHM}(the Full Width at Half Maximum) is measured to be 190 mV at 100 mV s^{-1}. A plot of peak current, i_p, vs the square root of scan rate, v, reveals an approximately linear relationship as shown in Figure 5.4.2. The diffusion coefficient, D, is estimated from the slope to be 1.4 x 10^{-10} cm^2 s^{-1} by using the general equation[2]:

$$i_p = (2.69x10^5)n^{3/2}AD^{1/2}v^{1/2}C_p \qquad (5.4.1)$$

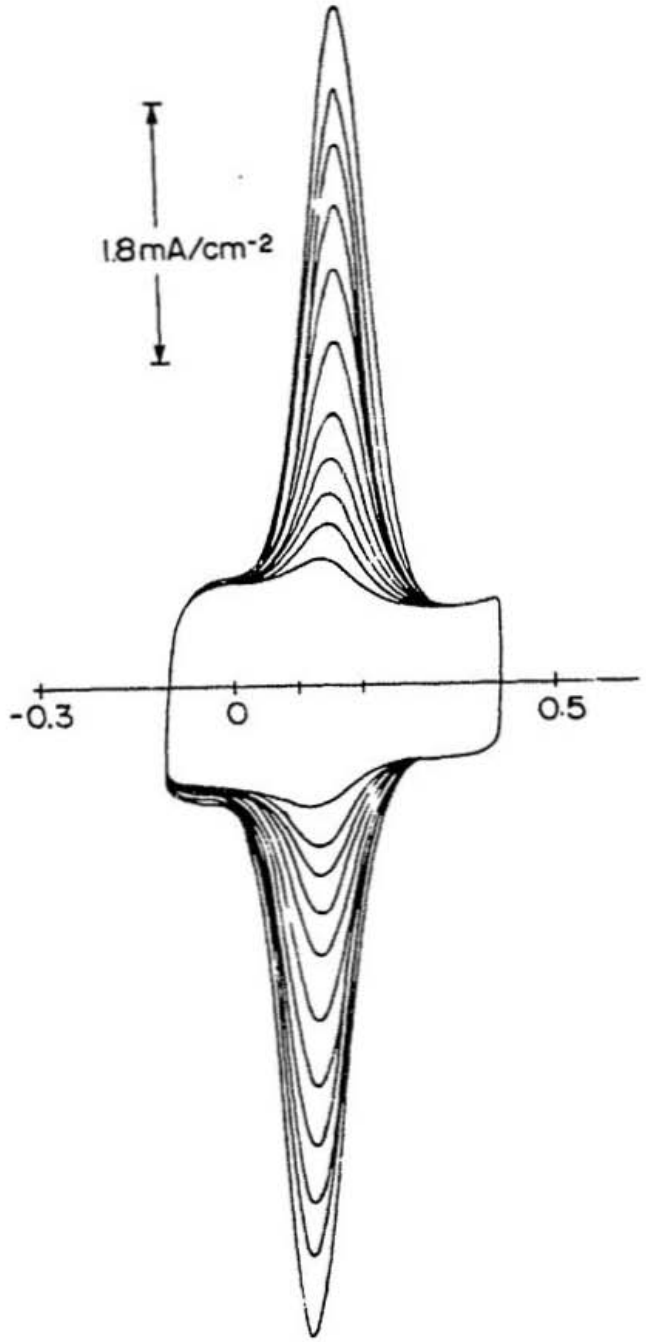

Figure 5.3.4. Cyclic voltammograms of a poly-PPTA^{+} coated Pt electrode. Peak currents increase during potential cycling in 0.1 mM $K_4Fe(CN)_6$/0.1 M KH_2PO_4 solution.

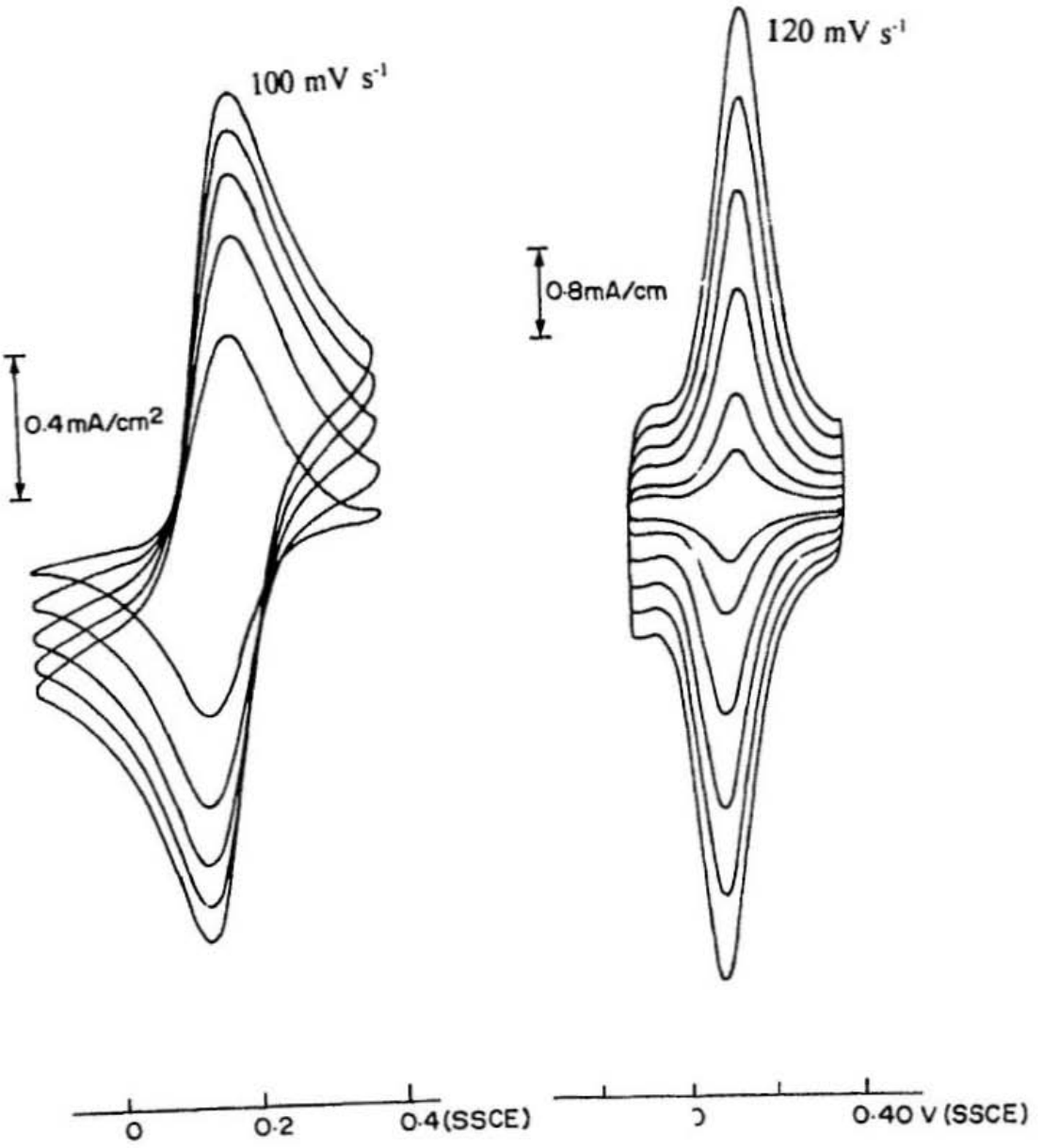

Figure 5.4.1. A comparison of the kinetics of ferrocyanide electrochemistry in (A) poly-MPMP$^+$, 0.21 μm; and in (B) poly-PPP$^+$,0.23 μm in $Fe(CN)_6^{4-}$ free 0.1 M phosphate buffer solution at pH = 2.25. Scan speeds were 20,40,60,80 and 100 mV s^{-1}.

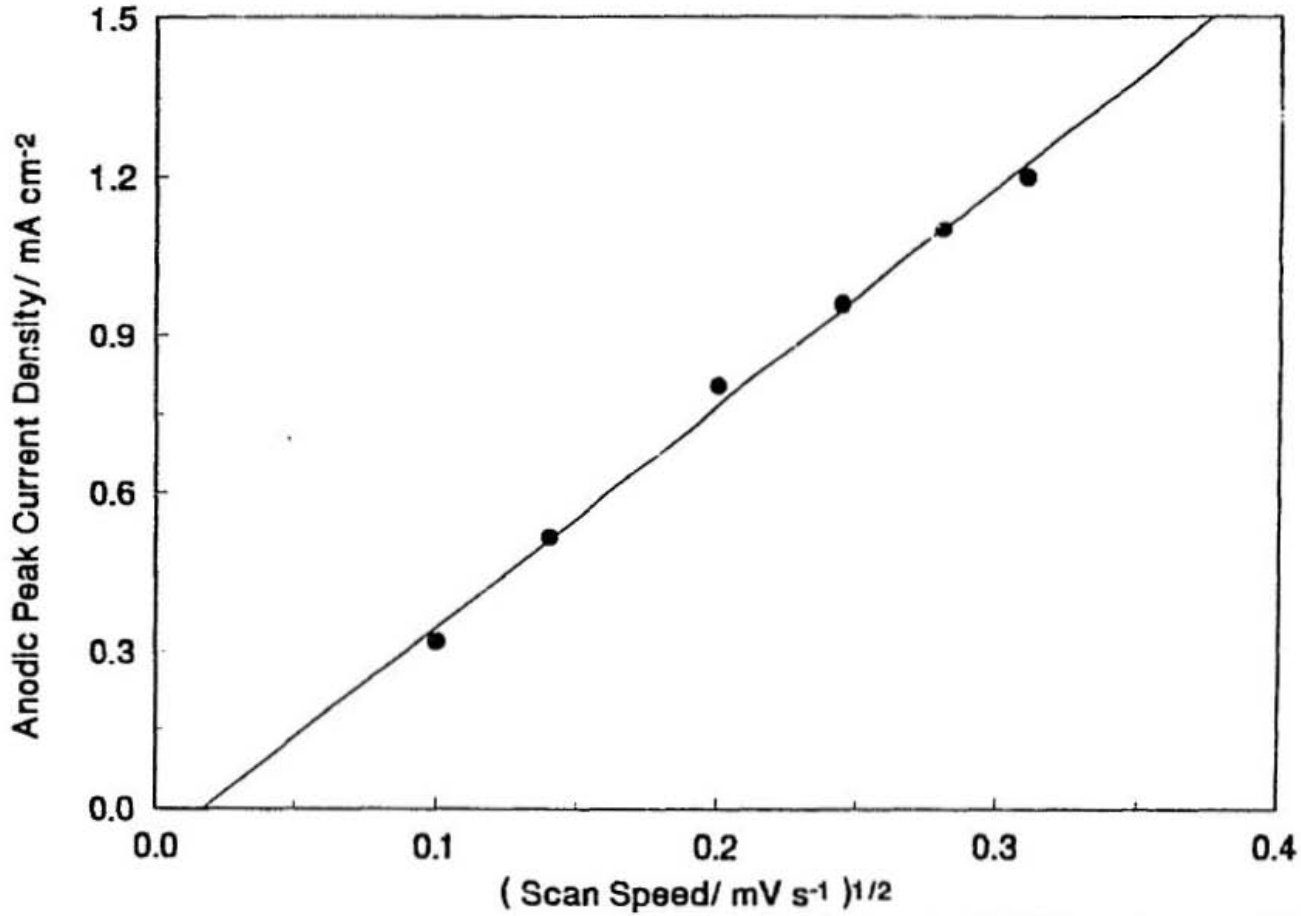

Figure 5.4.2. Plot of peak current density for ferrocyanide oxidation in poly-MPMP$^+$ *vs.* (scan rate)$^{1/2}$ in 0.1 M KH_2PO_4 containing no $K_4Fe(CN)_6$.

where C_p is the concentration of ferrocyanide in the film and other constants retain their usual meanings. These results demonstrate that the kinetics of ferrocyanide electrochemistry in poly-MPMP$^+$ are diffusion controlled and that the electron transport rate in the film is not fast enough to maintain equilibrium in the film at scan rates above 20 mV/s.

The diffusion coefficient of ferrocyanide in 1 mM $Fe(CN)_6^{4-}$, 0.1 M aqueous phosphate buffer solution was measured by rotating disc voltammetry to be 5.3 x 10^{-6} cm^2 s^{-1}. Therefore, the diffusion coefficient of ferrocyanide in the film is about four orders of magnitude lower than in solution.

Cyclic voltammetry was also used to study the kinetics of ferrocyanide electrochemistry in poly-PPP$^+$ as shown in Figure 5.4.1B. At all scan rates up to 100 n V s^{-1}, these cyclic voltammograms reveal sharp and symmetric peaks without diffusion tails. The E_{FWHM} is 140 mV for poly-PPP$^+$ at 100 mV s^{-1}. The plot of peak current *vs.* scan rate yields an excellent linear relationship as shown in Figure 5.4.3A.

The kinetics of ferrocyanide oxidation are different in poly-MPMP$^+$ and poly-PPP$^+$. The most important difference is in the dependence of the peak current on the scan rate. Figure 5.4.3 also shows plots of peak current vs scan rate for both films. A linear relationship was obtained for poly-PPP$^+$ (curve A), but there is significant curvature for poly-MPMP$^+$ (curve B). However, for poly-

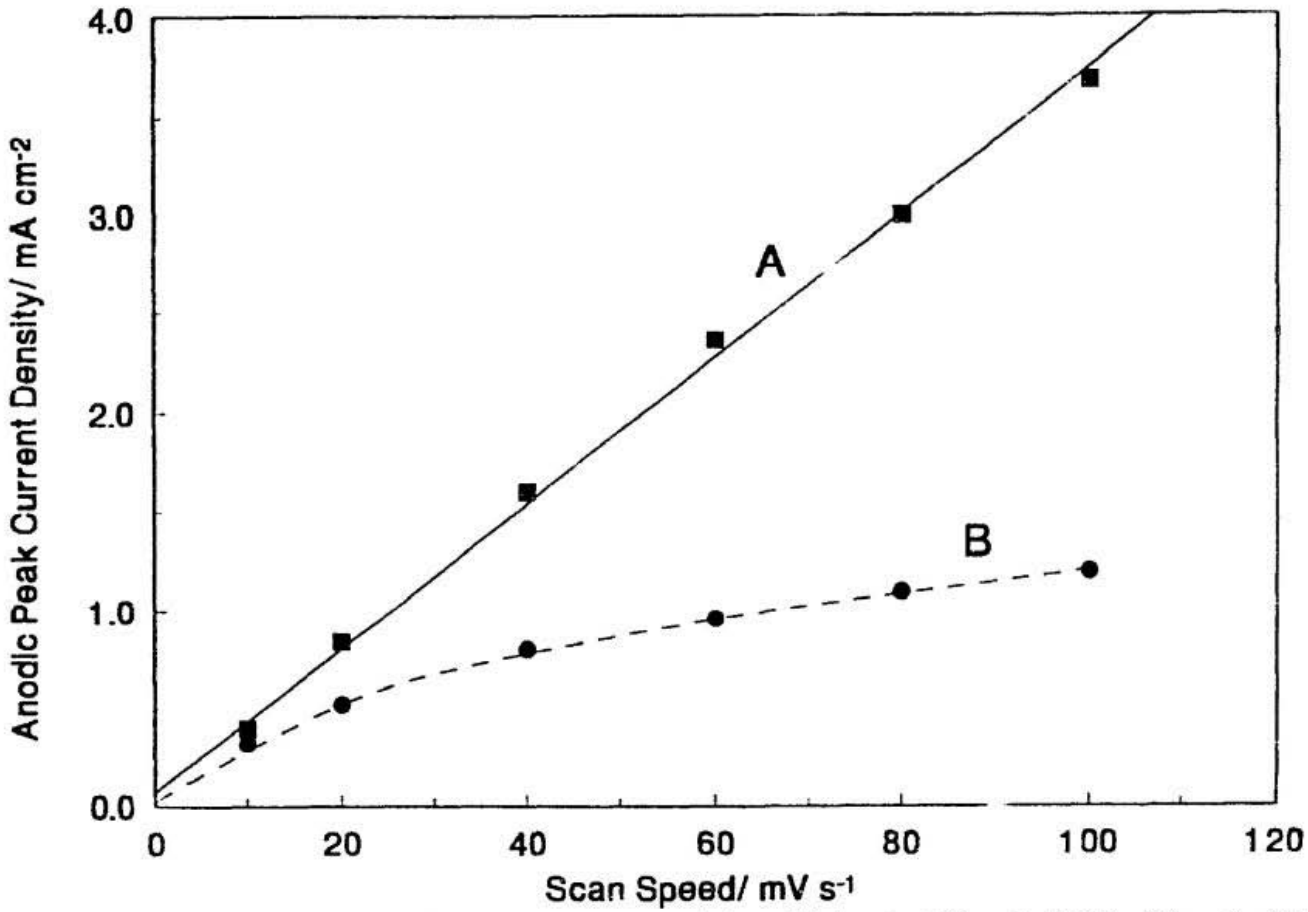

Figure 5.4.3. Plots of peak current density for ferrocyanide oxidation in (A) poly-PPP$^+$ (B) poly-MPMP$^+$ *vs.* scan rate in 0.1 M KH_2PO_4 containing no $K_4Fe(CN)_6$.

$MPMP^+$, an approximately linear relation exists between the peak current and the square root of the scan rate as shown in Figure 5.4.2. Murray[16] has discussed the relationship between the peak current and scan rate for a polymer coated electrode and its connection to the reaction kinetics. In the case of poly-$MPMP^+$, the charge transport rate is low and is dominated by a semi-infinite diffusion condition (the thickness of diffusion layer $<<$ film thickness). The peak current is proportional to the square root of the scan rate by the same equation as for species dissolved in solution and diffusing to the electrode. In contrast, the linear relation between peak current and scan rate indicates that all ferrocyanide in the poly-PPP^+ film remains in equilibrium with the electrode potential (absence of significant potential gradient within the film). Therefore, the charge transport must be fast. We can conclude that the reaction ($Fe(CN)_6^{4-} \leftrightarrow Fe(CN)_6^{3-}$) in poly-$PPP^+$ is much faster than that in poly-$MPMP^+$.

5.5 Discussion

Partition Coefficient of I^-: In Table 5.1, the I^- partition coefficients from water are much lower than those from acetonitrile. This is presumably due to the significant swelling of the polymer in water. The swelling in water is visible. When a 20 μm thick film with a dry diameter of 7.6 mm was soaked in aqueous

solution (0.1 M KH_2PO_4) for about an hour, an increase in diameter of 2 mm was observed. There is also an increase in the thickness as will be seen in chapter 6. The highly swollen film would leave more space between the polymer chains. Thus it may be easier for I^- anions to leave the positively charged sites and be exchanged with an electrolyte anion such as ClO_4^-. This could result in a lower partition coefficient.

Comparison of electrostatic binding of ferrocyanide by poly-MPMP$^+$ and poly-PPP$^+$: Both poly-PPP$^+$ and poly-MPMP$^+$ are cationic ion exchange polymers but the positively charged groups are located at different positions on the pyrrole ring. They can bind ferrocyanide by ion exchange at all the available sites. However, some differences have been noticed. The most significant difference is the kinetics of ferrocyanide electrochemistry in these films. The redox reaction of ferro/ferri-cyanide in poly-PPP$^+$ is much faster than that in poly-MPMP$^+$. The reason for the higher rate in poly-PPP$^+$ is presumably its higher electronic conductivity at the formal potential of ferrocyanide (0.14 V). At this potential poly-MPMP$^+$ is reduced ($E^{o'}$ = + 0.77 V) and has very low conductivity ($< 10^{-11}$ S cm^{-1}, Figure 4.2.7). In contrast, poly-PPP$^+$ is oxidized ($E^{o'}$ = -0.1 V) and the conductivity is about 10^{-5} S cm^{-1} (section 4.2.2). The conductivity for poly-PPP$^+$ is more than 6 orders of magnitude greater than the conductivity of poly-MPMP$^+$

at the same potential.

Another difference between the ion exchange properties of poly-MPMP$^+$ and poly-PPP$^+$ is that the ferrocyanide partition coefficient for poly-MPMP$^+$ is significantly lower than that for poly-PPP$^+$. This may be caused by the oxidized polymer chains which provide more positively charged sites in poly-PPP$^+$.

5.6 Conclusions

The ion exchange properties of poly-MPMP$^+$, poly-PPP$^+$ and poly-PPTA$^+$ have been studied. As a quantitative measure of ion exchange, partition coefficients of I^- in poly-MPMP$^+$, both in aqueous and acetonitrile solution, were obtained by potentiometry. The partition coefficient in water is significantly lower than that in acetonitrile, presumably due to swelling of the polymer in water. The

Ferrocyanide can be electrostatically bound, with excellent stability in all three polymers. The saturation concentrations for poly-MPMP$^+$ and poly-PPP$^+$ are similar at 1.4 M in aqueous solutions but the partition coefficient for poly-PPP$^+$ is about one order of magnitude higher than that for poly-MPMP$^+$. Cyclic voltammetry was used to study redox kinetics of bound ferrocyanide in the polymers. The peak current is approximately linearly related with the square root of the scan rate for poly-MPMP$^+$ but linearly related with scan rate for poly-

PPP^+. Charge transport in poly-PPP^+ is concluded to be much faster than in poly-$MPMP^+$ due to the significant difference in film conductivity at the formal potential of ferrocyanide. The enhancement in the charge transport rate for poly-PPP^+ and poly-$PPTA^+$ achieves one of the goals that prompted us to synthesize these 3-substituted polymers.

References

1. N. Oyama, T. Shimomura, K. Shigehara and F. C. Anson, J. Electroanal. Chem., 112 (1980) 271.

2. B. Zinger, and L. L. Miller, J. Am. Chem. Soc., 106 (1984) 6861.

3. G. Lian and S. Dong, J. Electroanal. Chem., 260 (1989) 127.

4. R. Noufi, D. Tench, and L. F. Warren, J. Electrochem. Soc., 128 (1981) 2596.

5. L. L. Miller, B. Zinger, and Q-N. Zhou, J. Am. Chem. Soc., 109 (1987) 2267.

6. N. Oyama and F. C. Anson, J. Electrochem. Soc., 127 (1980) 247.

7. H. Mao and P. G. Pickup, J. Electroanal. Chem., 265 (1989) 127.

8. P. G. Pickup, J.Electroanal. Chem., 225 (1987) 273.

9. B. Keita, D. Bouaziz, L. Nadjo and A.Deronzier, J. Electroanal. Chem., 279 (1990) 187.

10. S. Cosnier, A. Deronzier, J-C. Moutet and J. F. Roland, J. Electroanal. Chem., 271 (1989) 69.

11. J. R. Schneider and R. W. Murray, Anal. Chem., 54 (1982) 1508.

12. H. S. White, J. Leddy and A. J. Bard, J. Am. Chem. Soc., 104 (1982) 4811.

13. R. W. Murray in A. J. Bard (Ed.), Electroanal. Chem., Vol. 13, Marcel Dekker, New York, 1984, P.330.

14. A. J. Bard and L. R. Faulkner, Electrochemical Methods, Wiley, New York, 1980, P.228.

15. A. J. Bard and L. R. Faulkner, Electrochemical Methods, Wiley, New York, 1980, P.218.

16. R. W. Murray in A. J. Bard (Ed.), Electroanal. Chem., Vol. 13, Marcel Dekker, New York, 1984, P.204.

Chapter 6

Ion Transport in Poly-[1-methyl-3-(pyrrol-1-ylmethyl) pyridinium] (poly-$MPMP^+$)

Permeability to ions is one of the most important properties of conducting ion exchange polymers. Thorough understanding of ion transport in conducting polymers is of interest both in scientific significance and applications. Ion transport is associated with the processes of switching between the oxidized and reduced states[1]. The ion transport rate affects other properties such as ionic conductivity and electronic conductivity[2,3]. A thorough understanding of ion transport is the basis of many applications such as in batteries, displays and electrochemical devices[4]. Effective control of ion transport rates can lead to regulation of the rate of drug release in a human body or the release of a reagent into an automated analyzer in an industrial process[5,6].

This chapter describes the transport properties of different anions such as iodide, ferrocyanide, chloride and perchlorate within poly-[1-methyl-3-(pyrrol-1-ylmethyl)pyridinium] (poly-$MPMP^+$) in water and acetonitrile. The electroactive anions consist of two categories: low formal potential ($E^{o'} < 0.5$ V) anions and

high formal potential ($E^{o'} > 0.8$ V) anions.

6.1 Investigation of Transport of Electroactive Ions by Rotating Disc Voltammetry

Many efforts have been made to investigate ion transport rates in conducting polymers[7,8,9,10,11,12,13,14,15,16]. Among the methods used, rotating disc voltammetry (RDV) appears to be the most versatile method in the measurement of ion transport rates. A well defined transport region can be established and the theoretical treatment is analogous to that for classical rotating disc voltammetry. The disc surface is uniformly accessible to reactants and the solution diffusion layer thickness is precisely determined. Therefore, the ion transport in the film can be quantitatively determined without complications of external mass transport.

6.1.1 Transport of I^- within Poly-MPMP$^+$ in Acetonitrile

Figure 6.1.1 shows the principle of the RDV measurement. The substrate R is brought to the polymer surface by convection in solution and, if the film is not electronically conductive, diffuses through the film. It then reacts at the Pt/film interface and produces a current that reflects the mass transport rate. The electronic conductivity of the film must be sufficiently low to prevent the solute from reacting at the film/solution interface or within the film. Therefore, the

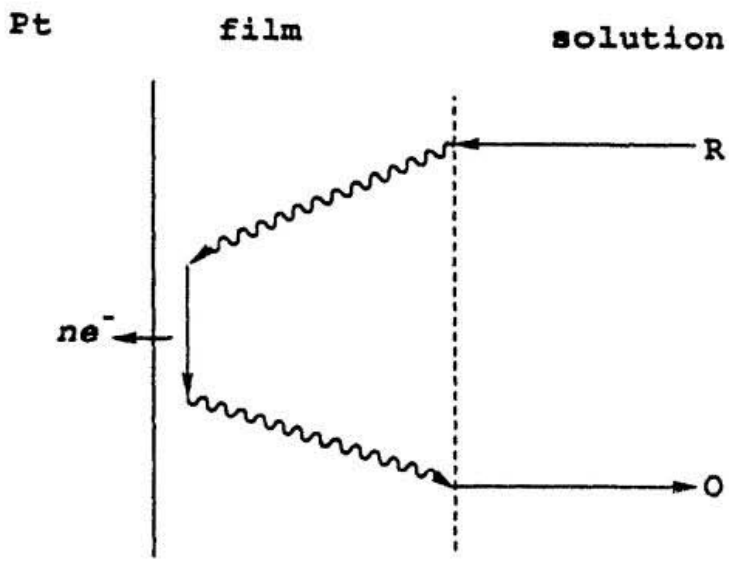

Figure 6.1.1. Schematic diagram of ion transport pathways within the polymer film and in solution during rotating disc voltammetry.

rotating disc voltammetry has to be operated at sufficiently low potential. This condition can be satisfied by choosing probe ions with low formal potentials (<0.5V for poly-MPMP$^+$). Iodine and ferrocyanide were selected as probe anions in this work because their oxidation potentials are below 0.5 V.

Rotating disc voltammetry at permeable polymer coated electrode has been described by Murray and coworkers[7]. The equation below from Murray's paper is based on a membrane diffusion model in which the film acts as a uniformly permeable barrier.

$$\frac{1}{1000i_l} = \frac{1}{nFAD_{s,pol}PC_s/d} + \frac{1}{0.62nFAD_s^{2/3}\nu^{-1/6}C_s\omega^{1/2}} \qquad (6.1.1)$$

The constants n, F, A retain the meanings defined in chapter 3 (section 3.1). $D_{s,pol}$ and D_s are the diffusion coefficients of the substrate within the film and in solution, respectively. P is the partition coefficient of substrate in the film as described in Chapter 5 (section 5.1.2).

The second term of the right hand side of equation 6.1.1 reflects the rate of solute diffusion through the Levich depletion layer. The diffusion coefficient D_s for the solute in solution is obtained from this term. The first term on the right hand side of the equation corresponds to the diffusion of the solute within the film. If diffusion in the film is very fast, the first term approaches zero. Consequently,

equation (6.1.1) will have a Levich form of ($i_l \propto \omega^{1/2}$), and a plot of i_l vs $\omega^{1/2}$ will be linear with zero intercept. If the diffusion of solute in the film is slower than in solution, the first term in equation (6.1.1) is not zero, and a plot of i_l^{-1} vs $\omega^{-1/2}$ is linear. This particular plot is called an inverse Levich plot and the intercept at infinite ω contains the diffusion coefficient $D_{s,pol}$. The $D_{s,pol}$ can be obtained if the partition coefficient P is known. Also, intercepts from inverse Levich plots should be proportional to film thickness while the slopes should be independent of film thickness and the same as for a bare electrode.

6.1.2 Transport of I^- within Poly-$MPMP^+$ in Acetonitrile.

Figure 6.1.2 shows rotating disc voltammograms for a bare Pt electrode and poly-$MPMP^+$ coated electrodes with film thicknesses ranging from 35 nm to 140 nm in acetonitrile containing 1.0 mM tetrabutylammonium iodide (But_4NI) and 0.1 M $LiClO_4$. Two waves with a current ratio of 2:1 are observed for the bare Pt electrode. The half wave potentials of +0.17 and +0.53 V correspond to the oxidation of I^- to I_3^- and I_3^- to I_2, respectively. In contrast to the behaviour observed for ferrocene (see Chapter 4, Figure 4.1.2), the I^- oxidation wave at poly-$MPMP^+$ coated electrodes rises at the same potential as at a bare Pt electrode. This indicates that the substrate, I^-, penetrates through the film and reacts at the Pt surface as schematically depicted in Figure 6.1.1. The limiting

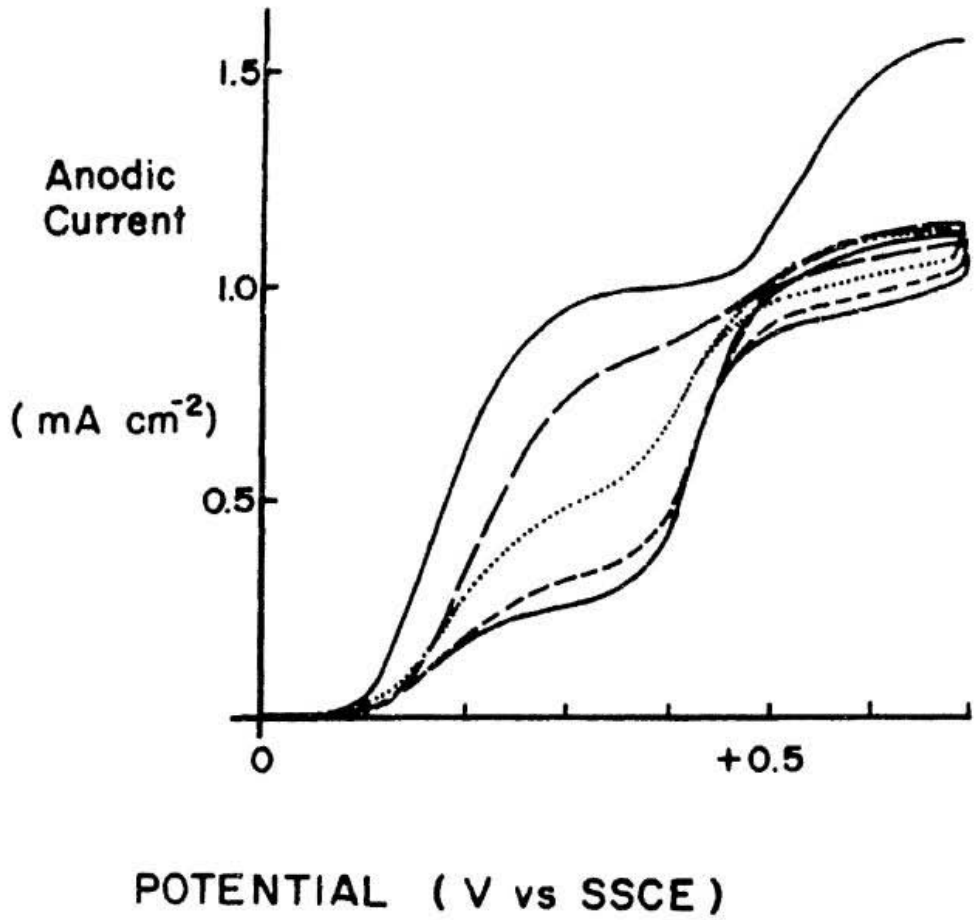

Figure 6.1.2. Rotating disk voltammetry of tetrabutylammonium iodide (0.1 mM) in 0.1 M $LiClO_4/CH_3CN$ at naked Pt(_____) and poly-MPMP$^+$ coated electrodes. Film thicknesses: 35(— —), 70(·····), 100(-----), and 140nm(_____,lower); rotation rate 2000 rpm and scan rate 20mV/s.

currents at about 0.3 V have been largely depressed due to the low ion transport rate within the film. This decrease becomes more significant with increasing film thickness.

Figure 6.1.3 shows that the limiting currents (i_l) at 0.3V increase with rotation rate (ω) but not with the normal $\omega^{1/2}$ dependence. The plot of i_l^{-1} vs $\omega^{-1/2}$ is linear with a non-zero intercept as shown in Figure 6.1.4. Normally, non-linear Levich plots and non-zero inverse Levich intercepts indicate slow reactions. Evidence that slow reaction is not limiting is the dependence on film thickness. This suggests that the rate controlling step is not the mass transport in solution (linear inverse Levich plots) but is mass transport in the film. The diffusion coefficient, $D_{s,pol}$, can therefore be determined by using equation (6.1.1). Data for a number of films with thicknesses ranging from 35 nm to 140 nm have been plotted in Figure 6.1.4. The parallel lines (constant slope) demonstrate that the I^- transport rate from solution to the film/solution interface is not changed despite the variation of polymer film thickness. A bare electrode yields a linear plot with the same slope and an almost zero intercept. However, the value of the intercepts for coated electrodes increases with increasing film thickness. Figure 6.1.5 shows that there is a linear relationship between the intercepts and the film thickness. The slope of the plot of intercept vs. film thicknesses gives an average value for $PD_{s,pol}$ of $(1.3 \pm 0.1) \times 10^{-7}$ cm^2 s^{-1}. The partition coefficient P is 240 (section

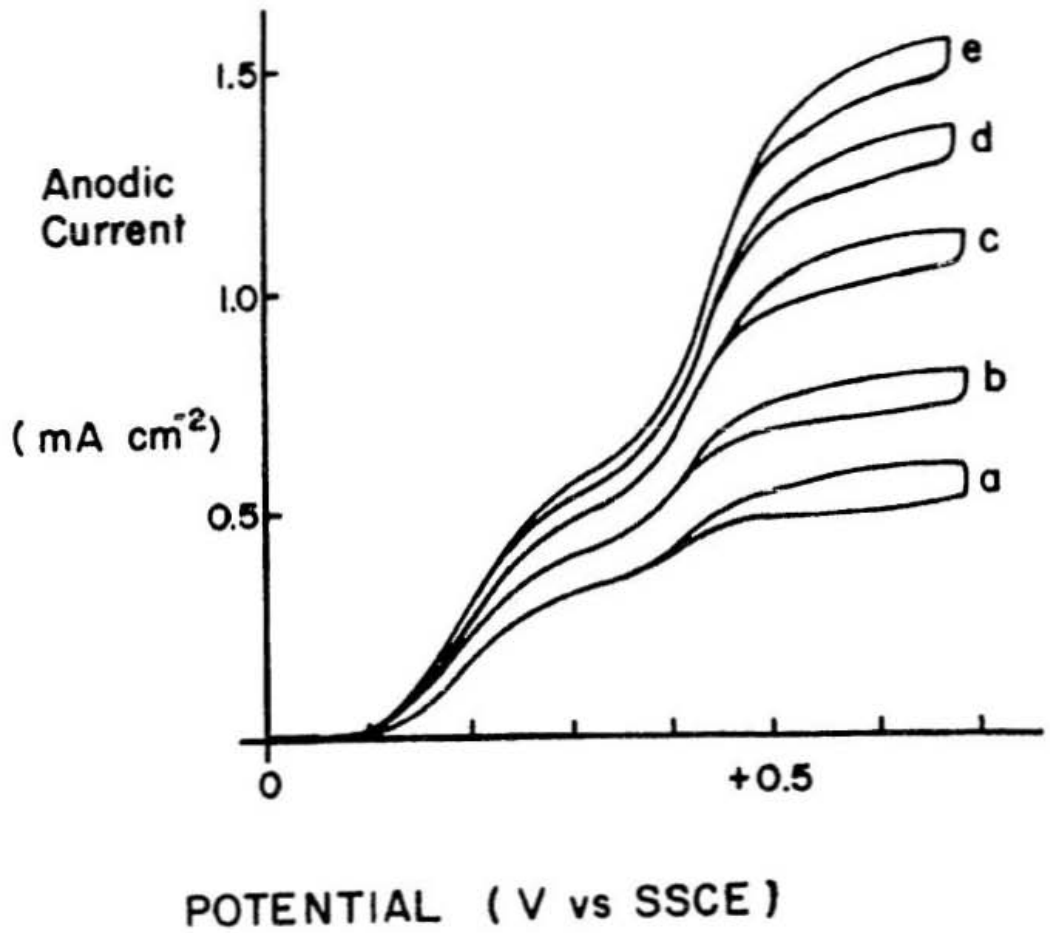

Figure 6.1.3. Rotating disk voltammetry of tetrabutylammonium iodide (0.1 mM) in 0.1 M $LiClO_4/CH_3CN$ at poly-$MPMP^+$ coated electrodes at different rotation rates: (a) 500, (b) 1000,(c) 2000, (d)3000, (e)4000 rpm. Film thicknesses 70 nm and scan rate 20mV/s.

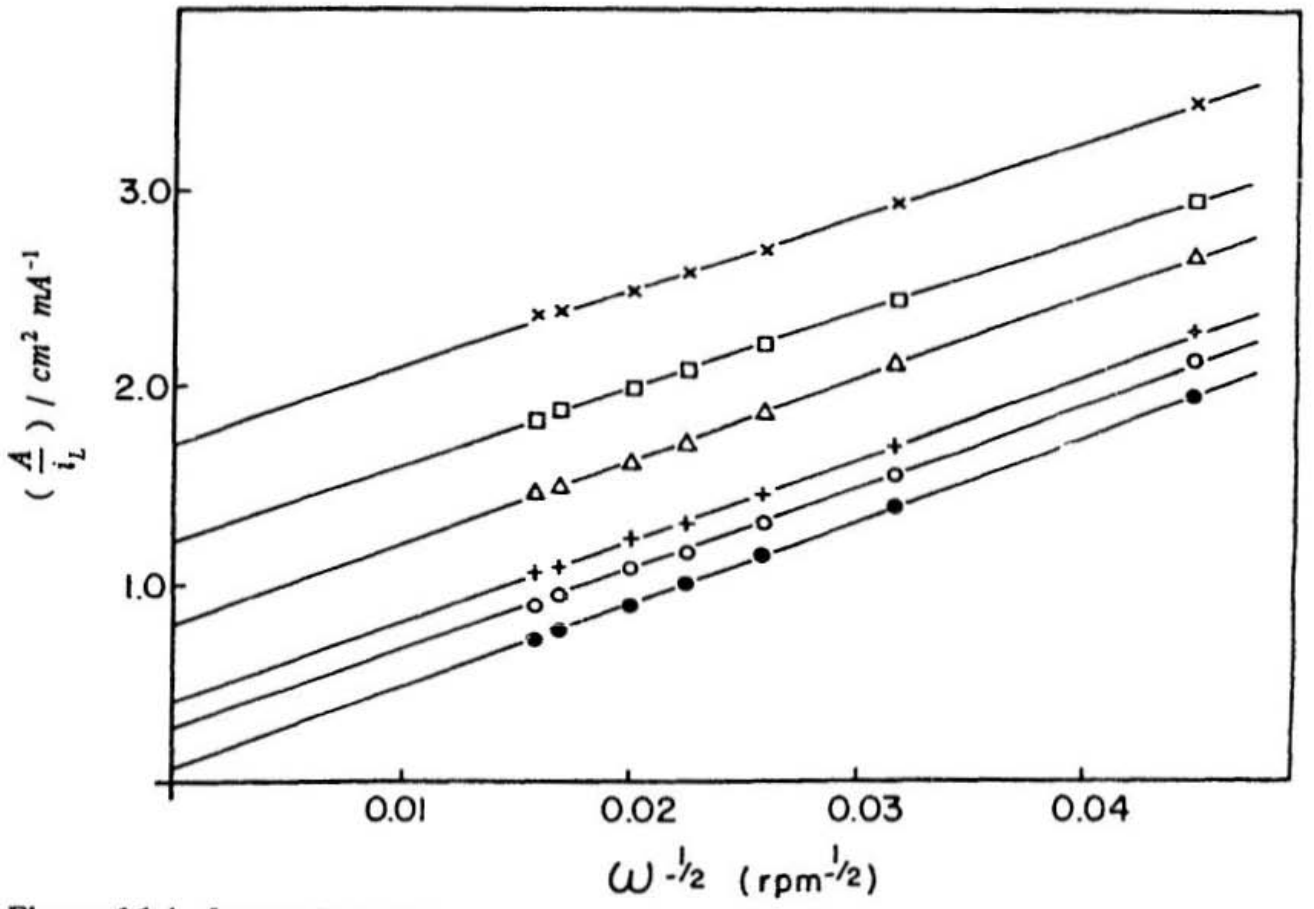

Figure 6.1.4. Inverse Levich plots for I^- (1.0 mM) oxidation at naked Pt (●) and poly-MPMP$^+$ coated Pt electrodes with film thicknesses: 18 (○), 35 (+), 70 (△), 100 (□), and 140 nm (×).

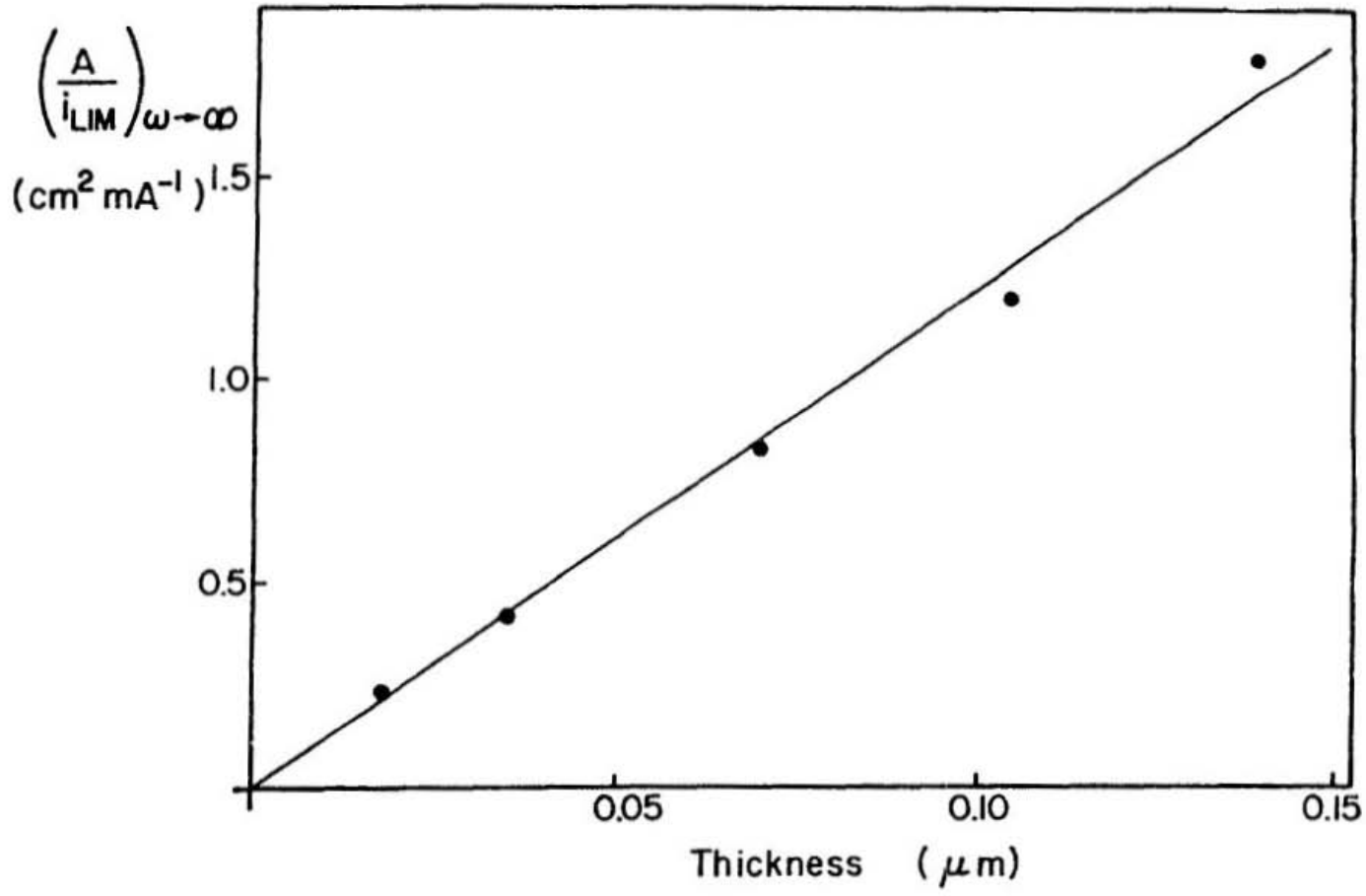

Figure 6.1.5. Plot of intercept vs film thickness for the inverse Levich plots shown in Figure 6.1.4.

5.1.2, Table 5.1), and, therefore, the I^- diffusion coefficient, within poly-$MPMP^+$ in acetonitrile, is 5.4×10^{-10} cm^2 s^{-1}.

6.1.3 Transport of I^- within Poly-$MPMP^+$ in Water

The transport of iodide in poly-$MPMP^+$ was also investigated in aqueous solution (1.0 mM, 0.1M $NaClO_4/H_2O$). However, under these experimental conditions, the half wave potential for I^- oxidation is 0.48 V which is too high to prevent interference from electronic conduction in the film. Fortunately, the electronic conductivity of poly-$MPMP^+$ can be permanently removed by potential cycling in aqueous solution as shown in Figure 6.1.6. When the potential is increased to about 1.40 V, the film loses its electrochemical activity and becomes non-conductive due to overoxidation[17]. To test for the possibility of structure change, a comparison of the partition coefficient measured for the deactivated films with that of virgin films was made. The results are listed in Chapter 5, Table 5.1. The absence of a significant difference in the partition coefficients between the virgin and deactivated films confirms that the structure of the polymer was not significantly changed by deactivation.

Figure 6.1.7 shows several rotating disc voltammograms for I^- oxidation through poly-$MPMP^+$ films (ranging from 0.2 to 0.5 μm) in aqueous solution. These rotating disc voltammograms show similar behaviour to that observed in

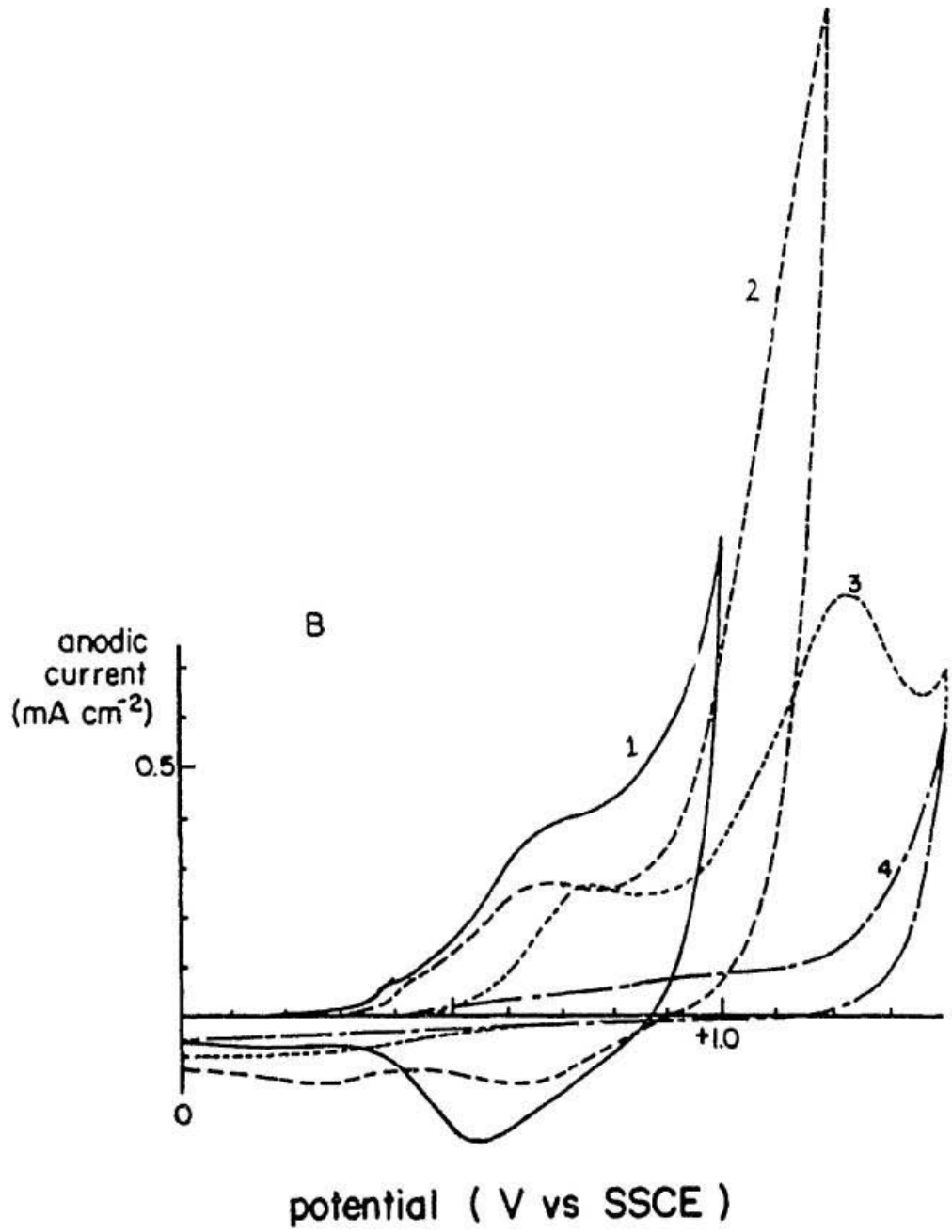

Figure 6.1.6. Cyclic voltammograms of four successive scans for a 0.3 μm poly-MPMP$^+$ film in 0.1 M $NaClO_4/H_2O$ solution. Scan rate 100mV/s.

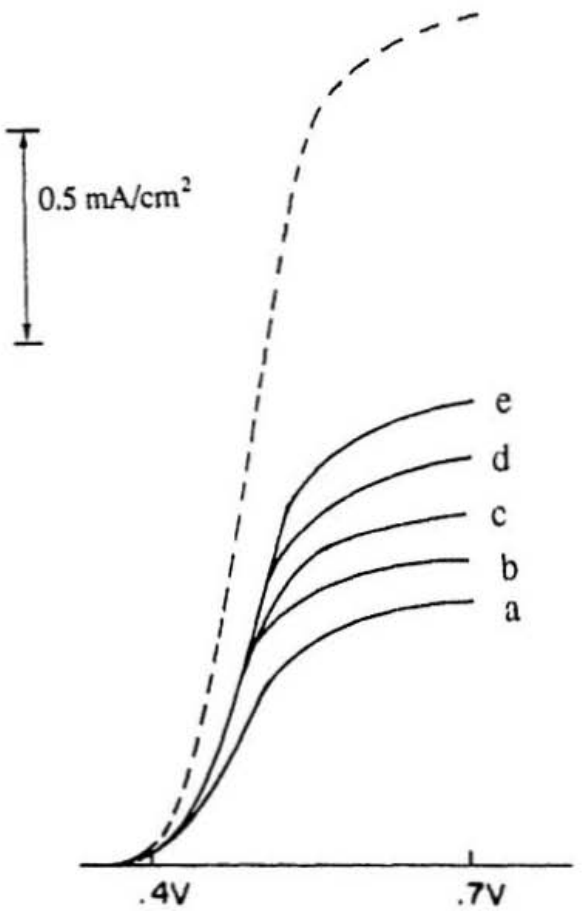

Figure 6.1.7. Rotating disk voltammetry of I^- (0.1 mM) in 0.1 M $NaClO_4/H_2O$ at a naked Pt electrode (dashed line, rotation rate 3600 rpm) and at poly-MPMP$^+$ coated electrodes at different rotation rates: (a) 400, (b) 900,(c) 1600, (d) 2500, and (e) 3600 rpm. Film thicknesses 0.2 μm and scan rate 20mV/s.

acetonitrile, and the product of diffusion coefficient and partition coefficient is similarly worked out to be $PD_{s,pol}$ = (2.8 ± 1.2) x 10^{-6} cm^2 s^{-1}. Dividing this product by the I^- partition coefficient in water (P = 19 ± 2 from Table 5.1), the I^- diffusion coefficient within poly-$MPMP^+$ in aqueous solution is found to be 1.5 x 10^{-7} cm^2 s^{-1}.

6.1.4 Transport of $Fe(CN)_6^{4-}$ within Poly-$MPMP^+$ in Water

Ferrocyanide transport within poly-$MPMP^+$ in water was also investigated by rotating disc voltammetry. Figure 6.1.8 shows rotating disc voltammograms for $Fe(CN)_6^{4-}$ at a bare electrode (dashed line) and a coated electrode (-x-) in 0.1 mM $Fe(CN)_6^{4-}$, 0.1 M KH_2PO_4/H_2O (pH = 2.5) solution. The voltammograms show similar features to those for iodide. The wave for ferrocyanide oxidization at the poly-$MPMP^+$ coated electrode rises at a potential similar to that at the bare electrodes. It indicates that ferrocyanide diffuses through the film and reacts at the Pt/film interface. The limiting current for the first wave at the polymer coated electrode is depressed owing to the sluggish transport of ferrocyanide in the film.

The same procedures used to calculate the diffusion coefficient for I^- (section 6.1.1) were used here. The intercepts of inverse Levich plots (Figure 6.1.9) were plotted against film thickness as shown in Figure 6.1.10 to yield the product, $PD_{s,pol}$, which is (4.4 ± 0.4) x 10^{-8} cm^2 s^{-1} for a series of films over the

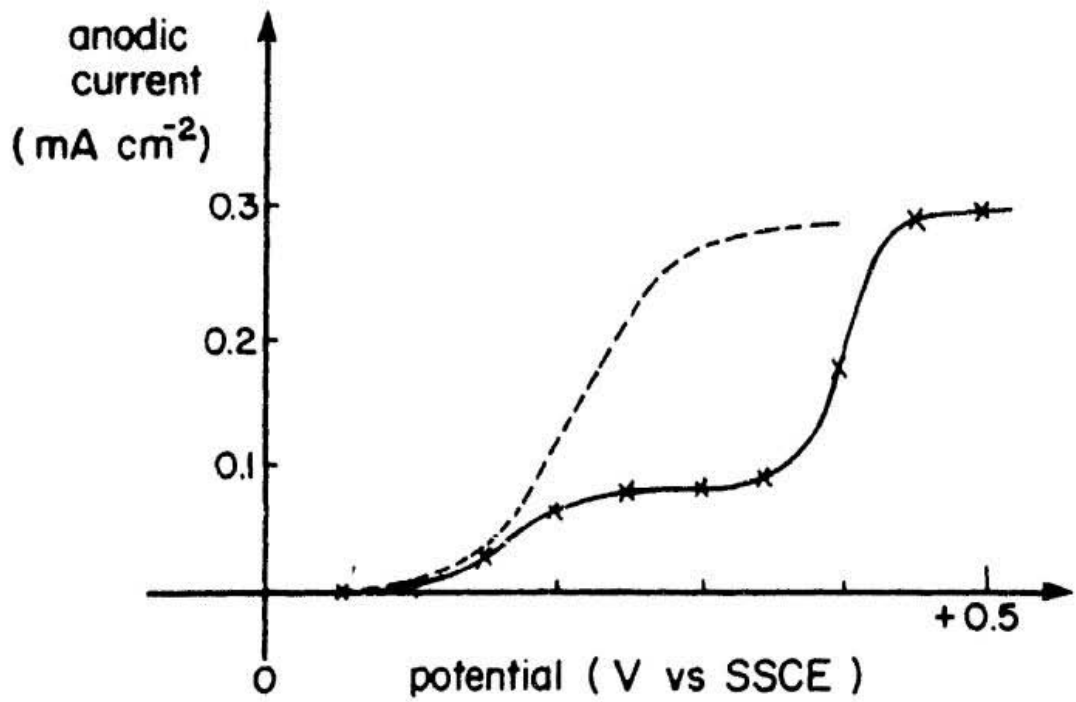

Figure 6.1.8. Rotating disk voltammograms of $Fe(CN)_6^{4-}$ (0.1 mM) in 0.1 M KH_2PO_4 at naked Pt (-----, 5 mV/s) and poly-MPMP$^+$ coated Pt (0.19 μm) electrodes (-x-), data points recorded after 20 s at each potential).

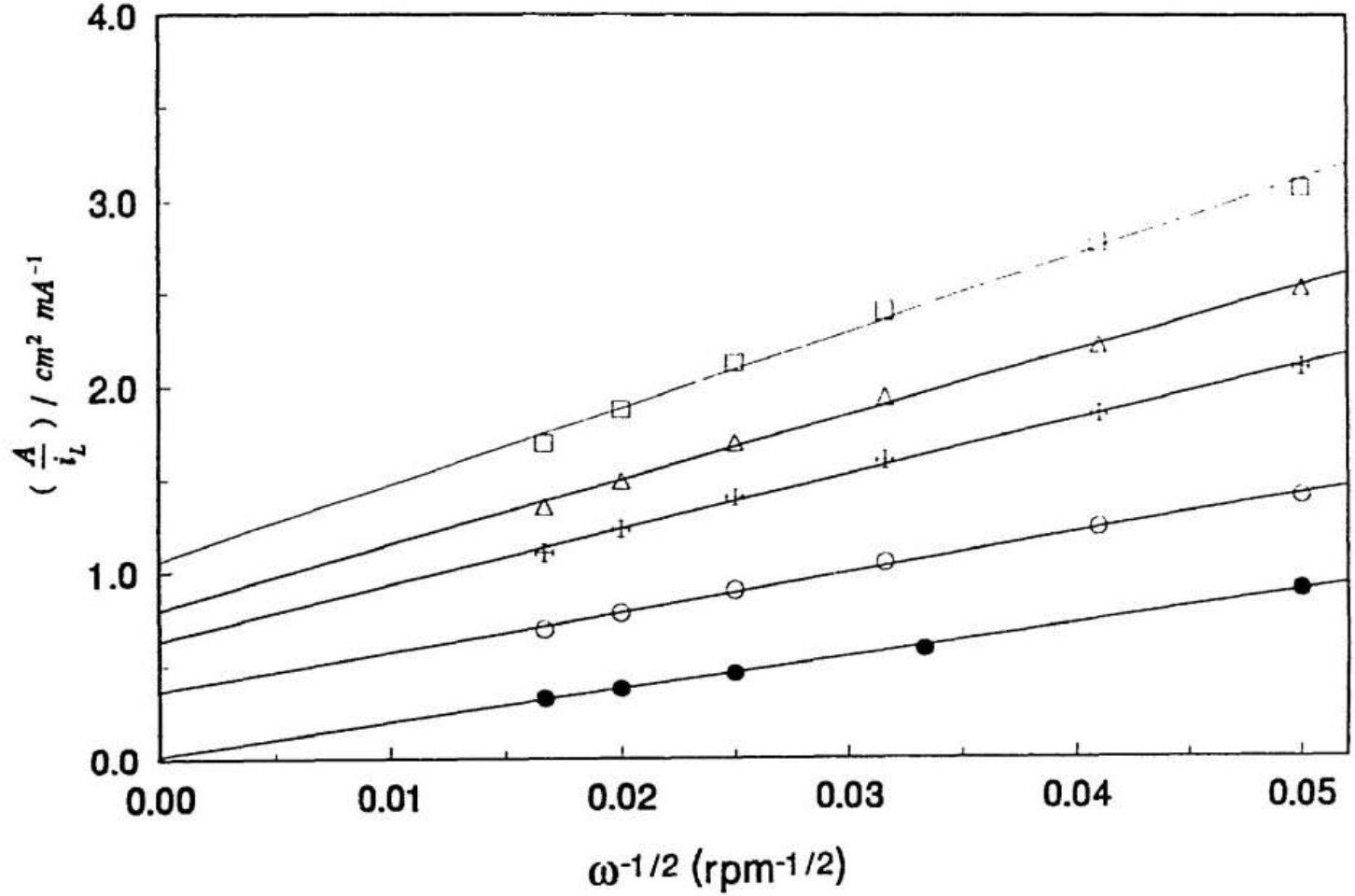

Figure 6.1.9. Inverse Levich plots for $Fe(CN)_6^{4-}$ (0.10 mM) oxidation at naked Pt (●) and poly-MPMP$^+$ coated Pt electrodes with film thicknesses: 50 (⊙), 100 (⊕), 150 (△), and 200 nm (□).

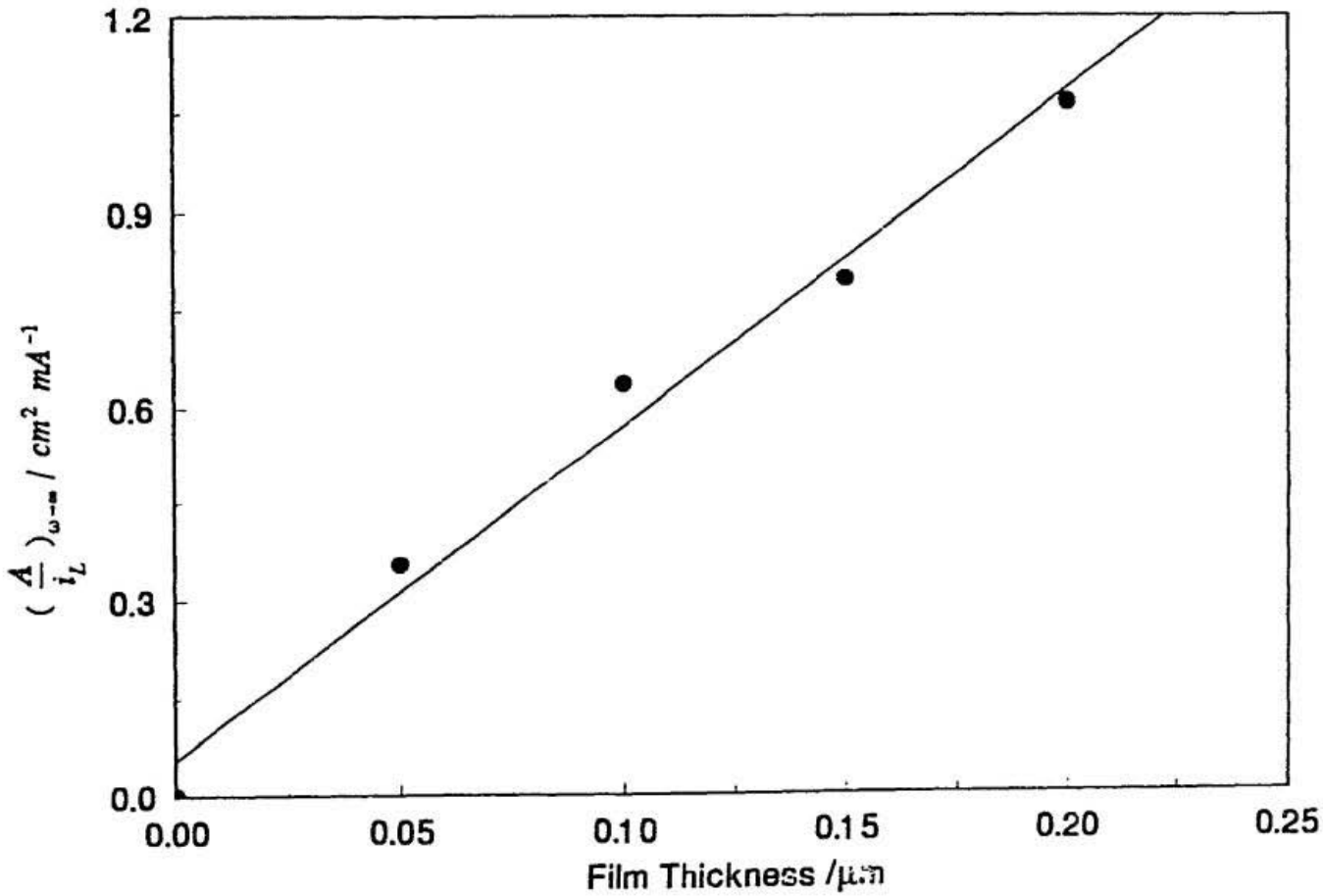

Figure 6.1.10. Plot of intercept *vs* film thickness for the inverse Levich plots shown in Figure 6.1.9.

thickness range from 50 to 200 nm. The slopes are not constant due to the decrease of $Fe(CN)_6^{4-}$ concentration during the experiments. The partition coefficient for ferrocyanide under the conditions of these experiments is 3.2×10^4 as reported in Chapter 5, section 5.2.2. The diffusion coefficient of ferrocyanide in poly-$MPMP^+$ is therefore $(3.2 \pm 0.3) \times 10^{-11}$ cm^2 s^{-1}. This value is more than 4 orders of magnitude smaller than the diffusion coefficient for I^- in the film under similar conditions. A likely explanation for this large difference is reconstruction within the film. Since the ferrocyanide carries a higher charge than iodide and four $MPMP^+$ units must be associated with each ferrocyanide, electrostatic cross-linking will occur and movement of the ferrocyanide ion will be restricted[18].

6.2 DC Ionic Conductivity Measurements

Ion transport was also studied by DC ionic conductivity measurements. This method is versatile for any anion, not limited by the electroactivity and the formal potential of the anion, and the operation is simple. Diffusion coefficients of anions can be obtained from the ionic conductivity of the polymer using the following equation[5,6]:

$$D_{s,pol} = 1000\sigma_i RT/F^2 C_p \qquad (6.2.1)$$

where σ_i, $D_{s,pol}$ and C_p are, respectively, the ionic conductivity of the film, the

anion diffusion coefficient in the polymer, and the concentration of the ion exchange sites. For poly-MPMP$^+$, the ion exchange sites are the pyridinium cations which have a concentration of 5.6 M (chapter 3, section 3.3). These positively charged sites allow anion migration through the film but cause exclusion of all cations from the film.

DC ionic conductivity measurements were carried out in a cell consisting of two compartments separated by the polymer film (shown in Figure 2.5.1). The ionic conductivity was measured perpendicular to the plane of the film as described in section 2.5. The film resistance was obtained by measuring the potential difference, ΔE_{DC}, between the two sides of the film when a constant current, i_{DC} passed through the film and solution assembly. The ionic conductivity, σ_I is obtained from the following equation:

$$\sigma_I = A\Delta E_{DC}/di_{DC} \qquad (6.2.2)$$

where A and d are the film area and thickness, respectively. The solution resistance was measured in the same cell without the polymer film between the two compartments and it was subtracted from the total resistance. The results for Cl^- transport are listed in Table 6.1 (next page).

The diffusion coefficients obtained by ionic conductivity measurements for all electrolytes and film thicknesses are in fair agreement. However, it appears that diffusion coefficients in KCl solutions are higher than those in

Table 6.1 Ionic conductivities and Cl^- diffusion coefficients for poly-$MPMP^+$ in aqueous solutions

electrolyte	film thickness (μm)	film resistance (Ω)	film conductivity (S cm^{-1})	$D_{s,pol}$ (cm^2 s^{-1})
1.0 M KCl	10	1.7	5.9×10^{-3}	3.1×10^{-7}
	21	2.5	9.1×10^{-3}	
	30	5.5	5.9×10^{-3}	
	40	6.7	6.2×10^{-3}	
0.10 M KCl	20	7.5	2.8×10^{-3}	1.3×10^{-7}
0.10 M But_4NCl	20	12	1.7×10^{-3}	8.2×10^{-8}
0.44 M But_4NCl	20	5.8	3.6×10^{-3}	1.7×10^{-7}

tetrabutylammonium chloride (But_4NCl) solutions of similar concentration. This can be explained by a contribution to the conductivity from the smaller K^+ ion since [in parallel conductivity measurements (see below)] the measured conductivity in the KCl/H_2O solution increases with time but no change is observed in But_4NCl/H_2O solution. Figure 6.2.1 shows the results of a parallel

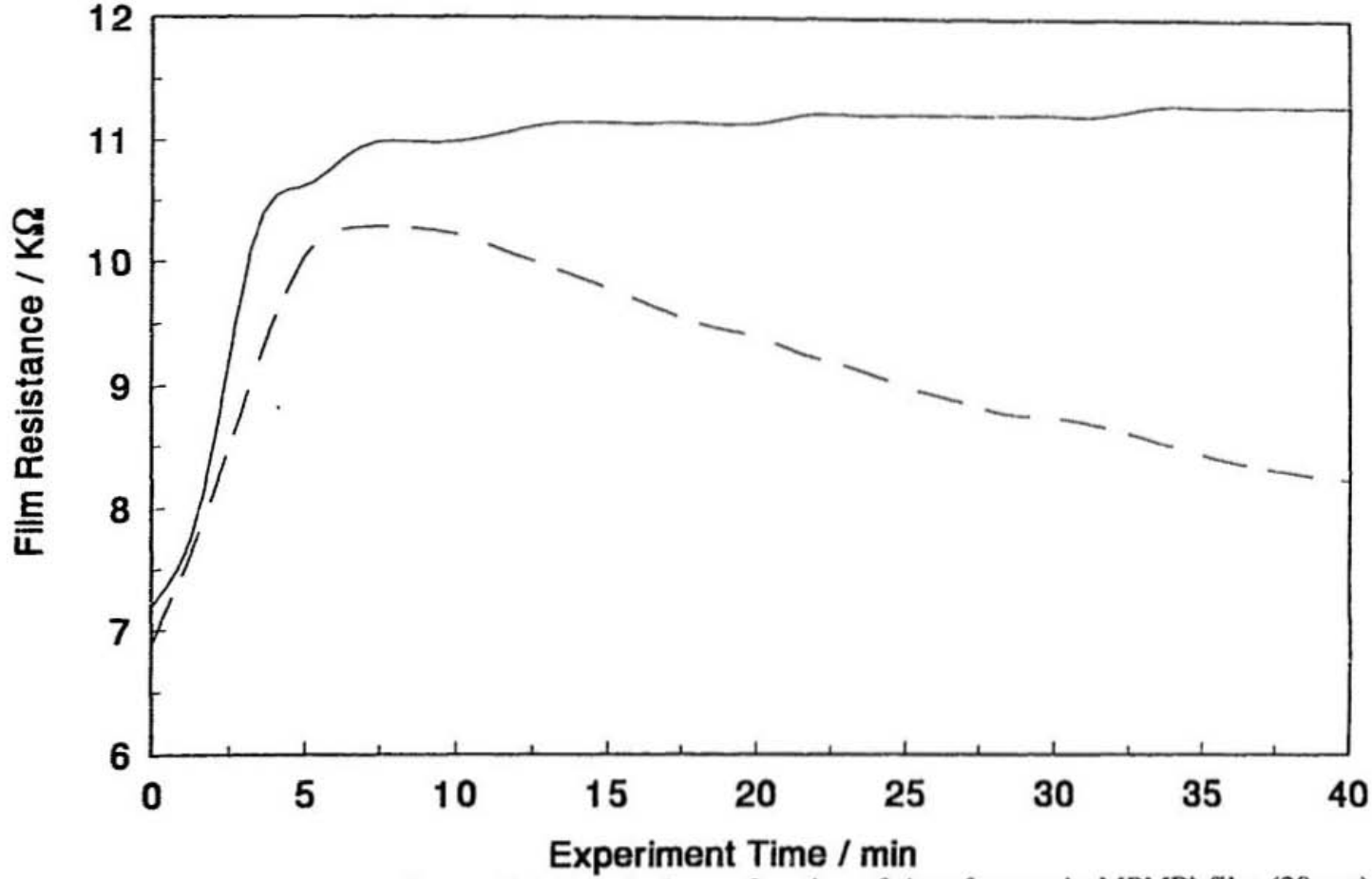

Figure 6.2.1. Ionic resistance (in parallel direction) as a function of time for a poly-MPMP$^+$ film (20 μm) in different electrolytes:(_____) in 1.0 M tetrabutylammonium chloride/H_2O and 1.0 M KCl/H_2O (----).

conductivity measurement in different electrolyte solutions. It demonstrates how the measured ionic resistance varies with time. The resistance in 1.0 M But_4NCl/H_2O (solid line) remains constant whereas the resistance decreases after a peak in 1.0 M KCl/H_2O (dashed line). All salt was washed out of the film before the experiment to ensure that But_4N^+ or K^+ is the only cation. The decreasing resistance with time in the KCl solution is presumably caused by conduction by K^+ which is driven into the film by the high solution concentration (1.0 M). The large But_4N^+ cation appears to be excluded from the polymer, even when it is at 2.0 M in solution. Thus, we can draw two conclusions from Figure 6.2.1. First, cation conduction can occur in the measurement of the ionic conductivity of poly-$MPMP^+$ in the presence of small cations, but can be eliminated by using large cations. Secondly, the diffusion coefficient obtained from the measurements in 1.0 M KCl is overestimated due to cation conduction.

A DC conductivity measurement was also carried out in an aqueous I^- (1.0 M KI) solution in the same manner as for Cl^-. The result is listed in Table 6.4 for comparison.

6.3 Estimation of Swelling Factor

As pointed out in Chapter 5 (Section 5.6), the poly-$MPMP^+$ swells significantly in aqueous solutions. The swelling of a polymer can be described by

swelling factor, s, which is the ratio of the swollen dimension (*e.g.* thickness) of a material over its dry dimension. This swelling factor for poly-MPMP$^+$ was estimated from the ionic resistances across the film in two directions as schematically shown in Figure 6.3.1 The variables s, d, R$\perp$ and R// are respectively the swelling factor, the dry film thickness, and the resistances measured perpendicular and in parallel to the plane of the polymer film. The perpendicular and parallel resistances are related to the polymer's resistivity as:

$$R_{\perp} = \rho sd/A \tag{6.3.1}$$

and

$$R_{/} = \rho l/sdw \tag{6.3.2}$$

where ρ, A, w and l are respectively resistivity, the area of the film in the perpendicular measurement, the width and the length of the film in the parallel measurement. The swelling factor can thus be calculated by using equations (6.3.1) and (6.3.2):

$$s = \sqrt{\frac{R_{\perp} A l}{R_{\parallel} d^2 w}} \tag{6.3.3}$$

The perpendicular resistance was measured using the cell shown in Figure 2.5.2 The parallel resistance was determined in the cell depicted in Figure 2.5.1. The experimental method has been described in Section 2.5, Chapter 2. A swelling factor of 3.2 was obtained for poly-MPMP$^+$ in 2.0 M Et_4NCl aqueous solution.

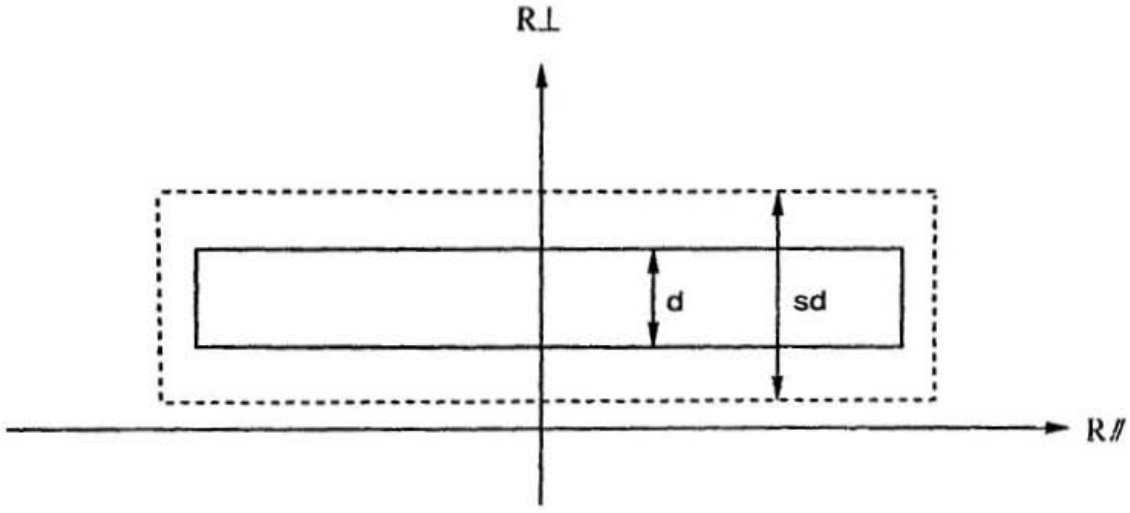

Figure 6.3.1. Schematic diagram of the estimation of the swelling factor. The solid box and dashed box represent the cross-sections of the dry film and the water swollen film respectively; d, sd, R⊥ and R// are respectively the dry thickness, wet thickness of the film, resistance measured perpendicular to the film, and resistance measured parallel to the film.

The amount of swelling is significant and it explains why ion transport in aqueous media is much faster than in acetonitrile solution where swelling was not observed. However, this number seems to be overestimated since the estimation is based on an assumption that the resistivity is identical in both perpendicular and parallel directions. If we identify the perpendicular resistivity as $\rho_\perp$ and parallel resistivity as $\rho_\parallel$, and use equation 6.3.1 and 6.3.2 we have:

$$R_\perp = \rho_\perp sd/A \tag{6.3.4}$$

and

$$R_\parallel = \rho_\parallel l/sdw \tag{6.3.5}$$

If the same film area (film plane) is used in both cases, then A = lw, we can combine equations 6.3.4 and 6.3.5 to give the swelling factor without any assumption:

$$s = \sqrt{\frac{\rho_\perp}{\rho_\parallel}} \times \frac{l}{d}\sqrt{\frac{R_\perp}{R_\parallel}} \tag{6.3.6}$$

We have:

$$s = 3.2 \times \sqrt{\frac{\rho_\perp}{\rho_\parallel}} \tag{6.3.7}$$

If $\rho_\perp > \rho_\parallel$, s > 3.2, the swelling factor is underestimated, and

if $\rho_\perp > \rho_\parallel$, s < 3.2, the swelling factor is overestimated.

Since the difference in the resistivity for the perpendicular and parallel directions

is not clear, dry thicknesses were still used in all measurements in aqueous solutions in this work.

6.4 Discussion

RDV for I^- transport in poly-MPMP$^+$ Rotating disc voltammetry has been a useful method in the study of ion transport in poly-MPMP$^+$. However, as pointed out by Peerce and Bard[19], the reaction of an electroactive solute at a polymer film coated electrode can have four possible modes and the use of equation (6.1.1) for these modes would yield diffusion coefficients with different physical meanings. The first mode is electronic conduction which certainly must be considered for a conducting polymer. Secondly, the oxidation or reduction could occur at the film surface *via* electron transport mediation by redox sites in the polymer film. The third mode is membrane diffusion by which the substrate virtually "dissolves" into the polymer and its transport in the film occurs by diffusion through the polymer phase. The last possibility is that the substrate can diffuse through the solvent in film imperfections which could be pinholes and/or channels with dimensions much greater than the size of the substrate.

The first possibility, electronic conduction through the polymer, can be excluded from the limiting current, which is less than at a bare electrode, but then

rises to the bare electrode value when the polymer becomes conductive at sufficiently high potential. If the first wave was due to electronic conductivity, it would rise smoothly to the bare electrode limiting current as for ferrocene in chapter 4. This argument can be quantitatively evaluated by the *in situ* electronic conductivity measurements in Chapter 4 (see Figure 4.2.6). The current by electronic conductance through the film is given by equation 4.1.8 with $x = d$:

$$i = \sigma sA/d$$

The conductivity can be calculated from Figure 4.2.6 for the potential at which the limiting current is measured (0.3 V for I^- and 0.23 V for $Fe(CN)_6^{4-}$), and the value of s (slope of E_{Pt} *vs.* $Ln\ d$ plot) is 0.046 from plot 4.1.6. Film thicknesses of 140 nm, for I^-, and 190 nm, for $Fe(CN)_6^{4-}$, were used. Table 6.2 gives the comparison of the possible current, i, from electronic conductance and the measured limiting current i_L from RDE.

Table 6.2 Comparison of the current density, i, of electron conduction with the limiting current density, i_L, in RDV experiments.

I^-		$Fe(CN)_6^{4-}$	
$i(\mu A/cm^2)$	$i_L(\mu A/cm^2)$	$i(\mu A/cm^2)$	$i_L(\mu A/cm^2)$
3.3	230	0.24	100

The limiting current is significantly greater than the current calculated from the electronic conductivity results for both anions. It demonstrates that the limiting current is not due to the film electronic conductivity.

The second possibility, mediation by redox sites in the film, can be discounted by consideration of the concentration of redox sites in the film. According to the partition coefficient results listed in Table 5.1, only 5 % of the available ion exchange sites [0.24M(I^-):5.6 M (pyridinium, section 3.3)] in acetonitrile and 0.36% (0.02M : 5.6M) in aqueous solution are occupied. There are not sufficient redox sites in the film to efficiently transport electrons by self-exchange (electron hopping). The relationship between the charge transport rate and redox site loading for quaternized polyvinylpyridine (QPVP) has been reported[20,21]. If the redox site (e.g. $Mo(CN)_8^{4-}$) loading in QPVP is less than 50% of the available sites, *ion diffusion* dominates the charge transport rate. Poly-MPMP$^+$ has similar structure and properties to QPVP. The relationship between the redox site loading and charge transport should therefore be similar for poly-MPMP$^+$. Thus, charge transport via redox sites is very unlikely with such a diminutive loading of I^-. The question of conduction *via* redox sites other than I^- can be resolved by the *in situ* electronic conductivity measurements in Chapter 4. The absence of an anodic current for ferrocene oxidation near the ferrocene formal

potential (see Figure 4.1.2) shows that no electron transport can occur in the reduced polymer at this potential, indicating the absence of other redox sites in the film.

The existence of pinholes or channels in the film can be negated by the limiting current dependence on film thickness shown in Figure 6.1.5. This relationship is evidence that the solute permeates through the film by membrane diffusion rather than by flowing through pinholes or channels with diameters much larger than the size of the ion. According to the theory[22] applicable to reaction at pinholes, the intercepts of the inverse Levich plots would be a function of the ratio of the pinhole diameter to spacing, not the film thickness. Furthermore, the difference in the diffusion coefficient between $Fe(CN)_6^{4-}$ and I^- implies the existence of size and charge discrimination. This would not be characteristic of reaction through pinholes in the film. In addition, the electron scanning microscopy pictures in Chapter 3 (Figure 3.2.2) show that the polymer is a dense material free of visible (SEM scale) pinholes and channels. The mode of membrane diffusion within poly-$MPMP^+$ seems most likely to be the model for the anions studied in this work.

RDV for $Fe(CN)_6^{4-}$ transport in poly-$MPMP^+$ Equation 6.1.1 may be used to treat rotating disc voltammetry data for $Fe(CN)_6^{4-}$ in poly-$MPMP^+$, as it was for

iodide.

The formal potential of ferrocyanide is 0.14 V, in the region where the polymer is non-conductive. Therefore, the possibility of electronic conduction by the film can be excluded using the same argument as was presented for I^-, referring to Table 6.2. The existence of pinholes or channels can be ruled out using the same arguments as for I^- transport in poly-$MPMP^+$ since the linear relationship between intercepts (from inverse Levich plots) and film thickness was also obtained. Because of the high concentration of $Fe(CN)_6^{4-}$ (1.4 M) in the film, the possibility of mediation by redox sites cannot be negated as easily as for iodide. However, a rough estimation of the $Fe(CN)_6^{4-}$ diffusion coefficient from the ion exchange data can help to exclude this possibility. According to the data in section 5.2.1, a 0.4 μm film completely loses bound ferrocyanide in 1.0 M $NaClO_4$ aqueous solution in 30 seconds. The $Fe(CN)_6^{4-}$ diffusion coefficient can be estimated from the relation $d = (2D_{ferrocyanide}\, t)^{1/2}$, where d is the thickness of the diffusion layer (approx film thickness) and t is the experimental time scale. The diffusion coefficient is calculated to be $2.7 \times 10^{-11} cm^2\ s^{-1}$, which is close to the value of $3.2 \times 10^{-11}\ cm^2\ s^{-1}$ from the RDV measurement. This similarity of the diffusion coefficients supports the mass transport mechanism under the RDV conditions.

Electron transport As discussed earlier, the first wave in the rotating disc voltammogram for $Fe(CN)_6^{4-}$ oxidation at the poly-$MPMP^+$ coated electrode (Figure 6.1.8) indicates that the $Fe(CN)_6^{4-}$ diffuses through the film and reacts at the Pt/film interface. It is interesting to note that the second wave for the coated electrode has features which are similar to rotating disc voltammograms for ferrocene oxidation (see Figure 4.1.2). The identical limiting currents for the coated electrode and the bare Pt electrode demonstrate that the ferrocyanide is now reacting at the film/solution interface. The electronic conductivity of the film has become sufficient at this potential (>0.5 V) to mediate the ferrocyanide oxidation. The mediated wave for the coated electrode has shifted to a higher potential compared to a bare electrode. Furthermore, the magnitude of the shift increases with increasing film thickness. The following table shows the relationship between the film thickness and half wave potential for the second (mediated) wave.

Table 6.3. Half wave potentials for the second ferrocyanide rotating disc wave at poly-$MPMP^+$ coated electrodes.

film thickness(μm)	0.0	0.05	0.2	0.3
half wave potential(V)	0.21	0.38	0.42	0.52

These data show the same trend of shifting half wave potentials with film thickness as was seen for ferrocene rotating disc voltammograms. Apparently, the film resistance causes these potential shifts according to the explanation in Chapter 4. The rotating disc voltammogram for ferrocyanide oxidation therefore implies that both ion transport and electronic conductivity may be simultaneously measured. The limiting current of the first wave gives ion transport information while the electronic conductivity can be calculated from the second wave. The probe ions diffusing within the film may not affect the electronic conductivity measurement as long as the electron transport rate (or electronic conductivity) of the film is higher than the ion diffusion rate so that a significant second wave can be observed as in Figure 6.1.8.

Comparison of the Results A summary of the ion transport measurements, is given in Table 6.4 (next page). The methods, RDV, DC and CA are, respectively, rotating disc voltammetry, DC ionic conductivity measurement and chronoamperometry[8]. From the results in Table 6.4, we can address five points. First, poly-$MPMP^+$ is very permeable to anions, especially in water. The diffusion coefficient of I^- in water (2.8×10^{-5} for I^-) is only about 200 times higher than in the polymer. The results in Table 6.5 can be compared with literature data for polypyrrole. An important result is that the diffusion coefficient of Cl^- in poly-$MPMP^+$ (1.2×10^{-7} cm^2 s^{-1}) is significantly higher than that in polypyrrole

Table 6.4. Summary of the ionic diffusivity measurements

ion	solvent	method	$D_{s,pol}(cm^2\ s^{-1})$
I^-	CH_3CN	RDV	5.4×10^{-10}
	H_2O	RDV	1.5×10^{-7}
	H_2O	DC	1.3×10^{-7}
$Fe(CN)_6^{4-}$	H_2O	RDV	3.2×10^{-11}
ClO_4^-	CH_3CN	CA	1.1×10^{-9}
Cl^-	H_2O	DC	1.2×10^{-7}

(3.4×10^{-8} $cm^2\ s^{-1}$)[23] in aqueous solution. This increase is due to the permanent positive sites which are responsible for the swelling of poly-$MPMP^+$. Secondly, poly-$MPMP^+$ is significantly more permeable in water than in acetonitrile. This is mainly due to the hydration and swelling caused by the high concentration of the positively charged sites in the film. Thirdly, similarly charged anions such as iodide, chloride and perchlorate have similar diffusion coefficients, both in aqueous solution and in acetonitrile. Fourthly, the mobility of ferrocyanide is much smaller than that of these singly charged anions owing to the high negative charge. This slowing down in diffusion rate may be caused by electrostatic cross-

linking since each $Fe(CN)_6^{4-}$ must associate with four $MPMP^+$ units. Finally, the RDV results are in excellent agreement with the DC conductivity measurements. This is additional evidence of the absence of electron transport by electron hopping between the redox sites partitioned in the film since only ionic conductance can be detected in DC conductance measurements.

6.5 Conclusions

Transport of iodide, ferrocyanide, and chloride in poly-$MPMP^+$ has been investigated by the techniques of rotating disc voltammetry, and DC ionic conductivity measurements. Rotating disc voltammetry is a convenient and precise method for the determination of diffusion coefficients of anions with low formal potentials. The results from this method are in excellent agreement with those from ionic conductivity measurements. The permeability to I^- ions of the reduced form of poly-$MPMP^+$ is similar to that of polypyrrole in acetonitrile but it is over three orders of magnitude higher than for polypyrrole in water. This is apparently due to hydration and swelling caused by the high concentration of positively charged sites (5.6 M). Identically charged anions, such as I^-, Cl^- and ClO_4^- have similar diffusion coefficients in both aqueous and acetonitrile solutions. The mobility of $Fe(CN)_6^{4-}$ is much lower than that of the monocharged anions, mainly

due to the high negative charge of the former.

The increased permeability of poly-$MPMP^+$ in water, compared to polypyrrole, makes it, and similar substituted pyrrole based polymers attractive, for a wide range of applications which require fast mass transport, such as batteries, electrolysis and electrocatalysis.

References

1. R.W. Murray, Ann. Rev.Mater. Sci., 45 (1984) 14.
2. A.F.Daiz, A.J. Logan, M. Krounbi, and J. Bargon, Mol. Cryst. Liq. Cryst., 83 (1982) 265.
3. L.F. Warren, and D.P. Anderson, F. Electrochem. Soc., 134 (1987) 101.
4. T. A. Skotheim (Ed.), Handbook of Conducting Polymers, Marcel Dekker, New York, 1986.
5. P. Burgmayer and R. W. Murray, J. Am. Chem. Soc., 104 (1982) 6139.
6. P. Burgmayer and R. W. Murray, J. Phys. Chem., 88 (1984) 2515.
7. T. Ikeda, R. Schmehl, P. Denisevich, K. Willman and R.W. Murray, J.Am. Chem. Soc., 104 (1982) 2683.
8. H. Mao, J. Ochmanska, C. D. Paulse and P.G. Pickup, Faraday Discuss. Chem. Soc., 88 (1989) 165.
9. H. Mao and P. G. Pickup, J. Phys. Chem., 93 (1989) 6480.
10. J. Rault-Berthlot, M. A. Orliac, J. Simonet, Electrochim. Acta, 33 (1988) 811.

11. E.W. Tsai, T. Pajkossy, K. Rajeshwar, and J. R. Reynolds, J. Phys. Chem., 92 (1988) 3560.

12. R. M. Penner, L. S. Van Dyke, and C.R. Martin, J. Phys. Chem., 92 (1988) 5274.

13. T. Osaka, K. Naoi, S. Ogano, and S. Nakamura, J. Electrochem. Soc., 134 (1987) 2096.

14. T. Mwaka, K. Naoi, and S. Ogano, J. Electrochem. Soc., 135 (1988) 1071.

15. J. B. Schlenoff, and J. C. W. Chien, J. Am. Chem. Soc., 109 (1987) 6269.

16. R. A. Bull, F.R. Fan and A. J. Bard, J. Electrochem. Soc., 129 (1982) 1009.

17. F. Beck, P. Braun and M. Oberst, Ber. Bunsenges. Phys. Chem., 91 (1987) 967.

18. T. Inour and F.C. Anson, J. Phys. Chem., 91 (1987) 1519.

19. P. J. Peerce and A. J. Bard, J. Electroanal. Chem., 112 (1980) 97.

20. N. Oyama, S. Yamaguchi, Y. Nishiki, K. Tokuda, H. Matsuda and F.C. Anson, J. Electroanal. Chem., 139 (1982) 371.

21. S. M. Oh and L.R. Faulkner, J. Electroanal. Chem., 269 (1989) 77.

22. R. Landsberg and R. Thiele, Electrochim. Acta, 11 (1966) 1234.

23. C. D. Paulse and P. G. Pickup, J. Phys. Chem., 92 (1988) 7002.

Chapter 7

Electrocatalysis of Ascorbic Acid Oxidation

In order to explore the application of the conducting ion exchange polymers prepared in this work to analytical chemistry, their electrocatalytic properties towards ascorbic acid oxidation were studied. Ascorbic acid is an important compound in mammalian brains and bodies. Electrochemical studies of ascorbic acid oxidation are therefore of particular interest for applications in biological systems[1]. There have been many reports of ascorbic acid's electrochemical properties, especially the electrocatalytic oxidation of ascorbic acid at carbon[2,3,4,5], mercury[6,7], and polypyrrole coated[8] electrodes. However, ascorbic acid oxidation at conducting ion exchange polymers has not previously been reported. In this chapter the catalytic properties of poly-MPMP$^+$, poly-PPP$^+$ and poly-PPTA$^+$ for ascorbic acid oxidation are discussed.

7.1 The Mechanism of Electrooxidation of Ascorbic Acid

7.1.1 General Mechanism

The electrochemistry of ascorbic acid has been studied since the nineteen

forties[9], and many oxidation mechanisms have been proposed. Figure 7.1.1 shows a widely accepted mechanism[10] for the electrooxidation of ascorbic acid. The value of the pKa (4.71) for the dissociation of ascorbic acid[11] indicates that most of the ascorbic acid exists as the monoanionic species [(2), Figure 7.1.1] in the solution at pH = 7. When the potential becomes sufficiently positive, a reversible one electron and one proton electrooxidation step, which yields an anion radical (3), has been proposed. The excess negative charge is spread over the conjugated bonds as shown by the dashed line in Figure 7.1.1. An irreversible one electron oxidation immediately follows the formation of the anionic radical to form dehydro-ascorbic acid (4). After the protonation reaction of (4) with water, compound (5) results. The transfer coefficient for ascorbic acid electrooxidation was measured and it was concluded that the second oxidation step (3 to 4) was the rate determining step[9]. The thermodynamic redox potential of ascorbic acid has been reported to be below 0 V *vs* a saturated calomel electrode (eg. ~ -0.2 V at pH = 7.4[8]). However, the measured oxidation potentials are usually found to be approx. + 0.3 V (pH = 7.4) *vs* SSCE on carbon electrodes[12,13], and the peak potential in cyclic voltammetry at a bare Pt electrode was reported to be at 0.58 V *vs* SSCE in 2 mM ascorbic acid in a pH 3.2 glycine aqueous solution[14]. These discrepancies, of the measured oxidation potential of ascorbic acid relative to the thermodynamic redox potential, indicate that there is a kinetic barrier for the

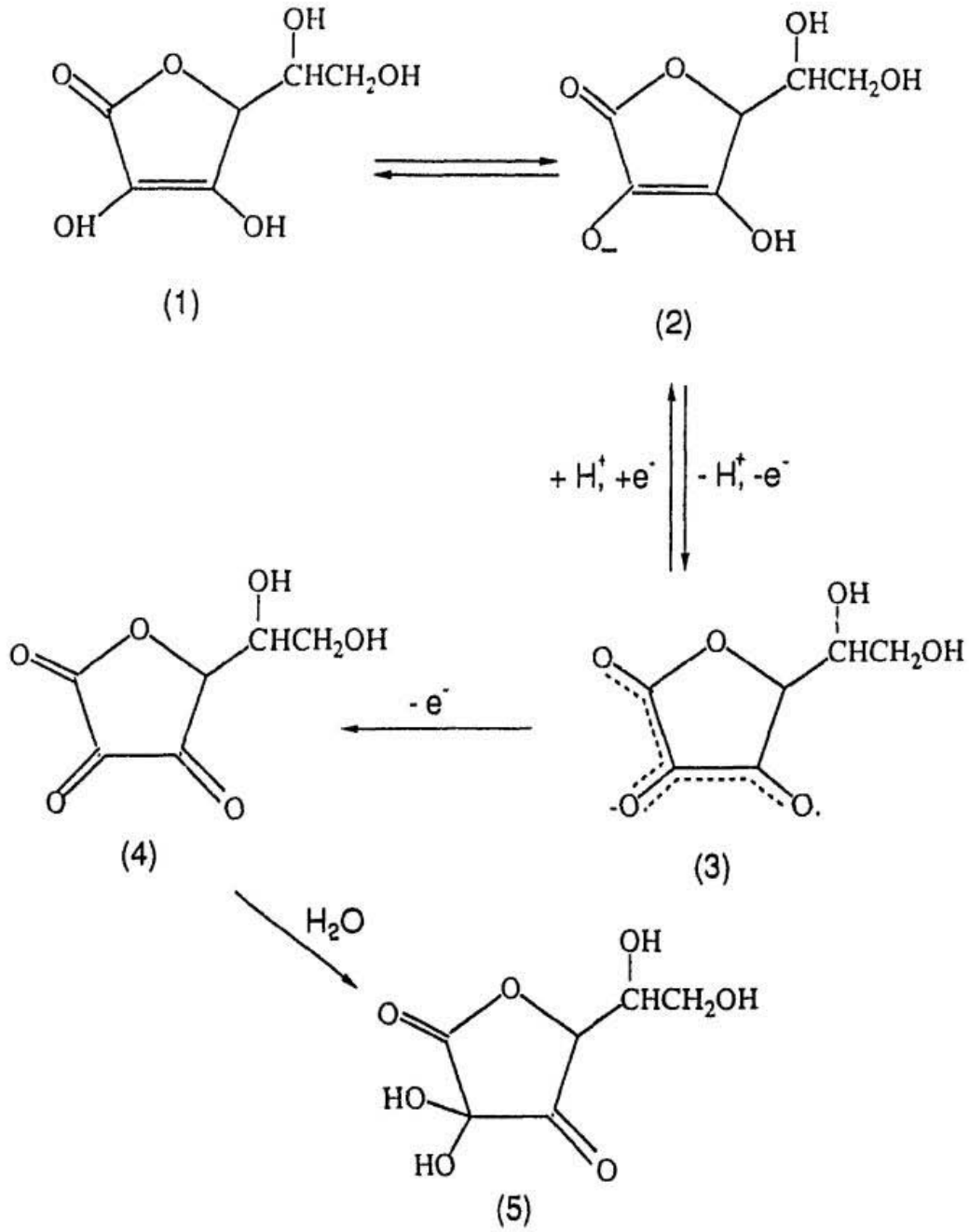

Figure 7.1.1. Proposed mechanism for the electrooxidation of ascorbic acid in solution at pH = 7.

reaction at the naked electrodes.

The influence of the rate constant on the peak potential can be seen from the equation[15] for an irreversible anodic reaction:

$$E_{p,a} = E^{o'} + \frac{RT}{(1-\alpha)n_{\alpha}F}[0.78 + Ln(\frac{D^{1/2}}{k^{o}}) + Ln(\frac{(1-\alpha)n_{\alpha}Fv}{RT})^{1/2}]$$

(7.1.1)

where $E_{p,a}$ and $E^{o'}$ are, respectively, the anodic peak potential and the formal potential of the reactant; k^{o} is the standard heterogeneous rate constant; α and n_{α} are, respectively, the transfer coefficient and the number of electrons involved in the rate-determining step; v is the scan rate; D is the diffusion coefficient; R, T and F retain their usual meanings. Although some limitations may exist in the use of this equation, it provides a good estimate of the relationship between the peak potential and rate constant. This equation predicts an logarithmic decrease in the anodic peak potential with the rate constant. A decrease in peak potential means that the kinetic barrier is depressed.

7.1.2. Mechanism of Electrooxidation of Ascorbic Acid at Cationic Ion Exchange Polymer Coated Electrodes

As has been discussed in previous chapters, the cationic ion exchange polymers, prepared in this work, contain a high concentration of positively charged

sites, and can be electronically conductive at potentials above their formal potentials. Also, they are permeable to anions in aqueous solution. Therefore, the mechanism of electrooxidation of ascorbic acid at electrodes coated with these polymers is different from that in solution in three main aspects; electrocatalysis, preconcentration and surface conditions.

I. Electrocatalysis Polypyrrole is a cationic polymer when it is oxidized, and the electrocatalysis of ascorbic acid oxidation at polypyrrole coated carbon electrode has been reported by Ewing and coworkers[8]. It is proposed that the catalysis of ascorbic acid oxidation at polypyrrole coated electrodes is due to an electrostatic interaction between the cationic polymer and the ascorbate (pH = 7.4). According to the mechanism in Figure 7.1.1, there could be an interaction between the dissociated anions (2), the anionic radicals (3), and the positively charged sites so that the kinetic barrier is decreased. A decrease in the peak potential is evidence of electrocatalysis.

The kinetics for electronically conducting and non-conducting polymer coated electrodes are different. For a non-conducting polymer, ascorbate has to diffuse through the polymer to be oxidized at Pt or within the polymer near the Pt. If the diffusion layer thickness is less than the film thickness, this process is similar to the case explained in section 7.1.1. Cyclic voltammetry would show a diffusion controlled shape (broad peak with diffusion tail) and the peak current will

be independent of the film thickness .

For a conducting polymer, the ascorbate in the film can react at any nearby polymer chain. In this case, one may consider a chain of the polymer as a conductive rod with many ascorbate anions electrostatically bound around the rod as schematically shown in Figure 7.1.2. Once the potential of the rod is sufficiently high, all of the ascorbate can rapidly be oxidized by the rod. The cyclic voltammetry should show a sharp peak without a diffusion tail. If the ascorbate anions are evenly distributed in the film, the longer the rod (meaning the thicker the film) the more ascorbate that would be oxidized to give more electrons (higher peak current) as long as electron transport in the film is fast enough to pass the electrons to the Pt surface. According to the discussion above, the ascorbate oxidation at a conductive cation ion exchange polymer coated electrode could be analogous to a thin layer electrode if the effect of the ascorbate in the solution is negligible (considering the higher concentration of ascorbate in the film because of the preconcentration). The following equation[16] therefore applies:

$$E_{p,a} = E^{o'} - \frac{RT}{(1-\alpha)n_{\alpha}F} Ln(\frac{ART\ k^{o}}{(1-\alpha)n_{\alpha}F\ v\ V}) \qquad (7.1.2)$$

where V is the volume of the film and other parameters have the same meanings as in equation 7.1.1. A decrease in peak potential also indicates a depression of

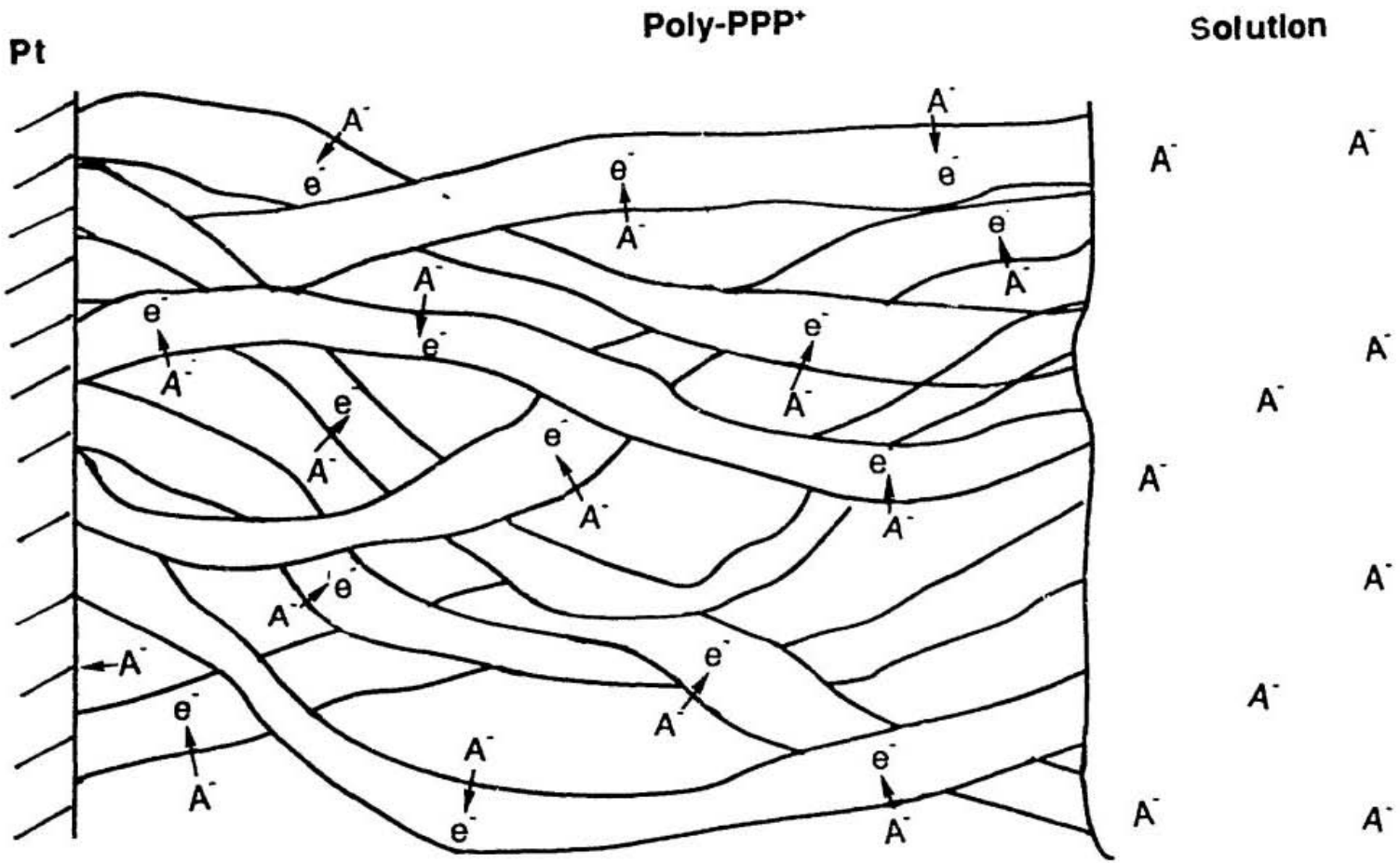

Figure 7.1.2. Schematic diagram of dissociated ascorbic acid oxidation at conducting polymer chains; (A^-) represents dissociated ascorbic acid.

the kinetic barrier in the reaction.

Another possible explanation of catalysis by conducting polymer coated electrodes might be that the number of active sites on the electrode surface is increased. It has been reported that ascorbic acid oxidation is very sensitive to the condition of the electrode surface[17,18,19]. Kuwana and co-workers[20] reported that the peak potential for ascorbic acid oxidation at an activated glassy carbon electrode (treated at 725 °C, $< 2 \times 10^{-6}$ torr) was shifted by 300 mV to a more negative potential and the peak current was almost doubled as compared to that at an untreated glassy carbon electrode. It was concluded that the treatment resulted in an increase in the density of active sites. Similar effects can occur at the conducting polymer coated electrode since the active surface area of the conducting polymer coated electrode is much greater than its geometric area.

II. Preconcentration An increase in peak current for a coated electrode, using cyclic voltammetry, is evidence for preconcentration of ascorbate in cationic ion exchange polymers. The peak current i_p for the case of a bare electrode, and a non-conductive polymer coated electrode when the diffusion layer thickness is less than the film thickness, can be represented by the following equation[15]:

$$i_p = (2.99 \times 10^2)\, n\, (1-\alpha) n_\alpha^{1/2} A C D^{1/2} v^{1/2} \qquad (7.1.3)$$

where n is the number of electrons per molecule of oxidized ascorbate, C is the

concentration of ascorbate either in solution or in polymer, and other parameters retain the same meanings as in equation 7.1.1. If we assume that the diffusion coefficient (D) for the coated electrode is similar to or less than that for bare electrode, and cyclic voltammetry is carried out in the same ascorbate solution, an increase in peak current for the polymer coated electrode indicates that the concentration of ascorbate in the film must be greater than in solution. The peak current is proportional to the ascorbate concentration (not amount of ascorbate in the film). Thus the peak current will be independent of film thickness.

For the case of conducting ion exchange polymers, the equation[16] for thin layer electrodes is used to explain the peak current for coated electrodes:

$$i_p = 0.368n(1-\alpha)n_\alpha F^2 \nu V C_p / 1000RT \qquad (7.1.4)$$

where C_p is the concentration of ascorbate in the film. It should be noted that the peak current is proportional to VC_p which is amount of ascorbate in the film, (not its concentration in solution). If we use $V = Ad$ (film area x film thickness), equation 7.1.4 becomes,

$$i_p = 0.368n(1-\alpha)n_\alpha A F^2 \nu d C_p / 1000RT \qquad (7.1.5)$$

Therefore the peak current is dependent on the film thickness.

7.2 Ascorbic Acid Oxidation at Polymer Coated Electrodes

7.2.1 Poly-[1-methyl-3-(pyrrol-1-ylmethyl)pyridinium], Poly-MPMP$^+$

Figure 7.2.1 shows cyclic voltammograms for the oxidation of ascorbate at a bare Pt (dashed line) and at a poly-MPMP$^+$ coated (1.7 μm) electrode (solid line), both in a phosphate buffer at pH = 7.4. Significant differences can be noted. First, the shapes of the cyclic voltammograms are distinctly different; ascorbate oxidation at the poly-MPMP$^+$ coated electrode produces a fairly symmetric peak with a well defined peak potential whereas the bare electrode produces a flat and lengthy tailed response. Secondly, under the same conditions the peak potential for the coated electrode is 0.07 V while for the bare Pt electrode it is about 0.30 V. The peak potential has been shifted by 230 mV. Thirdly, the peak current and the peak area are greatly enhanced at the poly-MPMP$^+$ coated electrode.

These differences in the cyclic voltammograms between coated and bare electrodes arise from two effects, electrocatalysis and preconcentration. The significant peak potential shift in the cyclic voltammogram indicates that the coated electrode catalyses ascorbate oxidation as discussed in section 7.1.2. However,

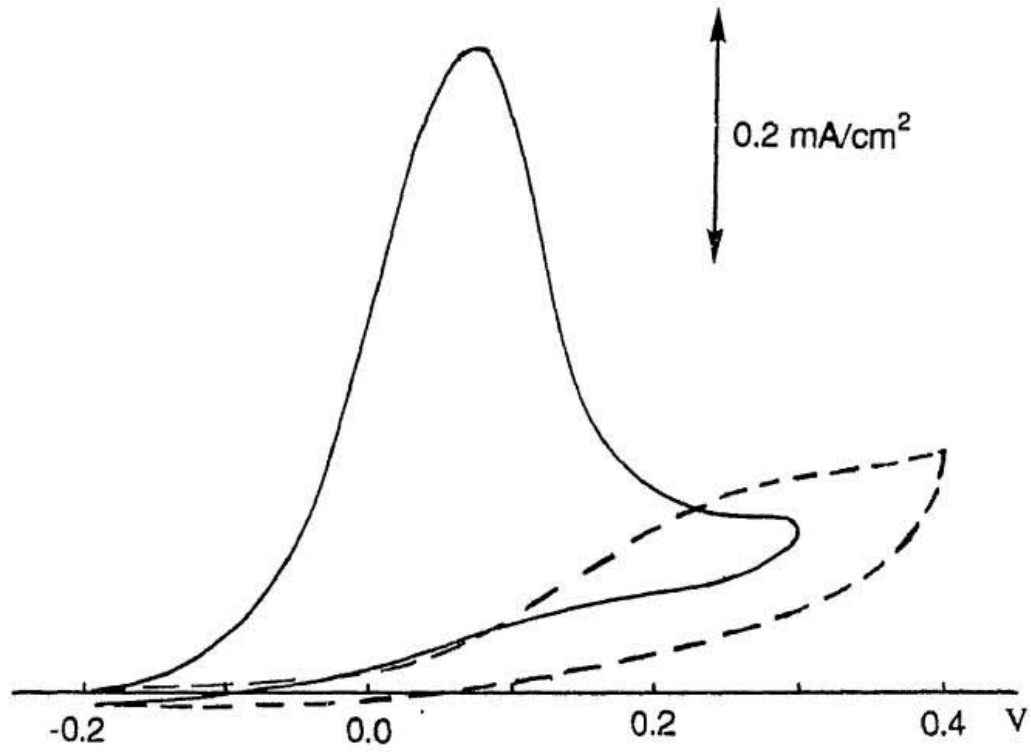

Figure 7.2.1. Cyclic voltammograms of ascorbate (0.5 mM) in 10 mM K_3PO_4 buffer (pH 7.4) at a naked Pt electrode (-----) and at a poly-MPMP$^+$ coated electrode (——); film thickness 1.7 µm; scan rate 100 mV/s.

the polymer, at the ascorbate oxidation potential (0.07 V), is not conductive. The electrode surface conditions may not be improved to catalyse the reaction since the polymer is reduced and non-conductive. The catalysis could only be due to an electrostatic interaction between the ascorbate and the positively charged pyridinium sites which stabilize the anion radicals. However, the ascorbate has to diffuse through the film and then react at or near the Pt surface.

The peak current at the poly-$MPMP^+$ coated electrode is 3.6 times higher than the peak current at the bare Pt electrode as shown in Figure 7.2.1. This increase in the voltammetric peak current provides evidence of preconcentration. The preconcentration shown by the peak current is due to high concentration of positive charge in the poly-$MPMP^+$ film. An electrostatic interaction between these cationic sites and ascorbate is presumably responsible for this preconcentration. An experiment was carried out similar to that used to investigate the electrostatic binding of ferrocyanide (section 5.2.2). A poly-$MPMP^+$ coated electrode was soaked in 0.5 mM ascorbic acid and 10 mM phosphate buffer (pH = 7.4) for 20 minutes. Then it was washed with water and transferred to an ascorbic acid-free phosphate buffer solution. The cyclic voltammogram of the electrode in this solution did not show ascorbate oxidation. Either the partition coefficient is low or the diffusion coefficient of ascorbate in the film is high enough that much of the ascorbate diffuses out of the film before it

can be measured. The weak binding of ascorbate compared to ferrocyanide is presumably due to its lower charge. Multiple charges are normally required for strong electrostatic binding. Although the peak current for ascorbate oxidation is much higher than at the naked Pt electrode, it is still very small compared to that for ferrocyanide at a poly-MPMP$^+$ coated electrode (Chapter 5). The following table shows the relationship between the peak current and film thickness for poly-MPMP$^+$ coated electrodes.

Table.7.1. Film thickness and peak current for poly-MPMP$^+$ in 0.5 mM ascorbic acid and 0.01 M phosphate buffer, pH = 7.4.

film thickness (μm)	0.6	1.3	1.5	1.7	1.9
peak current (μA)	1.3	1.9	2.1	2.2	1.8

Although there is an increase in peak current for film thicknesses less than 1.3 μm, the peak current ceases to increase when the film is thicker than 1.3 μm. This relationship between film thickness and peak current indicates that the ascorbate oxidation at poly-MPMP$^+$ fits the case for a non-conductive polymer coated electrode discussed in section 7.1.2, II.

At lower pH (2.3), the catalysis of ascorbic acid oxidation by poly-MPMP$^+$

was studied by rotating disc voltammetry. Figure 7.2.2 shows rotating disc voltammograms for ascorbic acid oxidation at poly-$MPMP^+$ coated (circles) and bare Pt (crosses) electrodes for a 0.32 μm thick film in 0.25 mM ascorbic acid in 0.1 M KH_2PO_4 buffer, pH = 2.3. The half wave potential for the coated electrode is about 20 to 30 mV lower than that of the bare electrode. The similarity in half wave potentials for the coated electrode and the bare electrode is evidence that the oxidation of the ascorbic acid occurs at the Pt/film interface. If the ascorbic acid reacted at the film/solution interface, the half wave potential would be more positive, similar to that observed for ferrocene (section 4.1). The electronic conductivity of the film is less than 10^{-11} S cm^{-1} at potentials below 0.2V and therefore the polymer cannot mediate the reaction. The ascorbic acid diffuses through the film and reacts at the Pt surface.

Although the catalysis by poly-$MPMP^+$ for ascorbic acid at this pH (2.3) is minimal, the reaction is catalyzed by the mediation of ferrocyanide. Figure 7.2.2 also shows ascorbic acid oxidation at the film preloaded with ferrocyanide (solid circles). The half wave potential is further decreased by 130 mV, as compared to the bare Pt electrode, and approximates the formal potential for ferrocyanide oxidation. The potential shift indicates that the electron transfer reaction is mediated by the ferrocyanide and occurs at the film/solution interface or within the film. However, the limiting current is not as high as that at the bare

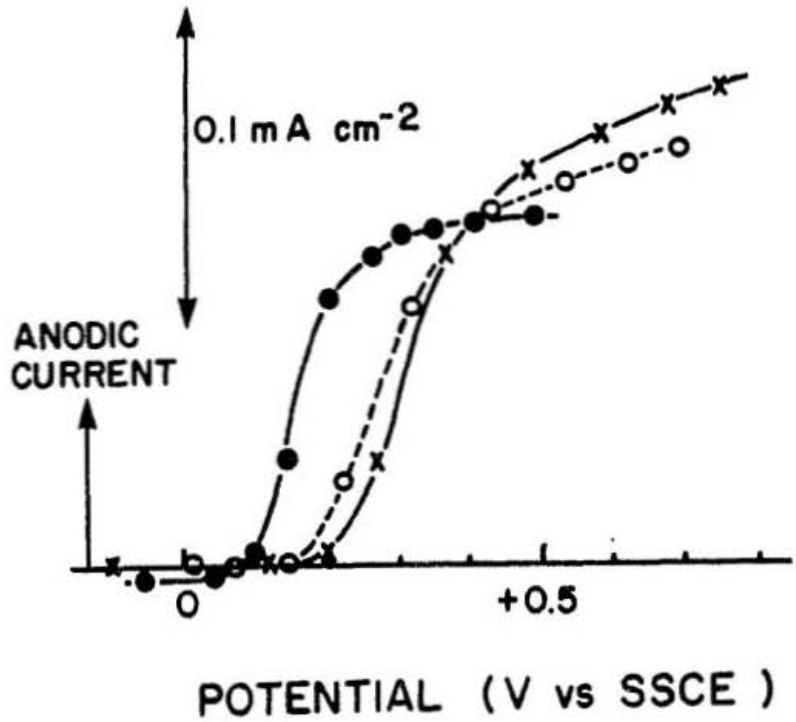

Figure 7.2.2. Rotating disc voltammograms of ascorbic acid (0.25 mM) in 0.1 M KH_2PO_4 buffer (pH 2.3) at a naked Pt electrode (X), a poly-MPMP$^+$ (O) and a poly-MPMP$^+$ coated electrode containing 1.3 M $Fe(CN)_6^{3-/4-}$ (●). Data points were recorded after the current had reached a constant value at each potential. Film thickness = 0.32 μm; rotation rate 400 rpm.

electrode. A slow ferrocyanide diffusion rate within the film may be the source of this decrease. More likely ferrocyanide cross-link electrostatically, reduces the diffusion coefficient for ascorbic acid. A plot of the limiting current *vs* the square root of the rotation rate was linear for the bare electrode but curved for the coated electrode. Inverse Levich plots were linear for both electrodes but a large intercept is observed for the coated electrode as shown in Figure 7.2.3. This demonstrates that there is some kinetic limitation within the film. One question that arises is why the limiting current for the poly-MPMP$^+$ coated electrode is higher when it is not loaded with ferrocyanide. This is presumably due to a decrease in the mobility of ascorbic acid in the film caused by electrostatic cross-linking of the film by ferrocyanide.

7.2.2 Poly-[1-(3-[pyrrol-3-yl]propyl)pyridinium], Poly-PPP$^+$

Poly-PPP$^+$ was also studied for electrocatalysis of ascorbate oxidation. Figure 7.2.4A shows a cyclic voltammogram of a poly-PPP$^+$ coated electrode in a 0.01 M K_2HPO_4/KH_2PO_4 buffer at pH = 7.4. When ascorbic acid was added to the solution a sharp anodic peak appeared at -0.03 V. This peak increased as the concentration of ascorbic acid was increased, as shown in Figure 7.2.4B. The ascorbate oxidation peak is greatly enhanced at the poly-PPP$^+$ coated electrode as

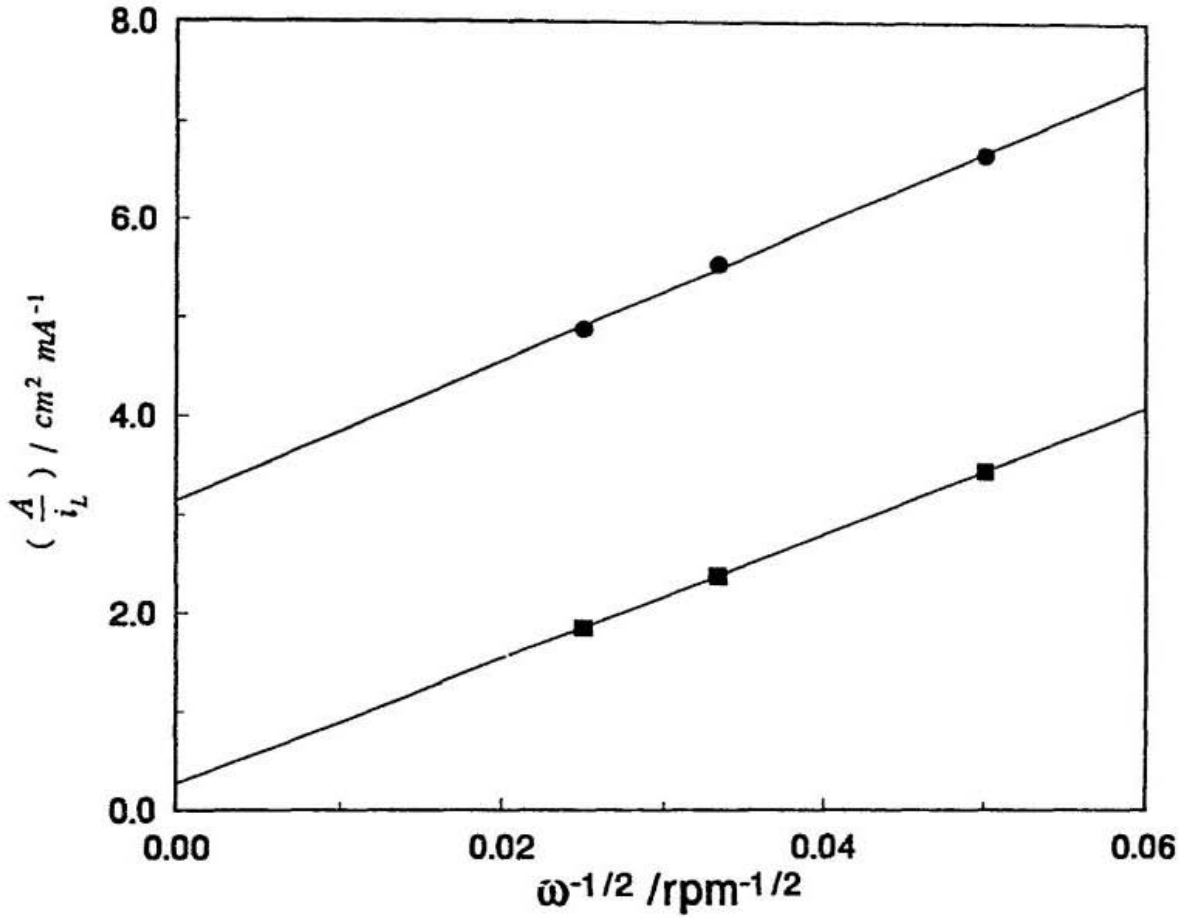

Figure 7.2.3. Inverse Levich plots for ascorbic acid (0.25 mM) oxidation at naked Pt (■) and poly-MPMP$^+$ coated Pt electrodes (●); film thickness = 0.62 μm.

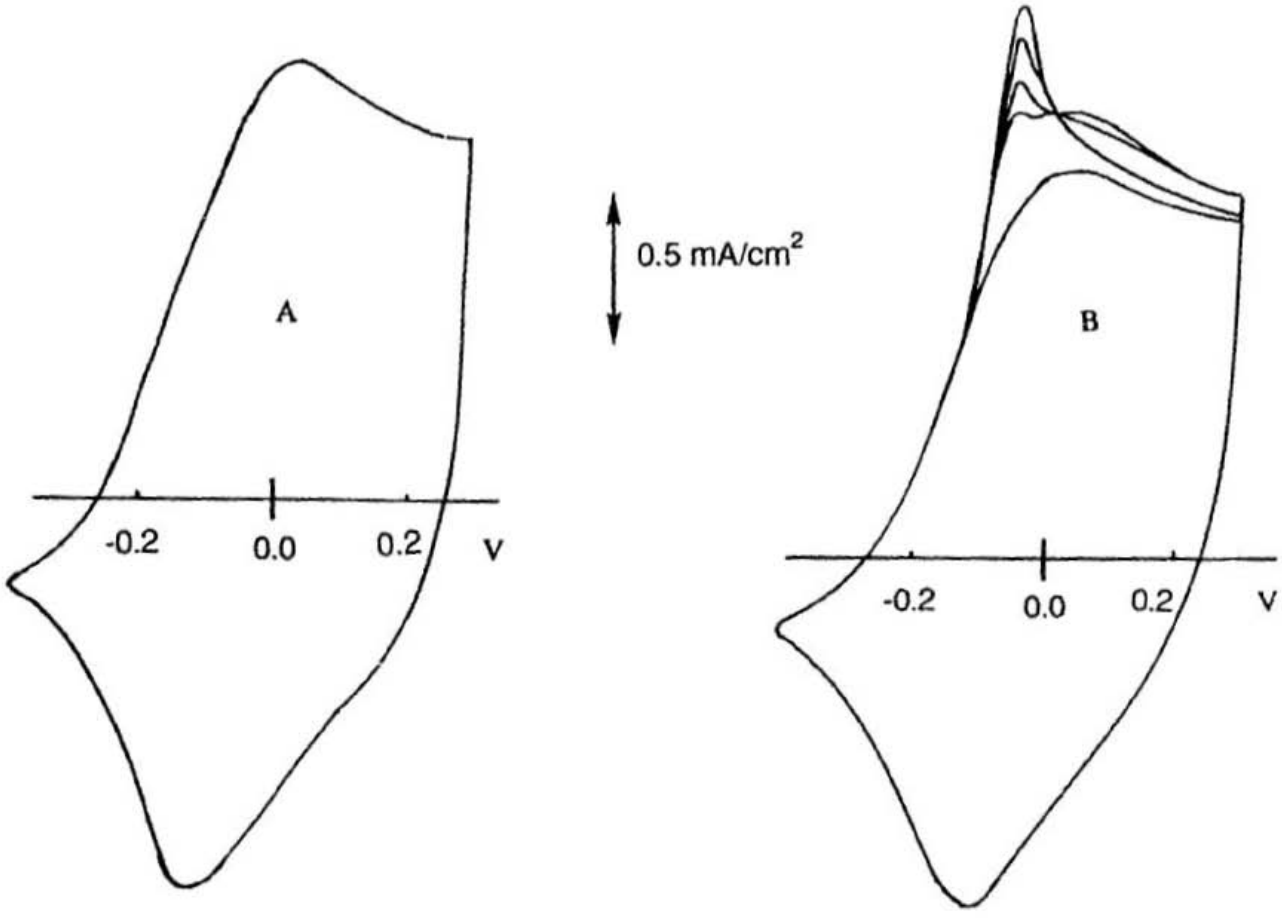

Figure 7.2.4. Cyclic voltammograms for poly-PPP* coated electrodes in 10 mM K_3PO_4 buffer (pH 7.4). (A) no ascorbic acid. (B) Peak current for ascorbic acid oxidation increases with adding ascorbic acid (approx.

compared to a bare electrode as seen in Figure 7.2.5. The solid and dashed lines are the voltammograms of ascorbate at a poly-PPP^+ coated electrode and a bare Pt electrode respectively. At the coated electrode, the peak potential shifts to below 0 V and the peak current increases by more than 10 times. The measured peak potentials and peak currents for ascorbate oxidation at different coating thickness are listed in Table 7.2.

Table 7.2. Cyclic voltammetry results for poly-PPP^+ coated Pt electrodes.

film thickness (μm)	peak potential (mV)	peak current (μA)
0.4	-55	1.4
0.8	-35	1.3
1.2	-5	2.2
1.4	-10	2.8
2	-15	3.8

The peak currents were measured from a base line approximated by a cyclic voltammogram of the film in a solution containing no ascorbic acid, (eg. Figure 7.2.4A). The E_{FWHM} (Full Width at Half Maximum) for ascorbate at the poly-

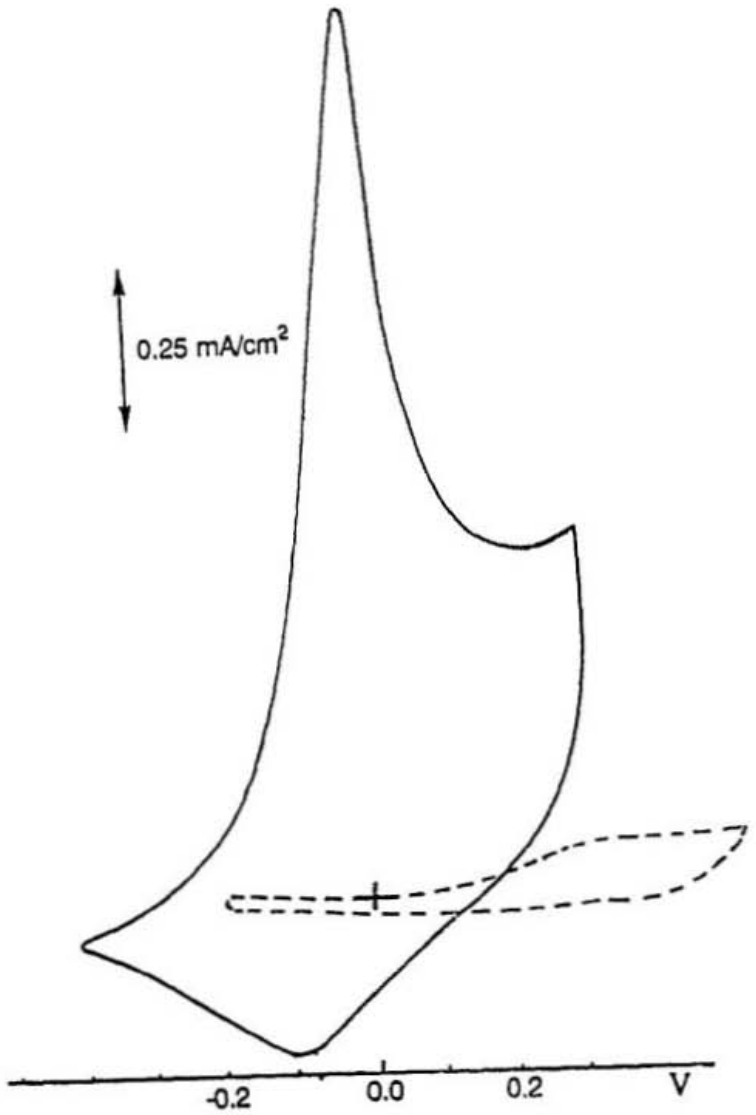

Figure 7.2.5 Cyclic voltammograms of 0.5 mM ascorbic acid in 10 mM K_3PO_4 buffer (pH 7.4) at a naked Pt electrode (-----) and at a poly-PPP$^+$ coated electrode (——). Film thickness = 1.4 μm; scan rate = 50 mV/s.

PPP^+ coated electrode is 92 mV which is measured at the half height from this base line to the peak.

The average peak potential from the table is -24 $\pm$ 20 mV. Although the peak potential dependence on film thickness is not consistent enough to draw any definite conclusion, it appears that thin films exhibit a lower peak potential. The increasing peak current with the increasing film thickness shown in Table 7.2 contrasts strongly with poly-$MPMP^+$ where the dependence on film thickness plateaued for thick films. The enhancement of the peak current with increasing film thickness can be used to improve sensitivity for determination of ascorbic acid in analytical applications (section 7.3).

7.2.3 Poly-[(3-[pyrrol-3-yl]propyl)trimethylammonium], Poly-$PPTA^+$

Figure 7.2.6A shows cyclic voltammograms of a poly-$PPTA^+$ coated electrode and a naked Pt electrode (dashed line) in 0.19 mM ascorbic acid and 10 mM K_2HPO_4 buffer (pH = 7.4) solution; Figure 7.2.6B is the cyclic voltammogram for the coated electrode in the same buffer containing no ascorbic acid. The ascorbate oxidation peak is very sharp and occurs at a potential of -40 mV. It is similar to the ascorbate peak at a poly-PPP^+ coated electrode (eg. Figure 7.2.5). The average E_{FWHM} from all voltammograms is 70 - 80 mV, which is even smaller than for poly-PPP^+ coated electrodes (average 92 mV). The similarity of

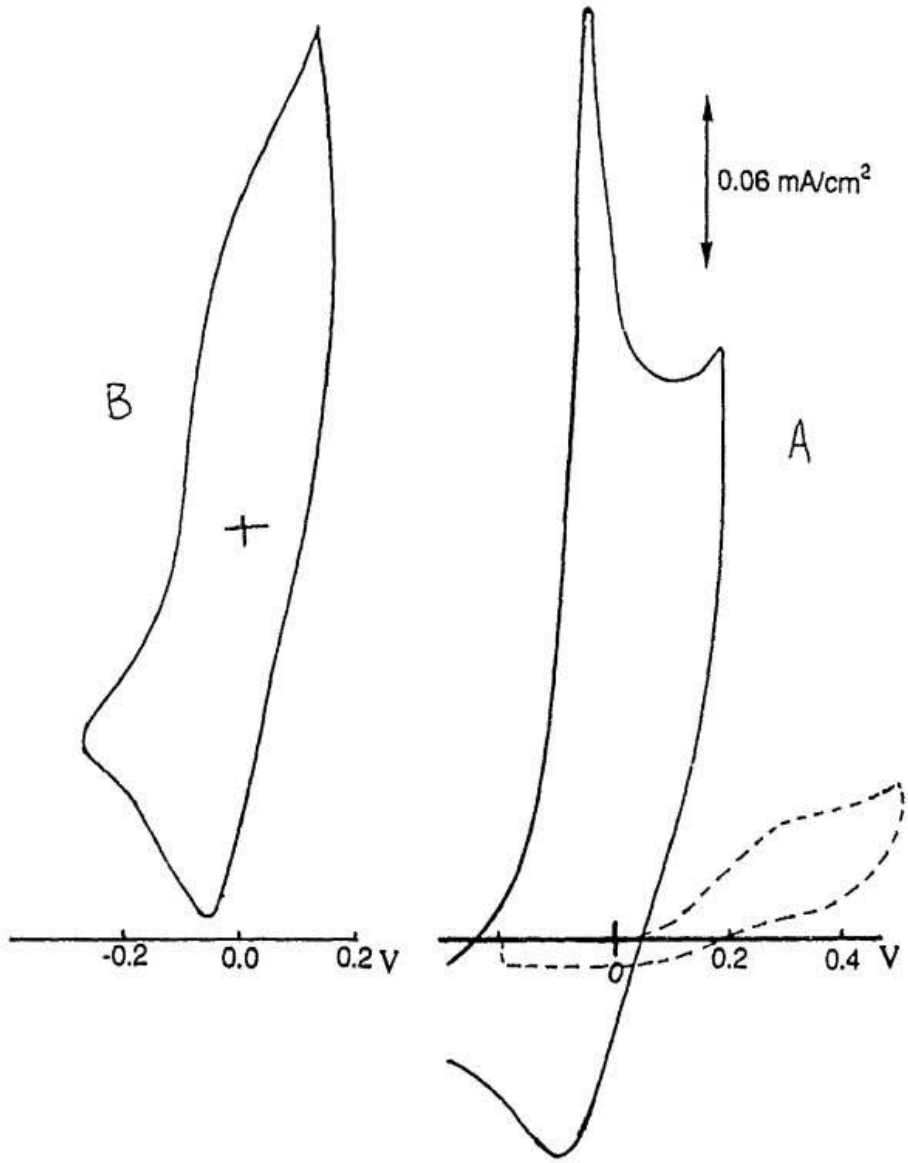

Figure 7.2.6. Cyclic voltammograms for (A) a poly-PPTA$^+$ coated electrode (——) and a naked Pt electrode (------) in 0.19 mM ascorbic acid in 10 mM K_3PO_4 buffer (pH 7.4); (B) a poly-PPTA$^+$ coated electrode in 10 mM K_2HPO_4 buffer (pH 7.4) containing no ascorbic acid. Film thickness = 1.2 μm; scan rate = 50 mV/s.

the cyclic voltammetry of ascorbate at poly-PPTA$^+$ and poly-PPP$^+$ demonstrates that the electrocatalysis is not greatly altered by the nature of the positively charged group on the polymer.

7.3 An Application in Analytical Chemistry

Conducting ion-exchange polymer coated electrodes have significant potential for application to analytical chemistry. As has been discussed in this chapter, all three of the ion exchange polymers examined demonstrated an enhanced, clear and analytically significant voltammetric peak for ascorbic acid. A development of a method for analysis of ascorbic acid in aqueous solution at pH 7.4 using these polymers is presented here. The ascorbic acid determination is simple. A polymer coated Pt disc electrode is immersed in the ascorbic acid containing solution for 5 minutes. A flow of nitrogen serves to stir the solution and remove oxygen. Then the electrode potential is scanned and the peak current observed is proportional to the bulk concentration of ascorbic acid. The polymer films are stable and can be reused for 8 to 10 times (washed with solution containing no ascorbic acid between runs) without significant decreases in the sensitivity. The peak current has been plotted against the bulk concentration of ascorbic acid, as shown in Figure 7.3.1, a linear relation (the slope of the log-log

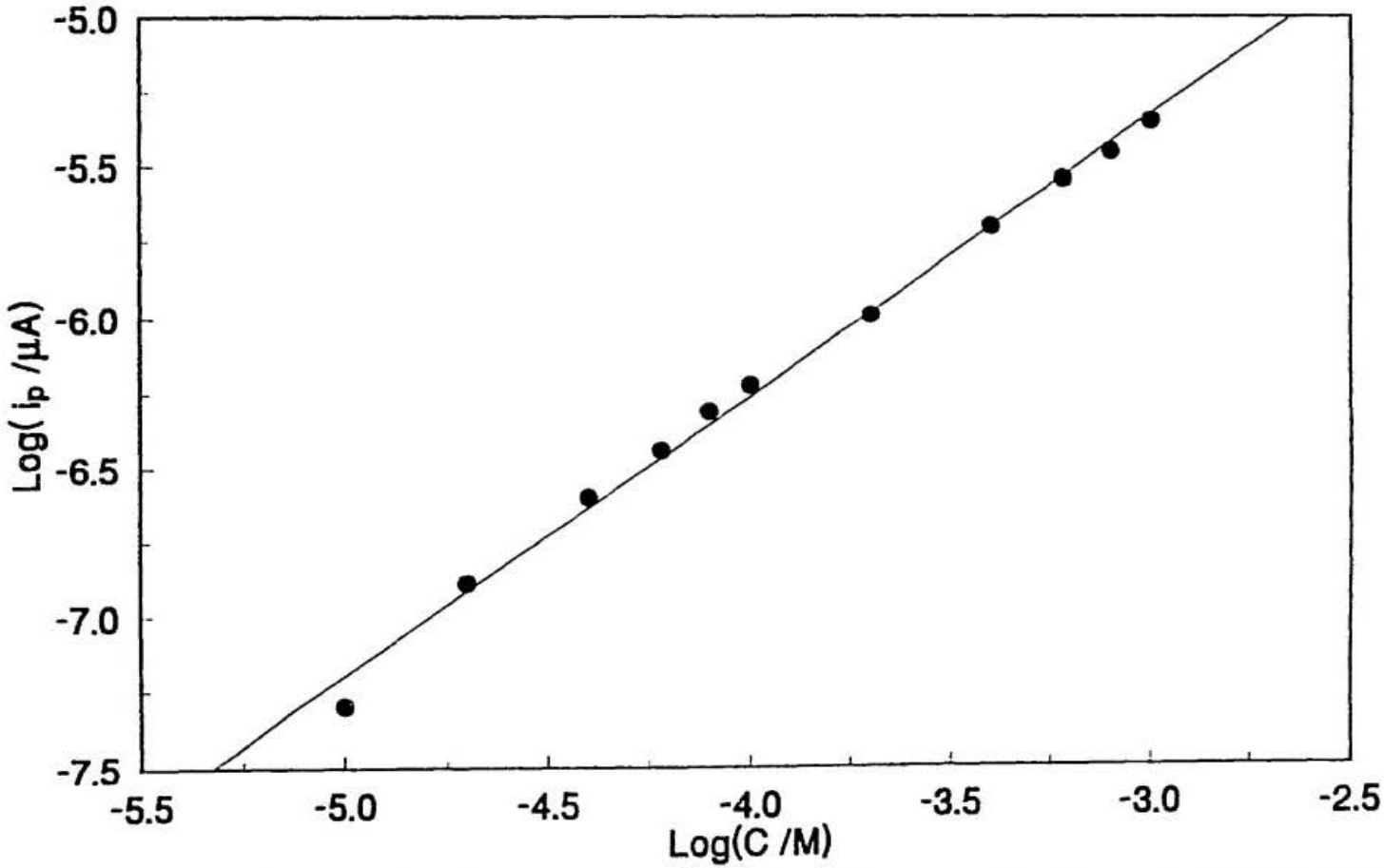

Figure 7.3.1. Calibration plot of peak current *vs* ascorbic acid concentration for a poly-MPM^{+}P^{+} coated electrode in 10 mM K_3PO_4 buffer (pH = 7.4). Film thickness = 1.7 μm; scan rate = 50 mV/s.

plot = 0.95) is obtained for a poly-$MPMP^+$ coated electrode. This plot can serve as a calibration curve in the analysis of ascorbic acid in the phosphate buffer solution at pH = 7.4. The detection limit is less than 10^{-5} M.

Figure 7.3.2 and Figure 7.3.3 show calibration curves for ascorbic acid analysis at poly-PPP^+ (slope = 0.75) and poly-$PPTA^+$ (slope = 0.60) coated electrodes respectively. Although the peak currents at these polymer coated electrodes are higher than for poly-$MPMP^+$, the detection limit is only about 5 x 10^{-5} M. The difficulty in operating at low ascorbic acid concentration is due to high background current on which the peak for ascorbate oxidation is superimposed. As has been discussed in section 7.2.2, the sensitivity can be increased by increasing the film thickness. However, the film thickness is limited by film adhesion to the Pt surface. Films thicker than 2 μm peel off from the electrode in aqueous solution.

No attempt has yet been made to investigate interferences or to apply these polymer coated electrodes to real samples. However, it is believed that conducting ion-exchange polymers will play an important part in the analytical determination of electroactive ions.

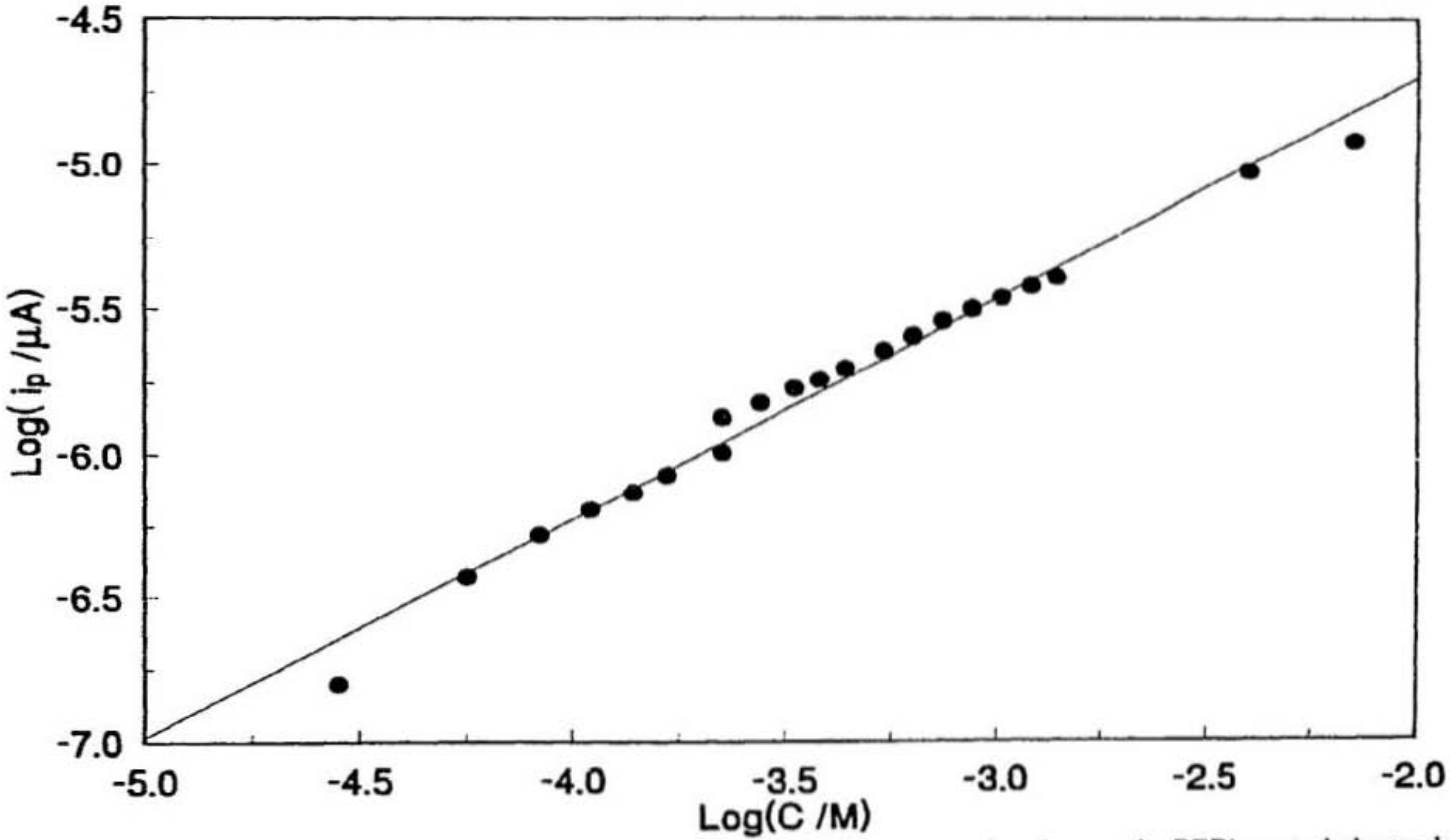

Figure 7.3.2. Calibration plot of peak current *vs* ascorbic acid concentration for a poly-PPP$^+$ coated electrode in 10 mM K_3PO_4 buffer (pH = 7.4). Film thickness = 1.8 µm; scan rate = 50 mV/s.

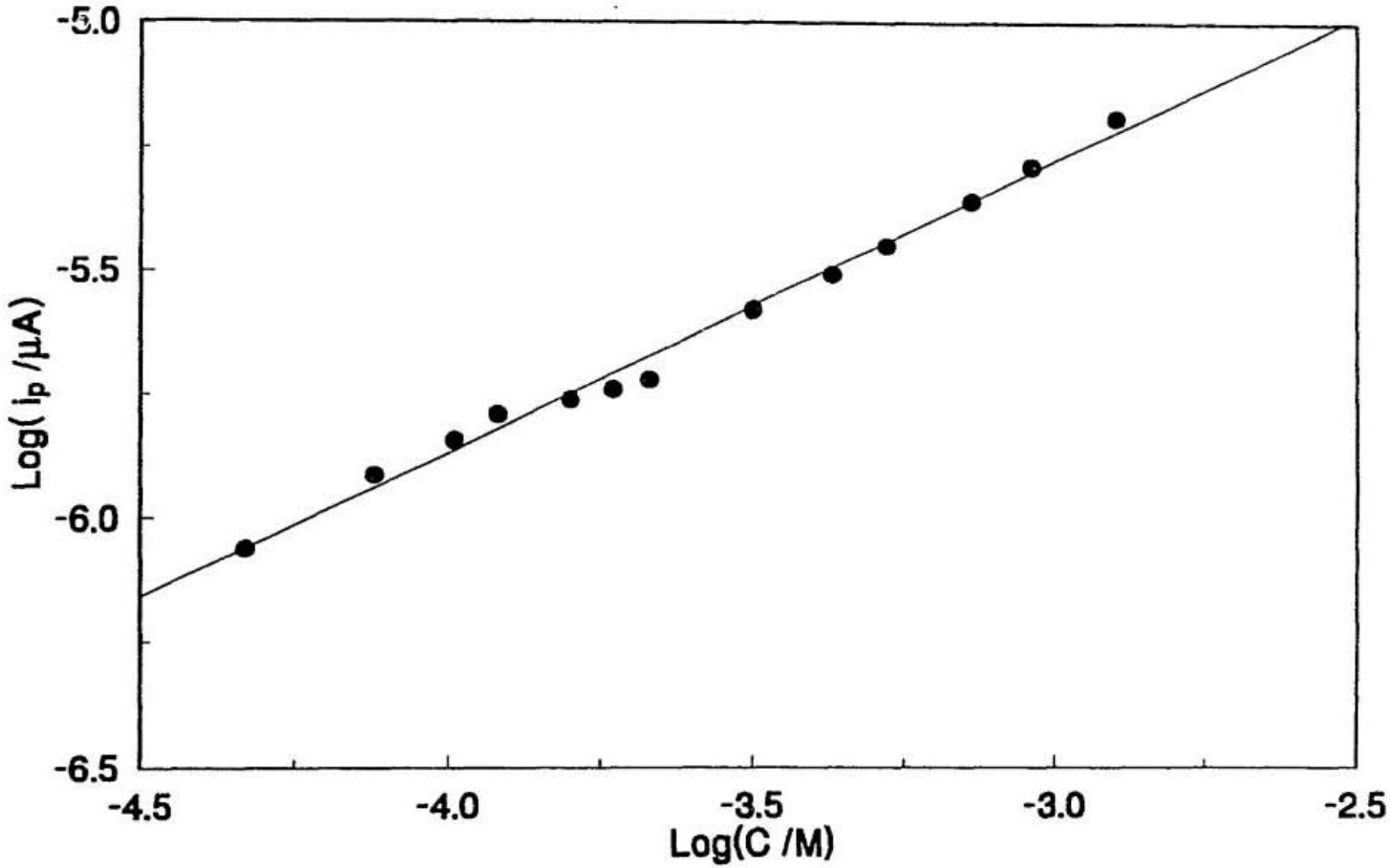

Figure 7.3.3. Calibration plot of peak current *vs* ascorbic acid concentration for a poly-PPTA$^+$ coated electrode in 10 mM K_3PO_4 buffer (pH = 7.4); film thickness = 1.4 μm; scan rate = 50 mV/s.

7.4 Discussion

Comparison with polypyrrole

All three polypyrrole-based anion exchange polymers, poly-MPMP$^+$, poly-PPP$^+$ and poly-PPTA$^+$, have demonstrated excellent electrocatalytic properties for ascorbate oxidation. For a comparison with polypyrrole, data are quoted from works by Lyons and Breen[21] on polypyrrole coated Pt electrodes, and Ewing and coworkers[8] on polypyrrole coated glassy carbon electrodes. The data are listed in Table 7.3 (next page) together with data from this work.

From the second column of Table 7.3, poly-MPMP$^+$, poly-PPP$^+$ and poly-PPTA$^+$ coated electrodes show lower peak potentials than polypyrrole coated Pt electrodes. The significant differences in peak potential (from 240 mV to -40 mV) for the polymers listed in Table 7.3 are probably due to a stronger electrostatic interaction. The potential difference between the polypyrrole coated and ion exchange polymers such as poly-PPP$^+$ and poly-PPTA$^+$ coated Pt electrodes indicates that the positively charged sites in the anion exchange polymers have greatly improved the catalytic properties of the polymer coated electrode. The ascorbate and the anion radicals (see Figure 7.1.1) can be stabilized to a greater extent in anion exchange polymers than in polypyrrole which has a lower concentration of cationic sites. This agrees with Ewing's postulation[8] that the catalysis of ascorbate oxidation at polypyrrole coated electrodes is due to an

Table 7.3. Comparison of cyclic voltammetry data for electrocatalysis of ascorbate oxidation at polypyrrole, poly-MPMP$^+$, poly-PPP$^+$ and poly-PPTA$^+$ coated electrodes.

polymer	E_p (mV)	peak current (μA cm^{-2})
poly-MPMP$^+$ [a]	70	333 (533)
poly-PPP$^+$ [b]	-10	487 (904)
poly-PPTA$^+$ [c]	-40	307 (464)
polypyrrole[d]	240	35
polypyrrole[e]	0	309

a. Experimental conditions: 1.7 μm thick films on Pt in 0.3 mM (or 0.5 mM) ascorbic acid with a scan rate 50 mV s^{-1} in 0.01 M phosphate buffer at pH = 7.4.

b. Same conditions as (a) but film thickness 1.4 μm.

c. Same conditions as (a) but film thickness 1.2 μm.

d. Data from reference 21 (measured from calibration curve). Experimental conditions: 1.4 μm thick films on Pt in 0.3 mM ascorbic acid with a scan rate 50 mV s^{-1} in 0.1 M NaCl at pH = 7.

e. Data from reference 8. Experimental conditions: 0.08 μm thick film on glassy carbon in 0.5 mM ascorbic acid in citrate and phosphate buffer containing 0.9% NaCl at pH = 7.4, scan rate 50 mV/s.

electrostatic interaction between the cationic polymer and the ascorbate. With the increased concentration of cationic sites in the anion exchange polymers, the electrostatic interaction should be more favourable.

A significant enhancement in peak current density for poly-$MPMP^+$, poly-PPP^+ and poly-$PPTA^+$ coated electrodes over polypyrrole coated electrodes can be noted in Table 7.3. The peak currents density for ascorbate oxidation at the ion exchange polymers reported in this work are approximately 10 times higher than at polypyrrole coated Pt electrodes. Preconcentration of ascorbate presumably occurs to a greater extent in the anion exchange polymers due to the higher concentration of cationic sites. The improved ascorbate oxidation signal could be advantageous when using the anion exchange polymers for applications in amperometric chemical sensors.

The catalytic properties for ascorbate oxidation at anion exchange polymer coated Pt electrodes is also compared to that at polypyrrole coated glassy carbon electrodes. The peak potentials are more negative for poly-PPP^+ and poly-$PPTA^+$ than that for polypyrrole. Poly-$MPMP^+$, however, shows a higher peak potential than does the polypyrrole coated glassy carbon electrode. This is presumably due to the low conductivity of the polymer at the potential of ascorbate oxidation. The peak currents (in parentheses) from all anion exchange polymers are higher than that from polypyrrole coated glassy carbon electrode at the same concentration (0.5

mM ascorbic acid).

Comparison of poly-MPMP$^+$ with poly-PPP$^+$ and poly-PPTA$^+$ Although all three of the ion exchange polymers demonstrate excellent catalytic properties for ascorbic oxidation, there are significant differences between the N-substituted polymer, poly-MPMP$^+$, and the 3-substituted polymers, poly-PPP$^+$ and poly-PPTA$^+$, namely from four aspects: full width at half maximum, peak potential, peak current and the relationship between the peak current and film thickness.

1. *Full width at half maximum* By comparing the cyclic voltammograms which appear in Figure 7.2.1, Figure 7.2.5, and Figure 7.2.6, it is observed that the anodic peak for ascorbate oxidation at a poly-MPMP$^+$ coated electrode is broader, and E_{FWHM} has a value of about 135 mV, compared with values of 92 and 65 mV for poly-PPP$^+$ and poly-PPTA$^+$, respectively. The responses at the 3-substituted polymer coated electrodes are sharp and more symmetric. This implies that the reaction at those electrodes is faster than at the N-substituted polymer coated electrode.

2. *Peak potential* There is a significant decrease of the peak potentials from poly-MPMP$^+$ to poly-PPP$^+$ and poly-PPTA$^+$ as listed in Table 7.3. The lower peak potentials for poly-PPP$^+$ and poly-PPTA$^+$ represent an increase in reaction rate compared to the peak potential for poly-MPMP$^+$. This can be related to the

different conductivity for these polymers. As has been mentioned in section 7.2.1, poly-MPMP$^+$ is non-conductive at the ascorbate oxidation potential whereas poly-PPP$^+$ and poly-PPTA$^+$ are oxidized so as to be conductive (6×10^{-5} S cm^{-1}). Therefore, ascorbate can react at the film/solution interface, within the film, and at the Pt surface, for these 3-substituted polymers. This is very much like an increase in the number of active sites for an electrode as discussed in section 7.1.2.

3. *The relationship between the peak current and film thickness* Table 7.2 shows a linear increase of the peak current with the film thickness for poly-PPP$^+$ but the peak current does not increase with film thickness as the film gets thicker, as shown in Table 7.1, for poly-MPMP$^+$. The significance of the peak current dependence on thickness for poly-PPP$^+$ can be seen in two ways. First, this dependence provides additional evidence for the preconcentration of ascorbate by ion exchange polymers. As mentioned in section 7.1.2, the peak current is proportional to the amount of the electroactive species in the film. Increasing the film thickness increases the number of the positively charged sites. Since the ascorbate [(2), Figure 7.1.2] is expected to be electrostatically bound by the cationic sites, the amount of ascorbate within the film must be increased as the film gets thicker. The dependence of peak current on film thickness therefore demonstrates that ascorbate is preconcentrated in the film.

Secondly, the dependence of peak current on film thickness indicates that the electron transport in the film is fast and the electrostatically bound ascorbate reacts within the oxidized polymer film and not at the Pt surface *via* diffusion through the film. The conductivity of the oxidized poly-PPP^+ and poly-$PPTA^+$ film ($E^{o'} \sim -0.1$ V) is presumably responsible for the high electron transport rate in the film, thus allowing the bound ascorbate to react with the polymer. In contrast with information in Table 7.2, the peak current does not significantly increase with film thickness for poly-$MPMP^+$ coated electrodes. This is also caused by the low conductivity of poly-$MPMP^+$ in the potential region of ascorbate oxidation. The levelling and eventually decrease in peak current may be due to an increase in the film resistance, which slows the rate of the ascorbate oxidation.

4. *Peak current* A higher peak current is observed for poly-PPP^+ than for poly-$MPMP^+$. According to the data in Table 7.1 for poly-$MPMP^+$ and Table 7.2 for poly-PPP^+, both polymers give about the same peak current for very thin films. When the films get thicker, the peak current increases linearly for poly-PPP^+ but does not increase significantly for poly-$MPMP^+$. Apparently, the peak current at poly-PPP^+ is higher than at poly-$MPMP^+$ for all films except the thinner films. This is presumably due to higher conductivity for poly-PPP^+ as discussed above. In addition, the higher peak current for poly-PPP^+ indicates a greater

preconcentration in poly-PPP$^+$ than in poly-MPMP$^+$. This is expected because the concentration of cationic sites in oxidized poly-PPP$^+$ is higher than in the reduced poly-MPMP$^+$. However, the peak current for poly-PPTA$^+$ is similar to poly-MPMP$^+$. The reason for this anomaly is not clear.

Combining the differences between the cyclic voltammograms of ascorbate at poly-MPMP$^+$ and poly-PPP$^+$ discussed above, it can be concluded that the improved catalytic activity of poly-PPP$^+$ (and poly-PPTA$^+$) is due to its enhanced conductivity at the ascorbate oxidation potential. The improvement in the catalytic properties obtained by moving the cationic groups to a 3-position has met our goal in synthesising such polymers.

7.5 Conclusions

The electrocatalytic properties of poly-MPMP$^+$, poly-PPP$^+$ and poly-PPTA$^+$, towards the oxidation of ascorbate have been studied by cyclic voltammetry and rotating disc voltammetry. At low pH, catalysis by the film itself is minimal but ascorbate oxidation is catalyzed by electrostatically incorporated ferrocyanide. In a neutral solution (pH = 7.4), cyclic voltammograms for ascorbate at these polymers show greatly enhanced peak currents which can be more than 10 times higher than for a bare Pt electrode. The peak potential for

ascorbate oxidation is shifted by as much as 350 mV to a more negative potential compared to a bare Pt electrode. Both electrostatic interactions and preconcentration of ascorbate by ion exchange are responsible for the catalysis by the polymers. These results have been compared with data for polypyrrole coated electrodes from the literature: peak currents are an order of magnitude higher than at the polypyrrole coated Pt electrodes and the peak potential is more than 300 mV more negative under similar experimental conditions. There are differences in the kinetics of ascorbate oxidation at the N-substituted (poly-MPMP$^+$) and 3-substituted (poly-PPP$^+$, poly-PPTA$^+$) pyrrole based polymers. The 3-substituted polymers show a faster electron transfer rate than the N-substituted polymer, mainly due to their higher electronic conductivity at the ascorbate oxidation potential. All three conducting ion exchange polymers show enhanced, analytically significant, peak currents which are linearly related to the bulk concentration of ascorbic acid. Calibration curves for the analysis of ascorbic acid in aqueous solution are presented.

References

1. G. Dryhurst, K. M. Kadish, F. Scheller, R. Renneberg, "Biological Electrochemistry", Academic Press, New York, Vol. 1, (1982) 256-277.

2. J. Facci and R. W. Murray, Anal. Chem., 54 (1982) 772.

3. K.J. Stutts and R. M. Wightman, Anal. Chem., 55 (1983) 1576.

4. J. F. Evans, T. Kuwana, M. H. Henne and G.P. Royer, J. Electroanal Chem., 80 (1977) 409.

5. M. A. Dayton, A. G. Ewing and R. M. Wightman, Anal. Chem., 52 (1980) 2392.

6. S. P. Perone and W. J. Kretlow, Anal. Chem., 38 (1966) 1760.

7. J. J. Ruiz and A. Aldaz, M. Dominguez, Can. J. Chem., 55 (1977) 2799 and 56 (1978) 1533.

8. R. A. Saraceno, J. G. Pack and A.D. Ewing, J. Electroanal. Chem., 197 (1986) 265.

9. Z. Vavrin, Collect. Czech. Chem., 14 (1949) 367.

10. J. J. Ruiz, A. Aldaz and M. Dominguez, Can. J. Chem., 55 (1977) 2799.

11. "Merck Index", 8th ed., P.105, Merck & Co., Inc., Rahway, New Jersey, 1968.

12. D. M. H. Kern, J. Am. Chem. Soc., 76 (1954) 1011.

13. K. J. Stutts, P. M. Kovach, W. G. Kuhr and R. M. Wightman, Anal. Chem., 55 (1983) 1632.

14. K-N. Kuo and R. W. Murray, J. Electroanal. Chem., 131 (1982) 37.

15. A. J. Bard and L. R. Faulkner, " Electrochemical Methods" , Wiley, New York, 1980, P.223.

16. A. J. Bard and L. R. Faulkner, " Electrochemical Methods" , Wiley, New York, 1980, P.412.

17. J. Zak and T. Kuwana, J. Electroanal. Chem., 150 (1983) 645.

18. S. Dong and T. Kuwana, J. Electrochem. Soc., 131 (1984) 813.

19. J. Zak and T. Kuwana, J. Am. Chem. Soc., 104 (1982) 5514.

20. I-F. Hu and T. Kuwana, Anal. Chem., 58 (1986) 3235.

21. M. E. G. Lyons and W. Breen, J. Chem. Soc. Faraday Trans., 87 (1991) 115.